

https://dspace.org/

Geotechnical optimisation of the Venetia open pit

Ekkerd, Josef Nicolaas

2013-01-30
http://hdl.handle.net/10539/12331

Downloaded from a DSpace repository. https://dspace.org/

GEOTECHNICAL OPTIMISATION OF THE VENETIA OPEN PIT

Josef Nicolaas Ekkerd

A research report submitted to the Faculty of Engineering and the Built Environment, University of Witwatersrand, in partial fulfilment of the requirements for the degree of Master of Science in Engineering.

December 2011

DECLARATION

I declare that this research report is my own, unaided work. The content covers work done at De Beers Venetia Mine, by the author as well as fellow staff members. It is being submitted for the Degree of Master of Science in Engineering in the University of Witwatersrand, Johannesburg. It has not been submitted before by the author for any degree or examination in any other university.

_____

Josef Nicolaas Ekkerd

31 December 2011

ABSTRACT

Venetia Mine is situated south of the confluence of the Shashi and Limpopo rivers, 80 km West of Musina and 36 km North-east of Alldays in South Africa. Venetia is an open pit, truck and shovel operation which commenced full production in 1993. Mining began on the Cut 4 design in 2006 with a final planned open pit depth of approximately 500m below surface at a maximum waste stripping rate of approximately 50 million tonnes per annum.

The country rock assemblages at Venetia are part of the Limpopo Mobile Belt and mainly consist of metamorphic and intrusive igneous rocks. The stability of the pit is structurally controlled and the structure can be divided into two main components, ductile structure (foliation) and brittle structures (major structures and joints). A dominant metamorphic foliation cross cuts all the geology which results in an anisotropic rock mass strength. The interaction between the brittle jointing and foliation also locally impacts on bench stability and subsequent bench performance. The slope design is therefore highly dependent on the orientation of the pit slopes relative to structural features.

Up to 2009 Venetia mine employed high energy blasting techniques, mainly focused on achieving high production rates and optimum fragmentation, to develop the final walls of the pit. Excavating the highwalls with conventional production blasting techniques resulted in extremely poor highwall conditions. In 2009 this practice was ceased and the mine started experimenting with limit blasting techniques on the final pit limits. The benefit of the limit blasting was however not quantified. That same year a revision and optimisation of the business plan was undertaken of which one aspect was the review of the slope angles and design sectors. The acceptance criteria, as recommended by the Guidelines for Open Pit Slope Design (Read and Stacey, 2009) were used by De Beers to determine the acceptable level of risk for the optimisation programme.

Rigorous reviews of actual pit slope performance were conducted for the North and Southern slopes. This indicated that the bench performance in the Southern slopes can be isolated to distinct areas. The South-western portion of the slope had the highest incidence of complete bench failures (43%) followed by the Southern section (17%). See Figure 2.1. In turn rock falls were prevalent in the North domain. This was aggravated by poor blasting resulting in the catch berms not being retained and thus not being effective at retaining rock falls. The

mechanisms that initiated the variable bench performance and rock fall risk were not well understood at that stage.

The first Cut 4 slope stability design was conducted in 2008 and defined only two major domains [North: 56° stack angle, South: 40° stack angle] (Contreras, 2008). The South slope design assumed a slope striking parallel to the orientation of the foliation. The analysis indicated that steeper stack angles are achievable in the North domain however a lower slope angle was recommended due to the perceived rock fall risk and mining practices at the mine. The rock fall risk was however not quantified. Review of the data supplied by the operation to the consultant indicated that the orientation of the S2 foliation and joint populations were extrapolated from old exposures in Cut 2. In addition to the above no groundwater table was available for the first design in 2008.

Thus considering the improvement in mining practices, lack of understanding regarding the actual slope performance and extrapolated data that was used in the design the author deemed it appropriate to re-evaluate the Cut 4 design in 2009. The optimisation study was scoped by the author and consisted of various phases (1 – 3).

Phase 1 was aimed at providing initial input parameters into the strategic business plan (SBP) regarding slope angles (savings on waste stripping) (Strouth, 2009; Gomez, 2010) and bench heights (potential to increase productivity) (Contreras, 2010; Steffen and Terbrugge, 2009). The only new data for this phase was limited scan line mapping that was collected by the mine in the South-western quadrant of the pit and thus similar constraints relating to the orientation of the S2 foliation, joint sets and groundwater applied.

Phase 2 ran concurrently with the above work and was aimed at defining the orientation of the S2 foliation, joint data and pore pressures in the toe of the slope. This phase consisted of structural mapping, drilling, instrumentation installation; and modelling of the geology and ground water table by Basson (2011a) and Liu et al. (2011) respectively.

For the final phase of the optimisation (Phase 3) the Geotechnical domain model and slope design was updated using the results from Phase 2 of the study. The updated design incorporated the updated groundwater table and considered the orientation of the pit slopes relative to the foliation; and consisted of bench, inter-ramp and overall slope analyses. Probabilistic limit equilibrium bench analyses were conducted by the author for every practical orientation of each domain, at various bench heights, using SWISA™ and PFISA™.

For the inter-ramp and overall slope design limit equilibrium probabilistic analysis were conducted using the programme SLIDE™. The anisotropic strength model in SLIDE™ was used to account for the S2 foliation.

The bench and inter-ramp analyses indicated that steeper angles are viable in a number of domains. The stability of the pit walls in the Southern domains is mainly controlled by their orientation in relation to the major S2 foliation. In contrast the stack angle in the North domain is not controlled by the S2 foliation and/or rock mass strength. Here the interaction between brittle jointing controls the maximum catch berm and subsequent stack angle. The numerical finite difference code, FLAC™, was used to validate the results of the limit equilibrium stack analysis. The validation indicated that the limit equilibrium modelling is conservative when compared to numerical modelling and it is recommended that future studies use the response surface methodology by Chiwaye and Stacey (2010), whereby numerical modelling is used, to estimate the risk (probability of failure).

Strategies to monitor the quality of mining practices and related rock fall risk have also been developed and incorporated into the Code of Practice and related standard operating procedures for the operation.

The results of the optimisation project was included into the mine's strategic business plan in 2011 and resulted in significant financial savings.

DEDICATION

To my daughter, Olivia: you are my inspiration.

ACKNOWLEDGEMENTS

The input of the following people and organisations are acknowledged:

- De Beers Venetia Mine: For sponsoring the project.
- The staff in the Venetia Geotechnical Department: For their support, efforts and perseverance.
- Dr. Ian Basson: For his ability to communicate and explain a complex geological problem.
- Dr. Marc Ruest: For being a good sounding board and mentor.
- Professor Thomas Stacey: For his patience, guidance and assistance.

TABLE OF CONTENTS

DECLARATION……...…….2

ABSTRACT……...…….3

DEDICATION……...…….6

ACKNOWLEDGEMENTS…….7

LIST OF FIGURES……12

LIST OF TABLES……..19

1. BACKGROUND 23

1.1 Introduction 23

1.2 Location and history 24

1.3 Geological setting Geological 27

1.3.1 Regional Geological Setting 27

1.3.2 Local Setting 28

1.3.3 On-Mine Geological Setting 30

1.3.3.1 Ductile Evolution 32

1.3.3.2 Brittle Overprint (Major Structures and Joint Sets) 37

1.3.4 Kimberlite Geology 41

1.4 Hydrological Setting 44

1.5 SUMMARY 44

2. JUSTIFICATION FOR OPTMISATION STUDY 46

2.1 SOUTHERN SLOPES 46

2.2 NORTH SLOPE 48

2.3 SUMMARY 50

3. SCOPE 52

3.1 AIMS 52

3.2 SPECIFIC OBJECTIVES AND LIMITATIONS 52

3.3 TECHNIQUES APPLIED BY THE AUTHOR 53

3.4 SUMMARY 54

4. LITERATURE SURVEY: SLOPE STABILITY AND DESIGN PRINCIPLES 55

4.1 PIT WALL AND OPEN PIT MINING TERMINOLOGY 55

4.2 OPEN PIT SEQUENCING 57

4.3 ACCEPTANCE CRITERIA 58
4.4 GEOTECHNICAL MODEL 61
4.5 ROCK MASS MODEL 62
4.5.1 Strength of Discontinuities 62
4.5.2 Anisotropy 75
4.5.3 Rock Mass Ratings 79
4.5.3.1 The Mining Rock Mass Rating and RQD 79
4.5.3.2 The Geological Strength Index (GSI) 84
4.5.4 Failure Criterion and Rock Mass Strength 87
4.6 HYDROLOGY 89
4.7 FAILURE MECHANISMS 92
4.7.1 Structurally controlled mechanisms 93
4.7.1.1 Planar Failure 93
4.7.1.2 Wedge failure 94
4.7.1.3 Toppling Failure 96
4.7.2 Rock mass (Circular) failure mechanisms 98
4.7.3 Combination of failure mechanisms 98
4.7.4 Failure mechanisms and scale effects 99
4.8 SLOPE DESIGN ELEMENTS AND TECHNIQUES 101
4.8.1 Bench Scale 101
4.8.2 Inter-ramp and Overall Slope Design and Methods 104
4.8.2.1 Application of Slope Stability Analysis Techniques 104
4.8.2.2 Stereographical and Empirical Estimates 106
4.8.2.3 Limit Equilibrium 107
4.8.2.4 Numerical Techniques 109
4.9 BLASTING 110
4.9.1 Blasting Techniques 110
4.9.2 Theoretical Blasting Damage Mechanism 112
4.9.3 Incorporation of Blast Damage into Slope Designs 114
5. PHASE 2 OPTIMISATION 118
5.1 GEOLOGICAL AND STRUCTURAL MODEL 118
5.1.1 Data Collection for Geological and Structural Model 118
5.1.1.1 Scan Line Mapping 118
5.1.1.2 Photogrammetry Mapping (SIROVISION^{TM}) 120
5.1.1.3 Mapping coverage 122
5.1.1.4 Borehole information 123

5.1.2 Review of Data and Development of Geological Model 127
5.1.3 Analysis of Structural Data (S2 Foliation and Brittle Jointing) 131
5.1.3.1 S2 Foliation 131
5.1.3.2 Brittle Joints 134
5.2 HYDROLOGICAL MODEL 138
5.3 SUMMARY 142
6. PHASE 3 OPTIMISATION 143
6.1 ROCK MASS MODEL 144
6.1.1 Intact strength 144
6.2 Weathering Horizon 148
6.3 Weighting of Data 149
6.4 Shear Strength of the Foliation 150
6.5 Tensile Strength 154
6.6 Triaxial testing and calculation of m_i 155
6.7 Density and Elastic Properties (Young's Modulus and Poisson's Ratio) 157
6.8 Rock Mass Ratings 160
6.9 Rock Mass Strength Properties 163
6.10 GEOTECHNICAL MODEL AND DOMAINS 166
6.10.1 Fall of Ground Analysis 166
6.10.2 Domain Boundaries 167
6.10.3 Tier 1 Major Domains 168
6.10.4 Tier 2 and 3 Domains 172
6.10.5 Geotechnical Block Model 173
6.11 SLOPE DESIGN AND OPTIMISATION 175
6.11.1 Bench height risk assessment 175
6.11.1.1 Stereographic Analysis 176
6.11.1.2 Empirical Analysis 177
6.11.1.3 Probabilistic Limit Equilibrium Bench Analysis 178
6.11.2 Inter-ramp Analysis 185
6.11.2.1 Empirical Inter-ramp Analysis 185
6.11.2.2 Limit equilibrium probabilistic analysis 186
6.11.3 Overall Slope Analysis 191
6.11.4 Ramp Width Design 193
6.12 SUMMARY 195
7. IMPLEMENTATION STRATEGIES AND CONTROLS 200

7.1 MEASURE BLASTING DAMAGE/ SUCCESS AND CLEANING PRACTICES ON THE FINAL LIMIT 200
7.1.1 Crest Lost on Benches in the Southern Domains 200
7.1.2 Crest Damage on Benches in the Northern and Southern Domains 202
7.1.3 Measuring Blasting and Final Pit Wall Excavation Effectiveness 204
7.1.3.1 Detailed rating system of benches 204
7.1.3.2 Crest and Toe Methods based on actual surveyed bench geometries 208
7.1.4 Blast Pattern Selection 211
7.2 QUANTIFICATION AND COMMUNICATION OF ROCK FALL RISK 214
7.2.1 Rock Fall Rating Systems 215
7.2.2 Application of ROFRAQ rating and Communication of Risk 221
7.3 SUMMARY 223
8. SUMMARY AND CONCLUSIONS 225
9. REFERENCES 232
APPENDIX A
APPENDIX B
APPENDIX C
APPENDIX D
APPENDIX E
APPENDIX F
APPENDIX G

LIST OF FIGURES

Figure 1.1 Locality Map (Taken from Google Maps ™). 25
Figure 1.2 A plan view of the planned Cut 4 pit showing the various pits and the split shell line. See Figure 1.3 for a section of the pit (15m Bench plan). 26
Figure 1.3 A section (A-B) through pit (See Figure 1.2 for the section line) showing the various planned Cuts (15m Bench plan). 26
Figure 1.4 Locality map showing the three distinct zones in the Limpopo Mobile Belt. Venetia Mine is located within the Central Zone (CZ) (Rigby et al., 2011). 27
Figure 1.5 The Venetia area of the Limpopo Belt, as mapped by Brandl (2000) showing the Beit Bridge Complex in the immediate vicinity of Venetia which consists of the Gumbu Group, Mount Dowe and Malala Drift Groups (Rigby et al., 2011). 29
Figure 1.6 Country rock map of the pit showing the major package boundaries, major structures and fold axial plane (Basson, 2011a). 32
Figure 1.7 The main deformation events from D3 onwards. The first deformation event is not resolvable, although it may have consisted of the juxtaposition of gneissic and metasedimentary units and is thus not represented graphically (Basson, 2011b). 34
Figure 1.8 Lower Hemisphere Stereographic Projections Showing the distribution of the brittle jointing and S2 foliation in the North and Southwest Domain. 34
Figure 1.9 Photograph of the S2 foliation in Biotite Bearing Gneiss. Note how the foliation separates on the biotite rich bands. 35
Figure 1.10 Photograph looking SE in the pit showing the S2 foliation in relation to the East Wall. Note how the planar failures decrease as the difference in strike between the S2 foliation and East wall increase. 35
Figure 1.11 Small-scale F3 folds, which refold F2 folds, at the contact between amphibolite (AM) and banded biotite gneiss (Rigby, et al., 2011). 36
Figure 1.12 “Crenulations” (in local mine terminology) or steeply NE- to NNE-plunging F4 folds on the surface of a biotite gneiss on the south face of the pit (Rigby, et al., 2011). 36
Figure 1.13 Photograph showing the MS1 Fault (Looking SSW along the strike of the fault). 39
Figure 1.14 MS3 structure in the East-wall of Cut 4 with the typical infilling. S2 is striking perpendicular to the wall. 40

Figure 1.15 MS3 structure, in the North-wall of Cut 4, with little to no infilling running parallel behind the face. This specific structure de-stabilised 6 benches. 40
Figure 1.16 Photograph showing the typical wedge failures that occur on the J2 and J4 joint sets in the North wall.....41
Figure 1.17 Plan of the pit showing all the kimberlite bodies in the pit. Note how K010, K016, K06 and K05 follow the Lezel-Tina trend.....42
Figure 1.18 North-South section through the pit showing the MVK and DVK kimberlites. 43
Figure 2.1 Historic bench performances in the South, South-Southwest and West-Southwest domains. 47
Figure 2.2 Percentage (%) catch berm since 2008 demonstrating the improvement in blasting practices. 49
Figure 2.3 Photograph of the North wall, looking North, comparing the bench retention pre- and post-2009 highwall conditions and bench retention (Scale: Benches = 12m). 49
Figure 4.1 Slope Design Terminologies adapted from Read and Stacey (2009) and Wyllie and Mah (2005). 56
Figure 4.2 Schematic illustrating the concentric and split shell mining concepts (after Gallagher and Kear, 2001). 57
Figure 4.3 The Definition of POF and its relationship with FOS according to uncertainty magnitude (after Tapia et al., 2007; taken from Chiwaye and Stacey, 2010). 59
Figure 4.4 The shear testing of discontinuities (after Hoek, 2002). 63
Figure 4.5 Some examples of in situ direct shear tests on discontinuities. (Romero, 1968; Hoek and Bray, 1981; Haverland and Slebier, 1972; Franklin and Dusseault, 1989; Brown, 1981).....64
Figure 4.6 Diagrammatic section through shear machine used by Hencher and Richards (1982). 65
Figure 4.7 Use of triaxial compression test to define the shear strength of veins or other defects with strong infills (Modified from Goodman, 1989). 66
Figure 4.8 Patton's experiment on the shear strength of saw-tooth specimens (Hoek, 2002). 67
Figure 4.9 Definition of 1st and 2nd order asperities on rough defects (From Wyllie and Norrish, 1996).....68
Figure 4.10 Effect of surface roughness and normal stress on the defect's friction angle (from Wyllie, 1992). 69

Figure 4.11 Defect roughness profiles and associated JRC values (Barton and Choubey, 1977). 71

Figure 4.12 Chart to estimate *JRC* from the maximum unevenness amplitude and the profile length (Barton, 1982). 72

Figure 4.13 Summary of scale effects in the shear strength components of non-planar defects. ∅ b is the basic friction angle, d_n is the peak dilation angle, s_a are surface asperities, and *i* is the roughness angle (Barton, 1980). 73

Figure 4.14 (a) Transversely isotropic specimen in triaxial compression (b) variation of peak strength at constant confining pressure with the angle of inclination of the normal to the plane of weakness to the compression axis (β). ∅ w in this case in the friction angle of the weakness (Brady and Brown, 2004). 75

Figure 4.15 Factor of safety of a 200m rock slope, with an inclination of 55^o, for different conditions of rock mass strength (Karzulovic and Read, 2009). 77

Figure 4.16 Simplified representation of the effect of rock bridges (modified from Wittke, 1990). 78

Figure 4.17 Graph for determination of joint spacing rating (after Laubscher, 1993; taken from Stacey, 2001). 81

Figure 4.18 The Geological strength Index – GSI (taken from Marinos et al., 2005). 85

Figure 4.19 The correlation between Bieniawski and Laubscher's RMR (after Terbrugge et al., 2004). 86

Figure 4.20 Showing the comparison of the effective stress states in a partly saturated slope and almost drained slope (Sjoberg, 1996). 90

Figure 4.21 Alternate piezometer installations in core or RC drill holes (Read et al., 2009) 91

Figure 4.22 (a) The conditions for planar failure (b) Release surfaces associated with a planar failure (c) Stereographic analysis showing the kinematic condition required for kinematic failure (Modified Wyllie and Mah, 2005). 94

Figure 4.23 (a) Typical wedge with line of intersection (b) Kinematic condition for wedge failure to occur illustrated on a stereonet (c) Kinematic conditions for wedge failure shown in section (d) Stereonet demonstrating the limit of wedge failure in relation to the strike of a slope, estimated at 20° (After Wyllie and Mah, 2005). 95

Figure 4.24 (a) Block Toppling (b) Flexural Topping (c) Block-Flexural Toppling (d) Secondary Toppling (e) Stereographic projection showing the kinematic conditions required for toppling (Modified from Wyllie and Mah, 2005). 97
Figure 4.25 Rock Mass or Circular Shear Failure Mechanisms (after Sjoberg, 2000). ...98
Figure 4.26 Theoretical complex failure (after Hoek et al., 2000). 99
Figure 4.27 Illustrating how the blockiness of the rock mass depends on the size of the rock slope: very blocky for the overall slope, blocky for the inter-ramp slope, and almost massive at the bench scale (Karzulovic, 2006). 100
Figure 4.28 The relationship between Bench Face Angle/Catch berm Width and Inter-ramp Angle after Ryan and Prior (2000). 101
Figure 4.29 Plan view of a catch berm width as defined by Ryan and Prior (2000) showing the crest and toe. 102
Figure 4.30 Illustration of symmetric conical distribution of failed material on a spill berm (Gibson et al., 2006). 104
Figure 4.31 The relationship between the complexity of failure mechanisms and analysis techniques (Stead et al., 2006). 105
Figure 4.32 The Haines and Terbrugge (1991) chart for estimating slope angles using the MRMR. 107
Figure 4.33 Demonstrating the economies of scale concept and the production benefit of improving fragmentation (Wyllie and Mah, 2005). 111
Figure 4.34 Showing a typical limit and pre-split drilling pattern. A trim blast at Venetia consists of production and buffer holes. 112
Figure 4.35 Showing the effect of the Disturbance factor introduced by Hoek (2002). 115
Figure 4.36 Diagrammatic representation of the transition between the in situ rock mass and blasted rock that is suitable for digging (Hoek, 2009).....116
Figure 4.37 Depth of damage zone for a 500m high slope (after Lorig, 2011). 117
Figure 5.1 Diagram representing a scan line and showing the waist high imaginary traverse. 119
Figure 5.2 Cameras used to take the images. 120
Figure 5.3 A SIROVISION™ screenshot showing a 3D image of an actual rock face at Venetia Mine. Structure traces (red, green and purple) denote actual structures. 121
Figure 5.4 Showing the scan line and SIROVISION™ mapping coverage. 122
Figure 5.5 Plan showing all the Venetia Resource Extension boreholes drilled since 2003 and the kimberlite ore bodies. 123

Figure 5.6 Showing the location of the boreholes that were selected for STEREOCORE™ analysis. 124
Figure 5.7 Showing an imported image in STEREOCORE™ of a drill core tray within the reference frame. 126
Figure 5.8 Showing the Stereographic projection and data display functionality of the STEREOCORE™ software 126
Figure 5.9 3D Geological model showing the F3 Fold and Fold Axial Plane (FAP3). 129
Figure 5.10 3D model and plan showing the structural volumes (after Basson, 2011a). 130
Figure 5.11 Pore pressure assumptions applied in the model (Contreras, 2008). 138
Figure 5.12 Showing a typical multi-level piezometer layout within one of the core holes (DWH020) in the North Wall. 139
Figure 5.13 A typical multiple VW piezometer installation in an angled core hole. 139
Figure 5.14 Showing the initial stand pipe piezometers and newly installed VW piezometer network. 140
Figure 5.15 A section through the model showing the groundwater table in the North Wall with and without a zone of relaxation (Liu et al., 2011). 141
Figure 5.16 A plan view showing the 3D groundwater table as modelled by Liu et al. (2011). 141
Figure 6.1 Plot of Beta angle after Jaeger (1960) versus uniaxial compressive strength for samples that failed on a discontinuity. 144
Figure 6.2 Showing the Uni-axial Test Results for those samples that failed through intact rock and on discontinuities. 146
Figure 6.3 Photograph of a Gneiss unit in the Venetia Pit showing the Biotite banding/foliation in the Gneiss. 147
Figure 6.4 Illustrating how the roughness or unevenness amplitudes were measured on a 500mm scale. 152
Figure 6.5 The largest failure to date in the Venetia pit (Tsheko, 2010) on 2 July 2003 in Cut 3. 153
Figure 6.6 FLAC plot showing the minimum principal stress distribution in the south slope. 163
Figure 6.7 Mine rock fall and slope instability incident analysis 166
Figure 6.8 Analysis of All Fall of Ground Statistics: Types of Failures 167
Figure 6.9 Analysis of fall of ground statistics for each tier 1 domain. 171
Figure 6.10 Tier 1 and 2 Geotechnical domains. 171

Figure 6.11 Showing the dip of the foliation in the Geotechnical block model. 173
Figure 6.12 Showing the intact rock strength of the various units in the Geotechnical block model. 174
Figure 6.13 The 2010 SRK bench height risk assessment study (Contreras, 2010). 175
Figure 6.14 Maximum inter-ramp angle calculated using the Ritchie Modified Criterion (Contreras, 2010). 177
Figure 6.15 Bench analysis results for 12m, 15m and 24m benches in STRV01 with an MS2 overprint. 181
Figure 6.16 Back break in STRV08. 182
Figure 6.17 (a) Design section South (S) showing the modelled GW table and Tier 2 domains in the South slope (b) the highest water table, from the lower most stack, that were used in the inter-ramp analysis. 186
Figure 6.18 The inter-ramp analysis for STRV1 in the North Domain. 188
Figure 6.19 The inter-ramp analysis for STRV8 GP indicating the lower inter-ramp angles are required to achieve the proposed acceptance criteria (FoS = 1.20-1.30 and PoF = 10%). 188
Figures 6.20 Limit Equilibrium Results (SLIDE™) for a 120m stack with no foliation. 190
Figures 6.21 Numerical Modelling Results (FLAC™) for a 120m stack with no foliation. 190
Figure 6.22 Overall slope limit equilibrium analyses for the WSW domain 192
Figure 6.23 Overall slope limit equilibrium and sensitivity analyses for the South domain. 192
Figure 6.24 Venetia mine ramp width design methodology (Mompati, 2009) 194
Figure 6.25 Back break results. 194
Figure 7.1 Photograph looking at the south wall, showing recent presplit results. The quality of the wall is very good, but the crest integrity could not be maintained. 201
Figure 7.2 Conceptual cross-sections showing how an increased collar length reduces the risk of damaging the crest of the bench behind a presplit line on the south pit wall (Andrieux, 2010). 202
Figure 7.3 Photograph of a well pre-splitted and cleaned final limit bench in Structural Volume 1. Note the damage near the crest of the bench. 203
Figure 7.4 Conceptual cross-sections (not to scale) looking east, showing how the blast holes in the previous (upper) bench have damaged the crest of the final wall in the lower bench (Andrieux, 2010). 203

Figure 7.5 Good Quality Blasting Example 2 (Meta-sedimentary rock type) (Ngoro, 2009). 206
Figure 7.6 Moderate Quality Blasting Example (Dolomite Rock type) (Ngoro, 2009)....207
Figure 7.7 Poor Quality Blasting Example (Kimberlite rock type) (Ngoro, 2009).....208
Figure 7.8 Showing an actual design limit in the 3D Mine Design and Modelling Package (GEMS) that contains the Geotechnical block model and mine design amongst others. 209
Figure 7.9 Showing the Polygons in 3D dimensions for a historic and current wall in the GEMS software. 209
Figure 7.10 % Catch berm since 2008 demonstrating the improvement in blasting practices. 211
Figure 7.11 Rockfall Hazard Risk Assessment and Classification for Venetia Mine-a comparison of the ROFRAQ, RHRON, RHRS systems (Rankhododo and Ekkerd, 2009). 219
Figure 7.12 Photograph Looking North-West (Rankhododo and Ekkerd, 2009).....220
Figure 7.13 Photograph, Looking South-East (Rankhododo and Ekkerd, 2009).....220
Figure 7.14 Photograph, Looking East (Rankhododo and Ekkerd, 2009).....220
Figure 7.15 Example of the Geotechnical Risk Sectors 222
Figure 7.16 Example of a Pit Hazard and Monitoring Map that is updated and distributed to mining production personnel on a monthly basis.....223

LIST OF TABLES

Table 1.1 Modified Country rock Lithologies after Rigby et al. (2011).....31

Table 1.2 The major units in the final pit walls of the pit (after Tait, 2007). 43

Table 2.1 Summary giving context to design reports from consultants.....51

Table 4.1 Definitions of slope components used in this project. 56

Table 4.2 Slope Design Acceptance Criteria. (Wesseloo and Read, 2009) 60

Table 4.3 Typical ranges of friction angles for a variety of rock types (after Wyllie and Mah, 2005). 65

Table 4.4 The different weighting on the Input parameters for Laubscher's (1990) and Bieniawski's (1989) RMR.....80

Table 4.5 The Mining Rock Mass Rating Classification (Laubscher, 1990).....80

Table 4.6 Adjustments for Joint Condition and Groundwater (Laubscher, 1990).....82

Table 4.7 Weathering Adjustment to MRMR (Laubscher, 1990). 83

Table 4.8 Adjustments to MRMR due to joint orientation (Laubscher, 1990).....83

Table 4.9 Adjustments for Blasting Effects (Laubscher, 1990).....84

Table 4.10 Various stability analysis techniques applicable to each stage of a project (Lorig et al., 2009).....106

Table 4.11 Showing the various limit equilibrium methods and their final equilibrium states (Curran, 2007). 108

Table 4.12 The advantages and limitations of numerical modelling techniques (Stead et al., 2001).....109

Table 4.13 The Blast Damage Mechanism after Williams et al. (2009).....113

Table 4.14 Guidelines for Estimating the Disturbance Factor, *D* (Hoek and Diederichs, 2006) 116

Table 4.15 Depth of blast damage (Hoek, 2009). 117

Table 5.1 Summary of the mapping dataset collected by the Venetia Geotechnical Department. 122

Table 5.2 Summary of the historic and modern drilling campaigns 124

Table 5.3 The structural volumes and their definition. 128

Table 5.4 Orientation of the S2 Foliation in each Structural Volume (Basson, 2011c) ..131

Table 5.5 Lower Hemisphere Equal Area Stereographic Projections (left) and Rosette Plots (right) for the S2 Foliation in each Structural Volume (Basson, 2011c).....132

Table 5.6 Lower Hemisphere Equal Area Stereographic Projections (left) and Rosette Plots (right) for the Brittle Joints in each Structural Volume. 135
Table 5.7 The joint data for each structural volume. 137
Table 6.1 The UCS results for all the country rock types and their mode of failure. 145
Table 6.2 The UCS results summarised for the fresh and weathered horizons. 149
Table 6.3 Percentage of each Rock per Geotechnical Domain (Structural Volume). 150
Table 6.4 The Average UCS and related Standard deviation for each Structural Volume (Domain) and sub-domain (weathered and fresh). 150
Table 6.5 Tri-axial shear testing on closed foliation (S2a). 151
Table 6.6 Results for shear tests on dry saw-cut surfaces. 151
Table 6.7 Joint roughness coefficient for all the rock types as obtained from pit mapping. 153
Table 6.8 The strength results of the foliation. 154
Table 6.9 The Brazilian tensile strength for the country rock units. 155
Table 6.10 The Brazilian tensile strength for the kimberlite units. 155
Table 6.11 The m_i results for the country rocks using Hoek (2002) and Cai (2009) methods. 156
Table 6.12 The m_i results for the kimberlite rocks using Hoek (2002) and Cai (2009) methods. 156
Table 6.13 Density of the country rock units. 157
Table 6.14 Weighted density for each country rock structural volume (domain). 157
Table 6.15 Density of the kimberlite units. 158
Table 6.16 Elastic properties (Young's Modulus and Poisson's ratio) of the country rock units. 158
Table 6.17 Elastic properties (Young's Modulus and Poisson's ratio) of the kimberlite units. 159
Table 6.18 Mining Rock Mass Ratings for the country rock units with no mining adjustments applied (Laubscher, 1990). 160
Table 6.19 Mining Rock Mass Ratings for the kimberlite units with no mining adjustments applied (Laubscher, 1990). 161
Table 6.20 Weighted Mining Rock Mass Ratings for the country rock units with no mining adjustments applied (Laubscher, 1990). 161
Table 6.21 Showing the results for the 2009 – 2011 window mapping dataset with and without foliation (no mining adjustments applied to the MRMR). 162

Table 6.22 Rock Mass Strength Properties for the various country rock domains.....164
Table 6.23 Rock Mass Strength Properties for the various kimberlite units. No weathered kimberlite present (mined out). 165
Table 6.24 Summary of the tier 1, 2 and 3 domains. 172
Table 6.25 The geometric properties of the Geotechnical block model. 173
Table 6.26 DIPS™ plots showing the major bench scale failure mechanisms in the pit. .176
Table 6.27 The various orientations of the slope for each Tier 2 domain that were considered in the bench analysis by the author. 179
Table 6.28 Maximum inter-ramp angle as obtained from the bench analysis. Results of the largest Tier 2 units are assumed for the Tier 1 domains for comparative purposes only. 182
Table 6.29 SWISA™ results of the bench analysis where wedges failed and where lower than the acceptability criteria. See Appendix C for the complete set of results. 183
Table 6.30 PFISA™ results of the bench analysis where wedges failed and where lower than the acceptability criteria. See Appendix D for the complete set of results.....184
Table 6.31 Empirical Estimate for the inter-ramp angles (Haines and Terbrugge, 1991). 185
Table 6.32 Inter-ramp angles obtained from Bench and Inter-ramp scale analysis with the controlling factors on stability. 189
Table 6.33 FLAC ™ and SLIDE ™ verification scenarios 189
Table 6.34 The results for overall slope analysis. 191
Table 6.35 Conceptual ramp widths taking into consideration back break from the bench analyses.....195
The final design parameters for each major tier 2 domain are given in Table 6.37. Historically stack heights at the mine was limited to 120m. Therefore Inter-ramp angles are stated at a maximum stack height of 120m. 198
Table 6.36 Comparison between the initial design, phase 2 and phase 3 inter-ramp angles. 199
Table 6.37 Final proposed inter-ramp angles and bench heights.....199
Table 7.1 The Final Limit Blasting and Cleaning Quality Assessment Form. 205
Table 7.2 The draft Anglo American Guideline for Bench Retention (Author unknown, 2009) 210
Table 7.3 Rating values for the RMD, JPS and JPO components of the BI (Lilly, 1992). 212

Table 7.4 Blasting Index Guidelines for Hard, Medium and Soft Rock Mass Conditions in the Venetia Pit. 213
Table 7.5 Blasting Index Guidelines (Taljaardt, 2010). 213
Table 7.6 Venetia mine size classification of failures (Ekkerd, 2010). 214
Table 7.7 Rock Fall Hazard Rating System (RHRS) (Hoek, 2002) 216
Table 7.8 RHRON – Ontario Rock Hazard Rating (Franklin and Senior, 1997) 216
Table 7.9 Template for collecting data for Rock Fall Risk Rating for Open Pit and Quarry Mines (ROFRAQ) (Alejano et al., 2008). 218
Table 7.10 ROFRAQ classification and guideline for remedial actions..... 222

1. BACKGROUND

1.1 Introduction

The design of a rock slope has a major impact on the economic viability, long term sustainability and safety profile of a mining operation. Investors and owners expect designs that will not only ensure a safe working environment but also maximise the return on investment. Corporate governance and socially responsible mining companies are not only a modern day given but an essential element for ensuring market leadership. Thus the loss of reputation due to a slope failure can have disastrous consequences for the modern mining company. "At the very least, any instability must be manageable. This applies at every scale of the walls, from the individual benches to the overall slopes" (Read and Stacey, 2009). Thus a delicate balance exists between achieving, and maximising, economic extraction while ensuring stability in a challenging engineering environment.

In the civil industry design is focused primarily on ensuring long-term reliability and use while in mining shorter life spans and higher levels of monitoring are taken into consideration. This however results in higher levels of risk and puts emphasis of good implementation strategies. Historically the level of risk was dependant of the risk appetite of the designer and or mining company. However in 2004 several international mining companies, including De Beers, initiated the Large Open Pit Project. This project culminated in the publication of the Open Pit Design Guidelines, in 2009, wherein slope design acceptance criteria are recommended (Read and Stacey, 2009).

Chapters 1 – 3 are structured to provide background information regarding the project site, optimisation programmes and techniques applied in the study. This chapter provides information relating to the location, mining method, geological and hydrological conditions at the project site (Venetia Mine). Emphasis is placed on the structural geology of the site since it has a major impact on the stability of the Venetia pit.

1.2 Location and history

Venetia is an open pit truck and shovel operation and one of seven active open pit operations in the De Beers Group of Companies. Mining began on the Cut 4 design in 2006 with a final planned open pit depth of approximately 500m below surface at a maximum waste stripping rate of approximately 50 million tonnes per annum. The mine is situated in the Limpopo Province about 27 km South of the confluence of the Shashi and Limpopo rivers, 80 km West of Musina and 36 km North-east of Alldays. See Figure 1.1. The mine is South Africa's largest producer of diamonds, thus maintaining the country's position as a prominent world producer.

The Venetia story begins on the farm Seta, 35 kilometres north-east of the present mine, where as early as 1903 diamond bearing gravels were discovered close to the Limpopo River. In 1969 De Beers began a reconnaissance programme to locate the source of these river deposits. The trail led to a farm called Venetia, where a cluster of kimberlite pipes were discovered in 1980. A thorough evaluation began the same year and the two largest pipes proved to be economically viable. A full feasibility study was commissioned in 1988 and approval for the project was granted in 1989. Construction of the mine began in January 1990, with full output being achieved in December 1992. Venetia inherited its name from the farm on which it is situated, while its emblem, the guardian lion, is the biblical symbol of Saint Mark, the patron saint of Venice.

The area is semi-arid with a mean annual rainfall at Pontdrift (SAWS station 0808253) of 366mm. Inflows into the pit generally occur from the fault zones and geological contacts. The passive groundwater inflow to the current pit is estimated at about 600m^3/day. The overall hydraulic conductivity of the country rocks is very low ~ less than 0.001m/day. In such rocks, active dewatering from perimeter of the pit will not be successful in reducing the relatively small amount of passive inflow to the pit. No significant water bearing structures that would constitute targets for dewatering boreholes have been encountered to date (Atkinson and Shchipansky, 2008).



Figure 1.1 Locality Map (Taken from Google Maps ™).

The two most economic kimberlite pipes (K01 and K02) at Venetia are currently being mined in a single open-pit operation with the future proposed K03 pipe being developed as a standalone pit. Venetia Mine employs a split shell mining method to strip waste and mine the associated ore. The split shell mining sequence is preferred since it allows for the merging of successive shell designs resulting in waste deferment and advancing revenue, leading to improved net present value (NPV) and cash flow. In the current plan, the mining sequence for the different split pits is as follows: Cut 3, Cut 4 North and Cut 4 South. See Figures 1.2 and 1.3.

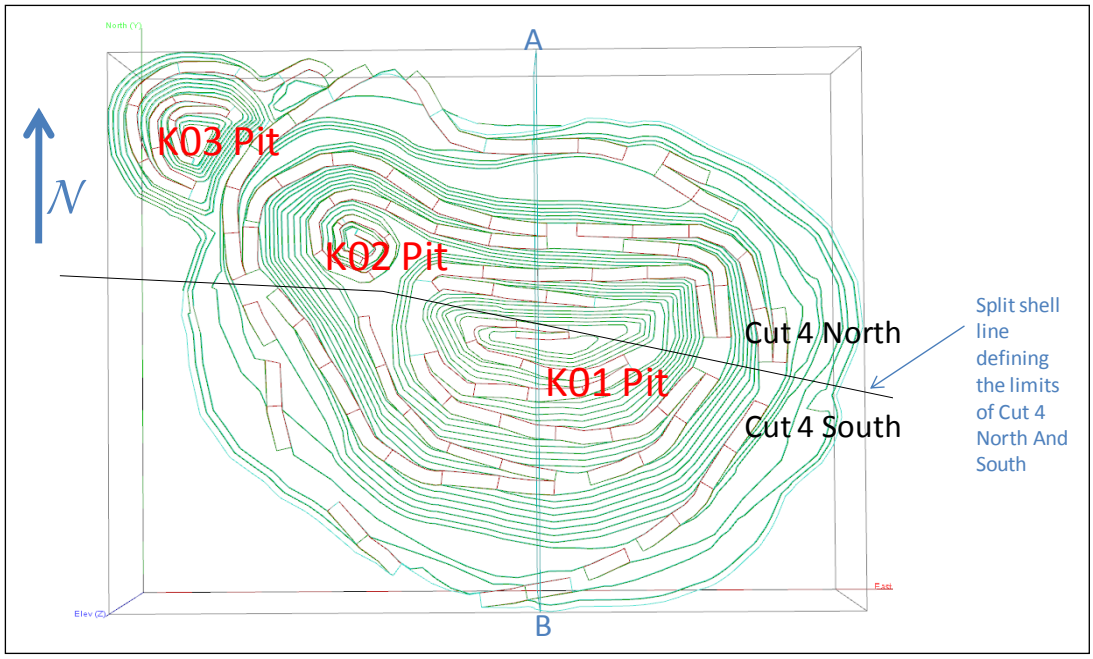


Figure 1.2 A plan view of the planned Cut 4 pit showing the various pits and the split shell line. See Figure 1.3 for a section of the pit (15m Bench plan).

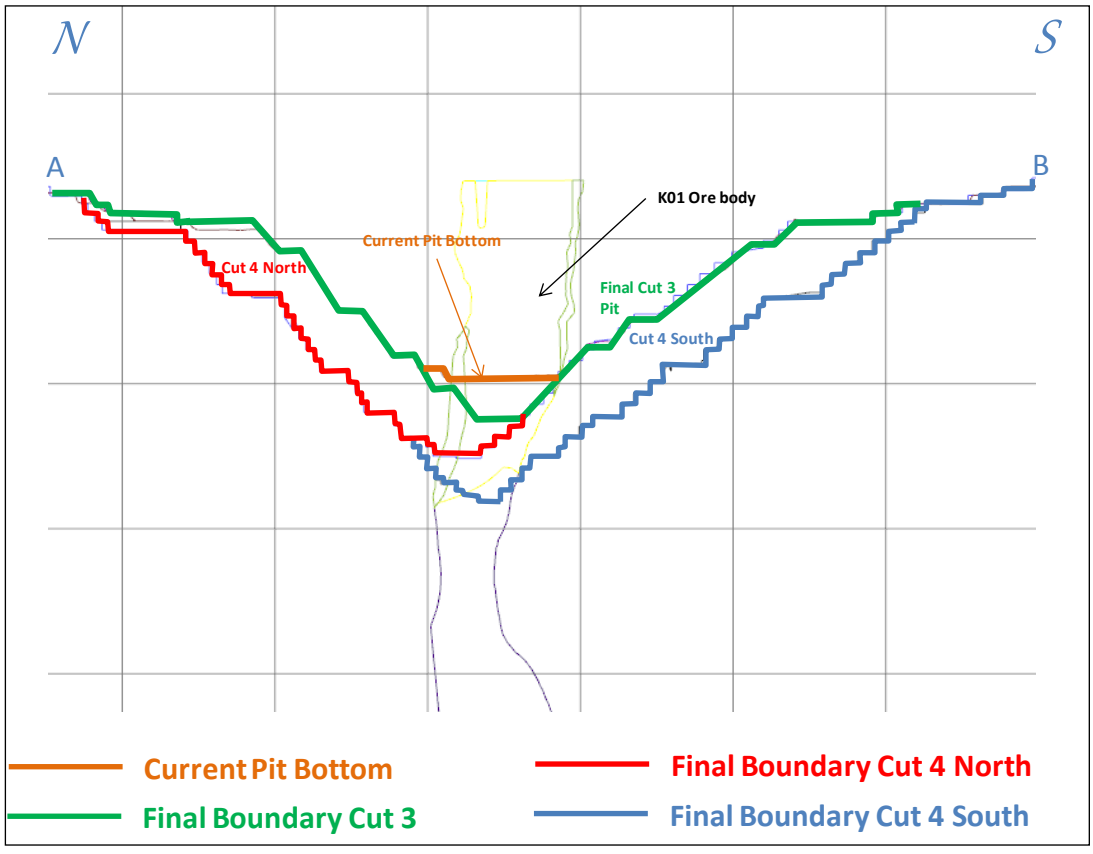


Figure 1.3 A section (A-B) through pit (See Figure 1.2 for the section line) showing the various planned Cuts (15m Bench plan).

1.3 Geological setting

1.3.1 Regional Geological Setting

The Limpopo Belt is located in between South Africa and Zimbabwe and runs in an East-north-easterly direction. See Figure 1.4. The belt is of high-grade metamorphic rocks that have undergone a long cycle of metamorphism and deformation that ended 2.0 billion years ago.

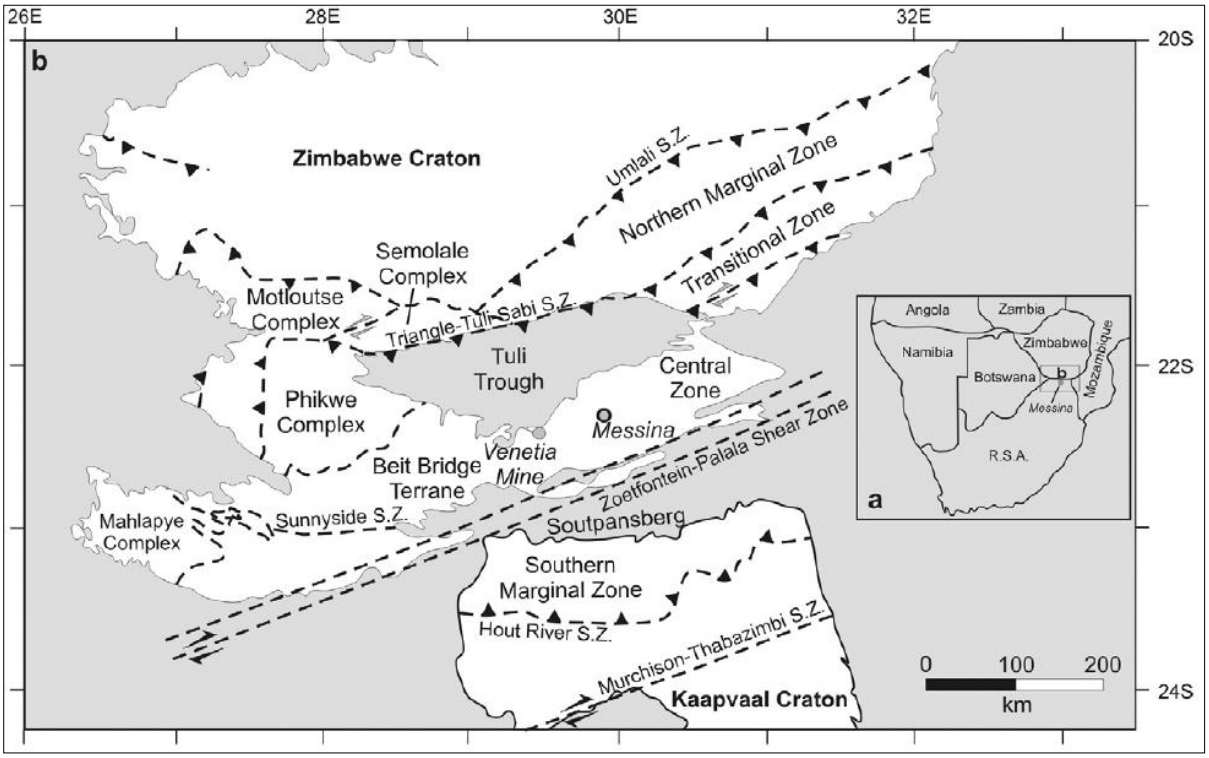


Figure 1.4 Locality map showing the three distinct zones in the Limpopo Mobile Belt. Venetia Mine is located within the Central Zone (CZ) (Rigby et al., 2011).

The terrane can be subdivided into three zones, each with a distinctive geological character and tectono-metamorphic fingerprint (Rigby et al., 2008):

- The Northern Marginal Zone (NMZ) is separated from the Zimbabwe Craton by a southward dipping ductile shear zone known as the North Limpopo Thrust Zone.
- Similarly, the Southern Marginal Zone (SMZ) is separated from the Kaapvaal Craton (KC) by the northwards-dipping Hout River Shear Zone.

- The Central (CZ) forms a lithologically diverse and distinct supracrustal sequence, which includes the Beit Bridge Complex (BBC); a diagnostic supracrustal unit composed of predominantly leucocratic quartzo-feldspathic gneiss, quartzite and marble with intercalated metapelitic gneiss, magnetite quartzite and mafic granulites (Rigby et al, 2011). Venetia mine is located within the Central Zone of the Limpopo Mobile. See Figure 1.4

1.3.2 Local Geological Setting

Venetia mine is located within the rocks of the Beit Bridge Complex. The Complex in the immediate vicinity of the mine consists of the metaquartzites of the Mount Dowe Group, the leucocratic and quartzofeldspathic gneisses of the Gumbu Group, and the "metasedimentary" rocks of Malala Drift Groups.

Barton et al. (2003) and Doorgapershad et al. (2003) postulated that the folded Gumbu Group in the immediate vicinity of the Venetia kimberlites forms a klippe or isolated, possibly Paleo-Proterozoic thrust slice, with an E-W trending, inward plunging synformal axis.

In geology, a nappe is a large sheet like body of rock that has been moved from its original position. Nappes form during continental plate collisions, when folds are sheared so much that they fold back over on themselves and break apart. A klippe (German for cliff or crag) is a geological feature of thrust fault terranes. The klippe is the remnant portion of a nappe after erosion has removed connecting portions of the nappe (Wikipedia, 2011). However according to Rigby et al. (2011) Venetia klippe is considered as speculative. They interpreted the structural style around Venetia as a product of "Ramsay-style" interference folding between NNE- and ESE-trending fold axes (shown as traces in Figure 1.5) and that the form of the Gumbu Group itself is dictated by interference folding: an E-W trending synform closes to the west of the Venetia kimberlites and displays possible refolding about a NNE-trending axis.

The core of this synform also contains Malala Drift gneiss, while the eastern extent of the synform's limbs display refolding and continuity with NNW trending units. The Venetia pit and kimberlites are located within this synform. The major right-lateral fault, which coincides with the local on-mine Lezel-Tina fault and shear system, also occurs in the regional mapping of Brandl (2000). See Figure 1.5.

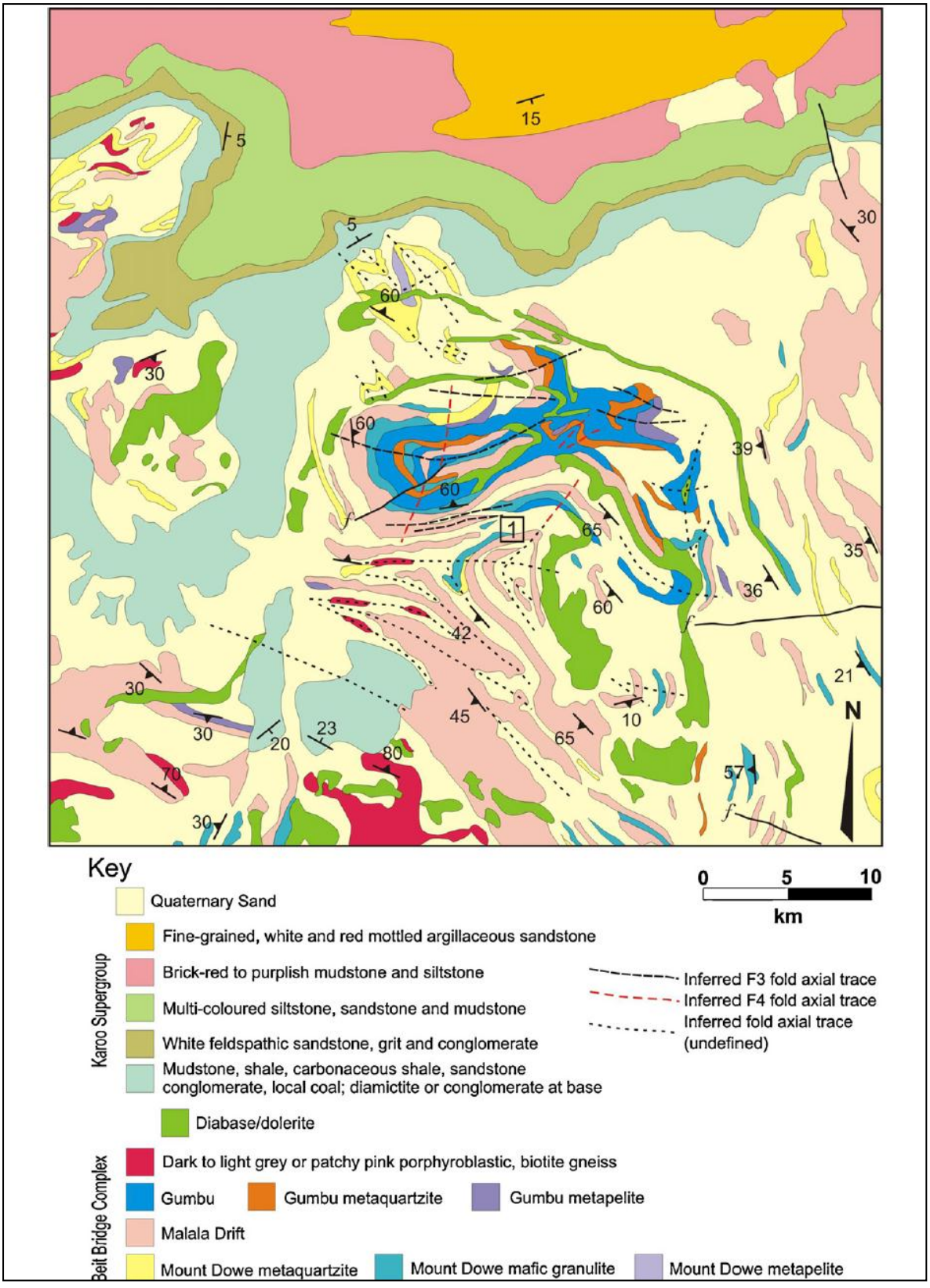


Figure 1.5 The Venetia area of the Limpopo Belt, as mapped by Brandl (2000) showing the Beit Bridge Complex in the immediate vicinity of Venetia which consists of the Gumbu Group, Mount Dowe and Malala Drift Groups (Rigby et al., 2011).

1.3.3 On-Mine Geological Setting

According to Barnett (2004), Basson (2005) and later Rigby et al (2011) the lithologies within and surrounding the Venetia Mine comprise a 'gneissic package' (12 lithologies) and a 'metasedimentary package' (6 lithologies, of which 3 are represented in Table 1.1). The 'gneissic package', representing the Malala Drift Group in the core of the large E- to ENE-trending synform consists of:

a) Biotite-bearing quartzofeldspathic gneiss (BBG),
b) Biotite schist (BS) and
c) Amphibolite/amphibolitic gneiss (AM). See Table 1.1 and Figure 1.6.

Each of these has their own "sub-units", which are distinguished on variable proportions of quartz, feldspar, garnet, sillimanite and the degree of retrogression. (Rigby et al., 2011) Lithologies of the metasedimentary package are less readily grouped into units. Metasediments exposed in the pit comprise fuchsite and fuchsite-muscovite quartzite (FQ), metapelite (PHY) and marble (MBL; Table 1.1). Cross-cutting both packages are pegmatite and dolerite dykes and sills. See Figure 1.6.

Table 1.1 Modified Country rock Lithologies after Rigby et al. (2011).

Package (mine Terminology)	Rock Type	Rock Type: Sub Unit	Mine terminology	Metamorphic mineralogy
Gneissic	BG	QFG	Quartzofeldspathic gneiss	Quartz-feldspar-biotite gneiss
		BBG	Banded biotite gneiss	Feldspar-biotite-quartz gneiss
		BG	Biotite gneiss	Feldspar-biotite-quartz gneiss
		ABG	Augen biotite gneiss	Feldspar-biotite-quartz gneiss
	BS	BS	Biotite schist	Biotite-feldspar-quartz schist
		CBS	Convoluted biotite schist	Biotite-feldspar-quartz schist
		GBS	Garnetiferous biotite schist	Biotite-feldspar-garnet-quartz schist
		GCBS	Garnetiferous convoluted biotite schist	Biotite-feldspar-garnet-quartz schist
		SBS	Silicified biotite schist	Biotite-quartz-feldspar-garnet schist
	AM	AM	Amphibole gneiss	Hornblende-feldspar-quartz gneiss
		GAM	Garnetiferous amphibole gneiss	Garnetiferous hornblende-feldspar-quartz-gneiss
		BAM	Biotite-bearing amphibole gneiss	Hornblende-feldspar-biotite gneiss
Metasedimentary	FQ	FQ	Fuchsitic quartzite	Fuchsite-muscovite quartzite
	PHY	PHY	Phyllite	Silimanite-biotite-muscovite-plagioclase-quartz schist
	MBL	MBL	Marble	Dolomitic marble
	LMST	LMST	Limestone	?
Late Stage Intrusions	DOL	DOL	Dolerite and Pegmatite Dykes and Sills	?
	KIM	VARIOUS	See section on Kimberlite Geology	?

The country rock geology can be broadly divided into a ductile component with a brittle overprint. The ductile evolution relating to the major Limpopo Orogeny is responsible for the main S2 foliation. The brittle overprint can be further sub-divided into bench scale joint sets and major structures that strike the length of the pit. See Figure 1.6.

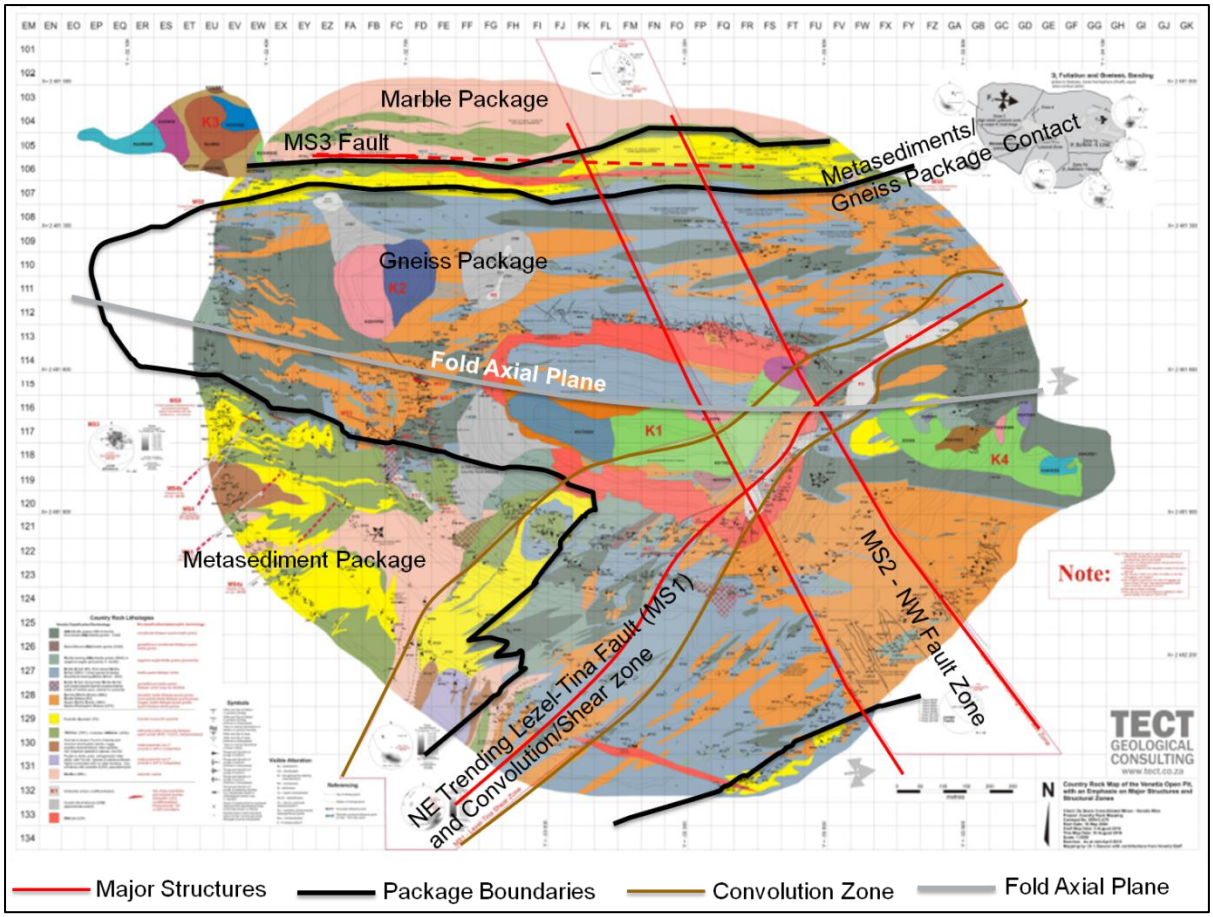


Figure 1.6 Country rock map of the pit showing the major package boundaries, major structures and fold axial plane (Basson, 2011a).

1.3.3.1 Ductile Evolution

Detailed structural mapping by Basson (2005, 2007, 2011a and 2011b) in Venetia pit delineated four ductile deformation events, termed D1-D4:

- D1: The first deformation event is not resolvable, although it may have consisted of the juxtaposition of gneissic and metasedimentary units. The first generation of planar fabric is termed S1 (S referring to planar fabric). It consists of alternating quartzofeldspathic and biotite-rich layers in biotite gneiss or plagioclase feldspar bands in amphibolites/hornblendite. The formation of S1, has obscured the original relationship between lithologies (e.g. intrusive, unconformable or thrusted), although sheared, biotite-rich contacts between the gneissic and metasedimentary packages (Table 1.1) are still observable.

- D2: S1 is refolded by F2 (F referring to folding) into tight to isoclinal folds that are predominantly overturned to the south (i.e. S-verging). S2, axial planar to F2 folds, forms the dominant foliation at Venetia. This foliation is largely parallel to gneissic and metasedimentary contacts. In most cases the orientation of S2 across the pit accords with the orientation of the E-W trending synform in Gumbu Group metasediments shown in Figure 1.5. The determination of F2 fold azimuths is not possible due to the tightness of F2 fold hinges (Rigby et al., 2011). See Figures 1.7.
- D3 – F3 refolds S2 and the flattened F2 and forms a large-scale F3 fold with a shallow to moderately plunging fold axis. A prevalent S3 axial planar foliation is not developed (Rigby et al., 2011), however local incipient/weak S3 foliation forms in local F3 parasitic folds (Basson, 2011a).The east-west trending synform in which the Venetia pit is located is classified as an F3 fold due to its relatively open (i.e. not isoclinal) form and lack of a penetrative axial planar foliation (Rigby et al., 2011). A fold axial plane (FAP3) subdivides the large F3 synform into, firstly, a northern block wherein S2 and lithological contacts are steeply N-dipping. The northern limb of the synform is vertical to overturned and steeply north-dipping. Secondly, a southern block wherein S2 and lithological contacts are moderately N-dipping may be defined. The southern limb is also north-dipping, although this has a shallower or more moderate dip, compared to the north limb. The exact form of the hinge zone of the large F3 synform is unknown (Basson, 2011a). See Figures 1.7 to 1.11.
- D4: D4, which was constrictional-prolate in nature, refolded S1, S2, F2. This last phase results in the transposition of the F3 fold axis and the formation of F4 and L4 (L referring to lineation) in the western portion of the pit. This process of constriction intensifies and results in the entrainment of the metasediments and formation of the Lezel-Tina Shear Zone / Zone of Convolution (LTSZ). See Figure 1.12.

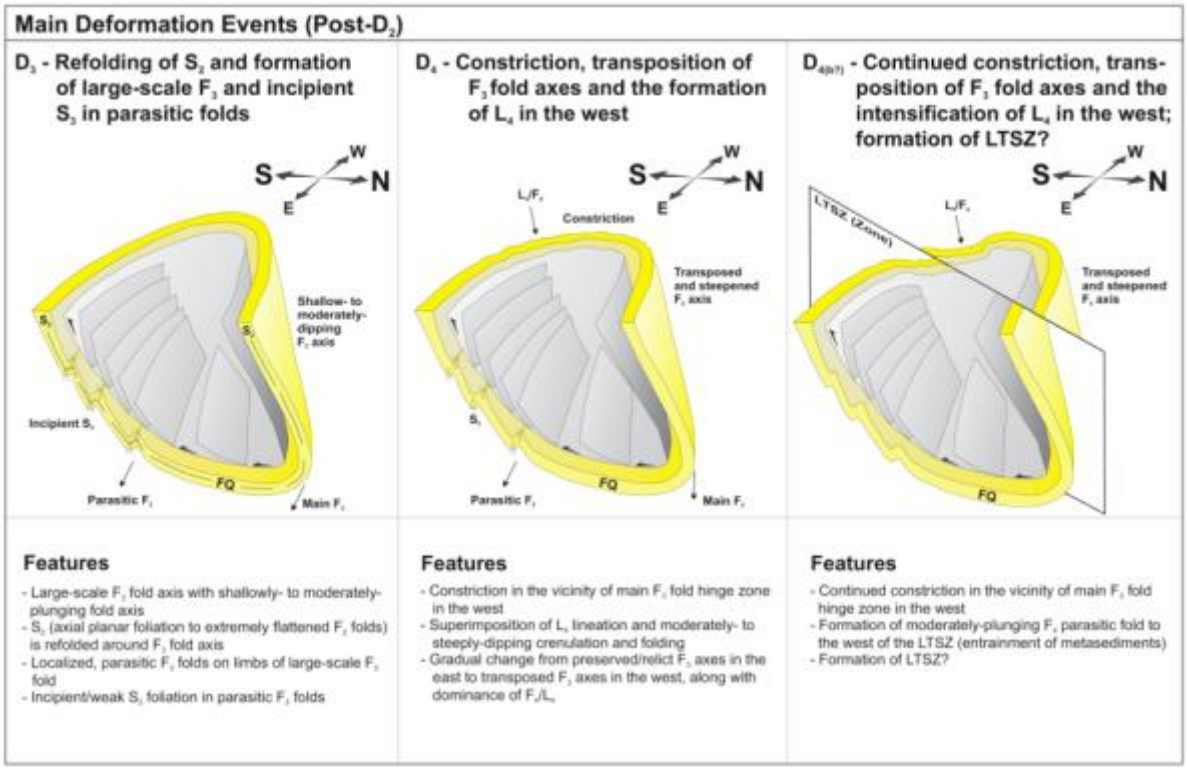


Figure 1.7 The main deformation events from D3 onwards. The first deformation event is not resolvable, although it may have consisted of the juxtaposition of gneissic and metasedimentary units and is thus not represented graphically (Basson, 2011b).

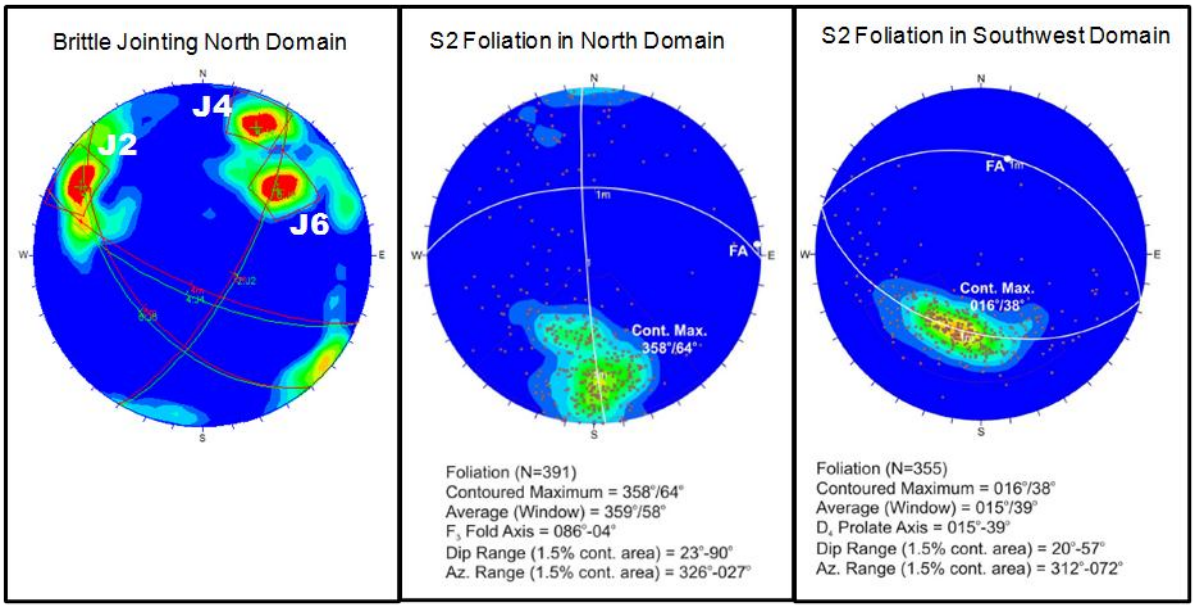


Figure 1.8 Lower Hemisphere Stereographic Projections Showing the distribution of the brittle jointing and S2 foliation in the North and Southwest Domain.

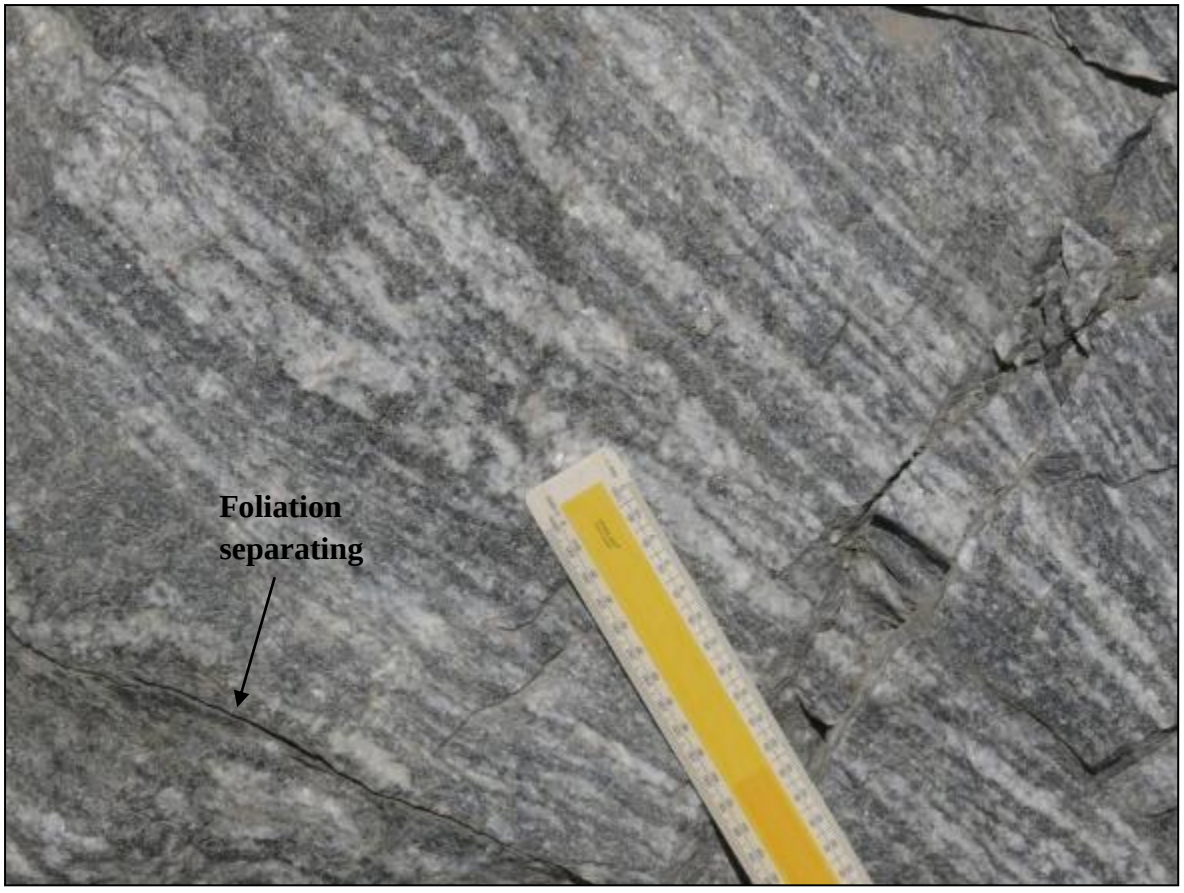


Figure 1.9 Photograph of the S2 foliation in Biotite Bearing Gneiss. Note how the foliation separates on the biotite rich bands.

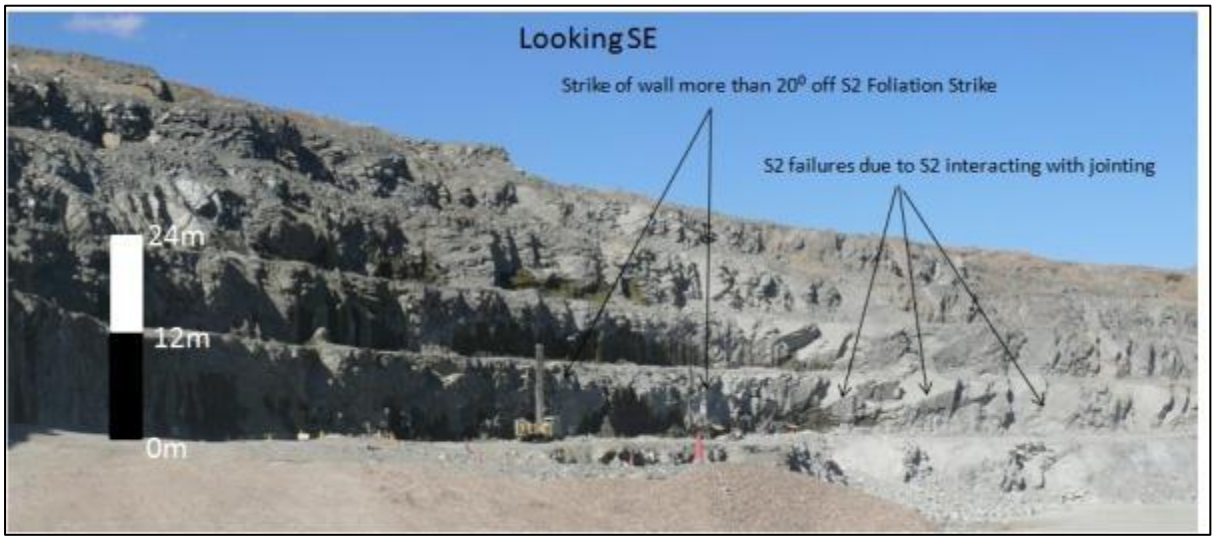


Figure 1.10 Photograph looking SE in the pit showing the S2 foliation in relation to the East Wall. Note how the planar failures decrease as the difference in strike between the S2 foliation and East wall increase.

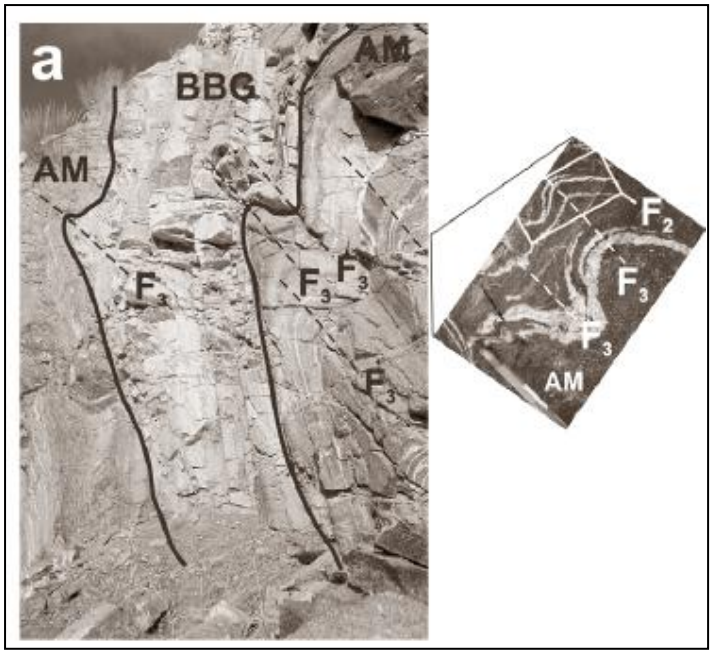


Figure 1.11 Small-scale F3 folds, which refold F2 folds, at the contact between amphibolite (AM) and banded biotite gneiss (Rigby, et al., 2011).

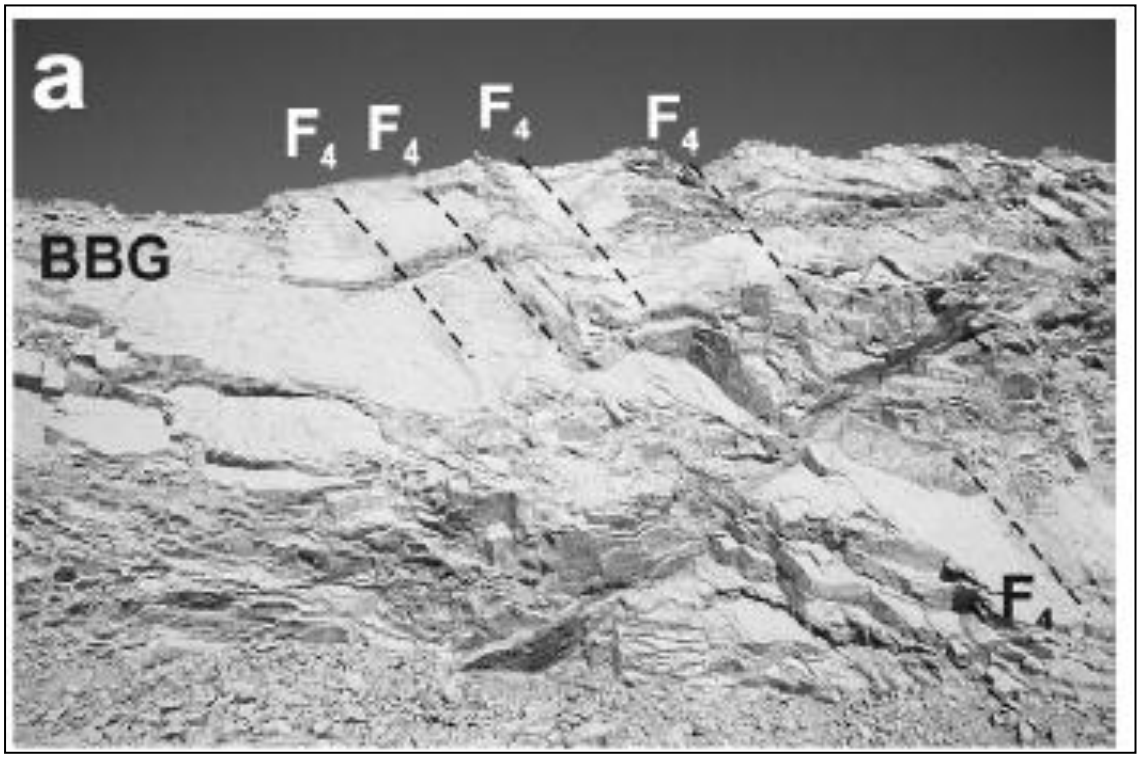


Figure 1.12 "Crenulations" (in local mine terminology) or steeply NE- to NNE-plunging F4 folds on the surface of a biotite gneiss on the south face of the pit (Rigby, et al., 2011).

1.3.3.2 Brittle Overprint (Major Structures and Joint Sets)

Barnett (2003) noted the following phases of brittle deformation:

1. Post-orogenic uplift prior to circa 2 Ga.
2. Rifting associated with the Early Proterozoic Waterberg sedimentary basins at circa 1.8 Ma.
3. Compression and impactogenic rifting during Early Palaeozoic amalgamation of Gondwana synchronous with the intrusion of the kimberlites.
4. Jurassic-Cretaceous rifting that forms the Karoo Basins in the Limpopo Belt.

The number of phases of deformation through which many of the faults and joints have been reactivated makes it difficult to create a reliable genetic model for the joint sets. The orientations of some of the sets do imply that they have been formed and reactivated at the same time as the faults during the brittle phase of the Limpopo Belt's development, post-2Ga (Barnett, 2003).

The existence of various major structures (MS: major structure) have been postulated by Basson (2007, 2011) however only sufficient evidence is available to define three major systems (termed MS 1 – 3). These are:

1. Lezel-Tina shear zone (MS1), trending North-east. Note Barnett (2007) defined it as a brittle zone, while Basson (2007 and 2011a) included ductile deformation features into this zone. Basson (2007) has interpreted the Lezel Fault as a reactivated shear or shears within a broad, lenticular zone of BS- and CBS-dominated gneissic material (the "Lezel-Tina Shear Zone"). Previously, the Lezel Fault was termed a "bounding fault" as it was thought to occur on the margin of the Lezel-Tina Shear Zone. Recent mapping suggests that this may not be the case. Several other NE- to ENE-trending faults, interpreted from aerial photographs, display significant movement (Basson, 2007). The dolerite dykes can be used as markers and are displaced all along the strike of this fault. Only a single mine wide fault trace has been modelled with a dip direction and dip of 327°/82°. See Figures 1.6 and 1.13.
2. Northwest fault zone (MS2): Basson (2007) highlighted several fault and fracture orientations that are observable on both the north and south faces of Cuts 3 and 4. These features are confined to, and/or more obviously expressed in the more brittle

units: biotite gneiss (BG), banded biotite gneiss (BBG) and quartzofeldspathic gneiss (QFG). The unit consists of faults and shallow dipping joints that are associated with this zone only (J6). The faults are widely spaced and have a limited strike (50m) with displacement (approximately 1m) and the zone varies in width from 130m to 320m; the zone is thicker in the gneissic units and thinner and/or more cryptic in biotite schist and its numerous varieties. Due to constraints on their propagation through biotite-dominated units, this zone is therefore not well represented in biotite-dominated lithologies such as BS, CBS and GBS (Basson, 2011a). This unit is thus not very prominent in the Northern portion of the pit. This one has been modelled with a dip direction and dip of 234°/62° (Basson, 2011a). Recent experience has shown that if present these structures can form significant wedges with MS3 in the North.

3. East-West striking structures (MS3) are late-kinematic, brittle-ductile to brittle structures that dip into the pit and are dilatational in origin (Basson, 2011a). The structures occur as discrete planes, usually maximum <1m thick, with infill varying from pink quartzofeldspathic pegmatite, quart-muscovite-tourmaline pegmatite, calcite veining to no infill at all. These structures typically have a dip direction and dip of 180°/40-50°. See Figures 1.14 and 1.15.

Historically four main joint sets have been identified and termed J1, J2, J4 and J6. Review of recent slope failures and extensive pit mapping indicated that the J2, J4 and J6 sets are still present within the current exposures. J6 is associated with the NW trending fault system (MS2). J2 and J4 are pervasive in the rock mass and the dip and strike vary slightly depending on the domain (Ekkerd et al., 2011). See Figure 1.8 and 1.16.

The most strongly developed sub-vertical joint set strikes NE-SW and is labelled J2 on the mine. The orientation is parallel to the Lezel shear system and Fault. The joint set is very likely related to the brittle reactivation of the Lezel shear zone and parallel shears. The J4 set strikes circa WNW-ESE, which is a common and very strongly developed Karoo aged dyke emplacement trend. The trend is known as Okavango dyke trend. However, not all the parallel dykes are Karoo aged and at least some of these dykes appear to have intruded older structures. The age of this prominent brittle fabric is therefore not known (Barnett, 2007).

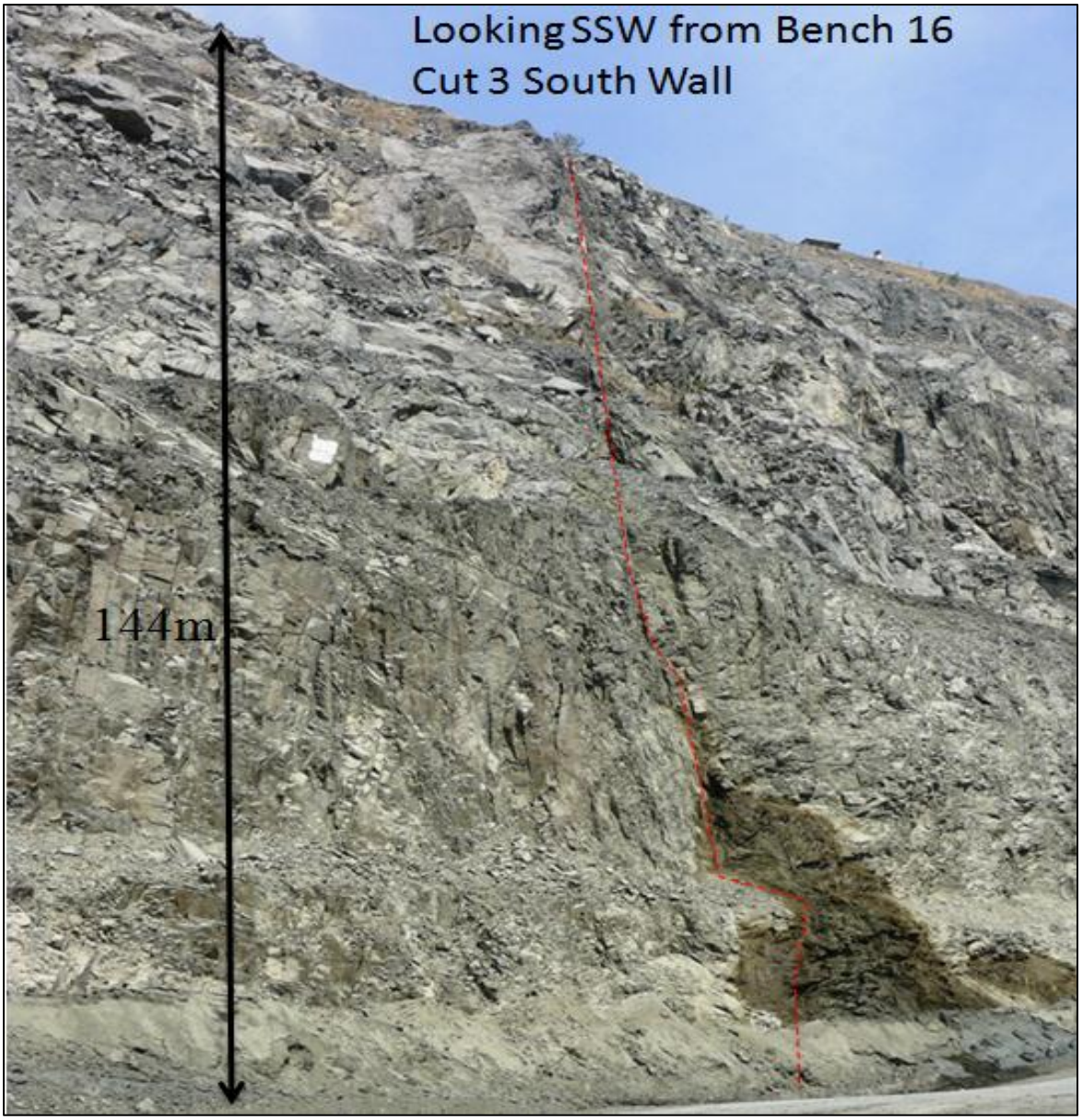


Figure 1.13 Photograph showing the MS1 Fault (Looking SSW along the strike of the fault).



Figure 1.14 MS3 structure in the East-wall of Cut 4 with the typical infilling. S2 is striking perpendicular to the wall.



Figure 1.15 MS3 structure, in the North-wall of Cut 4, with little to no infilling running parallel behind the face. This specific structure de-stabilised 6 benches.

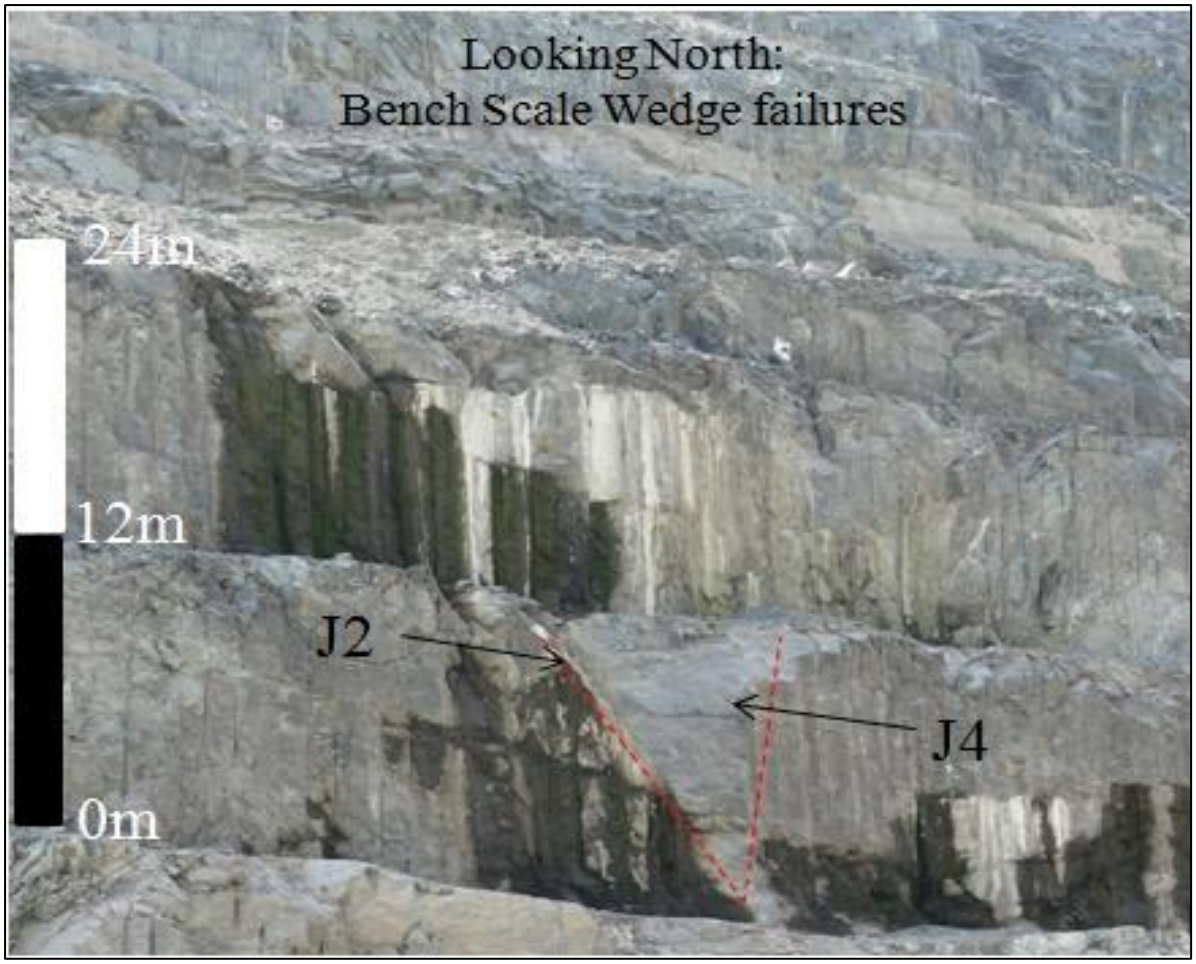


Figure 1.16 Photograph showing the typical wedge failures that occur on the J2 and J4 joint sets in the North wall.

1.3.4 Kimberlite Geology

Kimberlite is a volatile-rich, potassic ultrabasic igneous rock which occurs as small volcanic pipes, dykes and sills (Skinner and Clement, 1979).

The processes that led to the formation of kimberlite pipes are still being debated. This is the consequence of the fact that no modern kimberlite eruption has been witnessed, and a complete volcanic edifice has not been preserved in the geological record. Theories on proposed kimberlite pipe formation processes can be split into two main schools, namely those that favour the role of juvenile gases as the main driving force (magmatic model), and those that favour the interaction between magma and near-surface water (the phreatomagmatic or hydro-volcanic model) as the main process (Field et al., 2008).

The Venetia mine kimberlites were discovered by De Beers in 1980 through heavy-mineral sampling techniques. In all, 13 kimberlite bodies have been discovered in the immediate area. The Venetia kimberlite cluster consists of pipes that are slightly more irregular in shape because of the strong structural control of the country rock in which the kimberlites have intruded. The ore bodies of economic importance are K01, K02 and K03. See Figures 1.17 and 1.18.

The kimberlites are of Cambrian age. Phillips et al. (1999) determined an age of 519.2±0.6 Ma. No major slopes are planned in the kimberlite however applying sub-optimal slope angles could lead to either short term bench problems or under extraction at the end of the pit life. The major kimberlite facies that will remain in the final pit walls are given in Table 1.2.

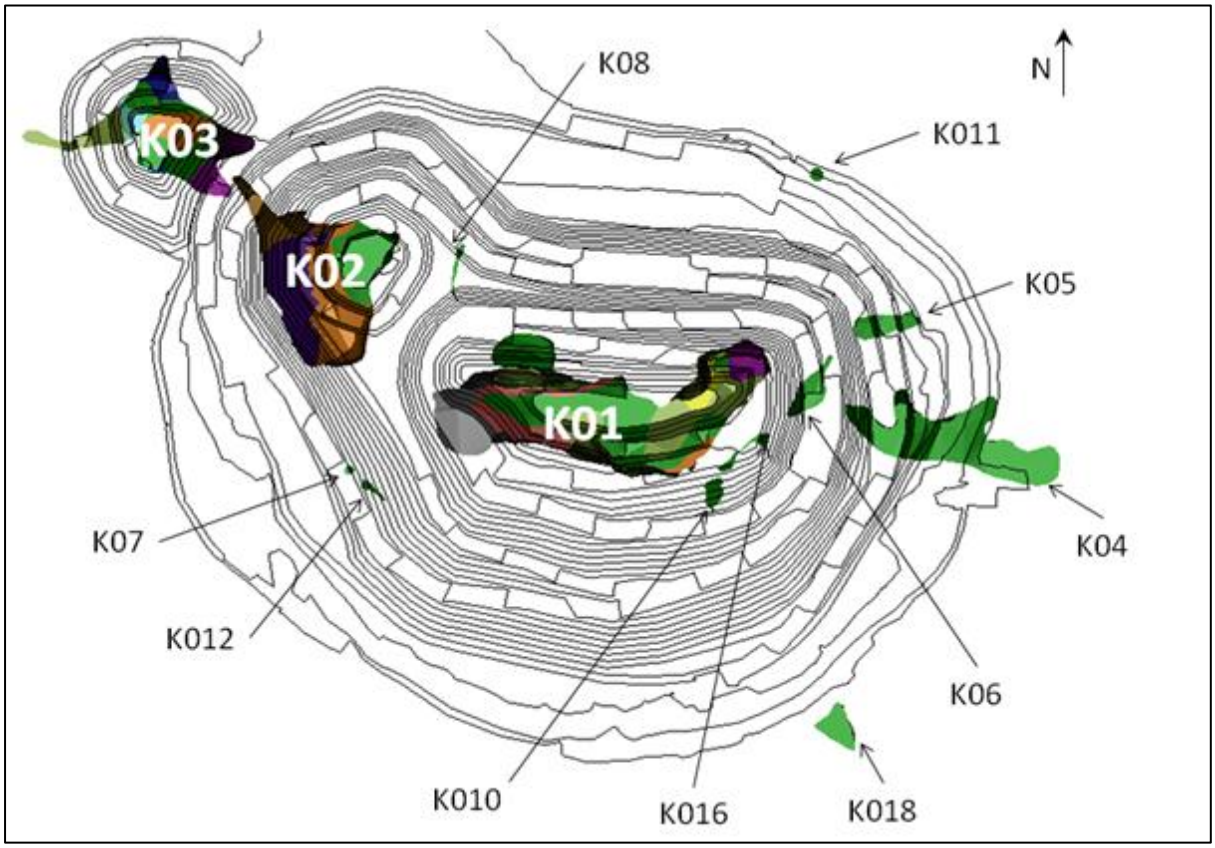


Figure 1.17 Plan of the pit showing all the kimberlite bodies in the pit. Note how K010, K016, K06 and K05 follow the Lezel-Tina trend.

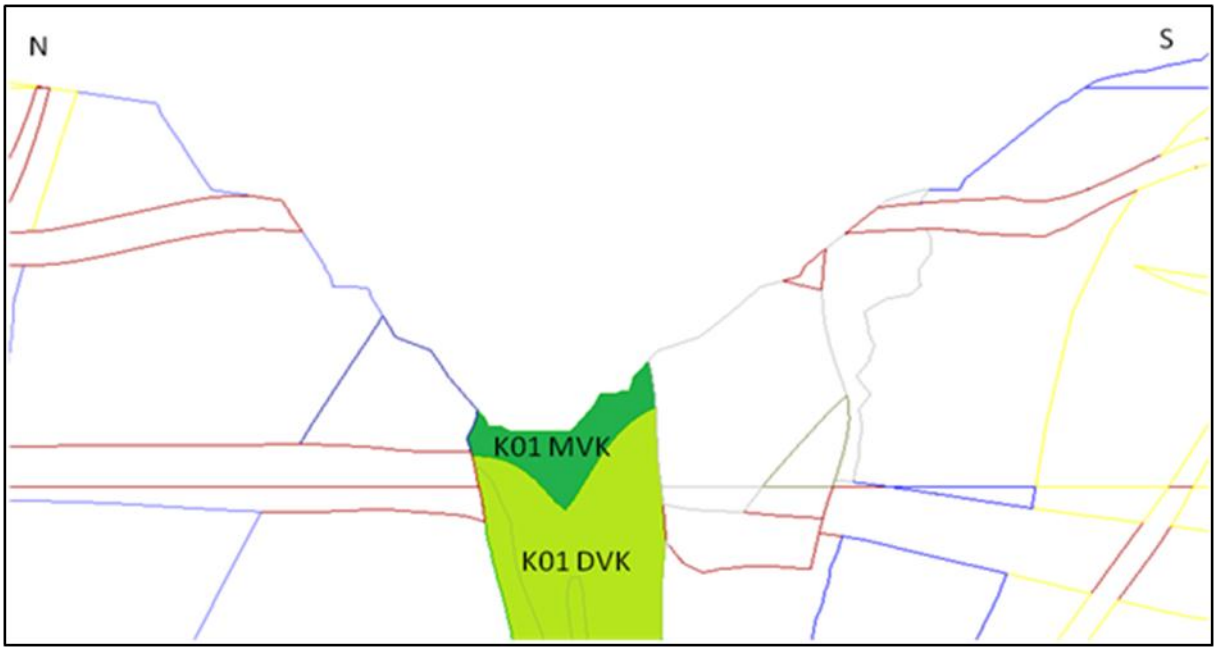


Figure 1.18 North-South section through the pit showing the MVK and DVK kimberlites.

Table 1.2 The major units in the final pit walls of the pit (after Tait, 2007).

Pipe	Type	Occurrence
K01	Massive Volcaniclastic Kimberlite (VK) Red, Volcaniclastic Kimberlite (Breccia) (RVK) and (RVKBR)	Dominant facies across pipe. Previously divided in half Western margin of pipe only. Extends to 400m below surface. Sharp contacts with MVK
	Dark Volcaniclastic Kimberlite (DVK)	Dominant at depth – seems to be main pipe filling facies <400m below surface
K02	Massive Volcaniclastic Kimberlite (VK) Country Rock Breccia (CRBR) Matrix Supported Volcaniclastic Kimberlite Breccia (MVKBR)	Found only in eastern side of pipe – modelled as pipe shaped body to bench 50 Very thick layers of CRBR found in K02West. Interbedded with VKBR units Common in western side of pipe. Often occurs as interbeds within layered breccias of K02West

1.4 Hydrological Setting

Inflows into the pit generally occur from the fault zones and geological contacts. The passive groundwater inflow to the current pit is estimated at about 600m^3/day. See Figures 1.6 for the major structures intersecting the pit. The overall hydraulic conductivity of the metamorphic country rocks is very low ~ less than 0.001m/day. In such rocks, active dewatering from perimeter of the pit will not be successful in reducing the relatively small amount of passive inflow to the pit. No significant water bearing structures that would constitute targets for dewatering boreholes have been encountered to date. Groundwater modelling and pore pressure monitoring has however indicated that some natural depressurisation of the highwalls has already occurred and will continue to occur as the pit deepens due to de-stressing or relaxation of the rock mass behind the highwalls (Atkinson and Shchipansky, 2008).

1.5 SUMMARY

The geology of Venetia mine is complex because it had a long and protracted geological evolution that was earmarked by various magmatic and metamorphic events. Thus ample and reliable information regarding the rock mass is required for slope design purposes.

The country rock assemblages at Venetia are part of the Limpopo Mobile Belt and mainly consist of metamorphic and intrusive igneous rocks. The stability of the pit is structurally controlled and the structure can be divided into two main components, ductile structure (S2 foliation) and brittle structures (major structures, MS1–3, and joints, J2, J4 and J6). The pit has been affected by several ductile deformation events, termed D1 to D4. However a dominant metamorphic foliation (S2) cross cuts all the geology which results in an anisotropic rock mass strength. The interaction between the brittle jointing (J2, J4 and J6) and S2 foliation also locally impacts on bench stability and subsequent bench performance. The slope design is therefore highly dependent on the orientation of the pit slopes relative to structural features.

No significant water bearing structures that would constitute targets for dewatering boreholes have been encountered to date however piezometer data have indicated the presence of

significant pore pressures within the pit walls. Active dewatering is however not deemed as viable due to the low permeability of the metamorphic rocks.

2. JUSTIFICATION FOR OPTMISATION STUDY

In 2009 a revision and optimisation of the business plan was undertaken of which one aspect was the review of the slope angles and design sectors. The following main opportunities were identified by the author:

2.1 SOUTHERN SLOPES

Initially the pit design was based on only two domains [North: mined at 56 degrees, South: mined at 40 degrees]. The 40 degree design assumed a slope striking parallel to the orientation of the conceptual foliation.

A survey of complete bench failures in Southern highwalls of Cut 3 was conducted in 2009. The survey indicated that the bench performance in the Southern slopes can be isolated to distinct areas. The South-western portion of the slope had the highest incidence of complete bench failures (43%) followed by the Southern section (17%). The southern slope was thus divided into additional sectors/domains by the author considering bench performance, slope orientation and geology:

- SSW: Metasediments, Dip direction of slope = approximately 35º – 45º, Eastern boundary is the contact between Gneiss and Metasediments. Poor bench performance
- WSW: Metasediments, Dip direction of slope = approximately 60º – 70º, Northern contact with the Gneiss. Good bench performance.

The reasons for the bench performance in each of these domains at that stage were not well understood.

The previous design was based on the Cut 4v25 shell; however the Cut 4 pit shell was updated and redesigned in 2009 for economic reasons which resulted in changes to the orientation of pit slopes. The kinematic impacts and/or benefits of these changes have never been assessed. A transition between the North and Southern domain was included in 2008 but this study was not extended to the rest of the pit. Review of the data supplied by the operation to the consultant indicated that the orientation of the S2 foliation and joint populations were extrapolated from old exposures in Cut 2. In addition to the above no groundwater table was available for the first design in 2008.

Thus based on the abovementioned reasons it was deemed appropriate to review the designs of the Southern slopes. See Figure 2.1.

.

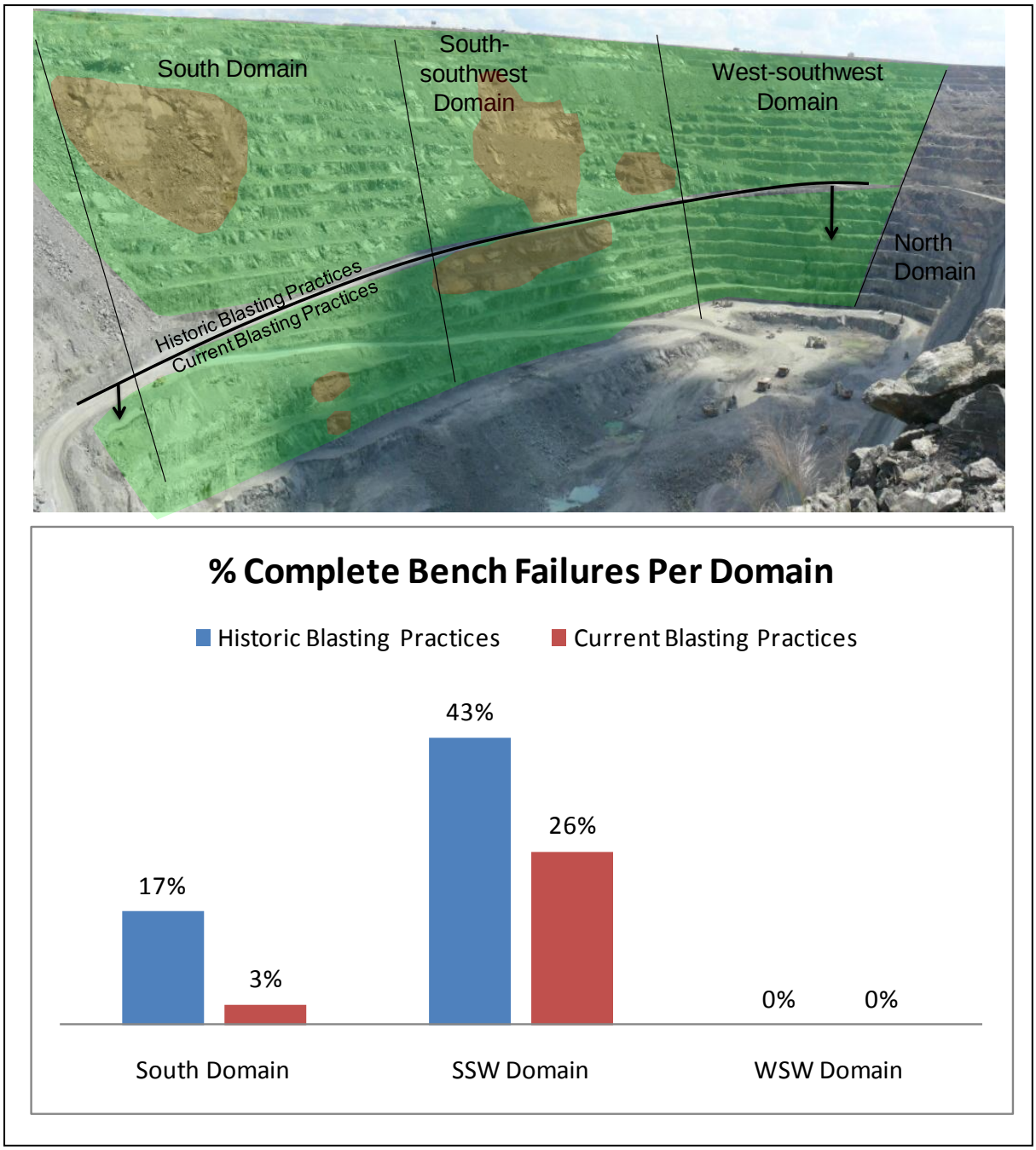


Figure 2.1 Historic bench performances in the South, South-Southwest and West-Southwest domains.

2.2 NORTH SLOPE

The North Slope Design was based on the slope design studies undertaken by SRK Consulting on behalf of Venetia mine in 2008 (Contreras, 2008). No information regarding the statistical and geometrical distribution of the major joint sets in Cut 4 was available for the analysis in 2008.

The stability analyses for overall and stack slope scales were performed with the programme SLIDE™, using the limit equilibrium methodology. Selected results of these analyses were verified with a stress-deformation analysis using the programme PHASE2™. The analysis indicated that steeper stack angles are achievable in this portion of the slope however a lower slope angle was recommended due to the perceived rock fall risk and the poor mining practices (blasting) at the mine. The rock fall risk was however not quantified.

Up to 2009 Venetia mine employed high energy blasting techniques, mainly focused on achieving high production rates and optimum fragmentation, to develop the final walls of the pit. Excavating the highwalls with conventional production blasting techniques resulted in extremely poor highwall conditions. In 2009 this practice was ceased and the mine started experimenting with limit blasting techniques on the final pit limits. The benefit of the limit blasting was however not quantified. The author used the definition as described by Ryan and Prior (2000) to define the actual catch berm width for the benches in the North domain. See Equation 2.1:

% Catch berm = actual catch berm width / design catch berm width x 100 [2.1]

The survey indicated that the new blasting techniques were effective resulting in a significant increase in catch berm potential (% catch berm).

Review of fall of ground data indicated that rock falls are prevalent in the North Domain. Poor blasting resulted in the catch berms not being retained and thus the catch berms did not act as an effective control to mitigate the rock fall risk. However the mechanism that initiates the rock fall was poorly understood.

It was therefore deemed appropriate to re-evaluate the angle for the North domain. See Figures 2.2 to 2.3.

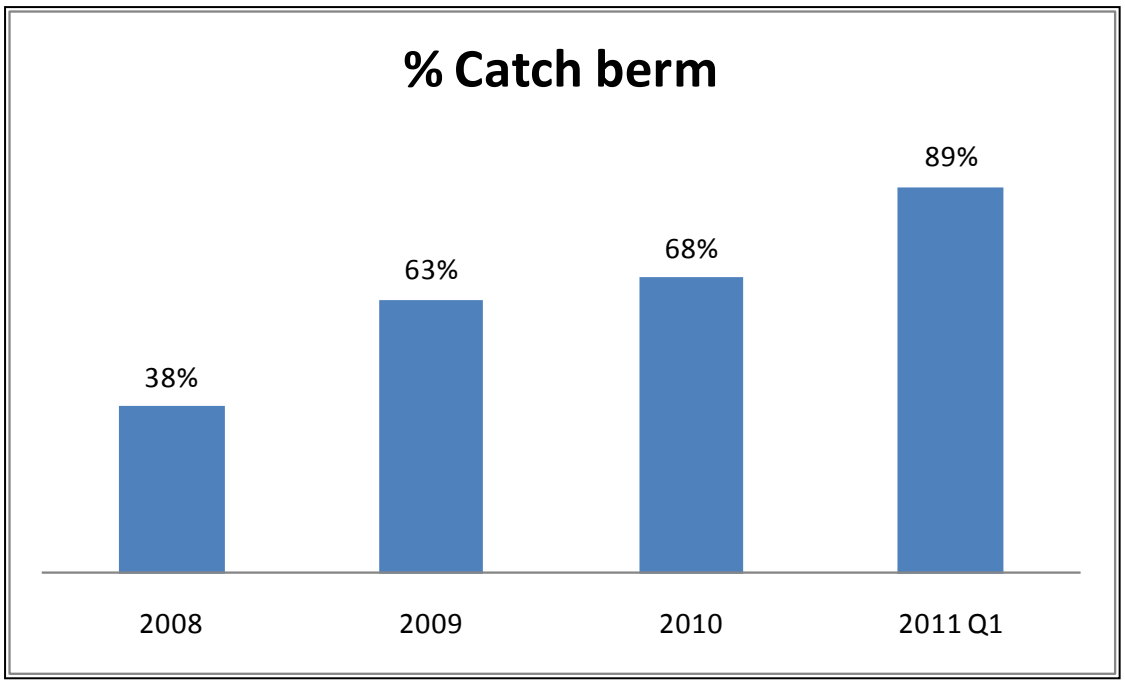


Figure 2.2 Percentage (%) catch berm since 2008 demonstrating the improvement in blasting practices.

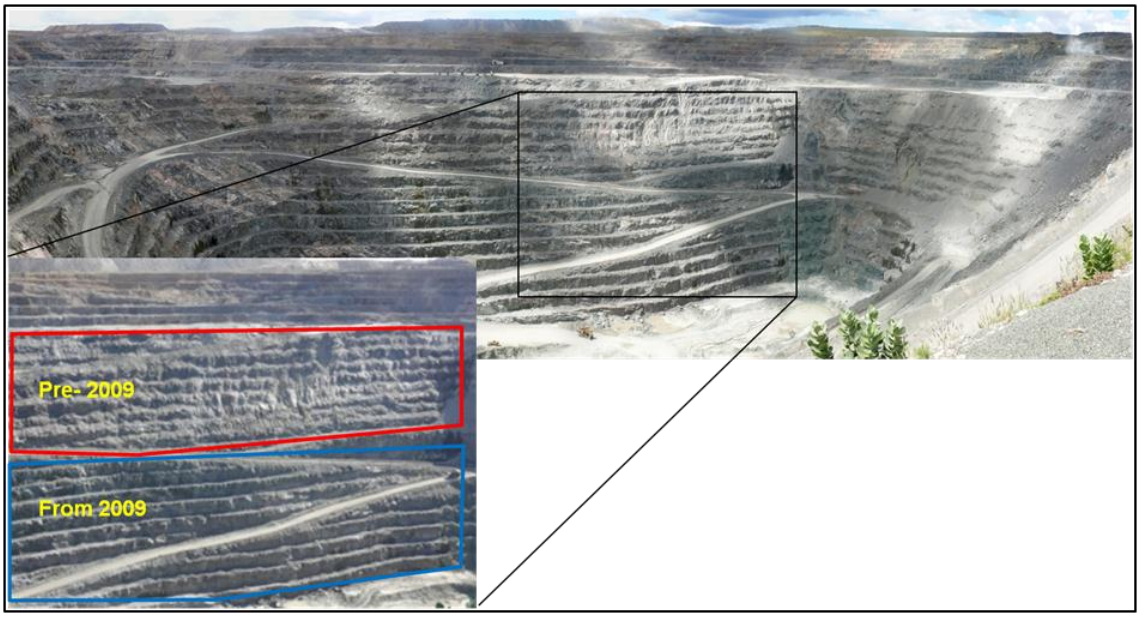


Figure 2.3 Photograph of the North wall, looking North, comparing the bench retention pre- and post-2009 highwall conditions and bench retention (Scale: Benches = 12m).

2.3 SUMMARY

Initial the pit design was conducted in 2008 and defined on only two major domains [North: mined at 56 degrees, South: mined at 40 degrees] (Contreras, 2008). The South Slope, 40 degree, design assumed a slope striking parallel to the orientation of the foliation. The analysis indicated that steeper stack angles are achievable in the North Slope however a lower slope angle was recommended due to the perceived rock fall risk and the mining practices at the mine. The rock fall risk was however not quantified.

Review of the data supplied by the operation to the consultant indicated that the orientation of the S2 foliation and joint populations were extrapolated from old exposures in Cut 2. In addition to the above no groundwater table was available for the first design in 2008.

Thus considering the improvement in mining practices, lack of understanding regarding the actual in pit performance and extrapolated data that was used in the design the author deemed it appropriate to re-evaluate the Cut 4 design in 2009. The optimisation study was scoped by the author and consisted of various phases (1 – 3).

- Phase 1 was initiated by the author post the review of the pit conditions as presented in this chapter and aimed at providing initial input parameters into the Strategic Business Plan (SBP) regarding slope angles (savings on waste stripping) (Strouth, 2009; Gomez, 2010) and bench heights (potential to increase productivity) (Contreras, 2010; Steffen and Terbrugge, 2009). The only new data for this phase was limited scan line mapping that was collected by the mine in the South-western quadrant of the pit and thus similar constraints relating to the orientation of the S2 foliation, joint sets and groundwater applied.
- Phase 2 ran concurrently with the above work and was aimed at defining the orientation of the S2 foliation, joint data and pore pressures in the toe of the slope. This phase consisted of:
    - Structural mapping, drilling, instrumentation installation conducted on mine and was supervised by the author;
    - Modelling of the geology and ground water table by Basson (2011a) and Liu et al. (2011) respectively.

- For the final phase of the optimisation (Phase 3) the Geotechnical domain model and slope design was updated, by the author, using the results from Phase 2 of the study. The updated design incorporated the updated groundwater table and considered the orientation of the pit slopes relative to the foliation; and consisted of a bench, inter-ramp and overall slope analysis. In addition to the above several strategies to monitor the quality of mining practices and related rock fall risk were developed and incorporated into the Code of Practice and related standard operating procedures for the operation. See Table 2.1.

Table 2.1 Summary giving context to design reports from consultants

Phase / Scoped or Initiated by Author			**Achievements**	**Restrictions**
Initial / No	Contreras (2008)	First Cut 4 Slope Design	Impact of S2 anisotropy on Slope design	S2 foliation and joint data conceptual, no modelled GW surface. Poor mining practice.
Initial / No	Atkinson and Shchipansky (2008)	First Cut 4 GW model	3D groundwater surface from strand pipe piezometers	Stand pipe piezometers installed too far from slope
Initial / No	Armstrong (2008)	Update SE Design sector	Mapping in SE quadrant of pit. Inter-ramp angle increased from 40° to 48° for SE	Limited mapping in SE quadrant only.
Phase 1 / Yes	Stroth (2009) and Gomez (2010)	Update WSW and SSW Design sector	Incorporate mine pit mapping. Inter-ramp angle increased from 40° to 53° for WSW and 40° to 41° for SSW	Only Scan line mapping in SSW and WSW quadrants
Phase 1 / Yes	Steffen and Terbrugge (2009) and Contreras (2010)	Bench Height Optimisation	Bench Height Optimised for current loading fleet	S2 foliation and joint data conceptual for large portions of the pit.
Phase 2 / Yes	Shchipansky and Atkinson (2010)	North Slope Pore Pressure Modelling	Incorporate angled VW piezometer data	For the North only
	Liu and Sterret (2011)	Update Venetia 3D GW model	Incorporate angled VW piezometer data from the South	
Phase 2 / Yes	Basson (2011a,b)	Update Venetia 3D Geological Model	Incorporate pit mapping and drilling data. Define S2 orientations and update domain model	

3. SCOPE

3.1 AIMS

The project aims to:

- Update and optimise the slope design for the Venetia K01 and K02 pits (Cut4V27 pit shell) and determine the factors that control stability in each of the domains.
- Ensure that the slope design at Venetia meets the new Open Pit Guidelines with the focus on acceptance criteria and accepted design practices (Read and Stacey, 2009).
- Define applicable implementation strategies to identify poor mining practices.

3.2 SPECIFIC OBJECTIVES AND LIMITATIONS

This study had the following specific objectives and limitations:

- Determine the factors that control the bench performance in the Southern Slopes.
- Determine the factors that result in the high rock fall rate in the North Slope.
- Propose design parameters that will take the above factors into account.
- Redefine the Geotechnical domains to take into consideration the above factors.
- Ensure that representative structural and hydrological information is obtained for each of the domains.
- Collate key the Geotechnical information for each domain into a three dimensional (3D) block model.
- Define design parameters for the various country rock units taking into consideration:
    - The country rock units that will be intersected by the Cut4V27 pit shell at depth.
    - The orientation of the proposed Cut4V27 pit shell in relation to structural features in the slope.
- The stability of the kimberlite stacks will be assessed but the optimisation of these is beyond the scope of the study.

- The angles of the overall slope are dependent on the amount and type of ramp systems and the optimisation therefore is beyond the scope of this work. The stability of the Cut4V27 overall slope will however be assessed
- Define applicable implementation strategies to identify poor mining practices.

3.3 TECHNIQUES APPLIED BY THE AUTHOR

The following techniques and tools were applied/used by the author for this study:

- Rigorous analysis of actual in-pit conditions and slope performance in order to provide defensible arguments for slope optimisation.
- Review and analysis of fall of ground data in order to outline and define Geotechnical domains and the factors that control stability in each of those domains.
- Scoping and supervising of drilling and instrumentation (piezometer) installation programme.
- Define and oversee the scope of work of Consultants.
- Supervise the collection of structural data.
- Collate all structural data and analyse brittle joint data for each domain.
- Literature surveys to determine suitable analytical and testing techniques.
- Re-define the rock mass model and summarise for each domain, which includes the calculation of rock mass ratings, analysis of laboratory rock testing data and calculation of rock mass and joint strengths.
- Construct a 3D Block model.
- Kinematic/Stereographic Analysis to demonstrate failure mechanisms.
- Empirical analysis of inter-ramp angles.
- Bench analysis using PFISA™ and SWISA™
- Limit equilibrium, SLIDE™ and finite difference, FLAC™, modelling to analyse for inter-ramp and or overall slope stability
- Oversee the development of rock fall and blasting effectiveness ratings.

3.4 SUMMARY

The current and previous chapters provided background information regarding the project site, optimisation programmes and techniques applied in the study.

The following chapter consists of a literature survey (Chapter 4) on slope design principles and is followed by an in-depth discussion on the optimisation (Chapter 5 – Phase 2 and Chapter 6 – Phase 3) and operational controls (Chapter 7 – Implementation Strategies).

Phase 1 was initiated by the author post the review of the pit conditions as presented in chapter 2 and aimed to provide initial input parameters into the Strategic Business Plan (SBP) regarding slope angles (savings on waste stripping) (Strouth, 2009; Gomez, 2010) and bench heights (potential to increase productivity) (Contreras, 2010; Steffen and Terbrugge, 2009). Phase 1 of the study suffered from the same shortcomings as the initial design however some of the outputs from Phase 1 were incorporated into the final design and are discussed in Chapter 6.

4. LITERATURE SURVEY: SLOPE STABILITY AND DESIGN PRINCIPLES

4.1 PIT WALL AND OPEN PIT MINING TERMINOLOGY

An open pit consists of various components (benches, ramps, bench stacks, Geotechnical berms, etc.) which in combination make up the overall slope or pit wall. Each of these components can be subdivided into various elements and their meaning varies from geographic location (Africa, Australia and or North America). The definition of the main slope components and their meaning according to geographic location and are illustrated in Figure 4.1 (Read and Stacey, 2009):

- Bench face (North America) = batter (Australia).
- Bench (North America) = berm (Australia): The flat area between bench faces used for rock fall catchment. The adjective ‘catch’ or ‘safety’ is often added in front of the term in either area.
- Berm (North America) = windrow (Australia): Rock piles placed along the toe of a bench face to increase rock fall catchment and along the crest of benches to prevent personnel and equipment falling over the face below. Note the potential confusion with the use of the term ‘berm’ for a flat surface.
- Bench stack or Inter-ramp: A group of benches between wider horizontal areas, e.g. ramps or wider berms left for Geotechnical purposes.

The removal of several benches below each other results in a stack or inter-ramp slope. The stack angle is also referred to as the inter-ramp angle. The combination of ramps and stacks results in an overall slope. Inter-ramp angles are always measured from crest to-crest or toe to-toe; whereas overall slope angles can only be measured from crest to-toe. See Figure 4.1. The above parameters are all determined by the Geotechnical Design. Thus it’s already evident that there are three scales of Geotechnical design for a pit: 1. Bench, 2. Inter-ramp and 3. Overall slope.

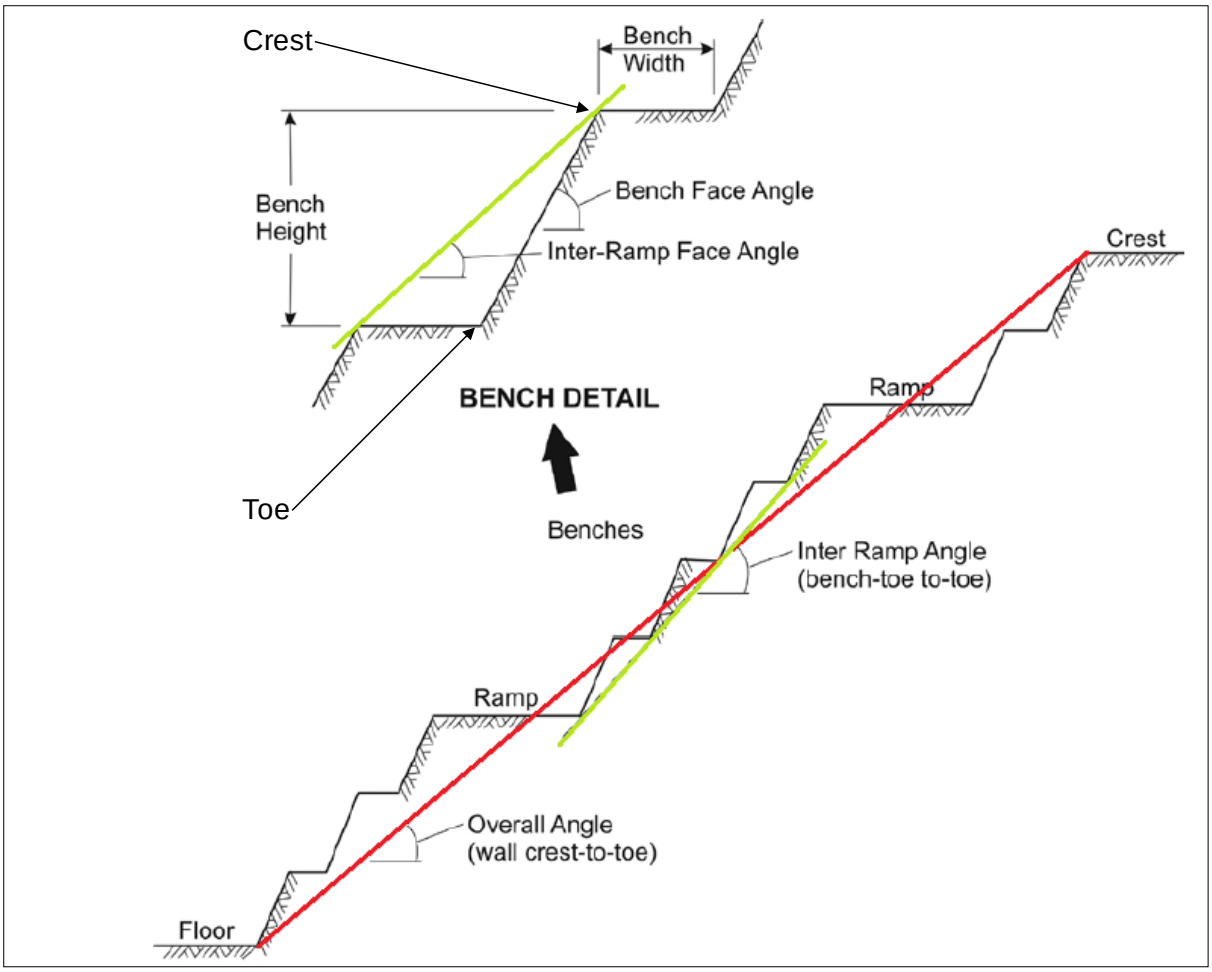


Figure 4.1 Slope Design Terminologies adapted from Read and Stacey (2009) and Wyllie and Mah (2005).

The slope design terms and definitions used for this project are largely based on well-established slope nomenclature used by previous South African design consultants and are given in the Table 4.1.

Table 4.1 Definitions of slope components used in this project.

Component	Definition
Bench	As per Figure 4.1. Consisting of bench height, berm and a batter angle
Berm	Bench width as defined in Figure 4.1
Bench Height	As defined in Figure 4.1
Batter	Bench Face angle as defined in Figure 4.1
Inter-ramp and Inter-ramp Angle	As defined in Figure 4.1
Overall Slope	As defined in Figure 4.1

4.2 OPEN PIT SEQUENCING

Typically open mines are either extracted in a concentric or split shell mining sequence. The concentric mining principle mines a waste cut or pushback 360° around the ore body thus waste stripping takes place all the way around the pit shell in successive waste cuts, each approximately 100m in width. The ramp geometry consists of independent ramp systems tracking all the way around the circumference of the pit in concentric rings (Gallagher and Kear, 2001). The only access to the ore in a concentrically mined pit is through the active production cuts and this creates production inefficiencies as well as safety hazards from rock falls from the upper benches where waste stripping is taking place. If for any reason one of the concentric ramps is cut off by a Geotechnical or operational problem, the entire ramp system is lost as there is no alternative access point (Barnett, 2002). Concentric mining is also only effective in pits with very shallow slopes (angle of repose is equal to slope angles) since these have the capacity to minimise the effect of blasting overspill (Kear, 2010).

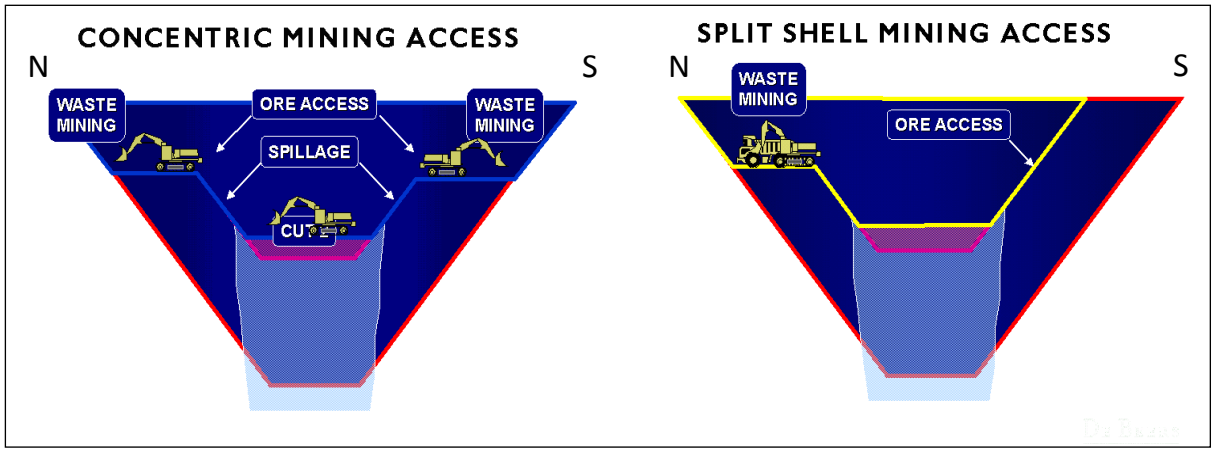


Figure 4.2 Schematic illustrating the concentric and split shell mining concepts (after Gallagher and Kear, 2001).

The split shell mining concept (See Figure 4.2) effectively creates two splits in the mine along an east west axis allowing one push back to take place before the other and has the following benefits (Gallagher and Kear, 2001):

- Unobstructed ore haul route access due to waste mining taking place on the opposite side of the pit to that of the ore ramp,

- Reduced blast waste spillage onto working areas, ore and access ramps by limiting it to one portion of the pit,
- Improved operational efficiencies due to less congestion of equipment in working areas,
- Increased flexibility in both operations and future planning, since the mining cut is split and is not being mined at once,
- Reduced Business Risk Period (BRP),
- Reduced waste tonnage profile due to the split in the mining cut and hence capital and operating cost.

In summary the split shell mining method enhances safety in the open pit environment by separating the mining operations to opposite sides of the pit allowing each operation to continue independently without adversely affecting the other one. However in order to mitigate the risk of blasting overspill, and subsequent rock fall risk, the following practices should to be in place:

- Ramps that are used as catchment should be cleaned on a regular basis and the build-up of overspill on the ramps should be prevented (Kear, 2010).
- Appropriate blasting practices should be put in place to minimise the heaving of material over the sidewall due to blasting (Stacey, 2010).

4.3 ACCEPTANCE CRITERIA

Risk can be defined as the probability of an event occurring and the consequence of that event (See Equation 4.1):

Risk = Probability x Consequence. [4.1]

Acceptance criteria or the appetite for risk, until recently, was either expressed as Factor of Safety (FoS) or Probability of Failure (PoF). The FoS is a deterministic measure of the ratio between the resisting forces (capacity= C) and driving forces (demand=D) of the system in its considered environment (See Equation 4.2).

$$FoS = \frac{C}{D} \quad [4.2]$$

The capacity factors are influenced by the shear strength of the rock mass, quality of lab testing, etc. The demand factors are in turn influenced by stress, mining practices, gravitational loading, etc. The uncertainty relating to each of these factors normally results in a minimum prescribed FoS for design purposes.

From Equation 4.1 it is evident that probability is an important factor in estimating risk. An alternative to deterministic methods, like FoS, are probabilistic methods of which the main aim is to calculate a PoF. Input parameters are described as probability distributions rather than point estimates of the mean values. By combining these distributions within the deterministic model used to calculate the FoS, the probability of failure of the slope can be estimated (Chiwaye and Stacey, 2010). Tapia et al. (2007) demonstrated a case where two slopes had a FoS of 1.35 and 1.50. The slope with the higher FoS also had the highest probability of failure thus illustrating the inadequacy of the FoS deterministic system. See Figure 4.3.

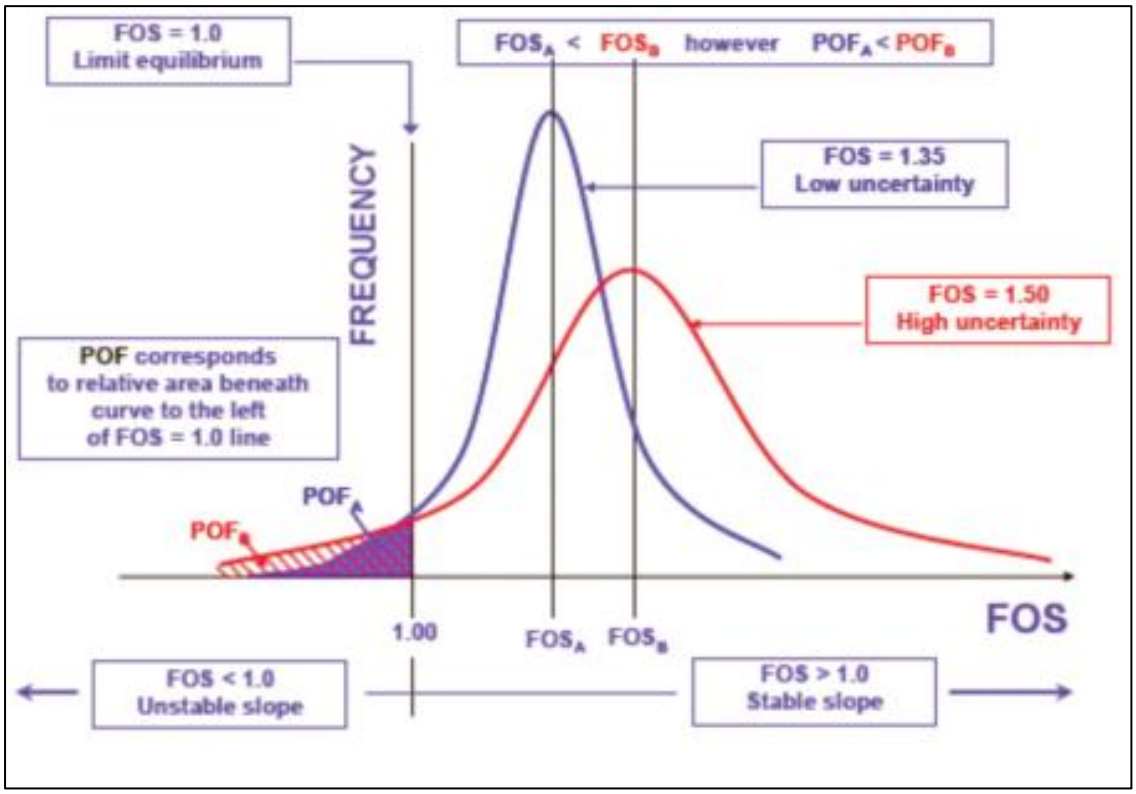


Figure 4.3 The Definition of POF and its relationship with FOS according to uncertainty magnitude (after Tapia et al., 2007; taken from Chiwaye and Stacey, 2010).

There are ways to calculate PoF of which option 1 is used most (Wesseloo and Reid, 2009):

- Option 1 – recognising the FoS as a random variable and seeking the probability of it being equal to or less than 1:

$$\mathrm{PoF} = \mathrm{P}[\mathrm{FoS} \leq 1] \quad [4.3]$$

- Option 2 – seeking the probability that the demand (D) exceeds the capacity (C):

$$\mathrm{PoF} = \mathrm{P}[\mathrm{C} - \mathrm{D} \leq 0] \quad [4.4]$$

One of the most popular probabilistic methods is the Monte Carlo method and at least 10 000 simulations are used to estimate the POF (Chiwaye and Stacey, 2010).

Slopes are designed to meet minimum risk criteria (factor of safety and/or probability of failure) or otherwise known as acceptance criteria. The acceptance criteria, as recommended by the 2009 Open Pit Design Guideline, are used by De Beers to determine the acceptable level of design risk (Wesseloo and Read, 2009). These are given in Table 4.2.

Table 4.2 Slope Design Acceptance Criteria. (Wesseloo and Read, 2009)

	Acceptance criteria			
Slope scale	**Consequences of failure**	**Factor of Safety (min) (static)**	**Factor of Safety (min) (dynamic)**	**Probability of Failure (max) P[FoS≤1]**
Bench	Low-high	1.1	NA	25-50%
Inter-ramp	Low	1.15-1.20	1	25%
	Medium	1.2	1	20%
	High	1.20-1.30	1.1	10%
Overall	Low	1.20-1.30	1	15-20%
	Medium	1.3	1.05	5-10%
	High	1.30-1.50	1.1	≤5%

Recent advances in acceptance criteria employ risk models in which the end objective is not stability but rather that safety is not to be compromised as the economic impact of the chosen slope angles is optimised. The traditional PoF criteria are used along with other parameters, such as poor mining practices to determine an overall PoF value by means of a fault tree analysis (This PoF is then incorporated into an event/consequence tree analysis of which the aim is to determine the final risk which can be stated as a probability of a fatality and/or NPV (Terbrugge et al., 2006). This process requires that the economic benefits of the slope angles be quantified and the involvement of top level management to define the appropriate controls and appetite for risk; and is thus beyond the scope of this research project.

4.4 GEOTECHNICAL MODEL

Geotechnical models are generated during the site investigation and mining phases and are used in the slope design process for the purpose of characterizing the rock mass for Geotechnical design and slope stability analysis. A Geotechnical Domain model consists of the following components or sub-models:

- Geological Model: The geological model presents a three-dimensional distribution of rock types that will be exposed and or intersected during mining operations. The material type categories can relate not only to lithology, but also to the degree and type of alteration, which can significantly change material properties, either positively (silicification) or negatively (argillization) (Read and Stacey, 2009).
- Structural Model: The purpose of the structural model is to describe the orientation and spatial distribution of the structural defects, such as jointing and faulting, which are likely to influence the stability of the excavation.
- Rock Mass Model: The rock mass model represents all geomechanical properties (for example, strength of structural defects, intact rock strength and rock mass rating) of the various geotechnical units/domains and needs a geological and structural model as framework.
- Hydrological Model: Groundwater pore pressure may have significant negative effects on the stability of an excavation or rock slope. This model includes the relevant hydrological properties and pore pressures of all the units in the vicinity of the project that will have an impact on the excavation design.

The Geology and Structural work is described in detail in other sections of this project. Thus only the Rock Mass and Hydrological sections are discussed in detail.

4.5 ROCK MASS MODEL

4.5.1 Strength of Discontinuities

All rock masses contain discontinuities such as bedding planes, joints and faults and in order to analyse the stability of this system of individual rock blocks in a slope, it is necessary to understand the factors that control the shear strength of the discontinuities which separate the blocks (Hoek, 2002). The strength of discontinuities is usually expressed as Mohr-Coulomb properties (friction angle, and cohesion) and can be measured by laboratory and in situ tests, field assessments of discontinuity geometry and or from back-analyses of structurally controlled failures.

The shear strength of discontinuities can be expressed by using the Mohr-Coulomb failure criterion, in which the peak shear strength is given by:

$$\tau_{max=}c_j+\sigma_n tan\varphi_j \quad [4.5]$$

where φ_j and c_j are the friction angle and the cohesion of the discontinuity for the peak strength condition and σ_n is the average value of the normal effective stress acting on the plane of the structure as illustrated in Figure 4.4. When the peak strength has been exceeded and relevant displacements have taken place in the plane of the structure, the shear strength is given by:

$$\tau_{res=}c_{jres}+\sigma_n tan\varphi_{jres} \quad [4.6]$$

where φ_{jres} and c_{jres} are the friction angle and the cohesion for the residual condition, and σ_n is the mean value of the effective normal stress acting on the plane as illustrated in Figure 4.4 (Hoek, 2002).

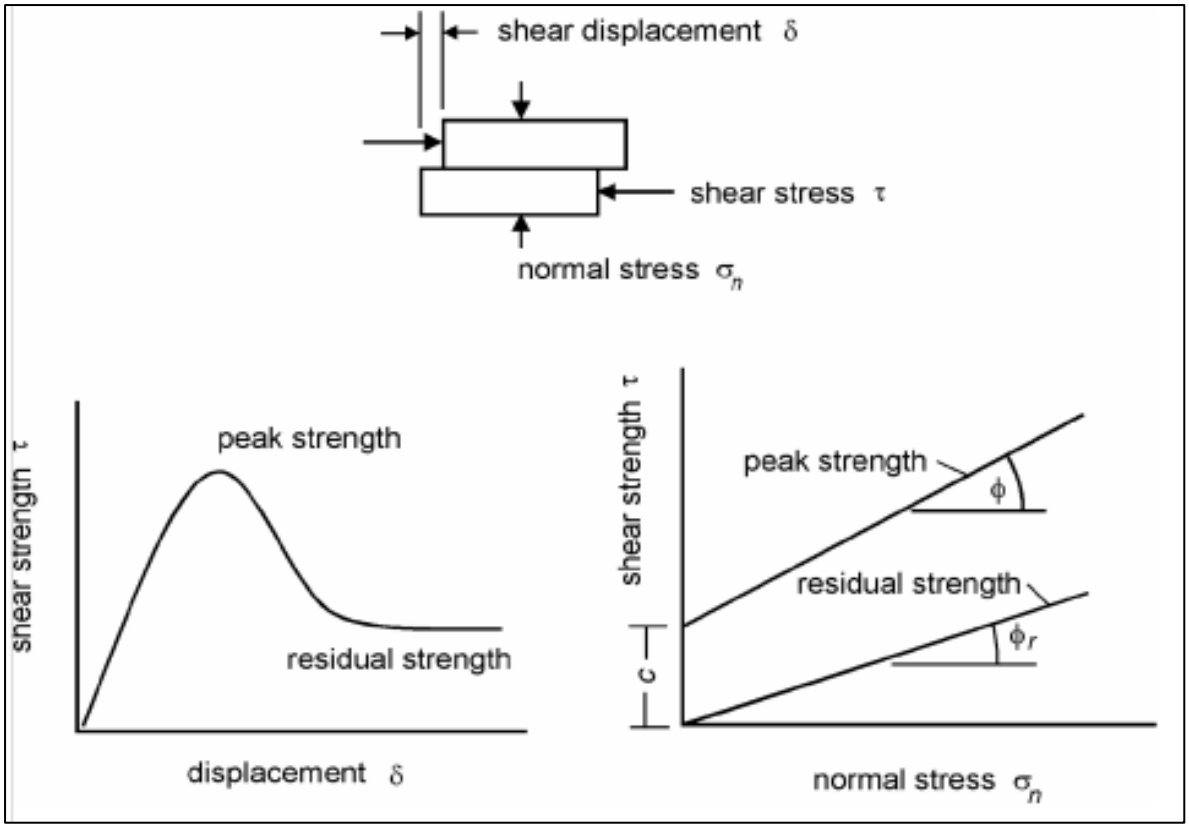
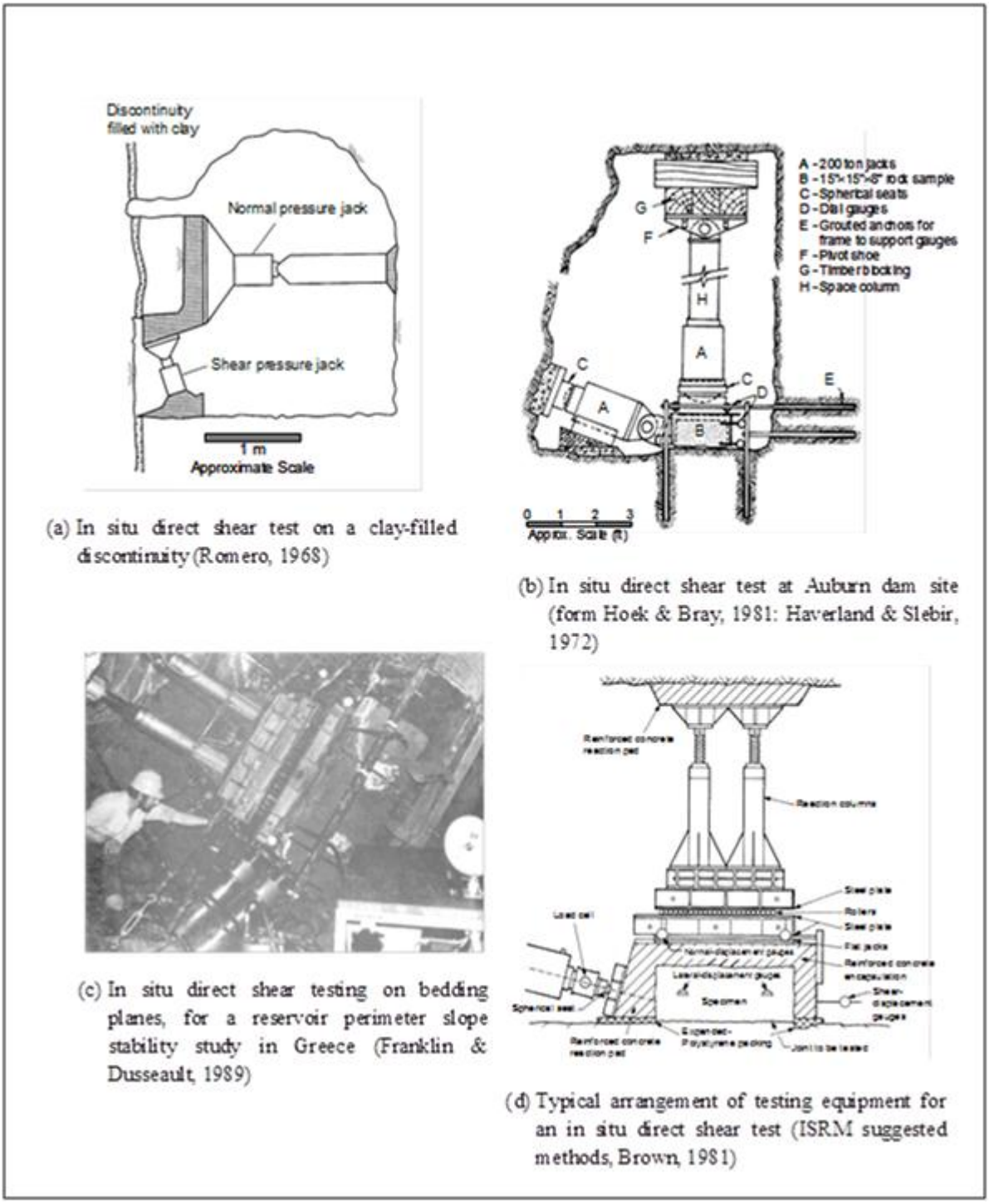


Figure 4.4 The shear testing of discontinuities (after Hoek, 2002).

Ideally, shear strength testing should be done by large-scale in situ testing on isolated discontinuities, but these tests are not commonly carried out because of the costs and related difficulty in exposing the discontinuity (Simons et al. 2001). See Figure 4.5. Thus a portable direct shear box testing machine is often used to test smaller lab-specimen scale samples.

The typical direct shear test procedure consists of using plaster to set the two halves of the specimen in a pair of steel boxes. A constant normal load is then applied using the cantilever, and the shear load gradually increased until sliding failure occurs. Measurement of the vertical and horizontal displacements of the upper block relative to the lower one can be made with dial gauges or more precise and continuous measurements with linear variable differential transformers (LVDTs) (Hencher and Richards 1989).



(a) In situ direct shear test on a clay-filled discontinuity (Romero, 1968)

(b) In situ direct shear test at Auburn dam site (form Hoek & Bray, 1981: Haverland & Slebir, 1972)

(c) In situ direct shear testing on bedding planes, for a reservoir perimeter slope stability study in Greece (Franklin & Dusseault, 1989)

(d) Typical arrangement of testing equipment for an in situ direct shear test (ISRM suggested methods, Brown, 1981)

Figure 4.5 Some examples of in situ direct shear tests on discontinuities. (Romero, 1968; Hoek and Bray, 1981; Haverland and Slebier, 1972; Franklin and Dusseault, 1989; Brown, 1981)

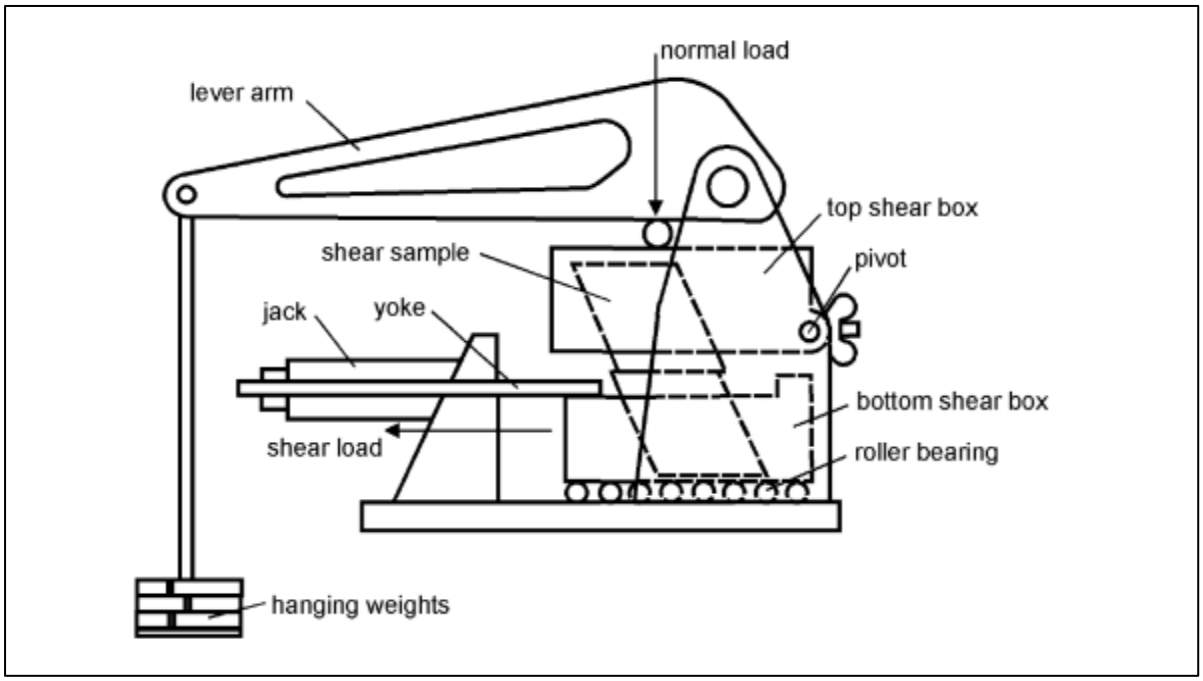


Figure 4.6 Diagrammatic section through shear machine used by Hencher and Richards (1982).

A typical shear testing machine, which can be used to determine the basic friction angle, is illustrated in Figure 4.6 Most shear strength determinations today are carried out by determining the basic friction angle, as described above, and then making corrections for surface roughness (Hoek, 2002). Typical basic friction angle ranges are given in Table 4.3

Table 4.3 Typical ranges of friction angles for a variety of rock types (after Wyllie and Mah, 2005).

Rock class	Friction angle range	Typical rock types
Low friction	20–27	Schists (high mica content), shale, marl
Medium friction	27–34	Sandstone, siltstone, chalk, gneiss, slate
High friction	34–40	Basalt, granite, limestone, conglomerate

An alternative method of estimated shear strength of discontinuities for laboratory scale samples is the triaxial shear testing technique as described by Goodman (1989).This method consists of a series of triaxial tests conducted on samples. If the failure planes in the samples are defined by a defect, of known orientation relative to the core axis (Figure 4.7a), then the normal and shear stresses on the failure plane can be computed using the pole of the Mohr circle (Figure 4.7b). In practice it can be very difficult to obtain failure on the exact same type of discontinuity in highly foliated or anisotropic rocks where the joint roughness can vary significantly.

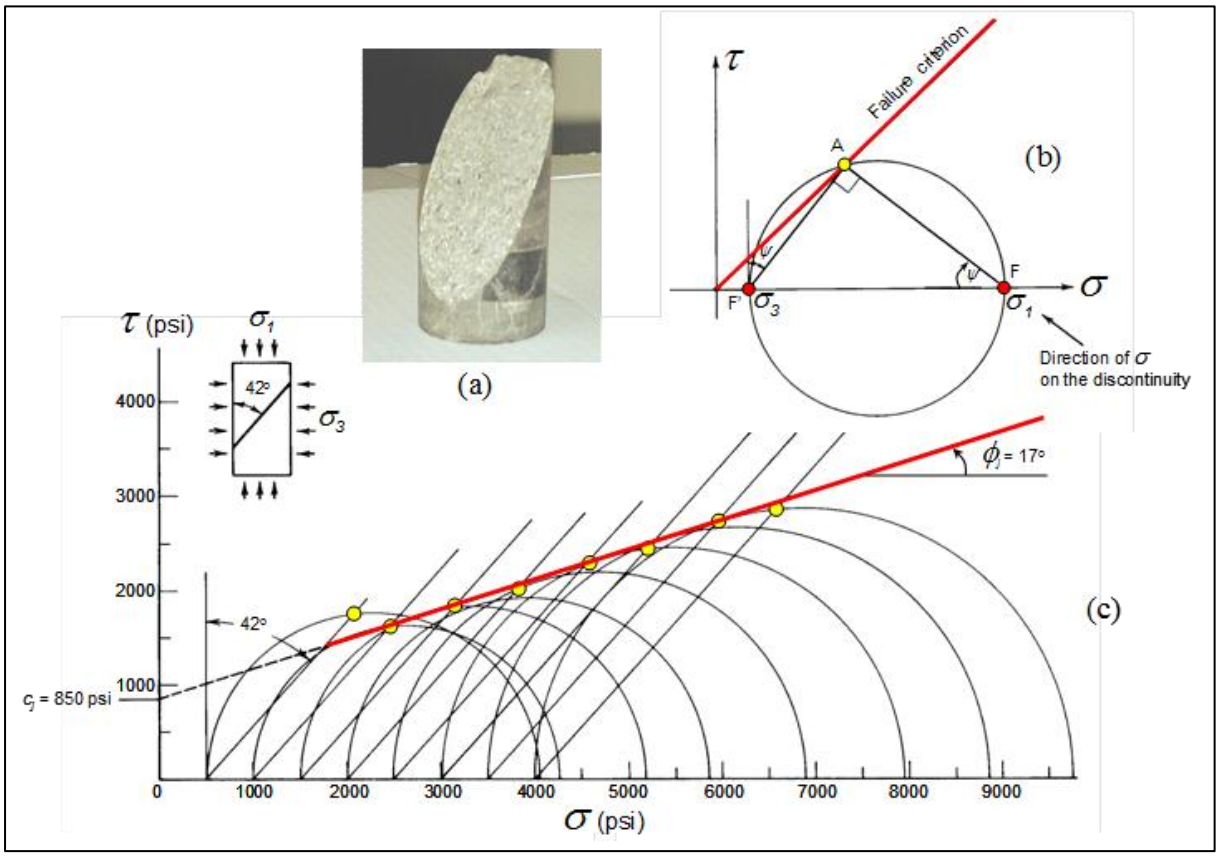


Figure 4.7 Use of triaxial compression test to define the shear strength of veins or other defects with strong infills (Modified from Goodman, 1989).

The laboratory tests show that, in general, the lower bound for the residual friction angle of a dry rock joint is given by the value of the basic friction angle of the material itself. The effect of surface roughness is to increase the residual friction angle. Thus, using the basic friction angle for the material provides a conservative estimate of the lower bound strength (Grasselli and Egger, 2003).

Patton (1966) who studied bedding plane traces in unstable limestone slopes concluded that for clean rough defects, the roughness increases the friction angle. The shear strength of Patton's saw-tooth specimens can be represented by:

$$\tau = \sigma_n tan(\varphi_b + i) \qquad [5.7]$$

Where φ_b is the basic friction angle of the surface and i is the angle of the saw-tooth face. See Figure 4.8.

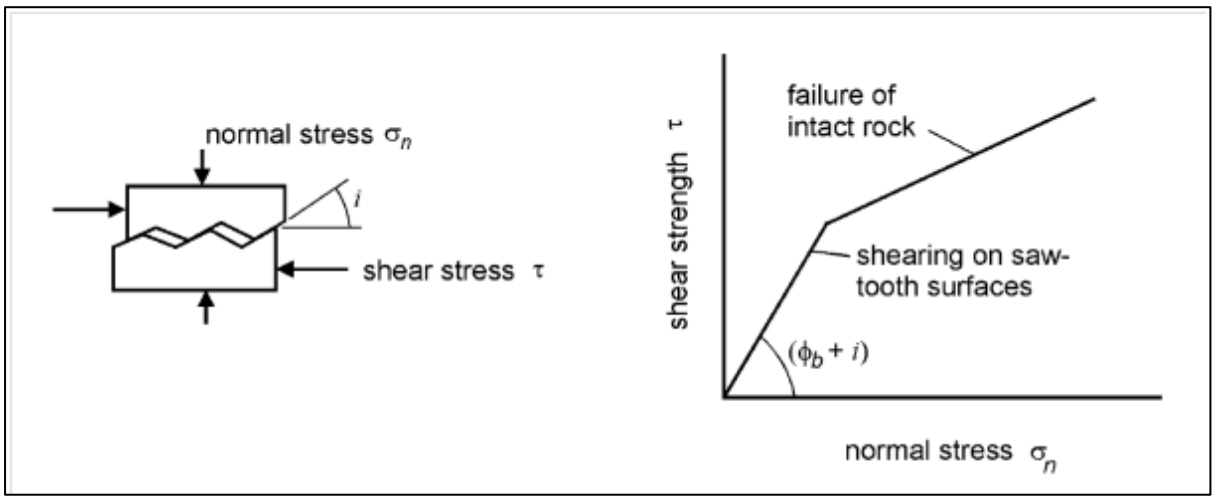


Figure 4.8 Patton's experiment on the shear strength of saw-tooth specimens (Hoek, 2002).

Patton (1966) suggested that asperities can be divided into first- and second-order asperities:

- First-order asperities: They correspond to major undulations of the discontinuity. They exhibit wavelengths larger than 0.5 m and roughness angles of not more than about 10° to 15° (Figure 4.9).

- Second-order asperities: Correspond to small bumps and ripples of the discontinuity with wavelengths smaller than 0.1 m and roughness angles as high as 20° to 30° (Figure 4.9). Patton (1966) indicated that only first-order asperities have to be considered to obtain reasonable agreement with field observations, but Barton (1973) showed that at low normal stresses second-order asperities also come into play.

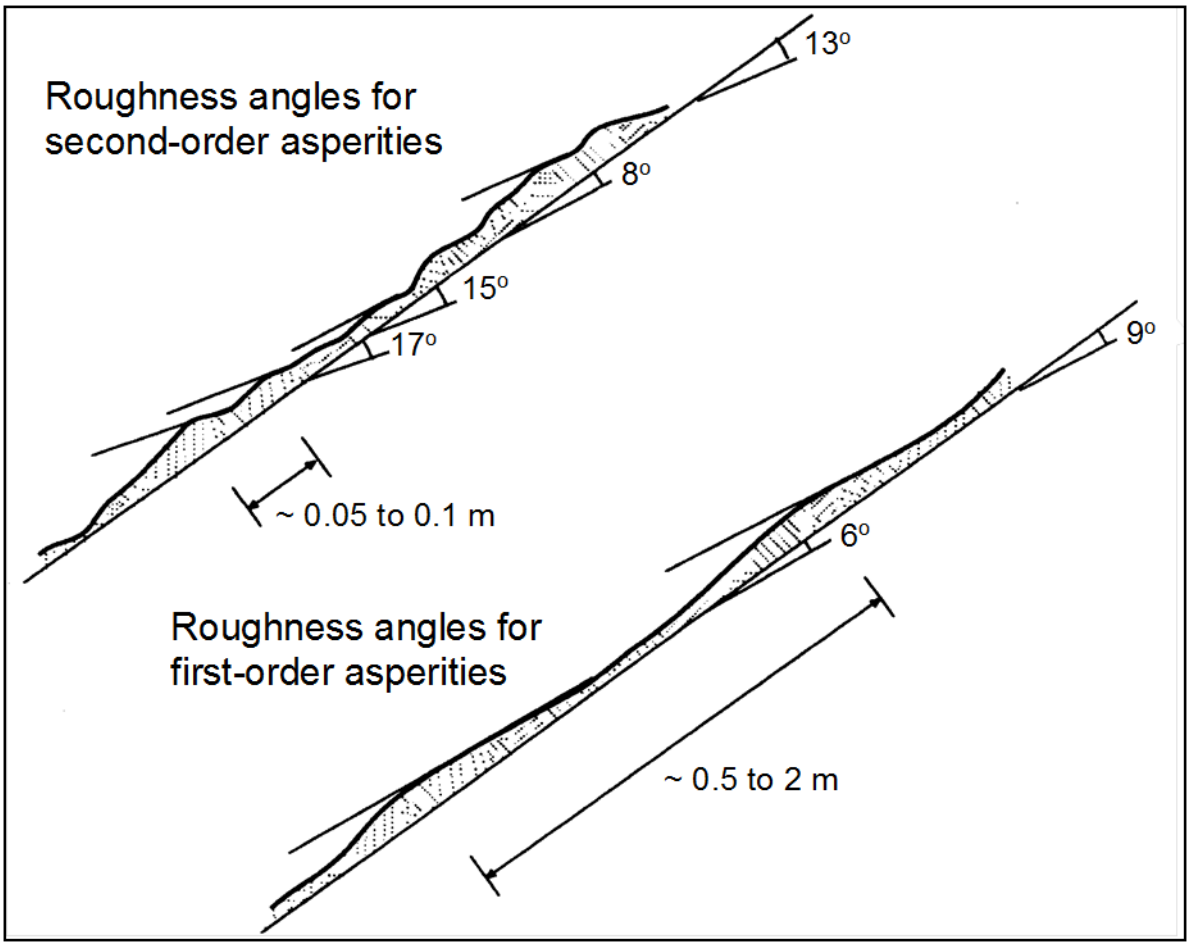


Figure 4.9 Definition of 1st and 2nd order asperities on rough defects (From Wyllie and Norrish, 1996).

Wyllie and Norrish (1996) indicated that the actual shear performance of the defects in rock slopes depends on the combined effects of the defect's roughness and wall rock strength, the applied effective normal stress, and the amount of shear displacement. See Figure 4.10.

Barton (1973) used the concepts of joint roughness and wall strength to introduce the non-linear empirical Barton-Bandis criterion for the shear strength of the defects in a rock mass.

The criterion excludes filled discontinuities and thus weathering and alteration can only be considered if the rock walls are in direct rock to rock contact. This means that the Barton-Bandis criterion cannot be applied to many of the geological environments found in pit slope engineering and should thus be applied with caution.

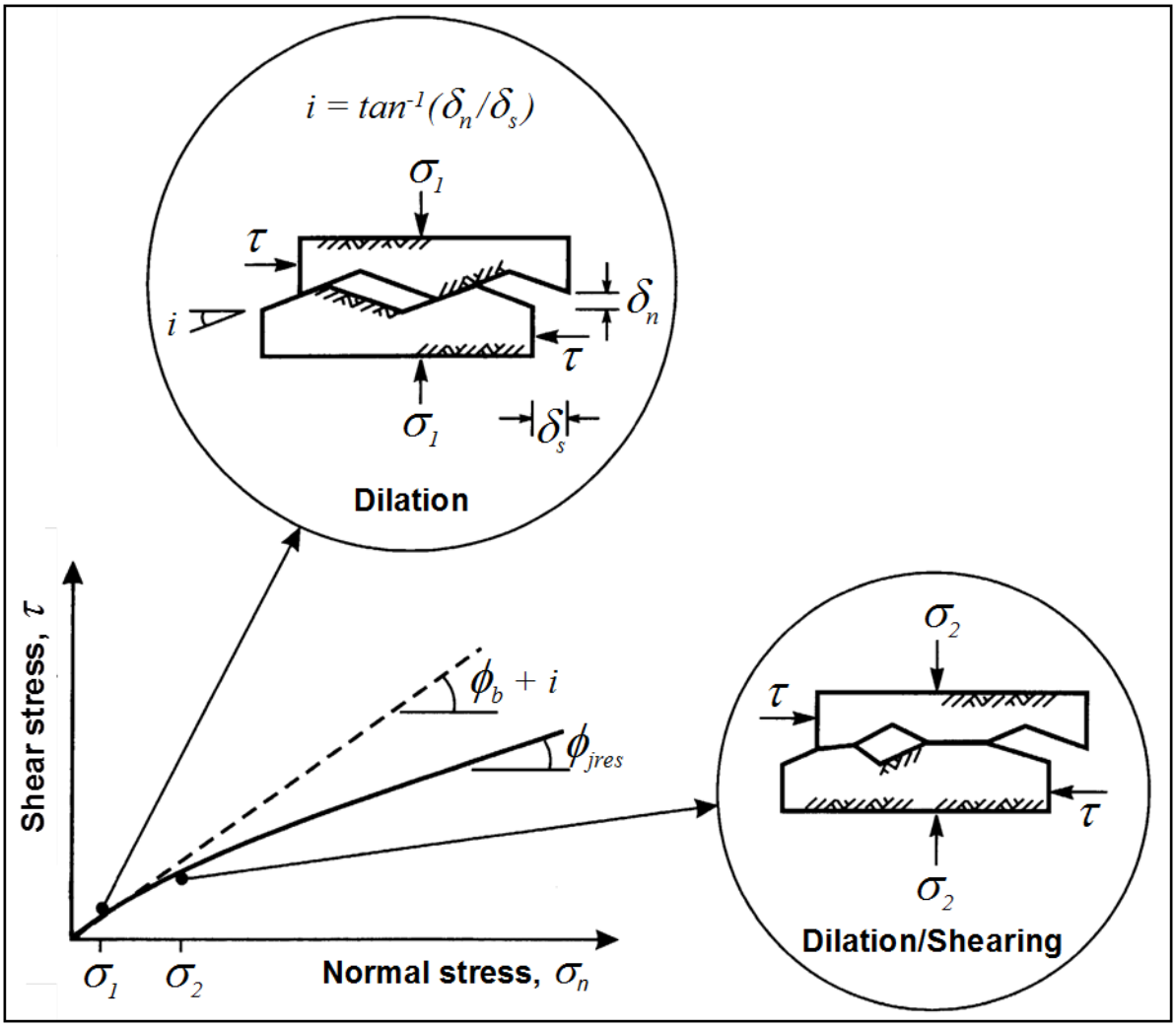


Figure 4.10 Effect of surface roughness and normal stress on the defect's friction angle (from Wyllie, 1992).

However the advantage of the Barton-Bandis (Barton and Bandis, 1990) criterion is that it includes explicitly the effects of surface roughness through the parameter JRC and the magnitude of the normal stress through the ration of *(JCS/σ_n):*

$$\tau_{\max} = \sigma_n \tan(\phi_j) = \sigma_n \tan(\phi_b + i) \quad [4.8]$$

where the friction angle of the defect, ϕ_j, is represented by the basic friction angle, ϕ_b, plus an increment *i* that depends on the roughness of the discontinuity and the magnitude of the effective normal stress relative to the uniaxial compressive strength of the wall rock. This increment is given by:

$$i = JRC \log_{10}\left(\frac{JCS}{\sigma_n}\right) \quad [4.9]$$

Thus the criterion defining the peak shear strength of a discontinuity can be written as:

$$\tau_{\max} = \sigma_n \tan\left(JRC \log_{10}\left(\frac{JCS}{\sigma_n}\right) + \phi_b\right) \quad [4.10]$$

where $\emptyset_b$ is the basic friction angle, JRC is the joint roughness coefficient, and JCS is the uniaxial compressive strength of the rock wall.

The joint roughness coefficient, JRC, varies from 0 for smooth, planar and slickensided surfaces to 20 for rough, undulating surfaces. There are a number of different ways of evaluating JRC:

- Visually compare the surface condition with standard profiles based on a combination of surface irregularities and waviness using profiles such as those shown in Figure 4.11. This method relies on judgment and experience and can be prone to error.
- Measuring of unevenness amplitude profiles and calculation of JRC using the graph as depicted in Figure 4.12.

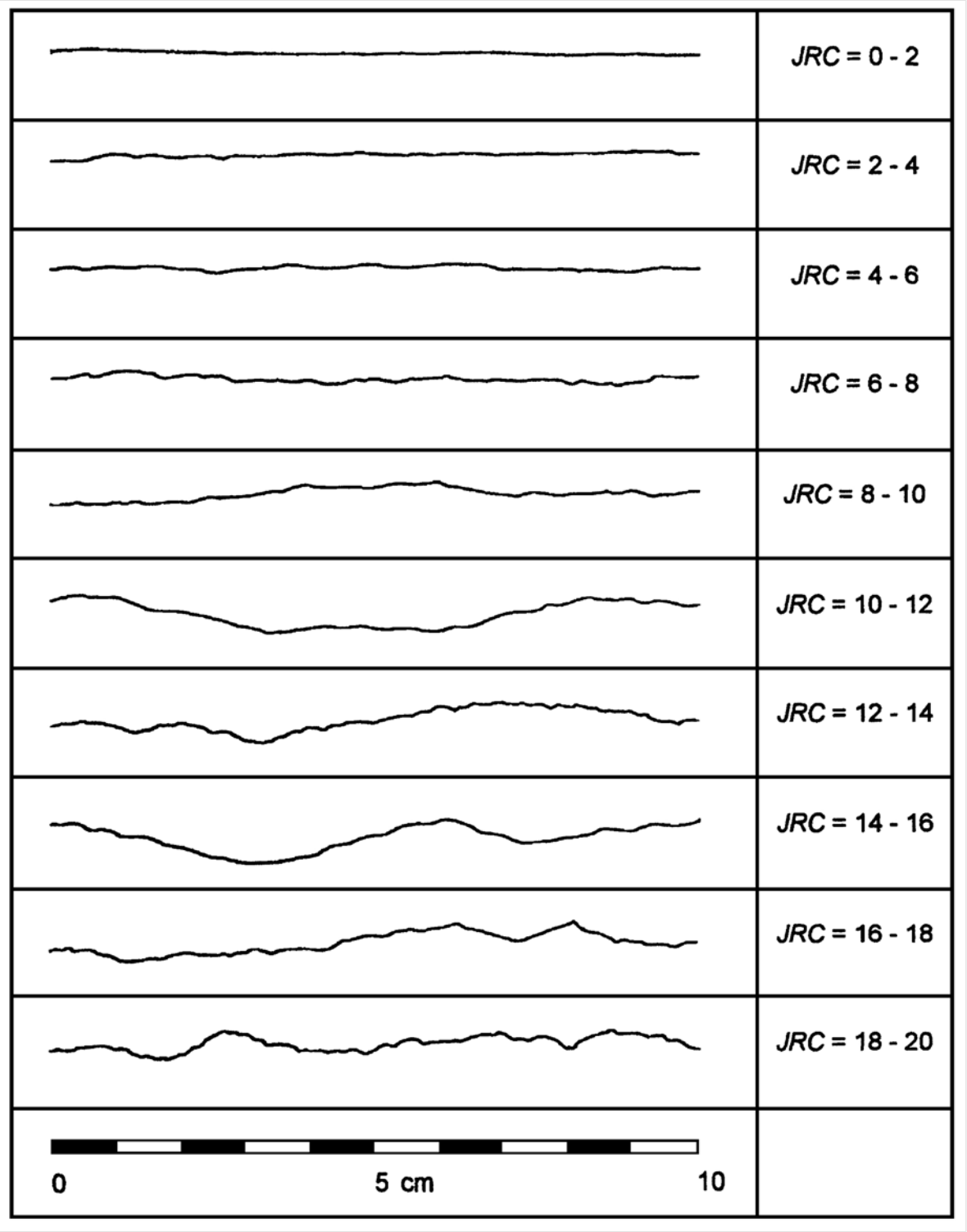


Figure 4.11 Defect roughness profiles and associated JRC values (Barton and Choubey, 1977).

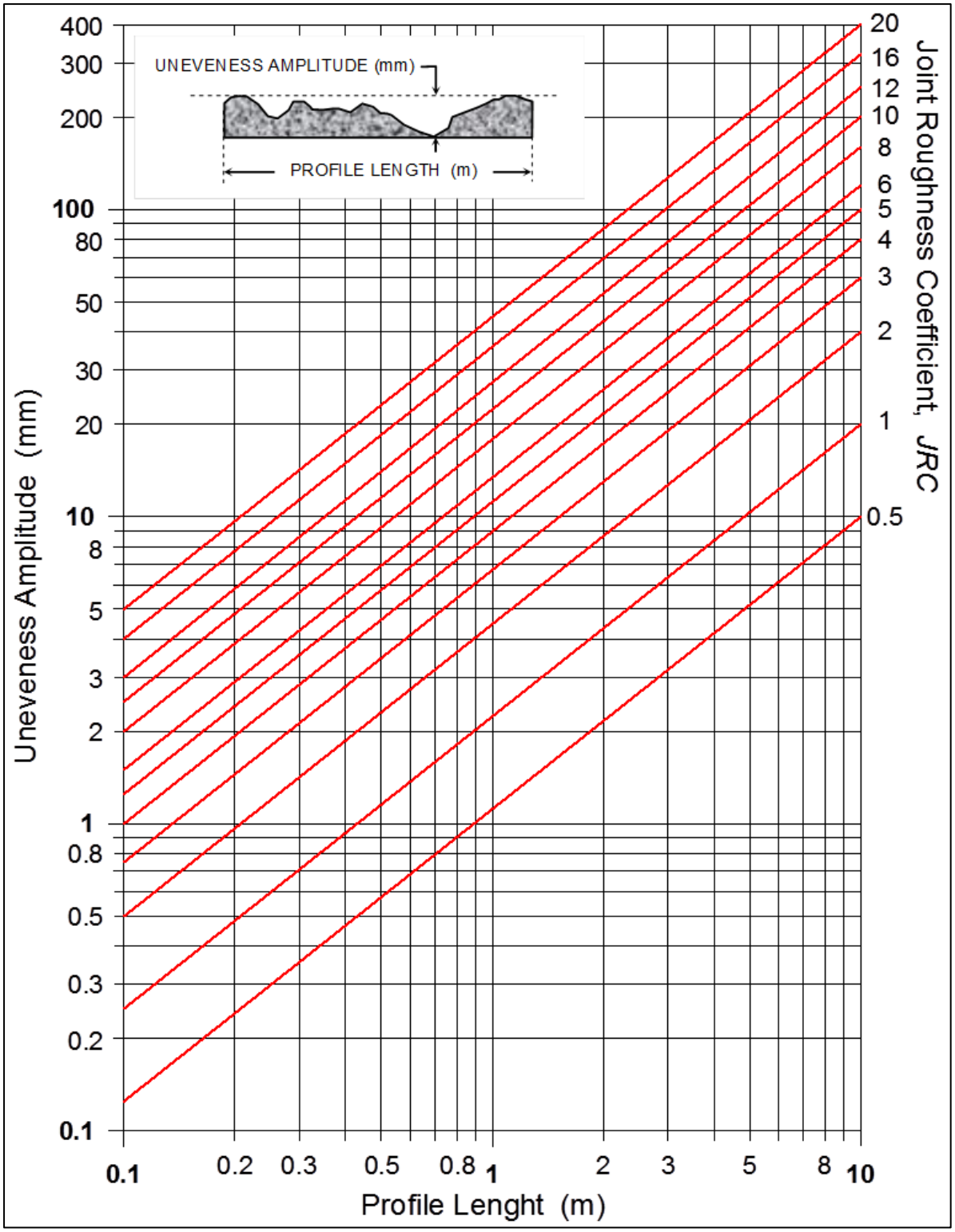


Figure 4.12 Chart to estimate *JRC* from the maximum unevenness amplitude and the profile length (Barton, 1982).

Karzulovic and Read (2009) noted that discussions about the effects of scale on the shear strength of defects as defined by the Mohr-Coulomb failure criterion are limited, but that the available data indicates that:

- Laboratory tests frequently over-estimate the shear strength of discontinuities, especially the cohesion;
- At low confinement and scales from 25 to 50 m, sealed structures with no clayey fillings have "typical" peak strengths characterized by cohesions ranging from 50 to 150 kPa and friction angles ranging from 25º to 35º.

Both JRC and JCS values are influenced by scale effects and decrease as the defect size increases. This is because small-scale roughness becomes less significant compared to the length of a longer defect and eventually large-scale undulations have more significance than small-scale roughness (Barton, 1980). See Figure 4.13.

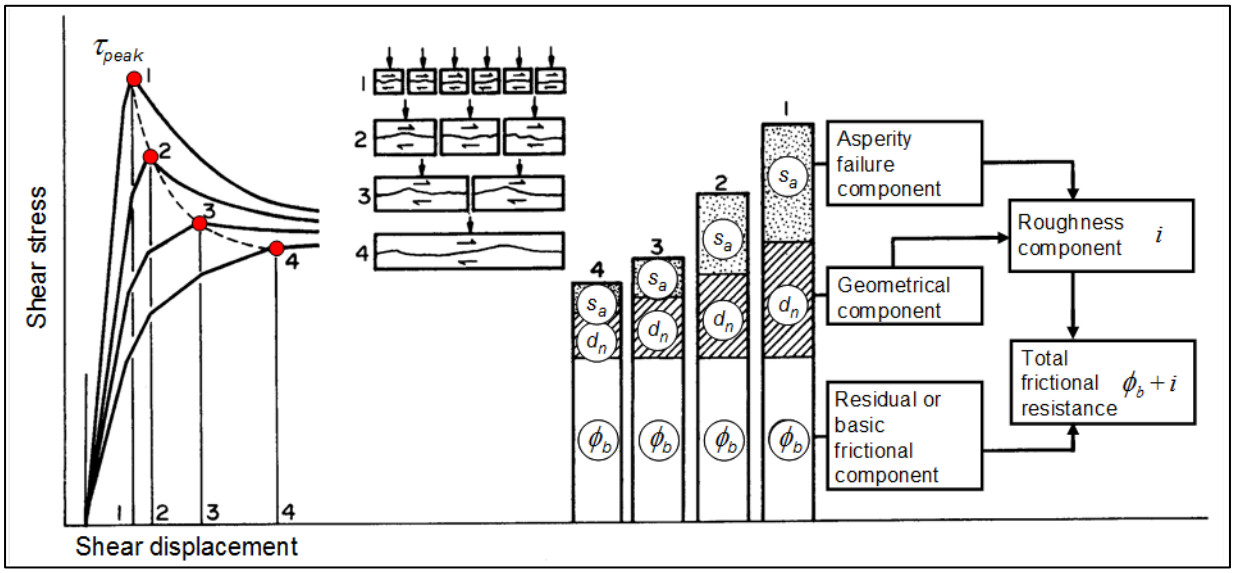


Figure 4.13 Summary of scale effects in the shear strength components of non-planar defects. $\emptyset_b$ is the basic friction angle, d_n is the peak dilation angle, s_a are surface asperities, and i is the roughness angle (Barton, 1980).

Bandis et al. (1981) studied these scale effects and found that increasing the size of the discontinuity produces the following effects:

- The shear displacement required to mobilize the peak shear strength increases.
- A reduction in the peak friction angle as a consequence of a decrease in peak dilation and an increase in asperity failure.
- A change from a "brittle" to a "plastic" mode of shear failure.
- A decrease of the residual strength.

To take into account the scale effect Barton and Bandis (1982) suggest reducing the values of JRC and JCS using the following empirical relations:

$$JRC_F = JRC_O \left(\frac{L_F}{L_O} \right)^{-0.02 JRC_O} \quad [4.11]$$

$$JCS_F = JCS_O \left(\frac{L_F}{L_O} \right)^{-0.03 JRC_O} \quad [4.12]$$

where JRC_F and JCS_F are the field values, JRC_O and JCS_O are the reference values (usually referred to a scale in the range from 10 cm to 1 m), L_F is the length of the structure in the field, and L_O is the length of reference (usually 10 cm to 1 m).

Karzulovic and Read (2009) noted that these relationships must be used with caution, because for long structures may produce values that are too low. Ratios of $JCS_F/JCS_O < 0.3$ or $JRC_F/JRC_O < 0.5$ are considered as conservative.

4.5.2 Anisotropy

Brady and Brown (2004) noted that some rocks will have anisotropic strength due to preferred orientation of the fabric or microstructure. Jaeger (1960) introduced a theory/case in which the rock contains well-defined, parallel planes of weakness whose normals are inclined at an angle β to the major principal stress direction. See Figure 4.14.

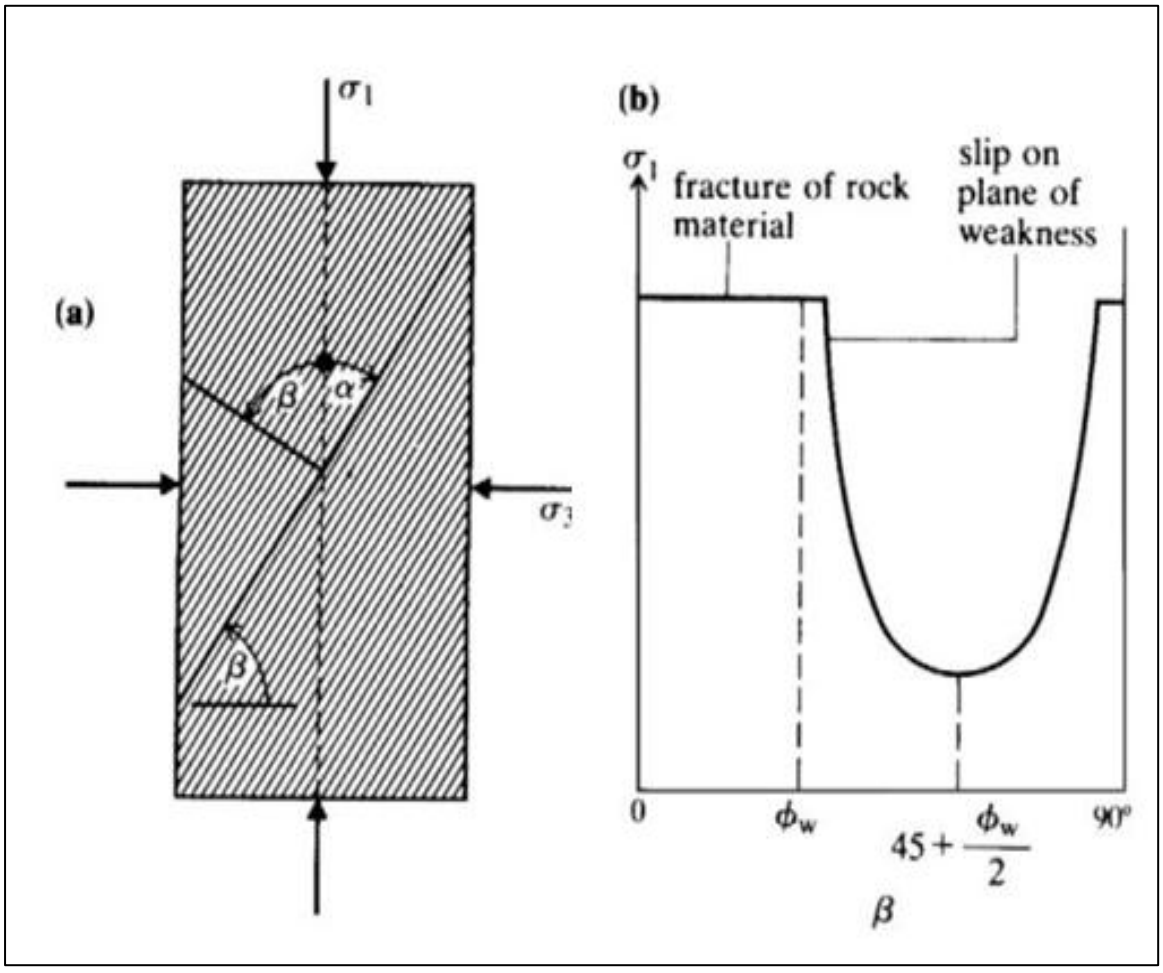


Figure 4.14 (a) Transversely isotropic specimen in triaxial compression (b) variation of peak strength at constant confining pressure with the angle of inclination of the normal to the plane of weakness to the compression axis (β). $\emptyset_w$ in this case in the friction angle of the weakness (Brady and Brown, 2004).

Brady and Brown (2004) noted that the plateau of constant strength at low values of β, or high values of β predicted by the theory (See Figure 4.13), is not always present in the experimental strength data and that thus they suggest that the two-strength model as proposed

by Jaeger (1960) provides an oversimplified representation of strength variation in anisotropic rocks.

Karzulovic and Read (2009) noted that where there are discontinuity sets parallel or sub-parallel to the slope, the shear strength of the rock mass cannot be assumed isotropic, because the rock mass is weaker in the direction of these discontinuities. Karzulovic (2006) demonstrated this principle by running several simplistic limit equilibrium models with an anisotropic rock strength function for four cases:

- No anisotropy,
- One discontinuity set is sub-parallel to slope,
- One discontinuity set is sub-parallel to the slope and day lighting in the face,
- Two sub-parallel joint sets of which only one is day lighting). See Figure 4.15.

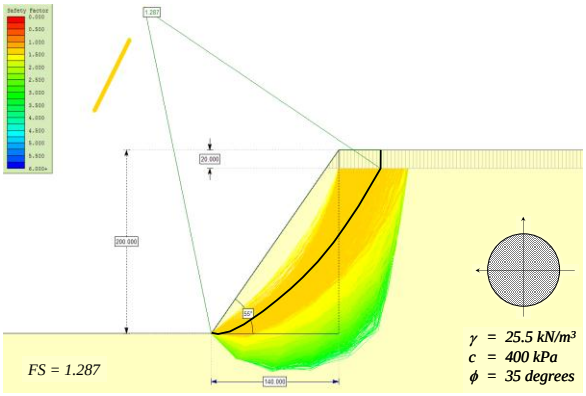
From Figure 4.14 it is clear that the rock mass shear strength is much smaller in the direction of the discontinuities. If discontinuities are persistent and can be assumed continuous for the slope being studied then the shear strength of the discontinuities can be assessed using the procedures described in the previous section. However if the discontinuities are non-persistent and their continuity is interrupted by rock bridges their shear strength will increase considerably. Unless the effect of rock bridges is accounted for, the shear strength of the discontinuities will be underestimated (Karzulovic and Read, 2009). This concept is illustrated by Wittke (1990) in Figure 4.16.

Case 1:

No discontinuity sets sub-parallel to slope.

Rock mass strength is isotropic.

FS = 1.29

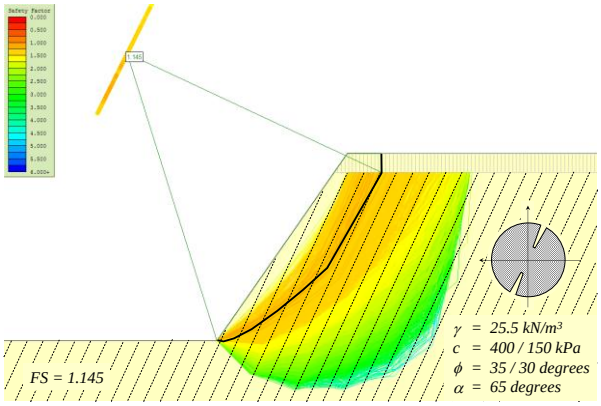


Case 2:

One discontinuity set is sub-parallel to slope, dipping 65° towards the pit.

Directional rock mass strength.

FS = 1.15

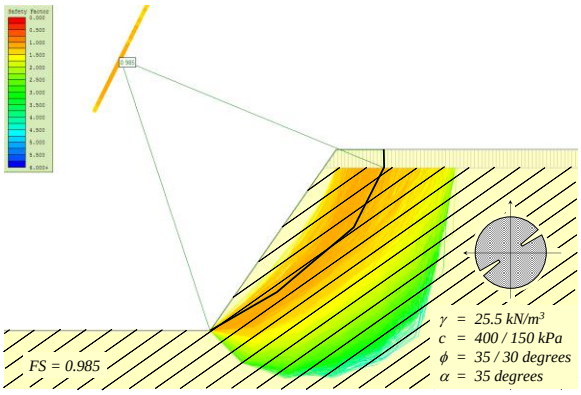


Case 3:

One discontinuity set is sub-parallel to slope, dipping 35° towards the pit.

Directional rock mass strength.

FS = 0.99



Case 4:

Two discontinuity sets are sub-parallel to slope, dipping 35° and 65° towards the pit.

Directional rock mass strength.

FS = 0.88

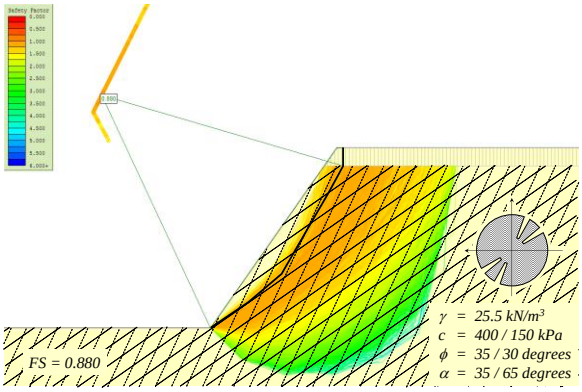


Figure 4.15 Factor of safety of a 200m rock slope, with an inclination of 55°, for different conditions of rock mass strength (Karzulovic and Read, 2009).

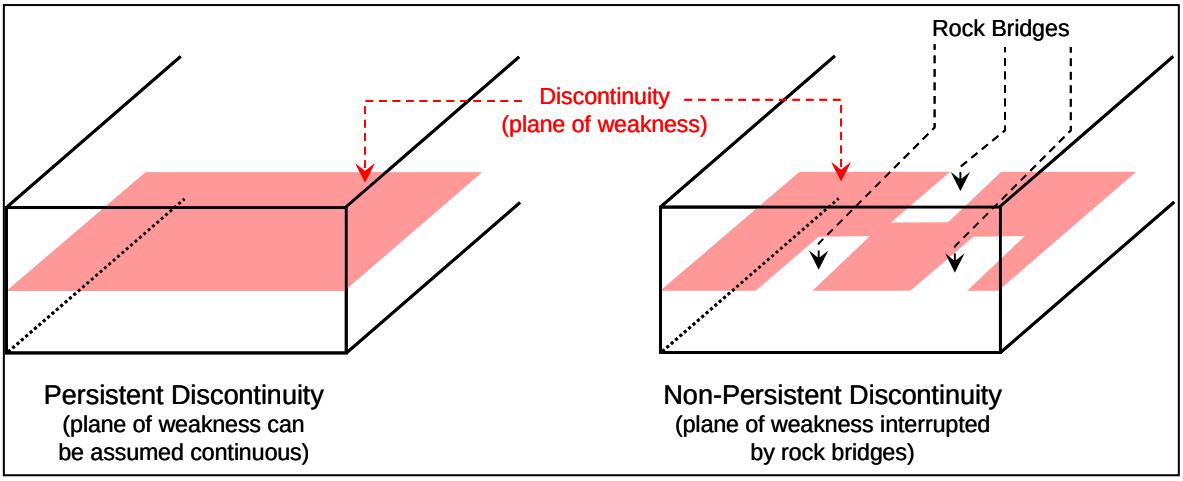


Figure 4.16 Simplified representation of the effect of rock bridges (modified from Wittke, 1990).

To account for the rock bridges Jennings (1972) proposed that equivalent strength parameters can be computed:

$$c_{eq} = (1-k)c + kc_j \qquad [4.13]$$

$$\tan(\phi_{eq}) = (1-k)\tan(\phi) + k\tan(\phi_j) \qquad [4.14]$$

where c_{eq} and ϕ_{eq} are the cohesion and friction angle of the equivalent discontinuity, c and φ are the cohesion and friction angle of the rock bridges, c_j and ϕ_j are the cohesion and friction angle of the discontinuities contained in the rock mass (joints), and k is the coefficient of continuity along the rupture plane given by:

$$k = \frac{\sum l_j}{\sum l_j + \sum l_r} \qquad [4.15]$$

where l_j and l_r are the lengths of the discontinuities and rock.

4.5.3 Rock Mass Ratings

4.5.3.1 The Mining Rock Mass Rating and RQD

Rock mass ratings work on basis of describing key geological features that will provide an indication of the quality of the rock mass with the aim of dividing it into Geotechnical domains for engineering applications. Rock mass ratings have been in use for decades and perhaps the oldest and best-known being that of Terzaghi, which was introduced for tunnel design in 1946. Bieniawski (1989) noted six specific objectives for rock mass classification:

- Identify the most significant parameters influencing the behaviour of a rock mass;
- Divide a particular rock mass formation into groups of similar behaviour, i.e. rock mass classes of varying quality;
- Provide a basis for understanding the characteristics of each rock mass class;
- Relate the experience of rock conditions at one site to the conditions and experience encountered by other practitioners;
- Derive quantitative data and guidelines for engineering design;
- Provide a common basis for communication between engineers and geologists.

Many massive underground mines start off as open pit operations (For example Koffiefontein Finsch and Palabora Mines). The Mining Rock Mass Rating (Laubscher, 1990) is perhaps one of the most popular rock mass classifications systems in use on massive mining operations since it is applicable to open pit design (Haines and Terbrugge, 1991) and massive underground methods (block caving). The MRMR system (Laubscher, 1977) was originally developed from Bieniawski's original classification (Bieniawski, 1973). Both systems were subsequently modified: the 1990 MRMR (Laubscher, 1990) and 1989 RMR (Bieniawski, 1989).

The MRMR system takes into account the same parameters as the Geomechanics system, but combines the groundwater and joint condition, resulting in the four parameters:

- Rock material strength (UCS)
- Rock Quality Designation (RQD)
- Joint spacing. See Figure 4. (Note the classification system allows for RQD and Joint Spacing parameters to be replaced by the Fracture Frequency per meter parameter)

- Joint condition and ground water. See Figure 4.17; and Tables 4.5 and 4.6.

Where RQD is defined as the ratio of the cumulative length of sticks of NX size core more than 100mm in length in a drill run to the total length of the drill run (Stacey, 2001):

$$\text{RQD\%} = \frac{\text{Total length of core} \geq 100\text{mm x } 100}{\text{Length of core run}} \qquad [4.16]$$

The weighting of the parameters are however different than Bieniawski' RMR system. See Table 4.4.

Table 4.4 The different weighting on the Input parameters for Laubscher's (1990) and Bieniawski's (1989) RMR.

Laubscher's RMR Input Parameters	Maximum Rating	Bieniawski's RMR Input Parameters	Maximum Rating
Intact Rock Strength (UCS)	20	Intact Rock Strength (UCS)	15
RQD	15	RQD	20
Joint Spacing	25	Joint Spacing	20
Joint Condition and Ground water	40	Joint Condition Groundwater	30 15

Table 4.5 The Mining Rock Mass Rating Classification (Laubscher, 1990).

Parameter	1		2		3		4	
	RQD		UCS		Joint Spacing		Joint Condition	
	RQD	Rating	UCS (MPa)	Rating	Joint Spacing	Rating	Joint Condition Including Groundwater	Rating
Range of Values	100-97	15	185	20	Refer Figure 4.16	25	Refer to Table 4.6	40
			184-165	18				
	96-84	14	184-165	16				
	83-71	12	164-145	14				
	70-56	10	144-125	12				
	55-44	8	124-105	10				
	43-31	6	104-85	8				
	30-17	4	84-65	6				
	16-4	2	44-25	4				
	3-0	0	24-5	2				
			4-0	0				

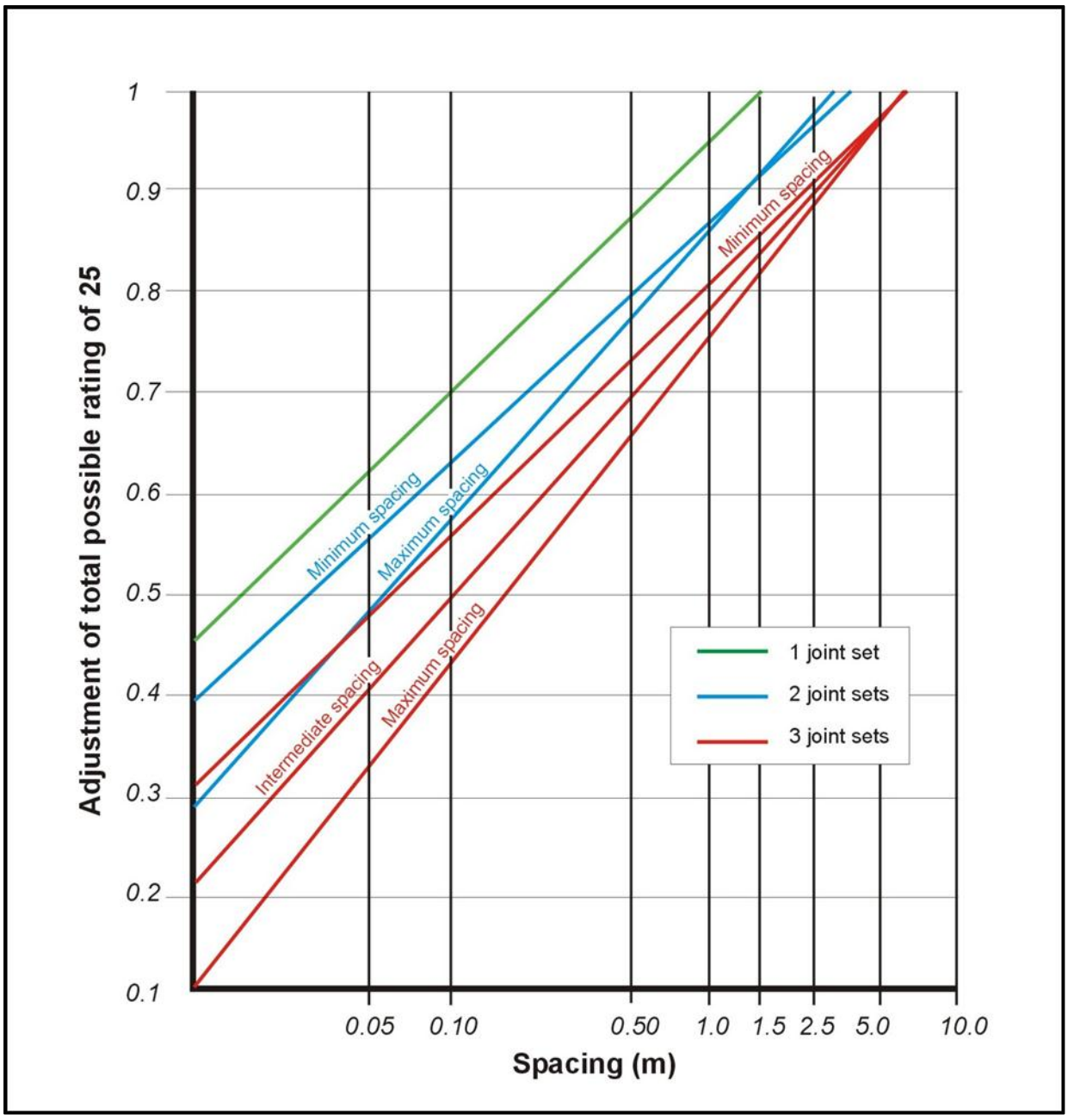


Figure 4.17 Graph for determination of joint spacing rating (after Laubscher, 1993; taken from Stacey, 2001).

Table 4.6 Adjustments for Joint Condition and Groundwater (Laubscher, 1990).

Parameter	Description		Dry Condition	Wet Conditions Moist	Moderate pressure 25-125 1/mm	Severe Pressure >125 1/min
A Joint Expression (large scale irregularities)	Multi-Wavy Directional		100	100	95	90
	Uni-Directional		95	90	85	80
	Curved		85	80	75	70
	Slight Undulation		80	75	70	65
	Straight		75	70	65	60
B Joint Expression (small scale irregularities or roughness	Rough stepped/irregular		95	90	85	80
	Smooth stepped		90	85	80	75
	Slickensided stepped		85	80	75	70
	Rough undulating		80	75	70	65
	Smooth undulating		75	70	65	60
	Slickensided undulating		70	65	60	55
	Rough planar		65	60	55	50
	Smooth planar		60	55	50	45
	Polished		55	50	45	40
C Joint Wall Alteration Zone	Stronger than wall rock		100	100	100	100
	No alteration		100	100	100	100
	Weaker than wall rock		75	70	65	60
D Joint Filling	No fill – surface staining only		100	100	100	100
	Non softening and sheared material (clay or talc free	Coarse	90	85	80	75
		Medium	85	80	75	70
		Fine	80	75	70	65
	Soft sheared material (e.g. talc)	Coarse	70	65	60	55
		Medium	60	55	50	45
		Fine Sheared	50	45	40	35
	Gouge thickness <amplitude of irregularity		45	40	35	30
	Gouge thickness <amplitude of irregularity		30	20	15	10

Laubscher's 1990 MRMR also accounts for environmental factors that will influence the strength of the rockmass by applying adjustments to take account of weathering of the rock mass, joint orientation relative to the excavation, mining-induced stresses and blasting effects. A weathering adjustment is relevant when rock types occur which are susceptible to deterioration over time. The adjustment percentages are given below in Table 4.7 (Laubscher, 1990).

Table 4.7 Weathering Adjustment to MRMR (Laubscher, 1990).

Rate of weathering and adjustments (%)					
Description of weathering extent	**6 months**	**1 year**	**2 years**	**3 years**	**4 + years**
Fresh	100	100	100	100	100
Slightly	88	90	92	94	96
Moderately	82	84	86	88	90
Highly	70	72	74	76	78
Completely	54	56	58	60	62
Residual soil	30	32	34	36	38

The orientations of the joints, and whether the bases of blocks formed by the joints are exposed, have a significant effect on excavation stability. The joint orientation adjustment depends on the orientations of the joints with respect to the vertical axis of the block (Stacey, 2001). The adjustment percentages are given in Table 4.8 below (Laubscher, 1990).

Table 4.8 Adjustments to MRMR due to joint orientation (Laubscher, 1990).

Number of joints defining the block	**Adjustment (%)** *Number of faces inclined away from the vertical*				
	70	75	80	85	90
3	3	-	2	-	-
4	4	3	-	2	-
5	5	4	3	2	1
6	6	5	4	3	2 or 1

The adjustments for mining induced stresses are essentially based on judgement and can vary from 120% for Good confinement to 60% for conditions with poor confinement, associated with numerous, closely spaced joint sets. The quality of blasting has an influence on the fracturing and loosening of the rock mass. Adjustments for blasting effects are given in Table 4.9 below (Laubscher, 1990).

Table 4.9 Adjustments for Blasting Effects (Laubscher, 1990).

Excavation Technique	Adjustment (%)
Boring	100
Smooth wall blasting	97
Good conventional blasting	94
Poor blasting	80

4.5.3.2 The Geological Strength Index (GSI)

Initially Bieniawski's RMR (Bieniawski, 1974) was used in the Hoek-Brown Criterion (Hoek and Brown, 1980). This was subsequently replaced by the Geological Strength Index (GSI) in 1995 (Hoek et al., 1995). The GSI system removed the double accounting of intact rock strength that was catered for in RMR and in the Hoek Brown criterion. Hoek et al (1995) determined that for better quality rock masses (GSI > 25), the value of GSI can be estimated directly from the 1976 version of Bieniawski's Rock Mass Rating (Bieniawski 1976), with the Groundwater rating set to 10 (dry) and the adjustment for joint orientation set to 0 (very favourable).

When the 1989 version of Bieniawski's RMR classification (Bieniawski 1989) is used, then GSI = RMR89' - 5 where RMR89' has the Groundwater rating set to 15 and the Adjustment for Joint Orientation set to zero. Thus for GSI values under 25 the chart must be used directly to estimate the GSI or alternatively calculated from Barton's Q (Barton, 1974):

$$GSI = \text{Bieniawski RMR 1976} = 9*\ln Q + 44 \qquad [4.17]$$

The chart for estimating GSI is given in Figure 4.18.

Often Laubscher's RMR is equated to that of Bieniawski's when the GSI is calculated. Terbrugge et al (2004) calculated the correlation between Bieniawski's RMR and Laubscher's RMR for a site investigation. The study indicated a very good correlation between Bieniawski and Laubscher's RMR. See Figure 4.19.

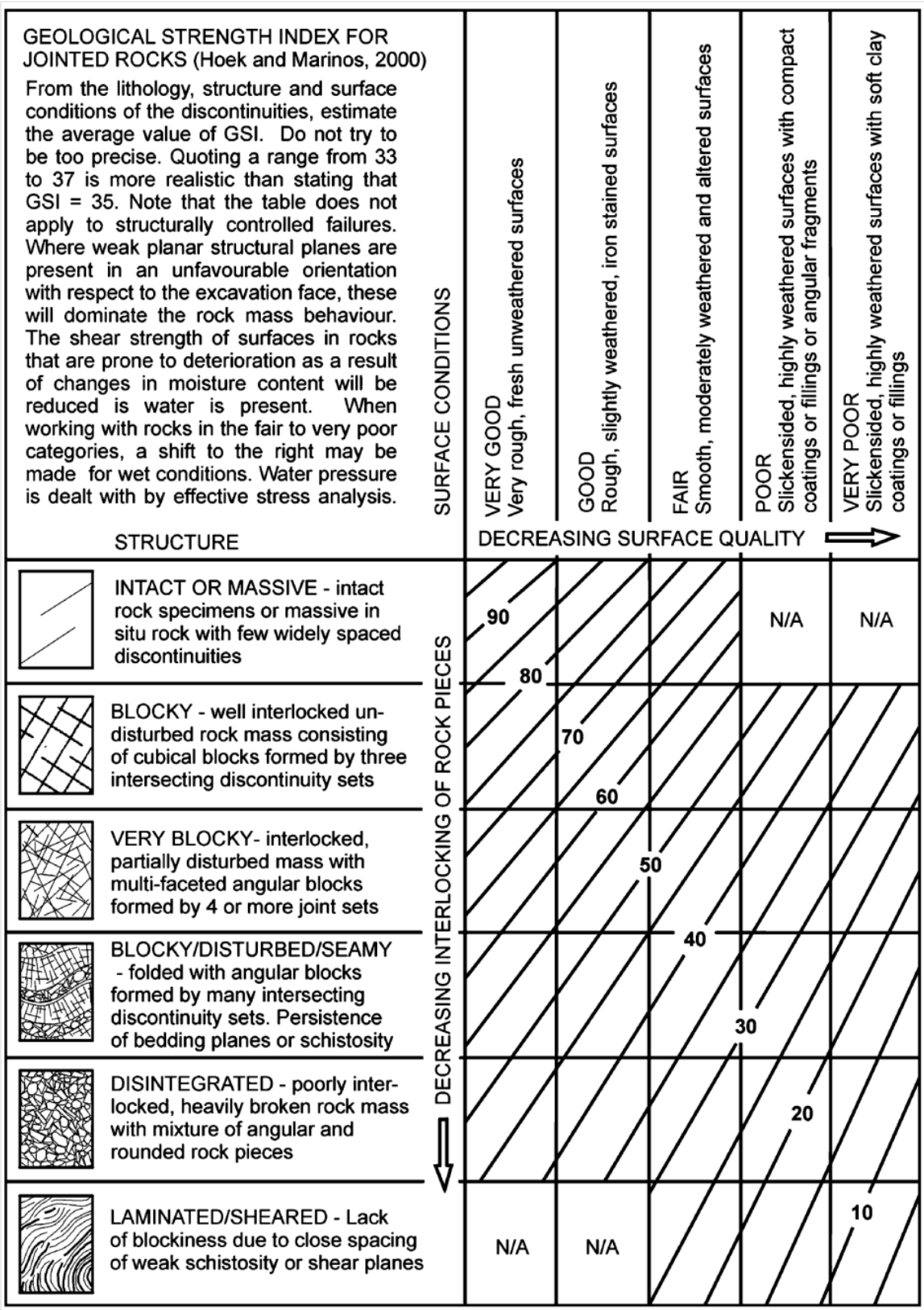


Figure 4.18 The Geological strength Index – GSI (taken from Marinos et al., 2005).

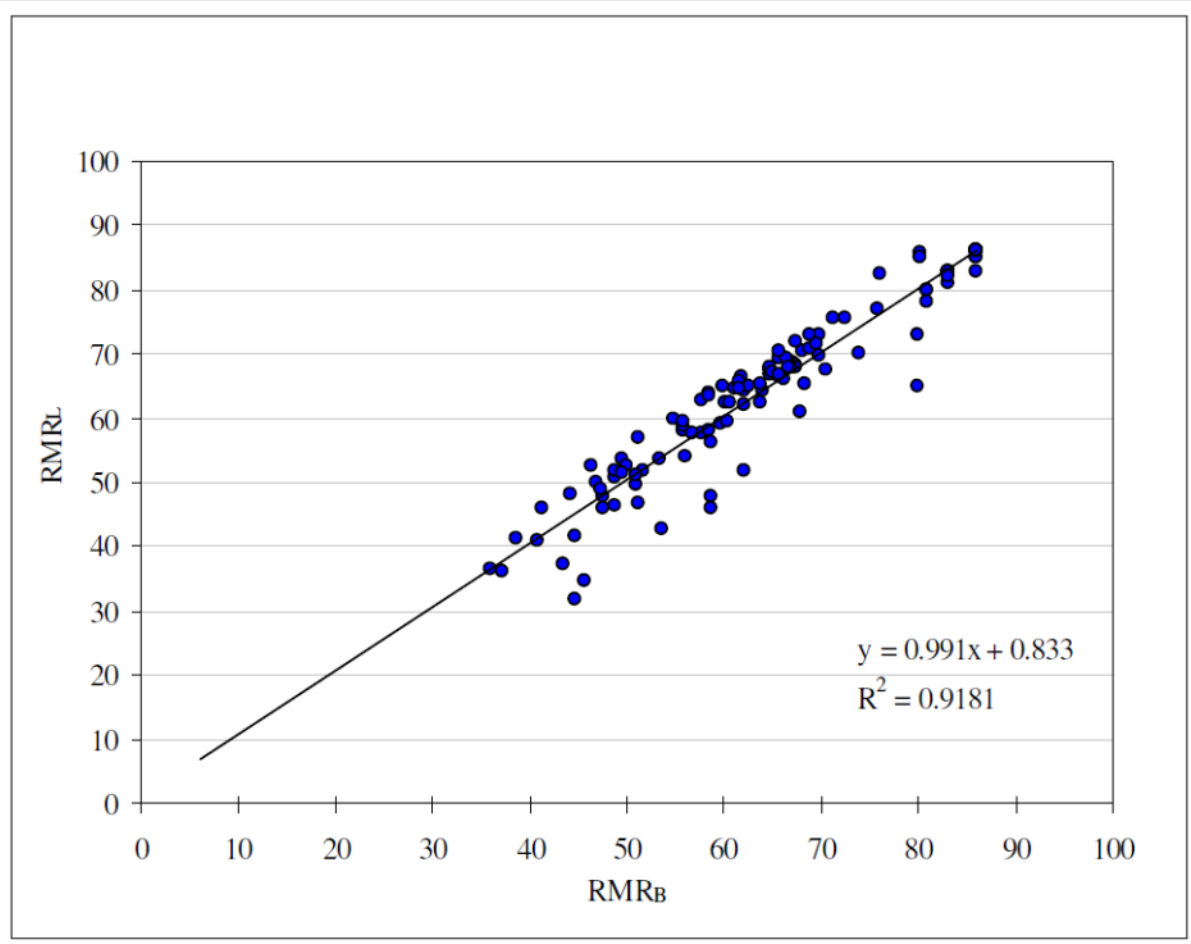


Figure 4.19 The correlation between Bieniawski and Laubscher's RMR (after Terbrugge et al., 2004).

4.5.4 Failure Criterion and Rock Mass Strength

The Hoek-Brown strength criterion was first developed in 1980 (Hoek and Brown, 1980a, 1980b) for the design of underground excavations in hard rock. The criterion was derived from the results of research into the brittle failure of intact rock. Complications arose early on in the use of the criterion since many problems were related to slope stability problems which were conveniently dealt with in terms of shear and normal stresses rather than the principal stress relationships of the original Hoek-Brown criterion (Hoek et al., 2002). The criterion was originally introduced in the form:

$$\sigma_1' = \sigma_3' + \sigma_c (m * \sigma_3'/\sigma_c + s)^{0.5} \quad [4.18]$$

Where:

σ_1' = major principle effective stress at failure

σ_3' = minor effective principal stress at failure

σ_c = uniaxial compressive strength of the intact rock

m = dimensionless material constant for rock

s = dimensionless material constant for rock, ranging from 1 for intact rock with tensile strength to 0 for broken rock with zero tensile strength.

Subsequently the criterion underwent several modifications with the final modification in 2002 (Hoek, 2002):

$$\sigma_1' = \sigma_3' + \sigma_{ci}\left(m_b \frac{\sigma_3'}{\sigma_{ci}} + s\right)^a \quad [4.19]$$

$$m_b = m_i \exp^{\left(\frac{GSI-100}{28-14D}\right)} \quad [4.20]$$

$$a = \frac{1}{2} + \frac{1}{6}\left(e^{-GSI/15} - e^{-20/3}\right) \quad [4.21]$$

$$s = e^{\left(\frac{GSI-100}{9-3D}\right)} \quad [4.22]$$

Where:

GSI = Geological strength Index

m_b = is a reduced value of the material constant m_i

s and a = constants

D = Damage factor accounting for blast damage and or stress relaxation ranging from D = 0 for undisturbed rock to D = 1 for very disturbed rock.

σ_{ci} = Uniaxial compressive strength of the intact rock material and

The rock mass modulus of deformation is given by (see above key to formula):

$$E_m(GPa) = \left(1 - \frac{D}{2}\right)\sqrt{\frac{\sigma_{ci}}{100}\, x\, 10^{\left(\frac{GSI-10}{40}\right)}} \qquad [4.23]$$

Note that the "switch" at GSI = 25 for the coefficients "s" and "a" was eliminated by the above equations. Best fit Mohr-Coulomb values (cohesion and friction angle) can be calculated from the Hoek-Brown criterion at a given confining stress (Hoek et al., 2002). The issue of determining the appropriate value of $sigma_3$ depends on the application and in the case of slopes Hoek et al. (2002) defined it as follows:

$$\frac{\sigma_{3max}'}{\sigma_{cm}'} = 0.72\left(m_b \frac{\sigma_{cm}'}{\gamma H} + s\right)^a \qquad [4.24]$$

σ_{cm} = rock mass strength as defined by Hoek et al. (2002)

γ = Unit weight of the rock

H = Height of the slope

m_i values should be determined from a series (usually five or more) of triaxial tests (Hoek and Brown, 1980a). Hoek (2002) noted that high quality triaxial test data will usually give a coefficient of determination r^2 of greater than 0.9. Cai (2009) noted that the m_i value depends on many factors such as mineral content, foliation, and grain size (texture) and not only on the rock type and that m_i can be estimated from this strength ratio (R):

$$m_i \approx \frac{\sigma_c}{\sigma_t}' = R \qquad [4.25]$$

Thus if the tensile strength, σ_t , and uniaxial compressive strength, σ_c ,are available, the strength ratio R, and indirectly m_i can be calculated (Cai, 2009).

4.6 HYDROLOGY

The effect of groundwater on slope stability can be illustrated with the effective stress concept which was developed by Terzaghi, which states:

$$\tau = c + (\sigma_n - p)tan\varphi \qquad [5.26]$$

Where:

τ	=	shear strength on a potential failure surface
p	=	fluid pressure (or pore pressure)
σ_n	=	total normal stress acting perpendicular to the potential failure surface
φ	=	angle of internal friction
c	=	cohesion available along the potential failure surface
$\sigma_n - p$	=	effective normal stress

Thus groundwater can have a negative effect on slope stability because of fluid pressure (p) acting within discontinuities and pore spaces that decrease the normal stress acting on the plane and thus reduces the shear strength (τ) of the surface. The presence of groundwater is defined by a water table where the pore pressure is 0 at the water table, positive below the water table and negative or zero above the water table. Thus the deeper the points of interest below the water table the higher the pore pressures. This effect is illustrated in Figure 4.20.

Beal et al. (2009) noted that the groundwater and related dewatering schemes at mines can be divided into five categories:

- Category 1 - Mines excavated below the water table within permeable rocks that are hydraulically interconnected: For this category, the general mine dewatering programme can adequately reduce pressure in all pit slopes, requiring no additional localised measures to dissipate pore pressure.
- Category 2 - Mines excavated below the water table that have low permeability rock occurring in part of their walls: For this category, the rock mass may not drain fully as the water table is lowered. The rock mass to be excavated has low permeability, and effective advanced dewatering is not possible or requires a long time to be successful. This category is applicable to Venetia Mine.

- Category 3 - Mines excavated below the water table that have perched groundwater zones: In other situations, perched groundwater zones may develop at higher elevations as the main water table is lowered
- Category 4 - Mines excavated in a fractured rock mass below the water table where sub-vertical geological structures form barriers to groundwater flow: For this category, the rock mass may not drain fully because geological structures act as impediments to horizontal groundwater flow, creating compartments of trapped water with unchanged (and therefore high) pore pressure.
- Category 5 - Mines excavated above the water table where seasonal precipitation leads to perched groundwater in upper stratigraphic intervals: For this category, control of pore pressure may be required even though the open pit is entirely above the water table.

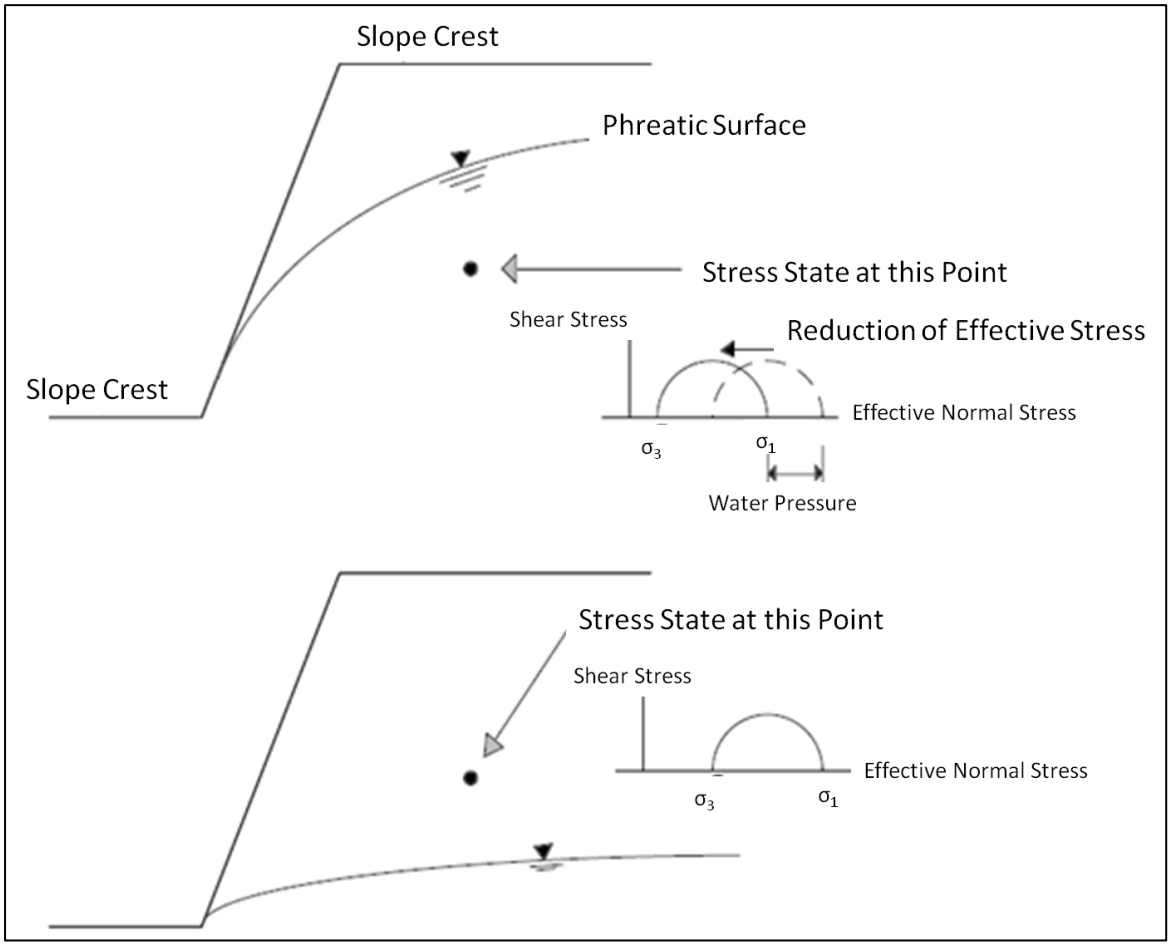


Figure 4.20 Showing the comparison of the effective stress states in a partly saturated slope and almost drained slope (Sjoberg, 1996).

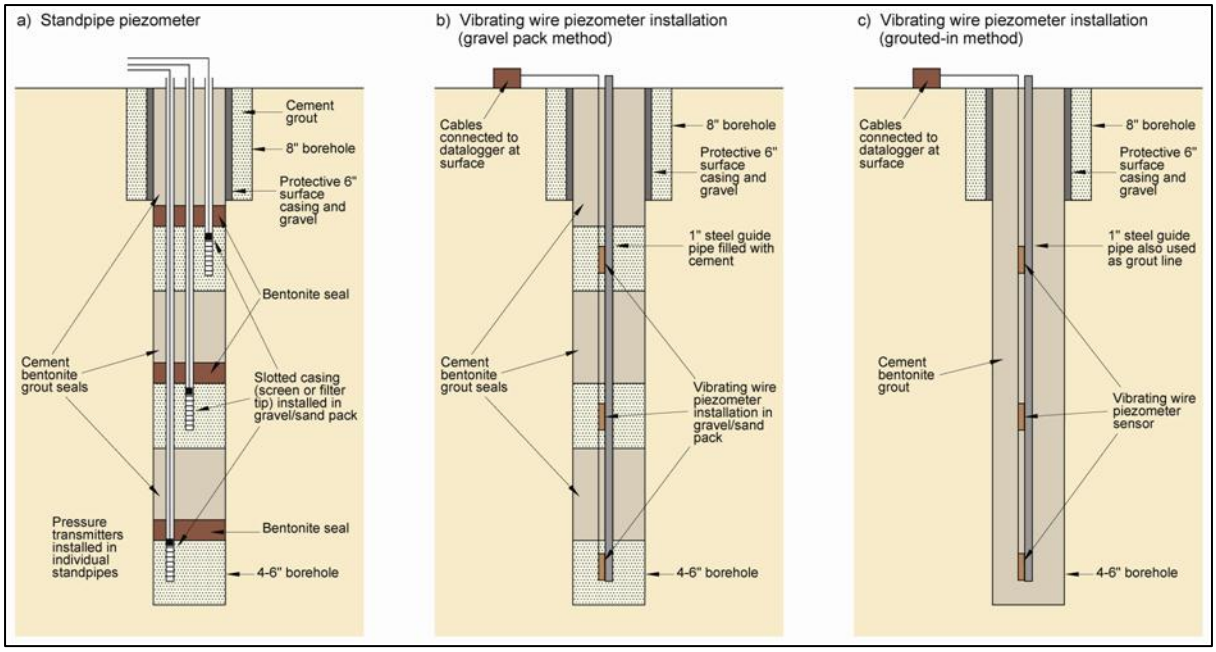


Figure 4.21 Alternate piezometer installations in core or RC drill holes (Read et al., 2009)

The measurement of groundwater pressure can be conducted using various types of piezometers ranging from standpipe to vibrating wire types. Standpipe piezometers can be used in rocks with high permeability, whereas in a closed system, an electrical piezometer is required for less permeable rocks (Hoek and Bray, 1981).

A standpipe piezometer consists of a filter tip or perforated interval of pipe of a desired length attached to the bottom of impermeable casing that extends to the surface. The level to which the water rises in the pipe is indicative of the average pressure over the perforated interval.

A vibrating-wire piezometer utilises a sensitive stainless steel diaphragm to which a vibrating-wire element is connected. Changing pressures cause the diaphragm to deflect, and this deflection is measured as a change in tension and frequency of vibration of the vibrating-wire element. See Figure 4.21.

4.7 FAILURE MECHANISMS

Traditionally open pit mining was conducted at relatively shallow depths < 500m and the design of those slopes could be divided into two distinct categories:

- The first category is for those designs that address structurally controlled failures that are kinematically controlled. This type of failure is commonly seen in slopes of up to 20 or 30 m high in hard jointed rock masses.
- 'The second category is that which includes non-structurally controlled failures in which some or all of the failure surface passes through a rock mass which has been weakened by the presence of joints or other second order structural features. An assumption commonly made is that these second order structural features are randomly or chaotically distributed and that the rock mass strength can be defined by a simple failure criterion in which 'smeared' or 'average' non-directional strength properties are assigned to the rock mass. The most common analyses are shear strength analyses that either make use of the Hoek Brown or Mohr Coulomb models. Thus only one mode of failure is considered in the design stage. This approach is frequently used for the analysis of the overall stability of large slopes where it is believed that no obvious failure mode presents itself' (Hoek et al., 2000).

Measurement of the in situ stress field in the vicinity of large slopes was seldom carried out because the impact of the in situ stress field was generally considered to be of minor significance. Although numerical analysis indicated that in situ stresses have no significant effect on the safety factor authors like Hoek et al (2000) stated that this assumption might only be adequate for small slopes and needs to be questioned for deeper slopes.

Thus limit equilibrium techniques, which do not take into account the effect of stresses, have been used with success to design shallow (<500m) rock slopes. However pit slopes are now commonly designed beyond 500m with some pits approaching 1000m. These deep slopes are entering realms where stresses are becoming significant, take longer to develop and could thus potentially also be exposed to time based strength reduction factors (Sjoberg, 2000).

4.7.1 Structurally controlled mechanisms

Structurally controlled failures follow the existing structures or defects within the rock mass and involve kinematic constraints and it is therefore necessary to have adequate knowledge of the orientation, strength and water pressure conditions in order to make sensible predictions about stability. Structural mechanisms rely heavily on field data, obtained through site investigations, where discrete structures have been identified and the extent of those features determined with accuracy. This type of analysis thus often focuses on distinct or dominant major structures that could be easily identified during a site investigation programme with second order structures (small scale) often ignored in the analysis. Thus only one mechanism at a time is considered in the analysis. The most common modes of structural failure are planar sliding, wedge sliding, and toppling (Simmons and Simpson, 2006).

4.7.1.1 Planar Failure

Planar failure occurs when a block of rock slides on a single plane dipping out of the face. There are several unique geometrical conditions for planar failure to occur:

- The plane on which sliding occurs must strike within approximately $\pm 20^{\circ}$ of the slope face.
- The dip of the plane must be less than the dip of the slope face, that is, $\psi_p < \psi_f$. Thus the sliding plane must daylight in the face.
- The dip of the sliding plane must be greater than the angle of friction of this plane, that is, $\psi_p > \varphi$. See Figure 4.22a.
- The upper end of the sliding surface either intersects the upper slope, or terminates in a tension crack.
- Release surfaces that provide negligible resistance to sliding must be present in the rock mass to define the lateral boundaries of the SLIDE™. Alternatively, failure can occur on a sliding plane passing through the convex portion of a slope (Wyllie and Mah, 2005). See Figure 4.22b.

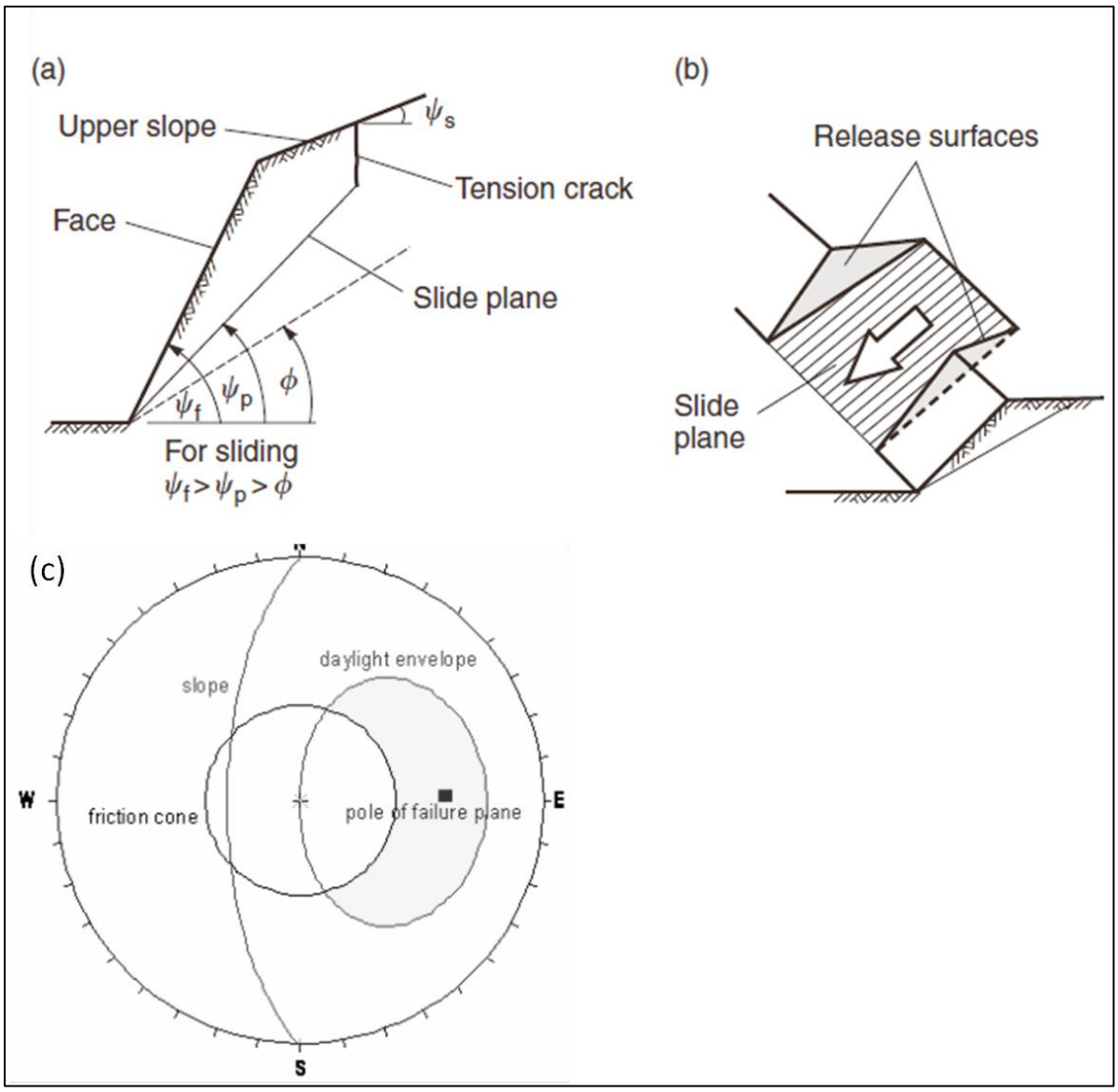


Figure 4.22 (a) The conditions for planar failure (b) Release surfaces associated with a planar failure (c) Stereographic analysis showing the kinematic condition required for kinematic failure (Modified Wyllie and Mah, 2005).

4.7.1.2 Wedge failure

Wedge failures can over a far wider range of geological and geometrical conditions than planar failure and occur where at least two continuous structures intersect and their line of intersection daylights in the rock face.

The following kinematic conditions are required to generate a wedge:

- As previously mentioned The line of intersection (ψ_i) must be flatter than the dip of the face (ψ_{fi}) but also steeper than the average friction angle (φ) of the two slide planes, that is $\psi_{fi} > \psi_i > \varphi$ (Wyllie and Mah, 2005).
- Structures included in the wedge analyses should strike at angles greater than 20° to the strike of the bench face (Lorig et al., 2009). See Figure 4.23.

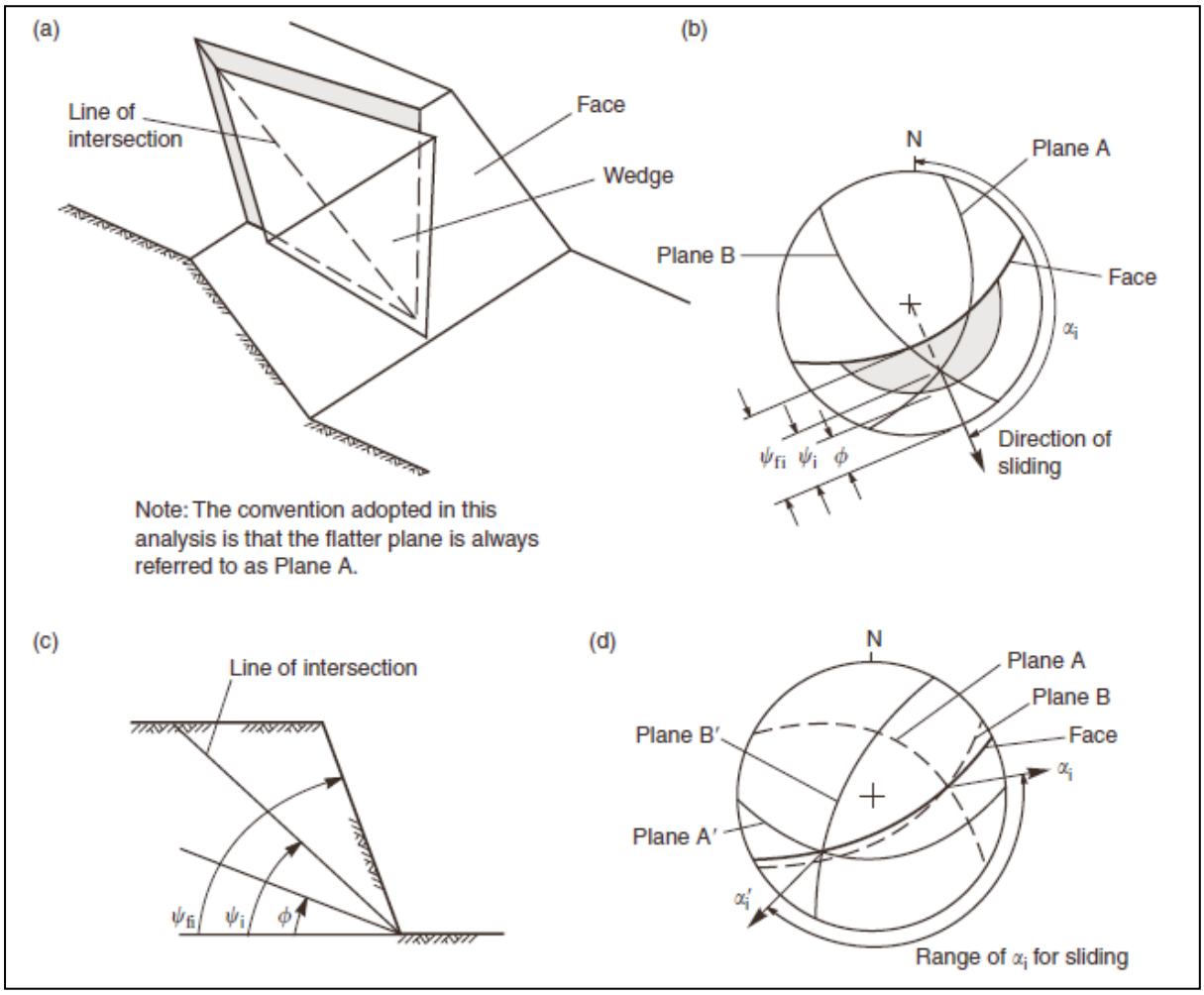


Figure 4.23 (a) Typical wedge with line of intersection (b) Kinematic condition for wedge failure to occur illustrated on a stereonet (c) Kinematic conditions for wedge failure shown in section (d) Stereonet demonstrating the limit of wedge failure in relation to the strike of a slope, estimated at 20° (After Wyllie and Mah, 2005).

4.7.1.3 Toppling Failure

According to Goodman and Bray (1976) and Wyllie and Mah (2005) toppling failures can be divided into four types:

- Block Toppling: Block toppling occurs when, in strong rock, individual columns are formed by a set of discontinuities dipping steeply into the face, and a second set of widely spaced orthogonal joints defines the column height. The short columns forming the toe of the slope are pushed forward by the loads from the longer overturning columns behind, and this sliding of the toe allows further toppling to develop higher up the slope. Typical geological conditions in which this type of failure may occur are bedded sandstone and columnar basalt in which orthogonal jointing is well developed.
- Flexural Toppling: Occurs where continuous columns of rock, separated by well developed, steeply dipping discontinuities, breaking in flexure as they bend forward. Typical geological conditions in which this type of failure may occur are thinly bedded shale and slate in which orthogonal jointing is not well developed.
- Block-Flexural Toppling: Toppling of columns in this case results from accumulated displacements on the cross-joints.
- Secondary toppling modes: In general, these types of failures are initiated by undercutting of the toe of the slope, either by natural mechanisms such as weathering, or by human activities. See Figure 4.24.

Goodman and Bray (1976) postulated that toppling failure will occur if the below conditions are met

- Condition 1: $(90^\circ - \psi_f) + \varphi_j < \psi_p$ [4.27]

  ψ_f = Dip of face (Proposed Stack Angle)

  φ_j = Friction angle of joint (Base Friction Angle of Foliation from Lab Testing)

  ψ_p = Dip of plane/joint

- Condition 2: The discontinuity dips into the face and strikes parallel or within 30° of the strike of the slope face.

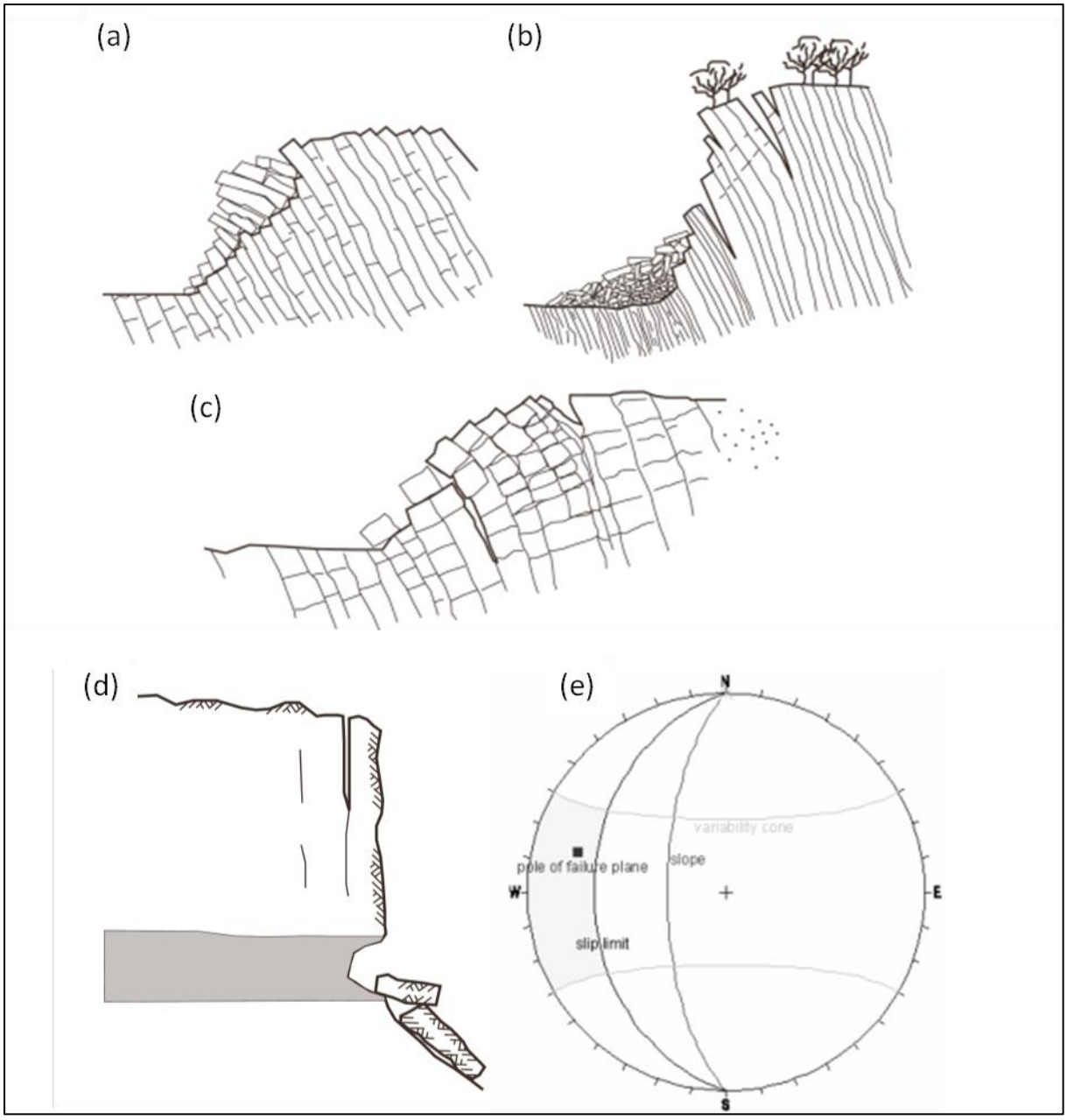


Figure 4.24 (a) Block Toppling (b) Flexural Topping (c) Block-Flexural Toppling (d) Secondary Toppling (e) Stereographic projection showing the kinematic conditions required for toppling (Modified from Wyllie and Mah, 2005).

4.7.2 Rock mass (Circular) failure mechanisms

Rock mass failures are known to develop in either soil, weathered rock masses or highly jointed rock masses where shearing of rock bridges occur. A characteristic circular shear surface is usually developed, and observed, in the event of failure in these rocks, and most stability theories are based upon this observation (Wyllie and Mah, 2005). Analysis for circular shear failure is frequently conducted using limit equilibrium or numerical modelling tools. Factors of safety calculated with limit equilibrium and numerical tools compare very well although differences in final slip surfaces have been observed by Sjoberg (2000). See Figure 4.25.

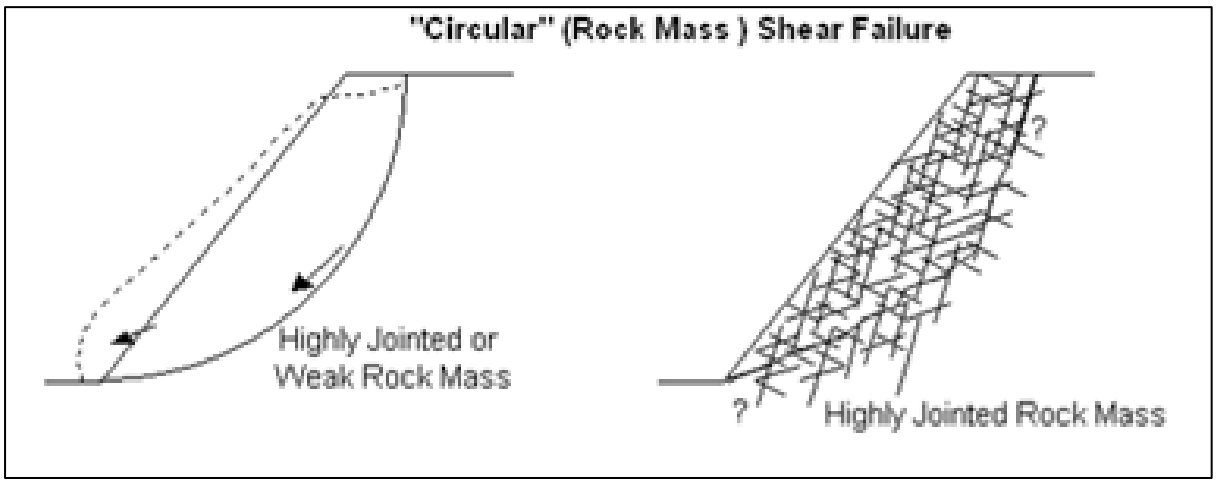


Figure 4.25 Rock Mass or Circular Shear Failure Mechanisms (after Sjoberg, 2000).

4.7.3 Combination of failure mechanisms

Various authors have noted the occurrence of complex failure mechanisms where more than one mechanism is present within the slope or slope failure (Hoek et al, 2000; Sjoberg, 2000; Dight, 2006). Examples include case studies where failures are clearly defined by faults at the back and on the upper portions of the failure. However towards the bottom of the failure no structural definition exists, See Figure 4.26. The following mechanisms could be present within this complex failure, these include:

- Failure on a major structure, direct shear strength model applicable.

- The Hoek-Brown failure criterion, for the central part of the failure and for the rock bridges in the step-path surface at the toe of the slope and
- Failure on existing joints forming the step path at the toe of the slope and thus Barton-Bandis failure criterion (Hoek et al., 2000). See Figure 4.26.

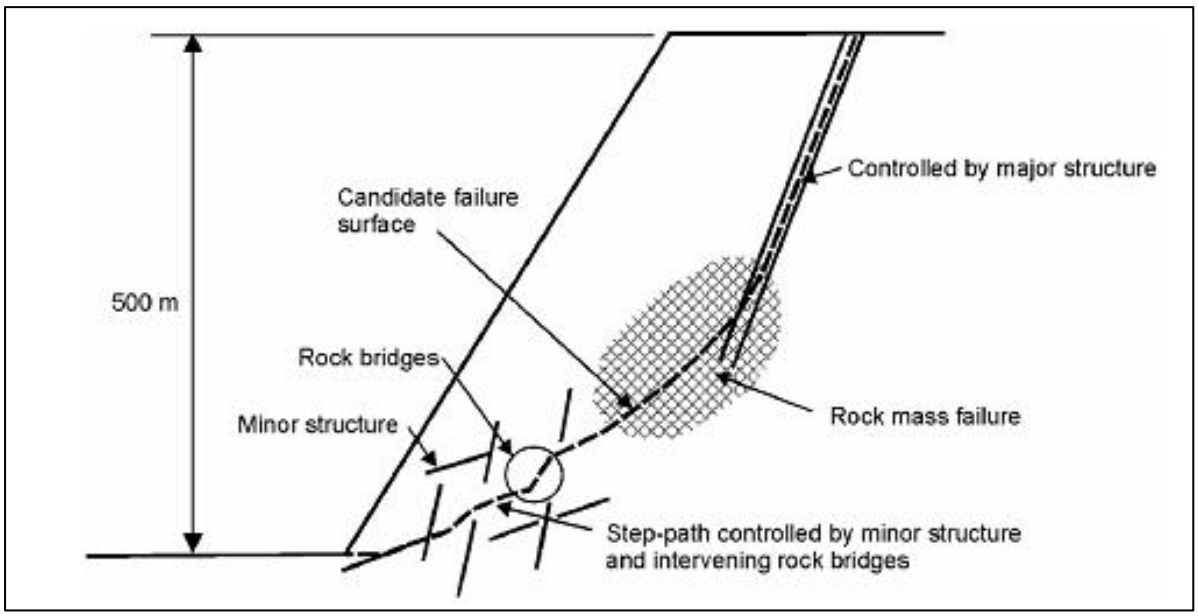


Figure 4.26 Theoretical complex failure (after Hoek et al., 2000).

4.7.4 Failure mechanisms and scale effects

Hoek and Karzulovic (2000) noted the effect of scale and the limitations of applying the Hoek-Brown criterion to slope stability problems. Karzulovic (2006) noted how this effect of scale can impact on the blockiness of the rockmass and associated failure modes and described three modes of failure related to scale:

- Structurally controlled failures: Rupture occurs only through structures. This is the case for planar and wedge SLIDEs, which are most likely to occur at bench and inter-ramp scale. In this case the strength of the structures is the most important parameter to assess the stability of the slopes.
- Failure with partial structural control: Rupture occurs partly through the rock mass and partly through the structures. This case usually occurs at inter-ramp and overall scale in rock masses with one structural set dipping towards the slope and/or where the failure surface is partially defined by a larger structure. In this case the strength of

the rock mass and the structures are both important to assess the stability of the slopes.

- Failure without structural control: Rupture occurs through the rock mass and is not affected by structures. This can occur at inter-ramp or overall slope scale in very fractured/very weak rock masses. In this case the strength of the rock mass is the most important parameter to assess the stability of the slopes. See Figure 4.27.

The above observation relates to the acceptance criteria and slope design practice where three (3) scales of design are considered: bench, inter-ramp and overall slope.

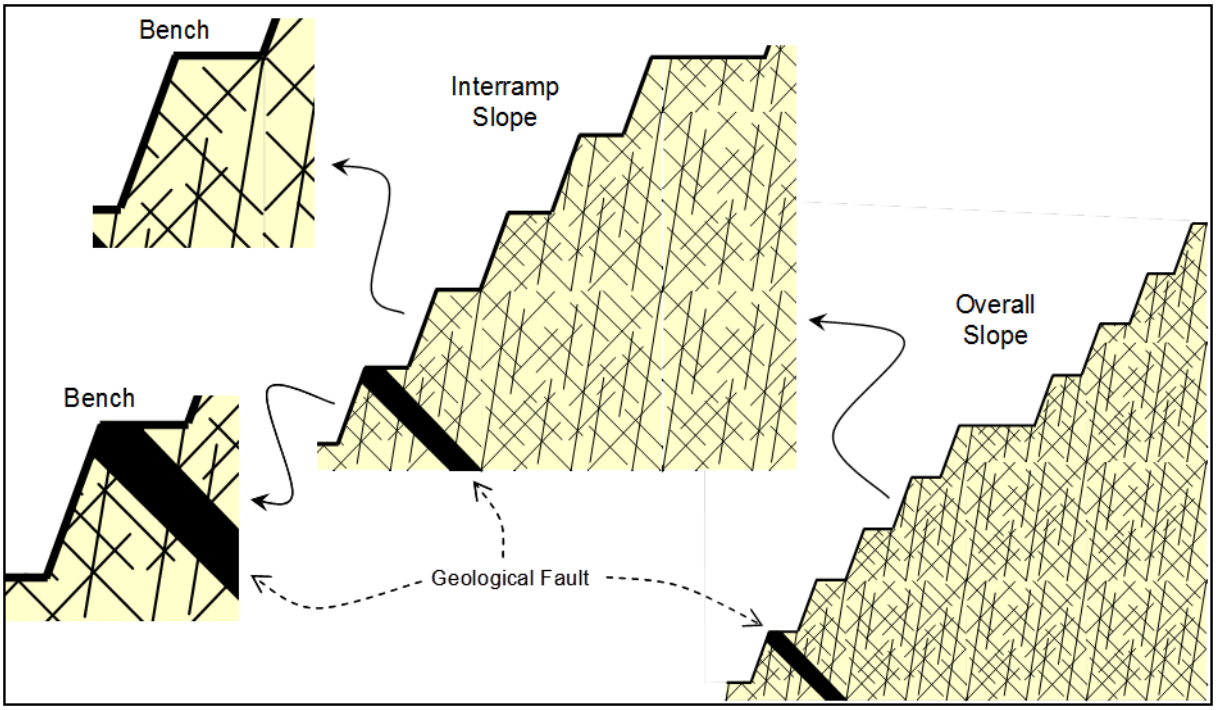


Figure 4.27 Illustrating how the blockiness of the rock mass depends on the size of the rock slope: very blocky for the overall slope, blocky for the inter-ramp slope, and almost massive at the bench scale (Karzulovic, 2006).

4.8 SLOPE DESIGN ELEMENTS AND TECHNIQUES

4.8.1 Bench Scale

Benches must be wide enough to retain possible hazardous rock falls. In hard rock operations where the stability is structurally controlled the bench design is the first stage in the slope design process, followed by the inter-ramp and overall slope analysis (Lorig et al., 2009).

Bench heights in large mining operations are typically 12m to 15m and the height is controlled by the available mining equipment that is used to drill, blast and load the bench (Ryan and Prior, 2000). There is a direct trigonometric relationship between the bench face angle (BFA) and remaining catch berm width (W). Thus only references to catch berm widths are made in this project. The maximum achievable bench face angle and related catch berm width determines the maximum inter-ramp angle. See Figure 4.28; Equations 4.28 and 4.29.

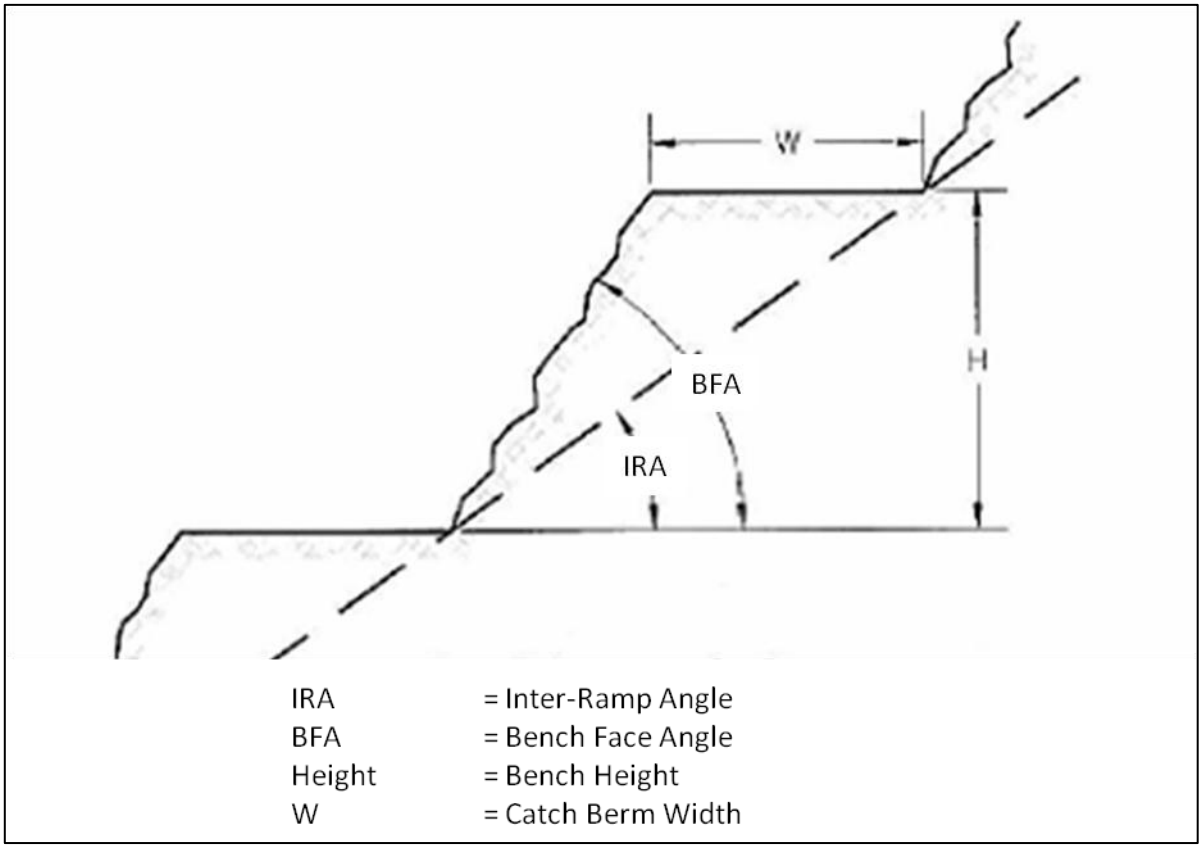


Figure 4.28 The relationship between Bench Face Angle/Catch berm Width and Inter-ramp Angle after Ryan and Prior (2000).

$$W = \frac{H}{\tan(IRA)} - \frac{H}{\tan(BFA)} \quad [4.28]$$

$$IRA = tan^{-1}(\frac{H}{W+HcotB}) \quad [4.29]$$

The catch berm width is controlled (See Figure 4.29) by the stability of joints and faults that intersect the bench. The stability of the structures is in turn influenced by:

- The orientation of the bench in relation to the structures.
- Blasting and related energies.
- Mechanical undercutting during loading and hauling operations.

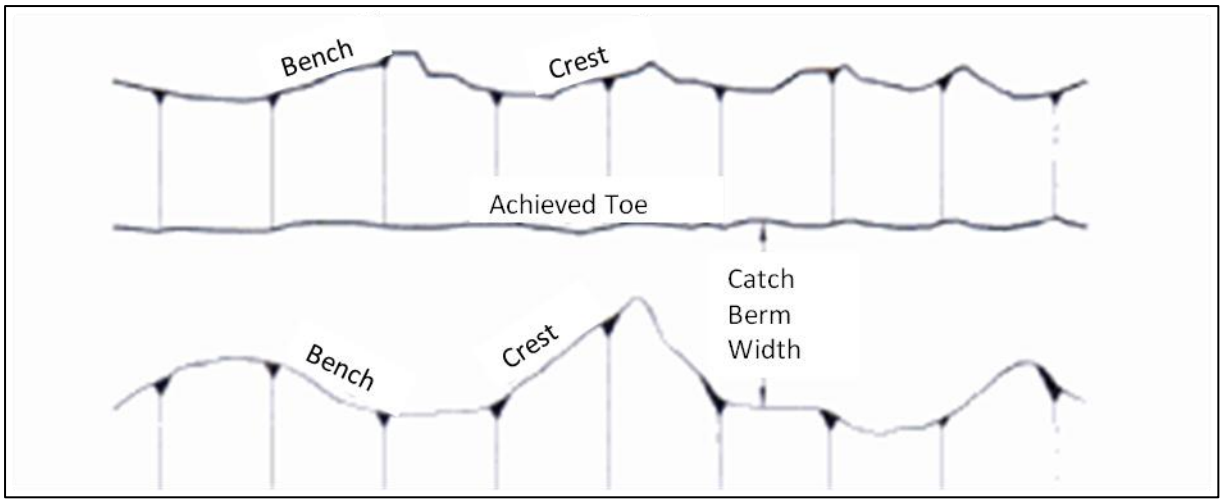


Figure 4.29 Plan view of a catch berm width as defined by Ryan and Prior (2000) showing the crest and toe.

The Modified Ritchie Criterion, developed by Call and Nicholas Inc. is often used to define the minimum catch berm width (Ryan and Prior, 2000). See Equation 4.30.

$$\text{bench width (m)} = 0.2 * \text{ bench height} + 4.5 \text{ m} \quad [4.30]$$

However Ryan and Prior (2000) have found that the problem is too complex for the application of a single criterion and that application of the Modified Ritchie Criterion results in very conservative catch berms. Instead a reliability approach was favoured by the authors.

Lorig et al. (2009) noted that it's neither practical nor economical to design benches to contain the spillage from every sliding plane or wedge failure. Instead, the limit is defined as the failed volume that can reasonably be contained on the bench.

Usually, this is 70–85% of the potential failed volumes. When calculating the failed volumes, structures included in the wedge analyses should strike at angles greater than 20° to the strike of the bench face. Planar failure structures should strike at angles of less than 20° to the strike of the bench face. Due to the low stresses involved and blast damage the cohesions of structures are often ignored in bench analysis (Lorig et al., 2009)

SWISA™ (wedge failure) and PFISA™ (planar failure) software developed by Itasca is based on the statistical analysis of the interaction between structures and the application of a catchment criterion to decide the appropriate bench geometry. The main characteristics of the SWISA™/PFISA™ analysis are the identification of unstable wedges/planes, the construction of cumulative distribution curves for the unstable volume and other geometrical parameters and the calculation of berm widths based on a comparison between the spill length of the critical volume and the catchment criterion (Itasca, 2011).

Although other commercially available software can also fulfil this functionality SWISA™/PFISA™ automates the process and uses the following basic data and their statistical information (average, standard deviation, maximum and minimum values) of:

- Wall orientation
- Joint sets (dip and dip direction)
- Bench face angle
- Bench height
- Cohesion and friction angle for the joints
- Unit weight of the rock

SWISA™/PFISA™ uses the spill width formula as described by Gibson et al. (2006). This method does not take into account the geometry of the wedge and therefore tends to overestimate the spill berm widths required (Gibson et al., 2006). See Equation 4.31 and Figure 4.30.

$$R = \sqrt[3]{\frac{6KV}{\pi}}\, x\, \frac{tan\alpha - tan\varphi}{tan\varphi . tan\alpha} \qquad [4.31]$$

V = volume of the failed material (m^3)

K = bulking factor (varying from 1.38 to 1.5)

α = bench face angle (°)

φ = angle of repose of the failed material (normally 38°) (Gibson et al., 2006)

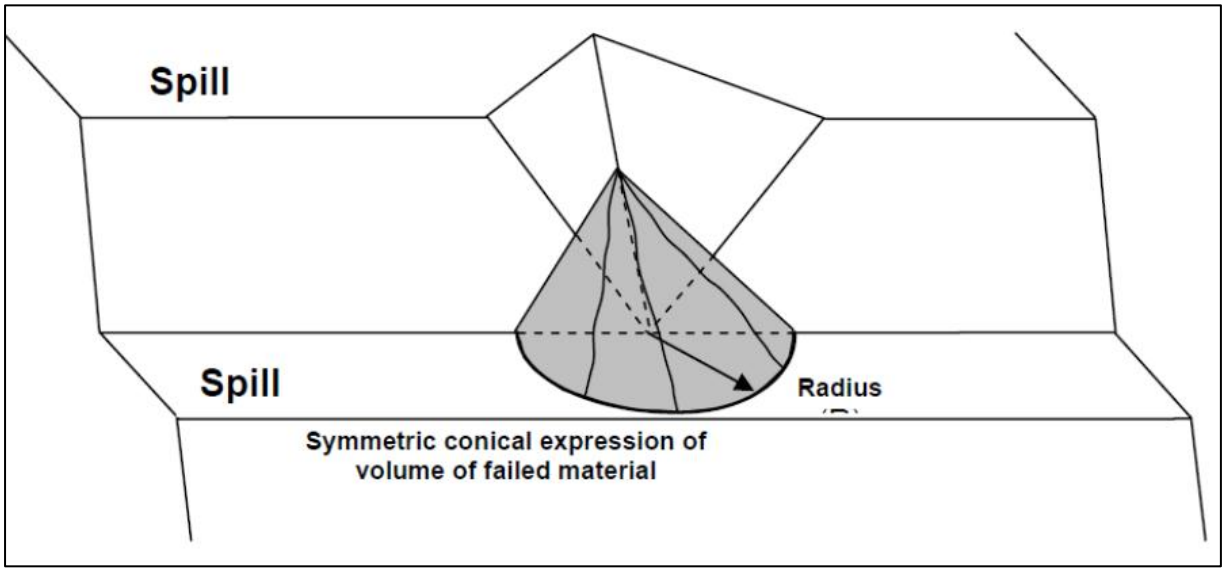


Figure 4.30 Illustration of symmetric conical distribution of failed material on a spill berm (Gibson et al., 2006).

4.8.2 Inter-ramp and Overall Slope Design and Methods

4.8.2.1Application of Slope Stability Analysis Techniques

The same kinematic techniques applied to bench analyses can be applied to an inter-ramp analysis but because of the greater heights inherent to inter-ramp slopes there is the possibility of more complex failure modes. The slope stability analysis technique will also depend on the complexity of the failure mechanism with numerical and hybrid/discrete modelling techniques being more applicable to complex failure mechanisms. Limit Equilibrium techniques are in turn applicable to situations where simple failure modes are assumed. (Stead et. al. 2006). See Figure 4.31.

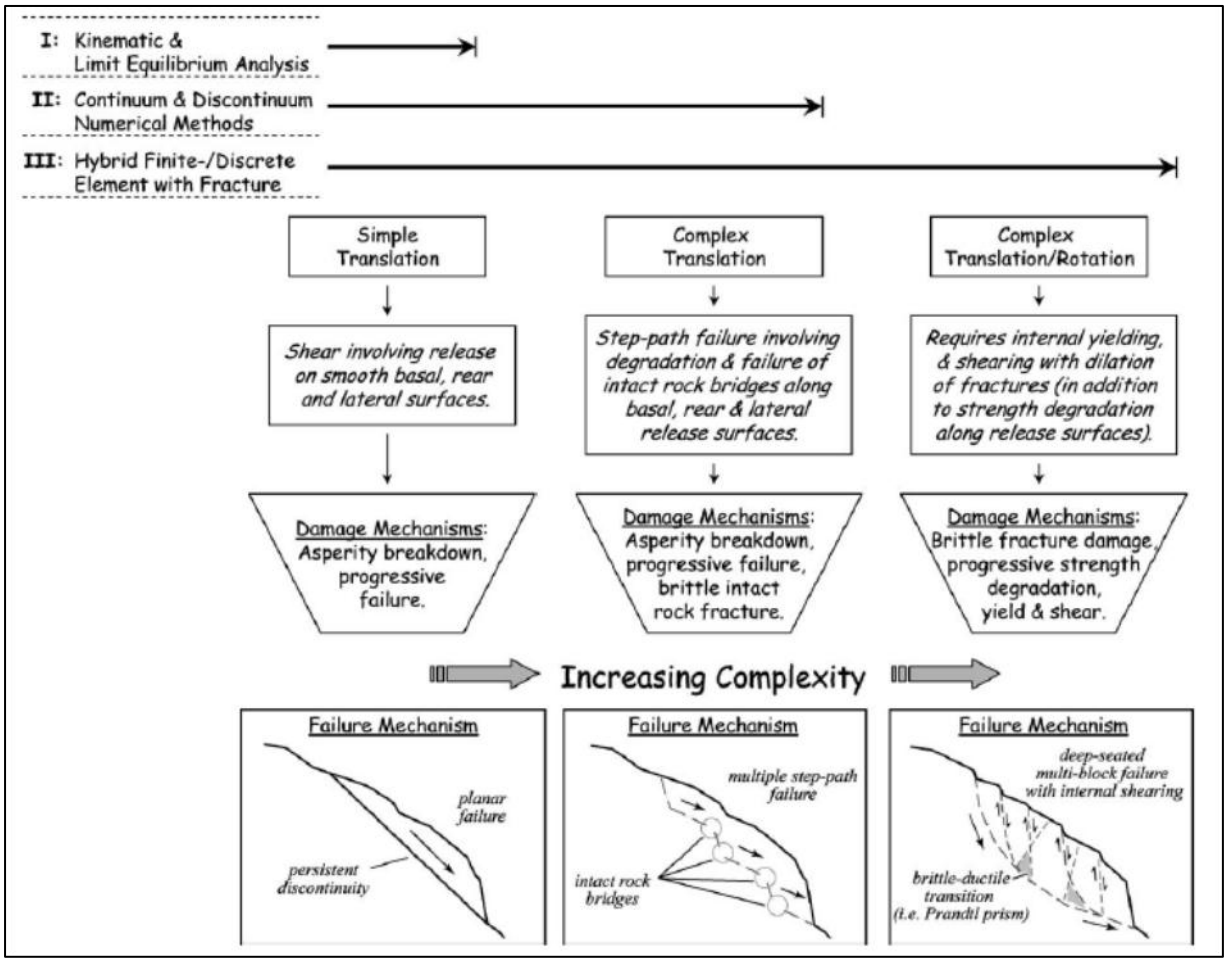


Figure 4.31 The relationship between the complexity of failure mechanisms and analysis techniques (Stead et al., 2006).

Lorig et al. (2009) described the most applicable analysis tools for each stage of a study. Empirical techniques are mainly limited to pre-feasibility studies and provide a good idea of initial slope angles that can be achieved in a rock mass. Limit Equilibrium techniques can be applied from the Pre-feasibility to Operations phase of a project or mine. See Table 4.10.

Table 4.10 Various stability analysis techniques applicable to each stage of a project (Lorig et al., 2009).

Method of stability analysis	Level 1: Conceptual	Level 2: Pre-feasibility	Level 3: Feasibility	Level 4: Design and Construction	Level 5: Operations
Empirical	¤	¤			
Limit equilibrium		¤	¤	¤	¤
Continuum and discontinuum numerical models			¤	¤	¤
Advanced numerical models			?	?¤	?¤

4.8.2.2 Stereographical and Empirical Estimates

The first step in any stability investigation is a detailed investigation of the rockmass and structure. Kinematic/Stereographical analyses are useful to determine whether the orientation of a specific discontinuity in relation to a pit wall can lead to instability by using friction cones, daylight and toppling envelopes. This technique primarily considers the orientation of a discontinuity and ignores important properties such as joint strength and groundwater. The stereographical techniques for the analysis of potential wedge, planar and toppling failure is given in Section 4.7.1.

Rock mass rating data are often available during the early stages of a project and can be collected with ease from drill core. One of the most widely used empirical techniques is that of Haines and Terbrugge (1991). The technique uses the MRMR as defined by Laubscher (1990) and the corresponding slope height to derive slope angles at various factors of safety. The technique also clearly specifies the limitations and areas where additional analyses are required over and above empirical estimates. See Figure 4.32.

Empirical and Stereographic techniques are usually only used up to the Pre-feasibility stage of a project or in the initial stages of an investigation study (Lorig et al., 2009).

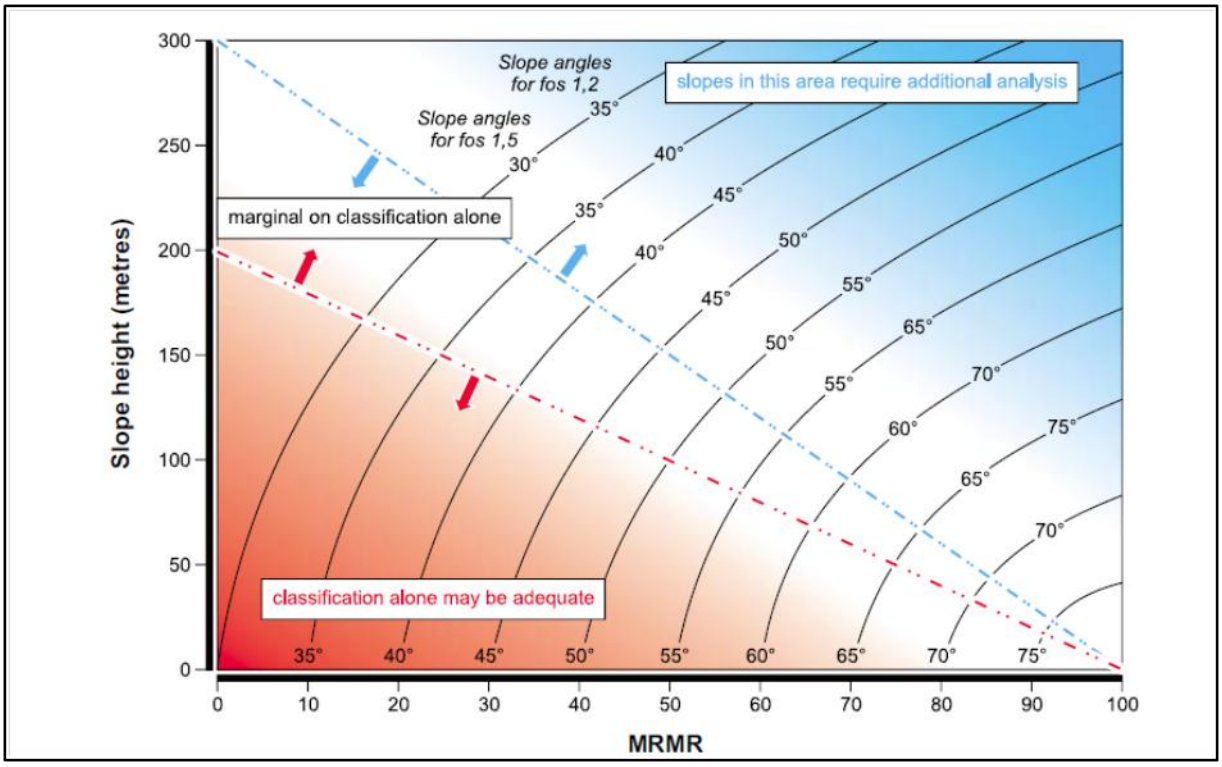


Figure 4.32 The Haines and Terbrugge (1991) chart for estimating slope angles using the MRMR.

4.8.2.3 Limit Equilibrium

Limit Equilibrium methods are particularly suited to translational failures where basal shear, lateral and rear release all take place on persistent structural features. Limit equilibrium methods have been well adapted to slope stability problems in jointed rock masses (Lorig, et, al., 2009) and the use of limit equilibrium methods still remains the most common adopted solution method in surface rock engineering although in many cases, major rock slope instabilities often involve complex internal deformation and fracturing (Stead et al., 2006). See Figure 4.31. The effect of joint persistence has been recognised early on. For example to account for a non-persistent failure plane, Terzaghi (1962) included an effective cohesion along the shear surface to allow for the increased resistance to shear failure provided by intact rock bridges. Thus methods that do not consider this phenomenon will derive more conservative results.

Limit Equilibrium methods are conservative in terms of their stability (both FOS and POF) estimates since they ignore complex mechanisms of rockmass failure and do not include

parameters, like dilatation angle, that tends to lead to greater stability (Chiwaye and Stacey, 2010).

Only three limit equilibrium methods satisfy force (x and y) and moment equilibrium, these are Bishop's rigorous, Spencer's and Morgenstern-Price. For hard rock slope stability, the preferred solution techniques are those of Spencer, Morgenstern and Price and Janbu, because they can model irregular failure surfaces (Lorig et al., 2009). See Table 4.11.

All of the complete equilibrium procedures (Spencer, Morgenstern and Price) of slices have been shown to give very similar values for the factor of safety. Thus, no complete equilibrium procedure is significantly more or less accurate than another. Spencer's procedure is the simplest of the complete equilibrium procedures for calculating the factor of safety (Duncan and Wright, 2005).

Table 4.11 Showing the various limit equilibrium methods and their final equilibrium states (Curran, 2007).

Method	**Force Equilibrium**		**Moment Equilibrium**
	x	***y***	
Ordinary	No	No	Yes
Bishop's simplified	Yes	No	Yes
Janbu's simplified	Yes	Yes	No
Lowe and Karafiath's	Yes	Yes	No
Corps of Engineers	Yes	Yes	No
Spencer's	Yes	Yes	Yes
Bishop's rigorous	Yes	Yes	Yes
Janbu's generalized	Yes	Yes	No
Morgenstern-Price	Yes	Yes	Yes

4.8.2.4 Numerical Techniques

Numerical analysis for slope stability problems can be divided into three categories:

- Continuum modelling
- Discontinuum modelling
- Hybrid modelling

Only Continuum and Discontinuum modelling will be discussed for the purpose of this project. See Table 4.12.

Table 4.12 The advantages and limitations of numerical modelling techniques (Stead et al., 2001).

Analysis method	Critical input parameters	Advantages	Limitations
Continuum modelling (e.g., finite element, finite difference)	Representative slope geometry; constitutive criteria (e.g., elastic, elasto-plastic, creep, etc.); groundwater characteristics; shear strength of surfaces; in situ stress state.	Allows for material deformation and failure. Can model complex behaviour and mechanisms. Capability of 3-D modelling. Can model effects of groundwater and pore pressures. Able to assess effects of parameter variations on instability. Recent advances in computing hardware allow complex models to be solved on PC's with reasonable run times. Can incorporate creep deformation. Can incorporate dynamic analysis.	Users must be well trained, experienced and observe good modelling practice. Need to be aware of model/software limitations (e.g. boundary effects, mesh aspect ratios, symmetry, hardware memory restrictions). Availability of input data generally poor. Required input parameters not routinely measured. Inability to model effects of highly jointed rock. Can be difficult to perform sensitivity analysis due to run time constraints.
Discontinuum modelling (e.g., distinct element, DDA)	Representative slope and discontinuity geometry; intact constitutive criteria; discontinuity stiffness and shear strength; groundwater characteristics; in situ stress state.	Allows for block deformation and movement of blocks relative to each other. Can model complex behaviour and mechanisms (combined material and discontinuity behaviour coupled with hydro-mechanical and dynamic analysis). Able to assess effects of parameter variations on instability.	As above, experienced user required to observe good modelling practice. General limitations similar to those listed above. Need to be aware of scale effects. Need to simulate representative discontinuity geometry (spacing, persistence, etc.). Limited data on joint properties available (e.g. jkn, jks).

Continuum modelling is best suited for the analysis of slopes that are comprised of massive, intact rock, weak rocks, and soil-like or heavily fractured rock masses. Most continuum codes incorporate a facility for including discrete fractures such as faults and bedding planes but are inappropriate for the analysis of blocky mediums. The continuum approaches used in rock

slope stability include the finite-difference (FLAC™) and finite-element methods (Phase2™).

Discontinuum methods treat the rock slope as a discontinuous rock mass by considering it as an assemblage of rigid or deformable blocks. The discontinuum analysis includes sliding along and opening/closure of rock discontinuities controlled principally by the joint normal and joint shear stiffness (Stead et al., 2001). Discontinuum codes require extensive knowledge of the rockmass and if utilized, it is essential that rigorous characterization of the rock mass be undertaken, particularly emphasising the discontinuity geometry with respect to the rock slope. Block size variation, joint persistence and joint spacing should be ascertained in order to constrain the discontinuum model input. This requires a further level of sophistication rarely carried out in most field mapping campaigns (Stead et al., 2006).

4.9 BLASTING

4.9.1 Blasting Techniques

Rock breaking or blasting by nature is a destructive process and if not controlled will lead to a significant amount of Rock Engineering related challenges. It is thus critical that Rock Engineering practitioners be involved in blasting operations and that they work with blasting practitioners on the selection and application of blasting techniques.

Large open pit mines depend on economies of scale to meet their business targets. Consequently, the trend in large open pit mining has been towards high energy blasting (production blasting) to increase downstream comminution and excavation performance coupled with large equipment that is capable of high levels of productivity. This increase in energy, defined by powder factor (See Equation 4.32), and rate of productivity threaten the integrity of the pit walls (Williams et al., 2009). Final wall controlled blasting techniques, also known as limit drilling and blasting, usually require smaller spaced drilling patterns and specialised charging techniques which inevitably lead to lower production volumes. Thus there is a constant trade-off between optimising blasting for fragmentation while limiting the damage to the highwalls. See Figure 4.33.

$$\text{Powder factor} = W_{ex} / V \qquad [4.32]$$

Where:

Weight of explosive per hole, W_{ex} = (diameter of explosive) × (unit weight of explosive) × (bench height − stemming length + sub-drill depth)

Volume of rock per hole, V = (bench height) × (burden) × (spacing)

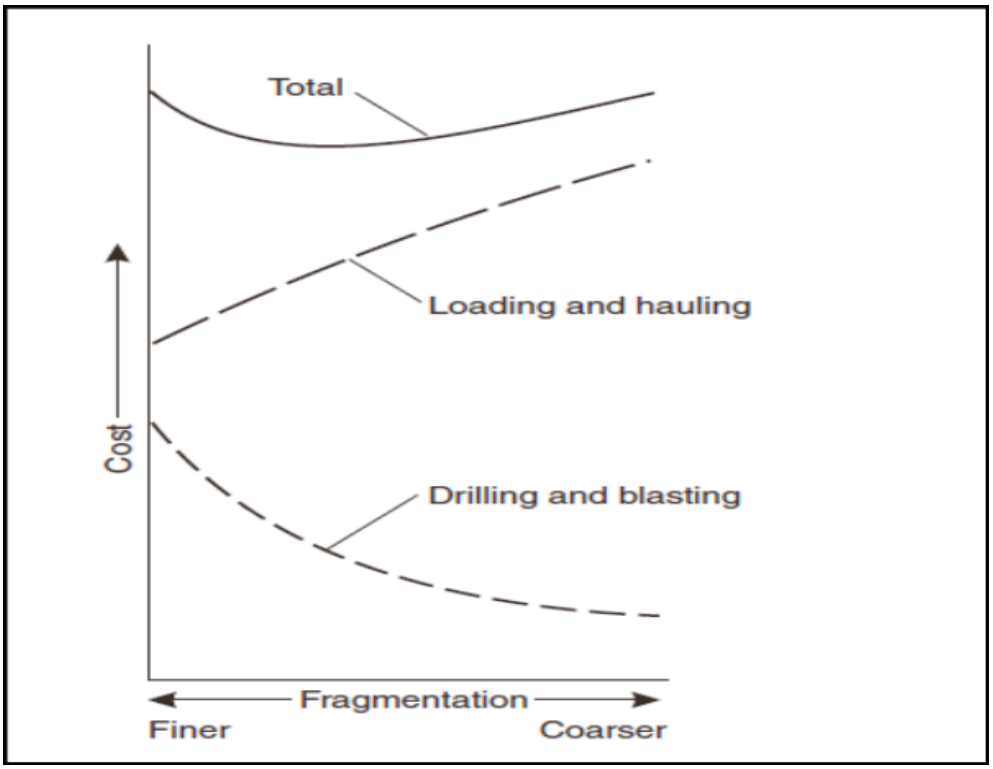


Figure 4.33 Demonstrating the economies of scale concept and the production benefit of improving fragmentation (Wyllie and Mah, 2005).

Three types of blasting are done at Venetia, these are:

- **Production blasting:** The main aim of this method is to break material in large volumes for extraction. In this type of blast the fragmentation of the rock is a key design objective and higher energies are generated when compared to limit blasting. Wider burden, spacing and powder factors are associated with this method.
- **Secondary blasting:** The main aim of this method is to break coarse blasted rock that could otherwise not be effectively loaded/ removed from the pit.

- **Limit Blasting:** This consists of Trim and Pre-split blasting of which the primary objective is to ensure a stable slope and minimise the occurrence of rock falls. Trim blasts are taken at the pit limits and have a reduced charge when compared to a production blast which helps to minimize the energy that is directed back into the sidewall. A trim blast pattern at Venetia typically consists of production holes and buffer holes. A typical Limit blast design is shown in Figure 4.34. Pre-split blasts are taken on the design limit and prevent the gases and compressive energy from the trim blast from moving into and disturbing the rock mass that will make up the future pit slope. A pre-split pattern consists of a single line of evenly spaced holes drilled on the final design limit and should be taken before the trim is blasted.

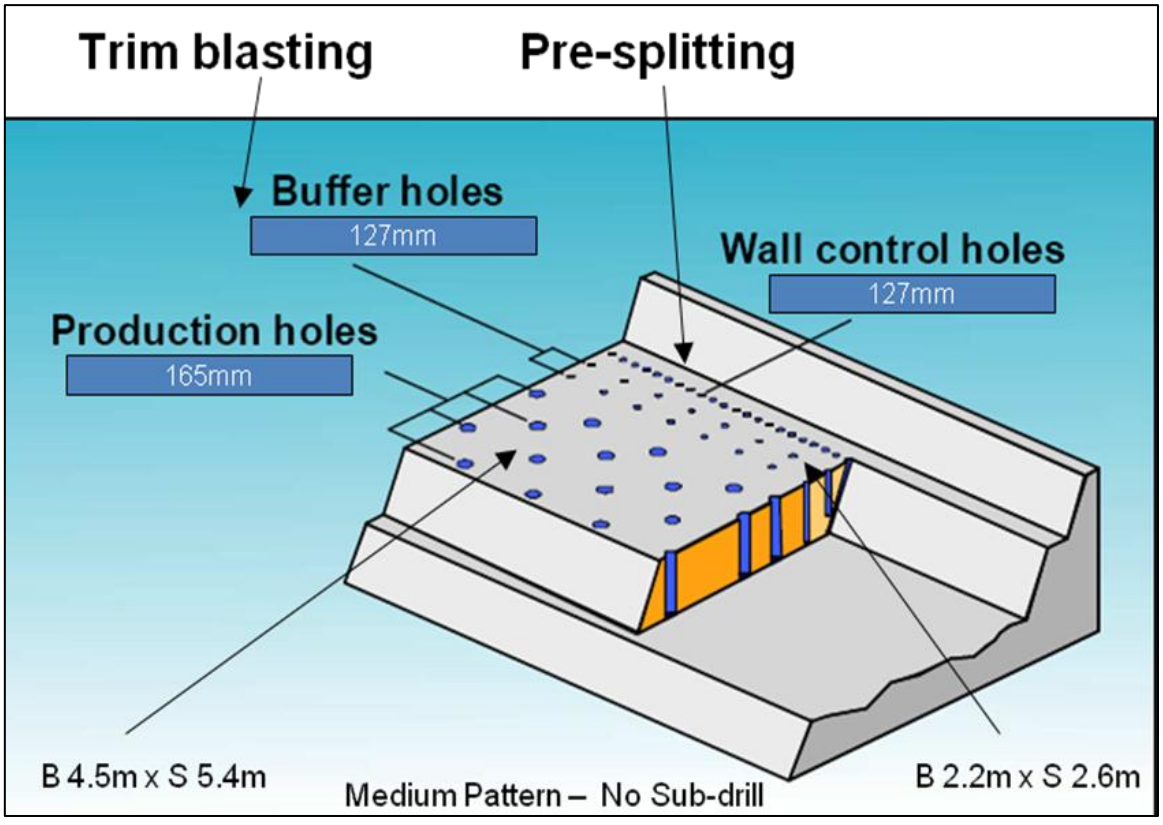


Figure 4.34 Showing a typical limit and pre-split drilling pattern. A trim blast at Venetia consists of production and buffer holes.

4.9.2 Theoretical Blasting Damage Mechanism

As stated initially blasting by nature is destructive and the rock is fractured by using explosives. If not controlled and applied correctly this could decrease slope stability.

"The blast damage mechanisms that cause reduction in slope stability can be categorized into near and far field effects. In the near field (less than 50 metres from the charge), shock, crack extension, gas related displacement and tensile failure are the major contributors to rockmass damage. In the far field (greater than 50 metres from the blast), the damage that results from blasting is mainly shear strength reduction and ravelling of loose material that eventually fills up the catch berms." (Williams et al., 2009)

Various authors (Williams et al., 2009), Wyllie and Mah (2005) and Brady and Brown (2004), have attempted to summarise the blasting damage mechanisms. The blasting damage mechanism as described by Williams et al. (2009) is given below in Table 4.13.

Table 4.13 The Blast Damage Mechanism after Williams et al. (2009).

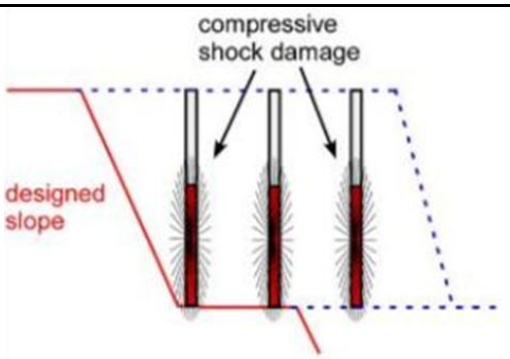
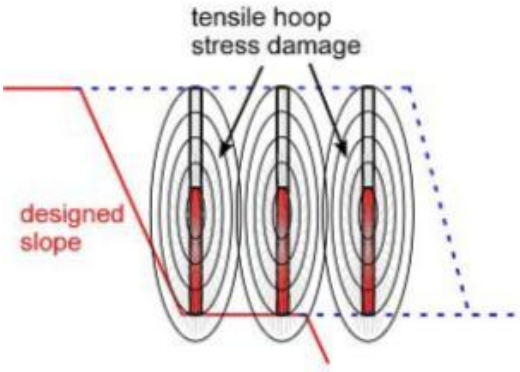
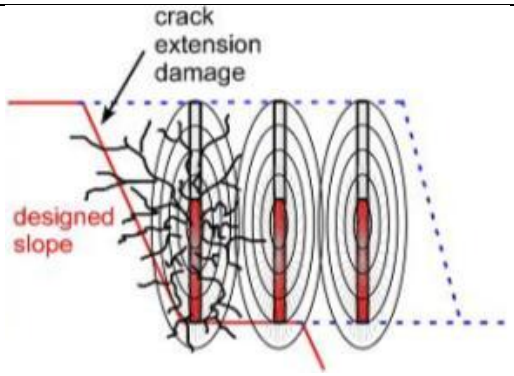
Phase 1 – Detonation and Crushing The explosive detonates and is quickly converted into a high temperature/pressure gas. The explosive column is consumed within 2 milliseconds, expands approximately 1000 times and generates theoretical borehole pressures in excess of 2000 MPa. Immediately around the blast hole, the high detonation pressures propagate a shock wave into the rock mass. The pressure of this initial shockwave is much greater than the strength and generates a zone of crushed rock two to three charge diameters in size.	
Phase 2 – Strain induced tensile failure Crushing and expansion of the blast hole reduces the pressure and the shock wave to a strain pulse. The strain pulse propagates through the rockmass at a rate equal to the P-wave or seismic velocity, compresses the rock radially which results in tangential tension or hoop stress. If the tangential tension is greater than the tensile strength of the rock, fractures are created (typically 20 to 30 charge diameters) that extend radially in all directions When the strain pulse reaches a rock/air interface (such as an open joint), the pulse is reflected back in tension and once again, if the tension is greater than the tensile strength of the rock, spalling occurs. Tensile fracturing and spalling relieves the stress within the rockmass to the point where new fractures from shock are not created.	

Table 4.13 Continuous

Phase 3 – Crack Expansion Damage

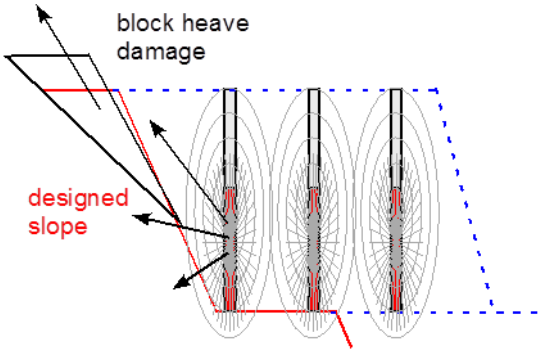
High pressure gases expand and penetrate into the rockmass. High pressure gases wedge into existing cracks and cause them to expand. As the cracks expand, they intersect with other cracks and produce a significant portion of the fragmentation. The envelope of damage created during tensile failure and crack extension is generally thought to be 20 to 30 charge diameters depending on the strength of the rock, explosives used and degree of confinement.



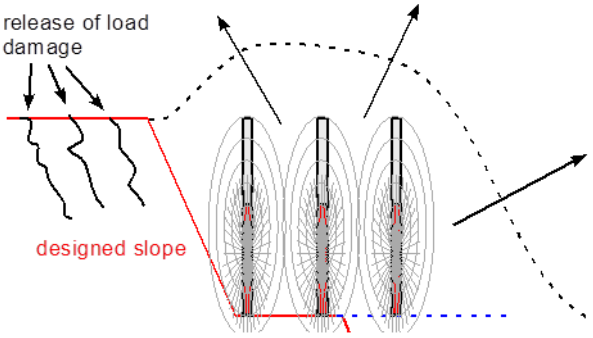
Phase 4 – Gas Penetration

Gas pressure bends and breaks the rockmass (flexural rupture) toward the path of least resistance. This can occur in any direction and can lead to excessive overbreak if relief away from the slope is not provided. In addition, if weak, adversely orientated discontinuities exist in the batter face, the expansion of gases can cause block heave beyond the designed slope. As the gases expand they also apply a load to the slope that is released as the blasted rockmass swells. If the initial load placed on the slope is excessive due to over confinement, tensile failure can occur well beyond the designed limit.

Block heave slope damage



Release of load damage



4.9.3 Incorporation of Blast Damage into Slope Designs

Blast damage results in a loss of rock mass strength due to the creation of new fractures and the wedging open of existing fractures by the penetration of explosive gasses (Hoek, 2000). The most widely used method to account for blast damage and or disturbance is called the D factor. The disturbance factor D was introduced by Hoek et al. (2002) and there is not a great deal of experience on its use (Hoek and Diederichs, 2006). D is a factor which depends upon the degree of disturbance to which the rock mass has been subjected by blast damage and

stress relaxation. It varies from 0 for undisturbed in situ rock masses to 1 for very disturbed rock masses (Hoek, 2002).

The influence of this disturbance factor can be large. This is illustrated in Figure 4.35 by a typical slope example in which σ_c= 50 MPa, m_i = 10, GSI = 50 and $\sigma_3$max = 1 MPa. D = 0 results in a ø= 50° and c = 585 kPa, while a disturbance factor of D = 1 results in ø= 36° and c = 279 kPa .

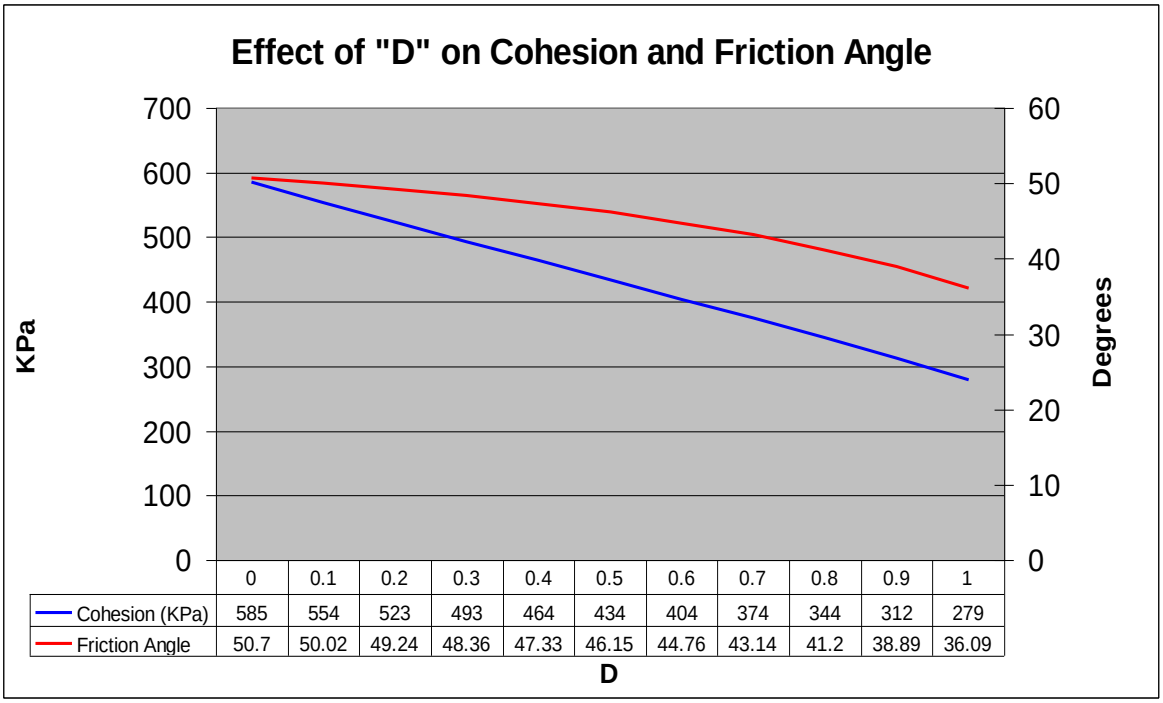


Figure 4.35 Showing the effect of the Disturbance factor introduced by Hoek (2002).

The extent and intensity of blasting damage varies due for each type of application. Hence, rather than attempt to present a table of recommended blasting damage values (D) Hoek and Diederichs (2006) chose to present a number of case histories which illustrated how the disturbance factor was incorporated into each analysis ranging from D=0 for no damage to D=1 for the maximum amount of damage. For a large open pit like the Chuquicamata open pit mine in Chile a value of D ~ 1 was suggested. Conversely small scale blasting in civil engineering results in modest rock mass damage, particularly if controlled blasting is used thus D=0.7 would be applicable (Hoek and Diederichs, 2006). See Table 4.14.

Hoek (2009) noted that downgrading the properties of the entire rock mass by the factor D will lead to unrealistically large slope failure predictions. Hence guidelines to estimate the depth of this zone were provided. See Figure 4.36 and Table 4.15. Lorig (2011) estimated a zone of disturbed rock of 50m assuming strain-softening behaviour in axisymmetric conditions. See Figure 4.37.

Table 4.14 Guidelines for Estimating the Disturbance Factor, *D* (Hoek and Diederichs, 2006)

Appearance of Rock Mass	Description of Rock Mass	Suggested Value of *D*
	Small scale blasting in civil engineering slopes in modest rock mass damage, particularly if controlled blasting is used as shown on the left hand side of the photograph. However, stress relief results in some disturbance.	*D* = 0.7 Good blasting *D* = 1.0 Poor blasting
	Very large open pit mine slopes suffer significant disturbance due to heavy production blasting and also due to stress relief form overburden removal.	*D* = 1.0 Production blasting
	In some softer rocks excavation can be carried out by ripping and dozing and the degree of damage to the slope is less.	*D* = 0.7 Mechanical excavation

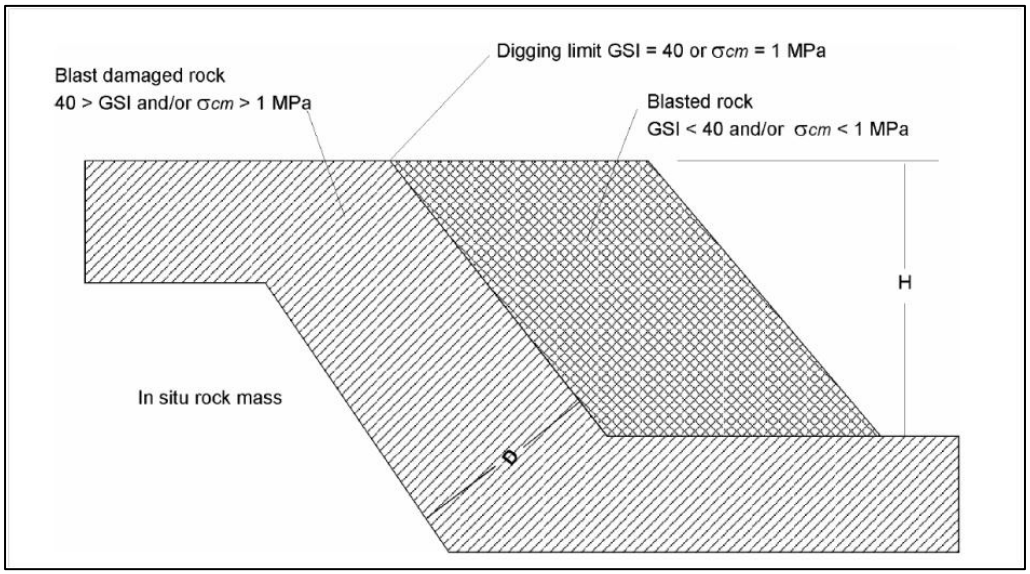


Figure 4.36 Diagrammatic representation of the transition between the in situ rock mass and blasted rock that is suitable for digging (Hoek, 2009).

Table 4.15 Depth of blast damage (Hoek, 2009).

Condition	D= Depth (m) of damage. (H= Height of the blast block (m)).
Large production blast, confined and with little or no control.	D = 2 to 2.5
Production blast with no control but blasting to a free face.	D = 1 to 1.5 H
Production blast, confined but with some control, e.g. one or more buffer rows	D = 1 to 1.2 H
Production blast with some control, e.g. one or more buffer rows, and blasting to a free face	D = 0.5 to 1 H
Carefully controlled production blast with a free face.	D = 0.3 to 0.5 H

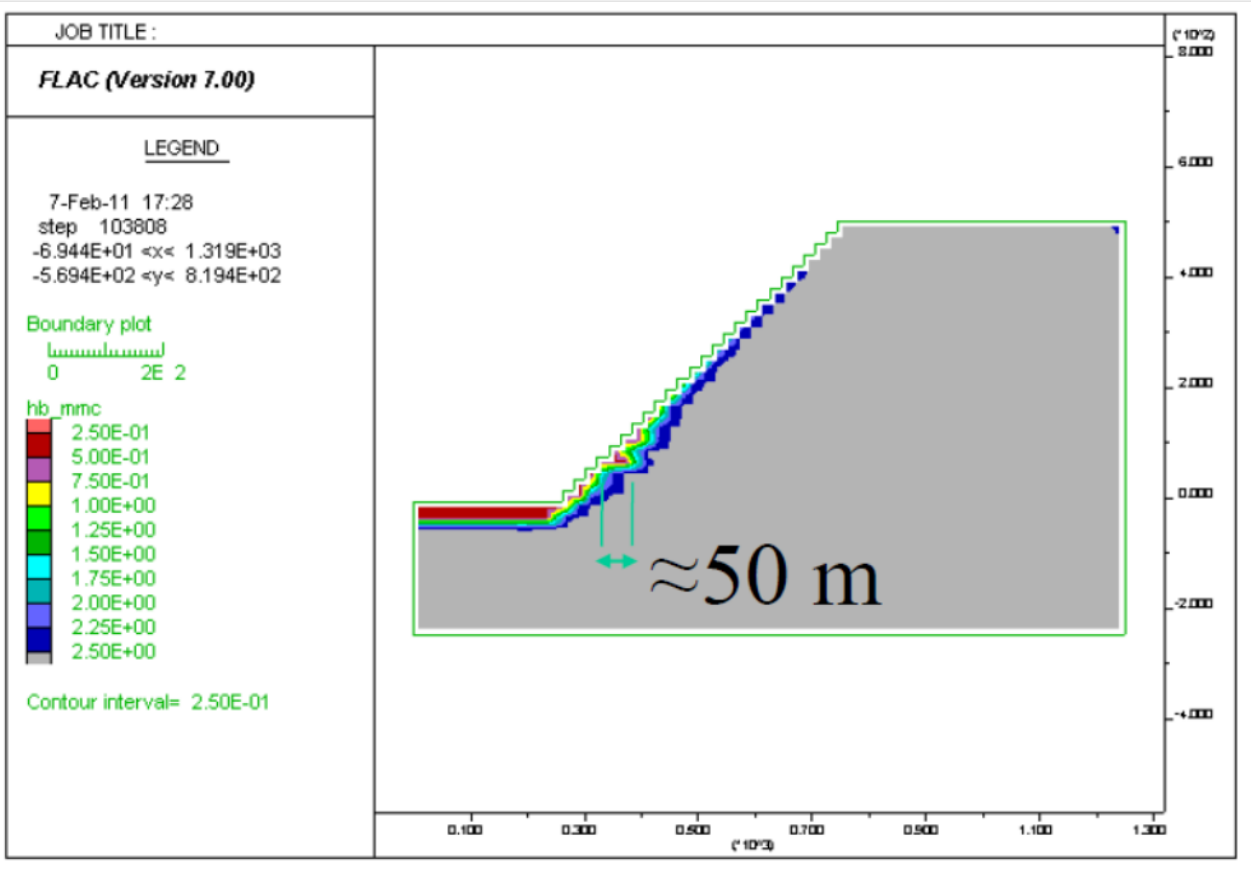


Figure 4.37 Depth of damage zone for a 500m high slope (after Lorig, 2011).

5. PHASE 2 OPTIMISATION

Phase 1 was initiated post the review of the pit conditions as presented in Chapter 2 and aimed at providing initial input parameters into the Strategic Business Plan (SBP) regarding slope angles (savings on waste stripping) (Strouth, 2009; Gomez, 2010) and bench heights (potential to increase productivity) (Contreras, 2010; Steffen and Terbrugge, 2009). This portion of the study suffered from the same shortcomings as the initial design however some of the outputs were incorporated into the final design and are discussed in Chapter 6, therefore this Chapter will only focus on Phase 2.

Phase 2 was scoped by the author with the aim of defining the orientation of the S2 foliation, joint data and pore pressures in the toe of the slope. This phase consisted of:

- Structural mapping, drilling, instrumentation installation conducted on mine and coordinated/supervised by the author;
- Modelling of the geology and ground water table by Basson (2011a) and Liu et al. (2011) respectively.

5.1 GEOLOGICAL AND STRUCTURAL MODEL

5.1.1 Data Collection for Geological and Structural Model

The structural data collection programme consisted of:

a) Pit Mapping (Scan Line Mapping and SIROVISION™),
b) Review of available borehole information.

5.1.1.1Scan Line Mapping

The initial mapping consisted of conventional scan-line mapping and was subsequently replaced with more efficient photogrammetry mapping technique, SIROVISION™. The programme was scoped and supervised by the author while mapping data was collected by staff in the Venetia Geotechnical Department.

Scan line mapping is done by collecting data with a structural compass on a pre-determined traverse. See Figure 5.1. The orientation and properties of each discontinuity on that traverse is recorded and described. Only discontinuities intersecting the pre-determined traverse are recorded in order to eliminate biased data capturing. Laubscher's (1990) descriptors for discontinuities were used. The method allows for the collection of detailed structural information. However it has the following disadvantages:

- The process is very time consuming.
- Large volumes of data have to be manually handled and interpreted by the user.
- Geotechnical personnel have to work at the rock face which increases the risk of injury due to rock falls.
- Structures, for example foliation dipping out of the face, that are sub-parallel to the traverse, i.e. that do not intersect the imaginary traverse line, are not recorded. Thus important structural aspects can be missed or under sampled.
- Structural compass readings depend on well exposed surfaces and most compasses are marked in 5 degree intervals thus making precise dip readings challenging.



Figure 5.1 Diagram representing a scan line and showing the waist high imaginary traverse.

5.1.1.2Photogrammetry Mapping (SIROVISION™)

Photogrammetry involves the use of two overlapping images called a stereo pair. The aim is to derive a position in 3D space of an object using the relationship of two images with a known position (X, Y, Z) (Grobler, 2008). The mine uses SIROVISION™ for this purpose. SIROVISION™ is a photogrammetry system that allows for the creation of 3D images of rock faces, the automated display and analysis of structural data.

The collection of field data is quick and seamless. A SIROVISION™ supported camera is used to take two overlapping pictures of a bench. The distance between the camera positions depends on the distance from the camera to the rock face. The camera positions are then surveyed in by a surveyor. The images with their coordinates are imported and processed in the software, which in turn creates a full 3D image of the bench in the provided coordinate system. The user has the option to either manually select the structure traces or allow for the system to select the traces. See Figures 5.2 and 5.3.



Figure 5.2 Cameras used to take the images.

The use of photogrammetry systems has the following advantages:

- It limits the time that Geotechnical personnel spend under the rock face.
- Larger areas can be mapped quicker and more efficiently.
- Larger populations of structures, including inaccessible structures are captured which results in statistically more representative data sets.
- An electronic record of the actual rock face is stored electronically.

The SIROVISION™ mapping programme was scoped and supervised by the author while mapping data was collected by staff in the Venetia Geotechnical Department.

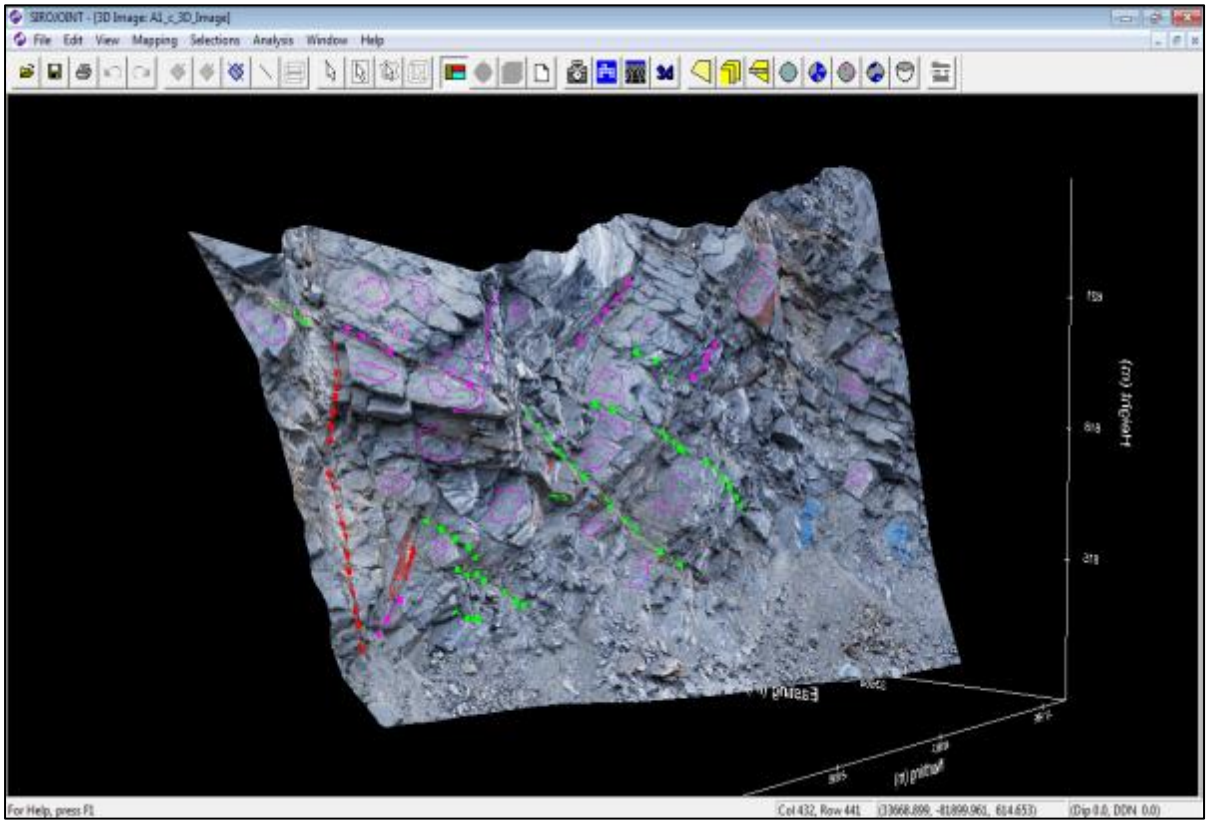


Figure 5.3 A SIROVISION™ screenshot showing a 3D image of an actual rock face at Venetia Mine. Structure traces (red, green and purple) denote actual structures.

5.1.1.3Mapping coverage

Most of the new exposures in Cut 4 were mapped. Scan Line Data is concentrated on the South-western side of the pit. The coverage from the pit mapping programme is given in Figure 5.4. The complete mapping dataset is given in Appendix B: Data Compact Disc.

Table 5.1 Summary of the mapping dataset collected by the Venetia Geotechnical Department.

Type	No of Scan lines / SIROVISION™ Surveys	Length / Area	Records
Scan Lines	31	1514m	1177 (559 Foliation)
SIROVISION™	117	N/A	7581 (4173 Foliation)

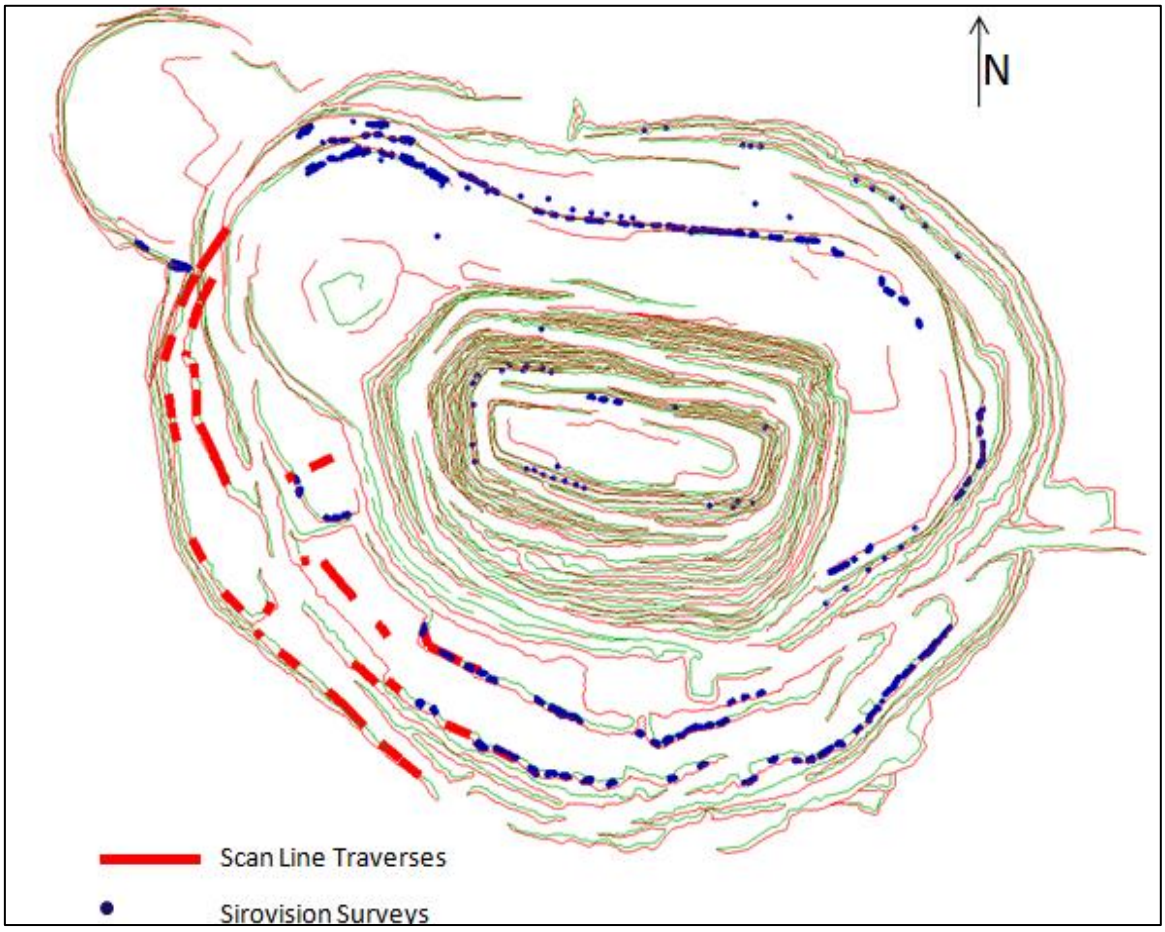


Figure 5.4 Showing the scan line and SIROVISION™ mapping coverage.

5.1.1.4 Borehole information

Over the years various drilling campaigns were undertaken at Venetia and a total of 800 boreholes were drilled. Of those only 59 were dedicated to Geotechnical and Dewatering investigation boreholes during the VREP programmes. In addition a limited number of those Geotechnical holes delivered quality orientated drill core. The data can be divided into historical and modern (VREP) drilling campaigns. These can be further sub-divided into the following datasets:

Historical:

- Anglovaal 1981 Copper Drilling Program (North of pit),
- Phase 1 Geotech Early 1993 delineation drilling,
- Phase 2 Geotech 1993 to 1997 delineation drilling,
- 1998 to 2002 Geotechnical Drilling Campaign.

Modern (VREP):

- VREP 1 Drilling Program 2004 to September 2006,
- VREP 2 Drilling Program September 2006 to 2009. See Figure 5.5 and Table 5.2.

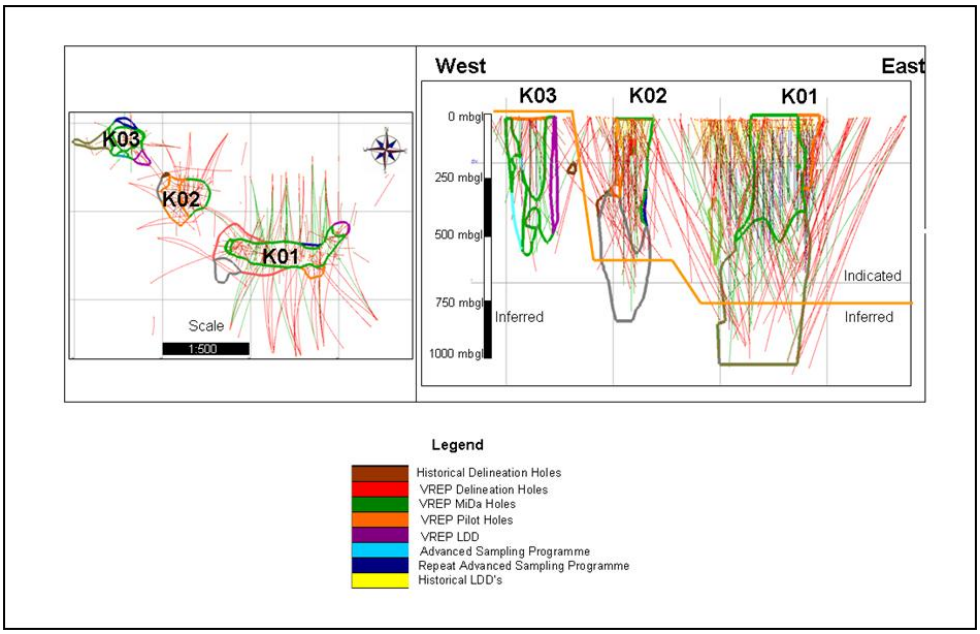


Figure 5.5 Plan showing all the Venetia Resource Extension boreholes drilled since 2003 and the kimberlite ore bodies.

Table 5.2 Summary of the historic and modern drilling campaigns

Campaign		Total Boreholes Drilled	Total Meters Drilled
Historical	Anglovaal	23	6 043
	Dewatering	7	4 768
	Geology	497	101 076
	Geotech	67	19 276
VREP	Core	199	116 332
	Dewatering	8	3 185
	Geotech	59	35 761
	Gmt	20	1 353
	Total	880	287 795
STEREOCORE™	Geotech	38 of 59	23 627

A total of 38 boreholes (23 627m) with quality orientated drill core, were selected from the Modern (VREP) dataset for STEREOCORE™ analysis. See Table 5.2. From the STEREOCORE™ analysis 15583 foliation records were identified and used in the study. The location of the boreholes is shown in Figure 5.6.

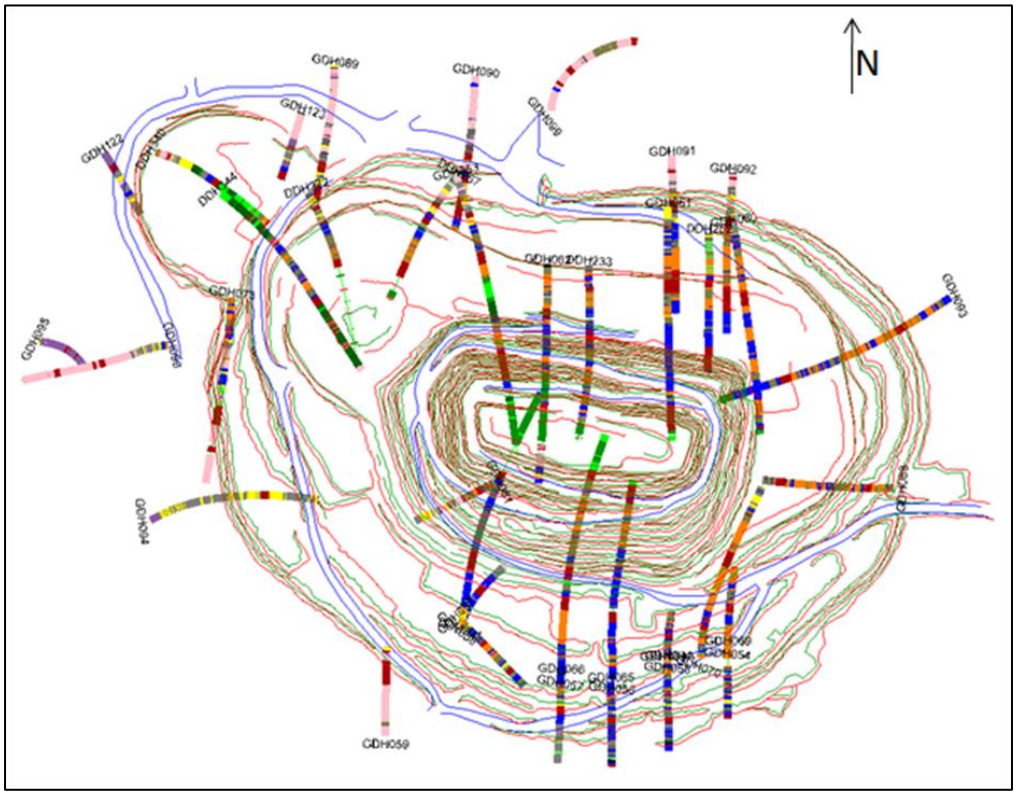


Figure 5.6 Showing the location of the boreholes that were selected for STEREOCORE™ analysis.

STEREOCORE™ is photogrammetric software that uses digital images to calculate core recoveries, RQD and the dip and dip direction of structural features in orientated drill core. A reference frame is placed around each core tray. This reference frame is used by the software to create a virtual 3D model of the core. Any digital camera can then be used to photograph the core in this reference frame. The image is the imported into the software and depth referenced.

The core is then remotely logged (Geological, Structural and Geotechnical) from within the STEREOCORE™ software and the images are annotated such that QA/QC is fast and easy without necessarily requiring direct access to the core. In addition the data is immediately available for analysis. The system also allows for the tagging and stereographic display of various structure types (Orpen, 2011). See Figures 5.7 and 5.8.

The use of this system has the following advantages:

- It provides an auditable digital database of the specific core and core logging.
- Eliminates human error often associated with manual logging techniques.
- Saves significant time and allows for processing and immediate analysis of large amounts of data.

Dr John Orpen (Orpen, 2007) was contracted by Venetia Mine in 2007 to analyse the data for 38 boreholes using the STEREOCORE™ system. The data was however never incorporated into the geology model or design.

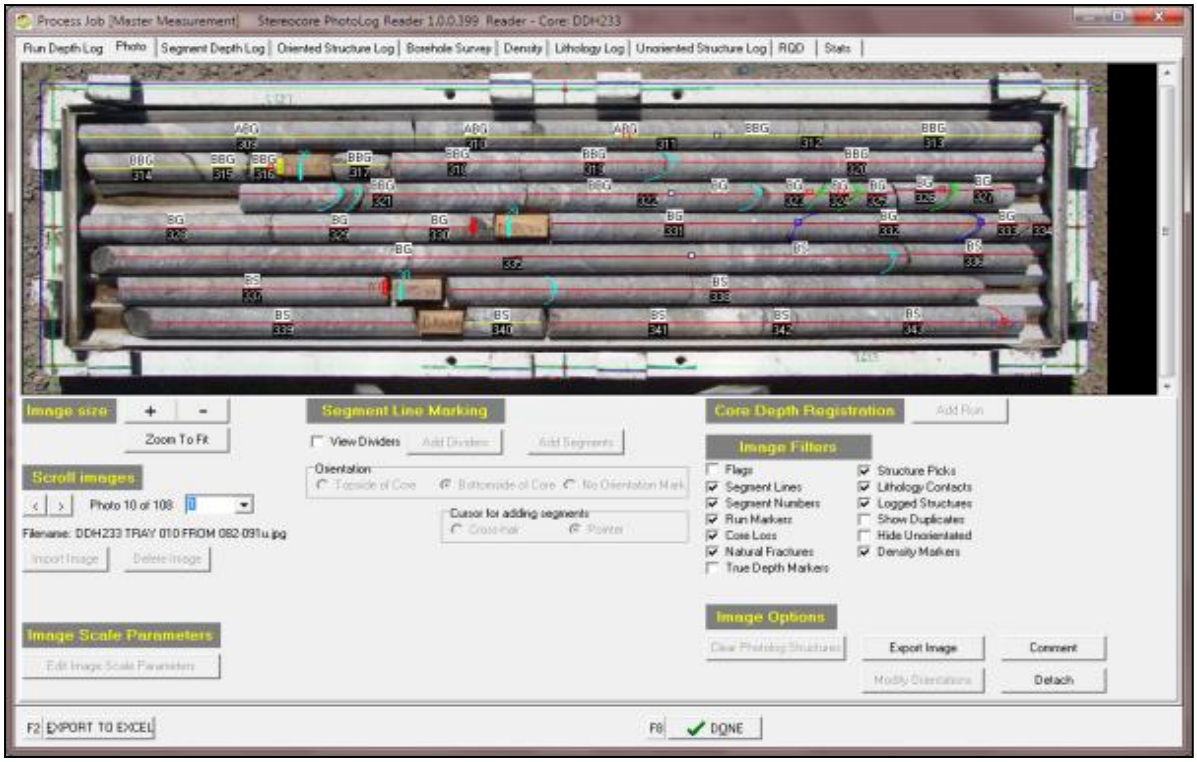


Figure 5.7 Showing an imported image in STEREOCORE™ of a drill core tray within the reference frame.

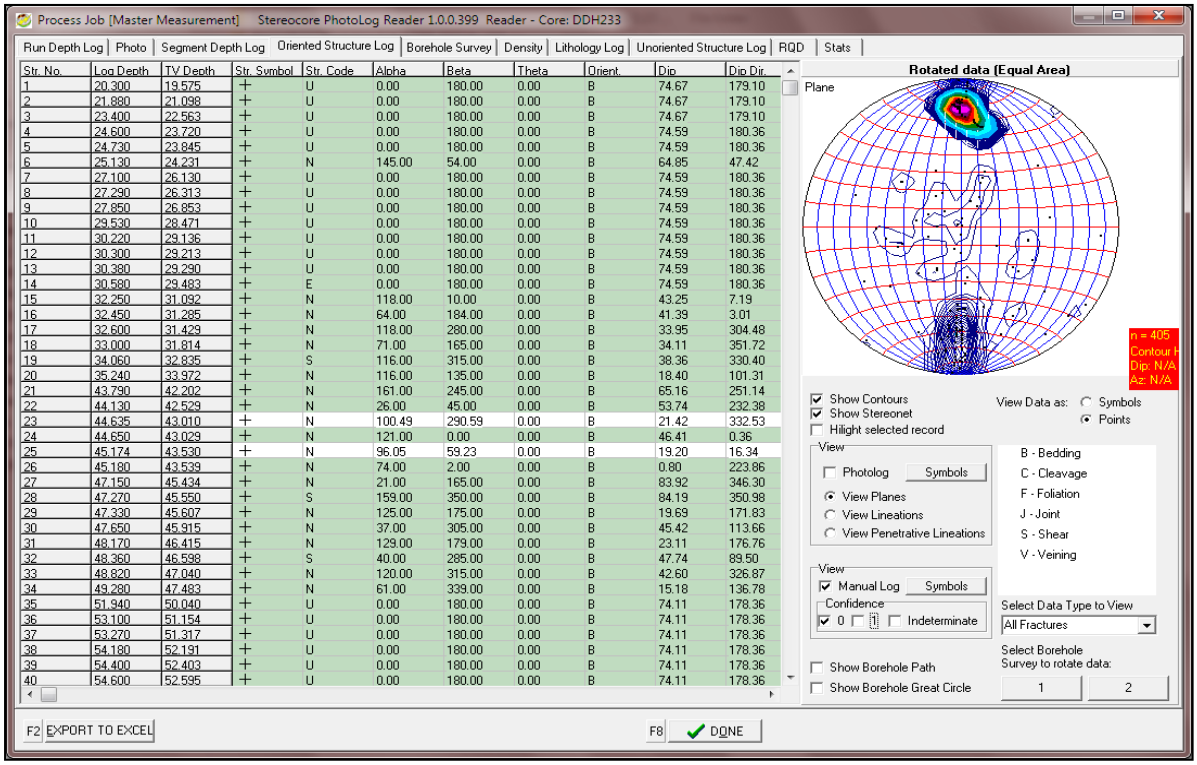


Figure 5.8 Showing the Stereographic projection and data display functionality of the STEREOCORE™ software.

5.1.2 Review of Data and Development of Geological Model

Since 2005 a significant amount of structural work was undertaken and several pit maps of the geology was derived based on mapping conducted between 2005 and 2010 in Cut 3 and 4 exposures (Basson, 2005; 2007; 2011).

The last major geological and structural model update was done in 2007 by De Beers and was largely based on the underground study exploration drilling and observations in Cut 2. Unfortunately the development of the model did not keep pace with the latest information and observations (See Basson, 2005; 2007; 2011) and the model that was built in 2007, and subsequently used in the 2008 slope design study contained conceptual orientations of the S2 foliation that were extrapolated from Cut 2 and 3.

One of the main assumptions in the 2007 model was that the Lezel-Tina Shear Zone is mainly due to brittle activation. However Basson (2007, 2011) described the Lezel-Tina Shear Zone as an elongated, lensoid, curviplanar zone that resulted from ductile to brittle-ductile deformation of Central Zone units with the style of ductile deformation similar to that in the adjacent gneissic units.

In 2010 Tect Consulting was contracted by the author to:

- Analyse the newly collected structural pit mapping information, incorporate all the historical geological pit mapping and drilling information and update the current 3D geological model;
- Update the geology model and further sub-divide the model into unique structural volumes. Structural volumes are characterized by an internally consistent suite of characteristics, such as a consistent fault style and orientation, consistent foliation orientation or confinement to a particular lithological unit or package.

The following methodology was followed by Basson (2011a) in the sub-division of the structural domains:

- The Venetia kimberlites are situated within a large F3 synform, which is asymmetrical and south-verging. The foliation measured in both limbs of the large F3 synform is S2. The large F3 fold axial plane or “FAP3” was modelled by Basson

(2011a) in 3D and a surface was used to subdivide the large F3 synform into a large Northern block wherein S2 and lithological contacts are steeply N-dipping and, secondly, a large southern block wherein S2 and lithological contacts are moderately N-dipping (Structural Volumes 4, 5, 6 and 7). See Figure 5.9.

- The volumes North and South of FAP3 were further subdivided into their various lithological packages, and then further subdivided according to their position west or east of the Lezel-Tina Shear Zone.
- The cross-cutting Lezel-Tina Shear Zone was re-modelled and included as a separate volume with respect to adjacent volumes defined by S2 and lithological packages (Structural Volume 8).
- The NW fault zone consists of brittle NW trending faults or joints that overprint the ductile deformed rocks. This zone was modelled to overlap the structural volumes in order to simulate the overprinting effect and is named Structural Volume 9.
- The ductile structure (S2 foliation) is not present with the cross cutting late stage emplaced diabase sills and dykes. All the diabase sills and dykes were classified as Structural Volume 10. See Table 5.3 and Figure 5.10 for a summary and location of the structural volumes (STRV1-STRV11) respectively.

Table 5.3 The structural volumes and their definition.

	S2 FOLIATION		
Structural Volume	**In Relation to Fold Axis (FAP3)**	**Lithological Package**	**In Relation to Lezel-Tina Fault**
STRV1	North	Gneiss	West
STRV2	North	Gneiss	East
STRV3	North	Metasediment	West
STRV4	South	Gneiss	West
STRV5	South	Gneiss	East
STRV6	South	Metasediment	West
STRV7	South	Metasediment	East
STRV8 GP	N/A	Gneiss	N/A
STRV8 MP	N/A	Metasediment	N/A
STRV9	N/A	N/A	N/A
STRV10	N/A	Diabase	N/A
STRV11	N/A	Marble	N/A

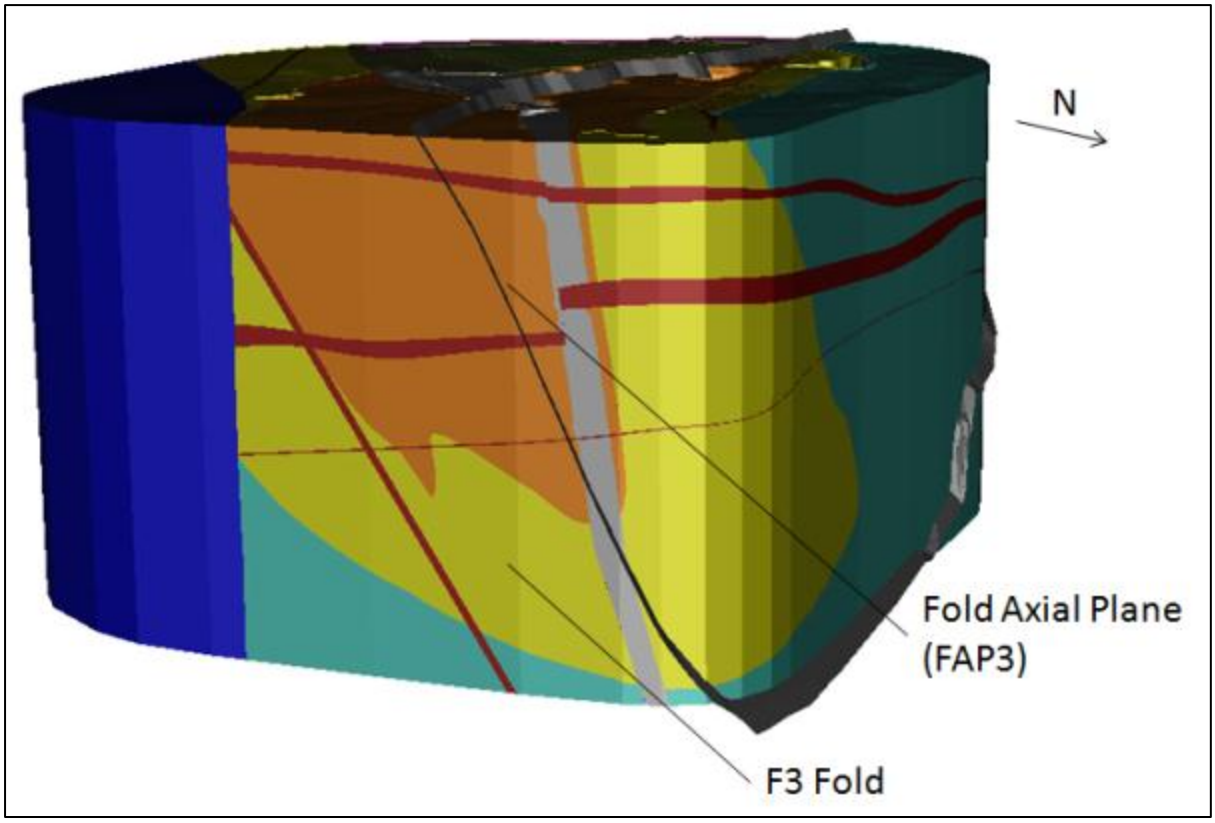


Figure 5.9 3D Geological model showing the F3 Fold and Fold Axial Plane (FAP3).

.

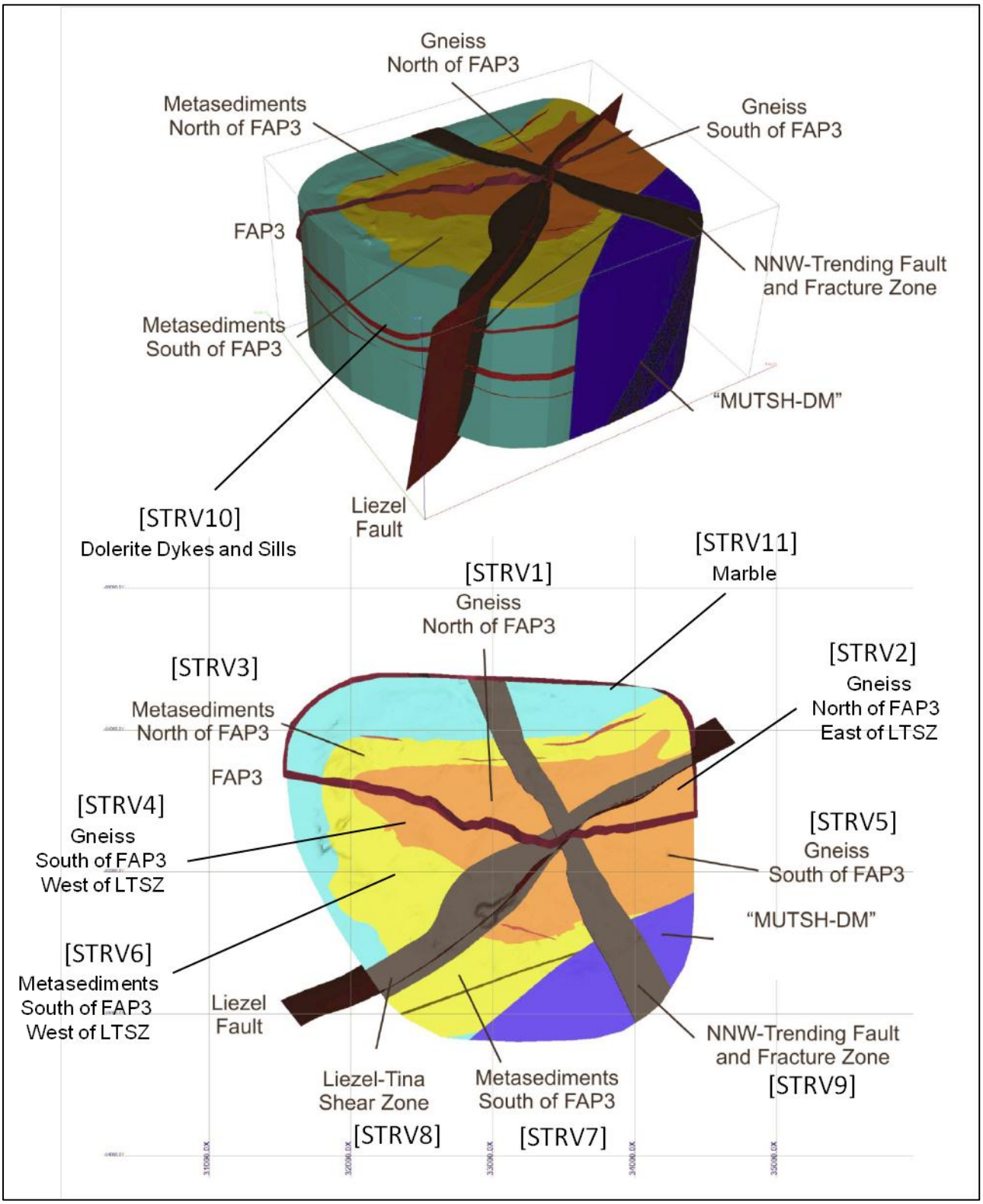


Figure 5.10 3D model and plan showing the structural volumes (after Basson, 2011a).

5.1.3 Analysis of Structural Data (S2 Foliation and Brittle Jointing)

5.1.3.1 S2 Foliation

From previous sections it is clear that the country rock geology is complex. The SIROVISION™, scan line and STEREOCORE™ information was thus, on request of the author, reviewed by the Mine's Structural Geology Consultant (Dr Ian Basson), as part of the abovementioned review and update of the geology models, who selected and recommended the most representative dataset for each Structural Volume (Basson, 2011c). See Tables 5.4 and Table 5.5. The complete data set (on mine data set and Basson Historical Mapping) are presented in the form of equal area lower hemisphere stereonet and rosette plots in Appendix B.

Table 5.4 Orientation of the S2 Foliation in each Structural Volume (Basson, 2011c)

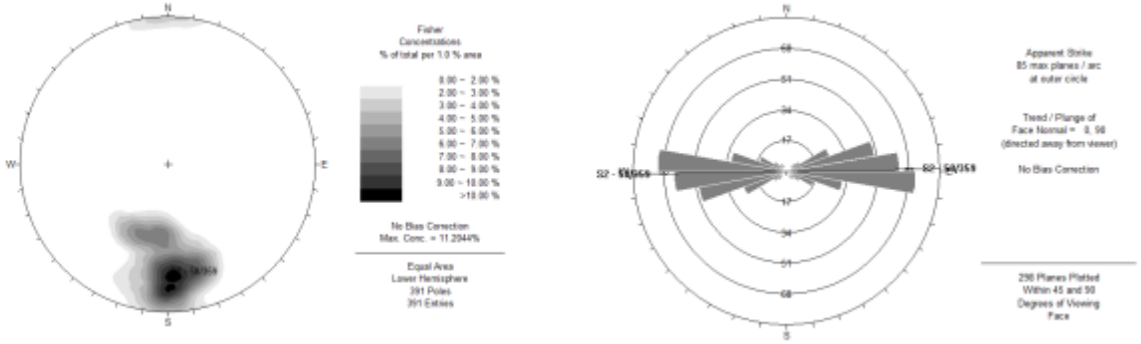
Structural Volume	Dip (°)	Standard Deviation Dip (°)	Dip Direction (°)	Standard Deviation Dip Direction (°)
STRV1	58	15	359	15
STRV2	58	15	338	15
STRV3	63	10	7	11
STRV4	39	8	22	25
STRV5	55	13	343	18
STRV6	39	8	15	25
STRV7	39	18	340	34
STRV8	45	10	19	24
STRV9	53	13	348	13

Key	
FM (Basson's Mapping)	Face mapping data, collected by Silva compass-clinonometer (Tect Consulting/Basson)
SR (Venetia Mine)	SIROVISION Data collected by Venetia Mine in 2009-2010
SC (Venetia Mine)	Scan line mapping data (Brunton compass-clinometer) collected by Venetia Mine in 2010-2011
DH (Orpen, J, 2007)	Oriented drillhole data (primarily STEREOCORE-derived) collated by Venetia Mine. Originally derived by Dr John Orpen in 2007.

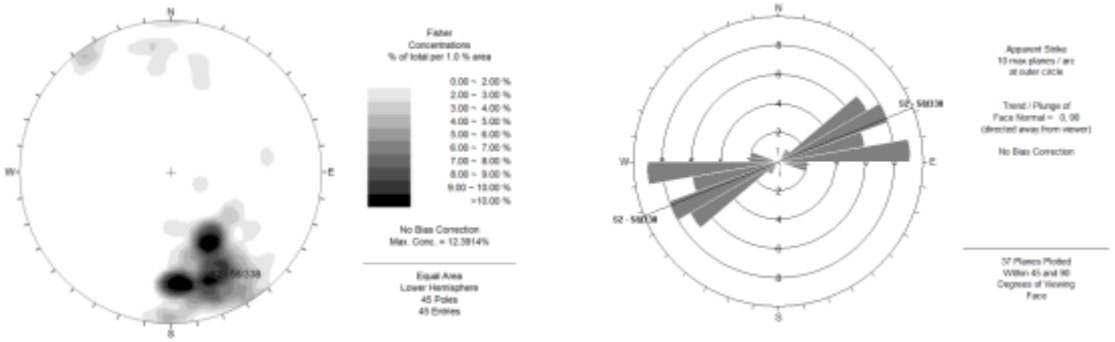
Table 5.5 Lower Hemisphere Equal Area Stereographic Projections (left) and Rosette Plots (right) for the S2 Foliation in each Structural Volume (Basson, 2011c).

DIPS™ Plots constructed by the author from raw data

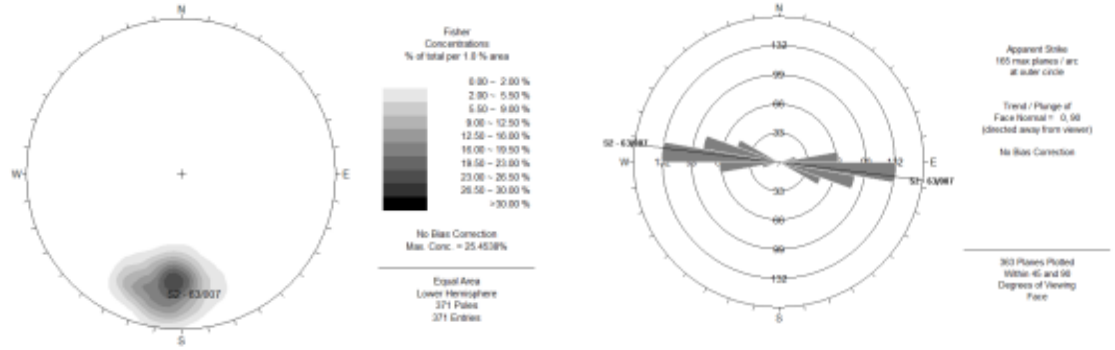
Structural Volume 1: 58°/359°



Structural Volume 2: 58°/338°



Structural Volume 3: 63°/007°



Structural Volume 4: 39°/022°

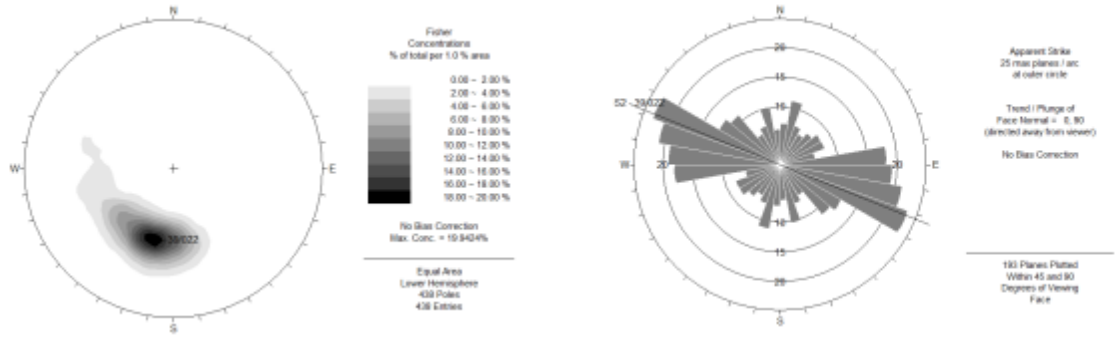
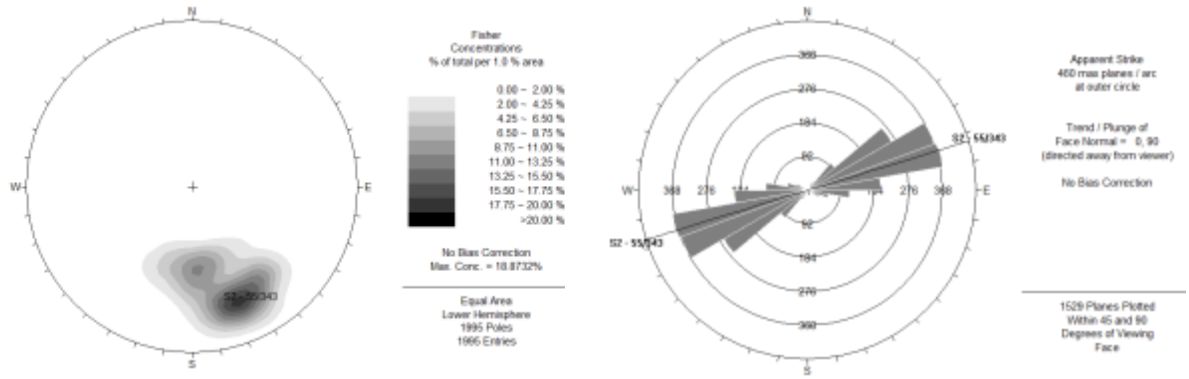
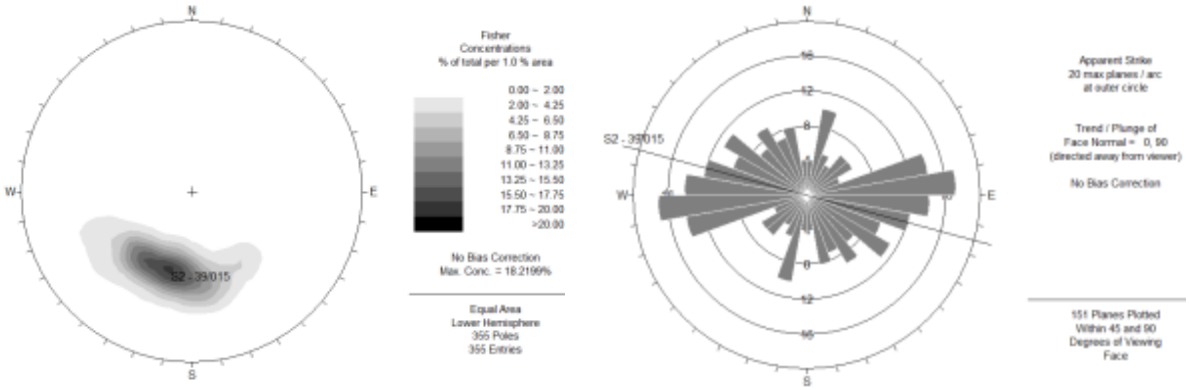


Table 5.5 Continues

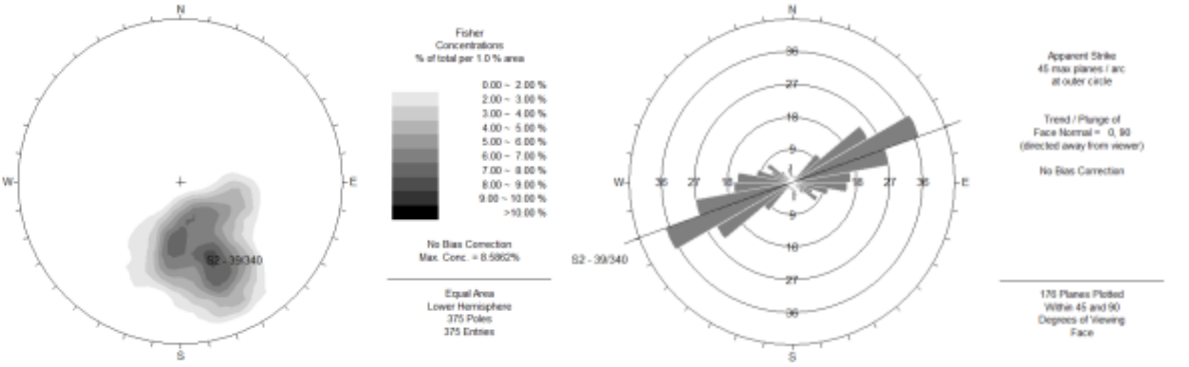
Structural Volume 5: 55°/343°



Structural Volume 6: 39°/015°



Structural Volume 7: 39°/340°



Structural Volume 8: 45°/019°

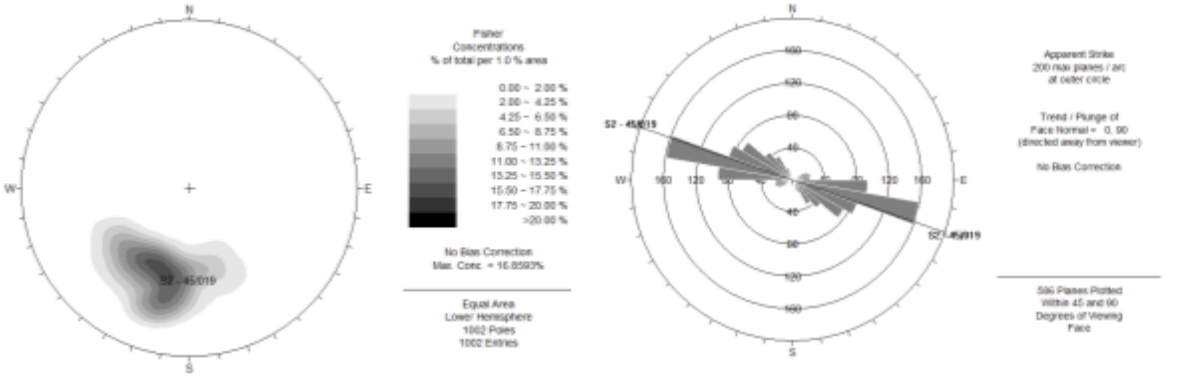
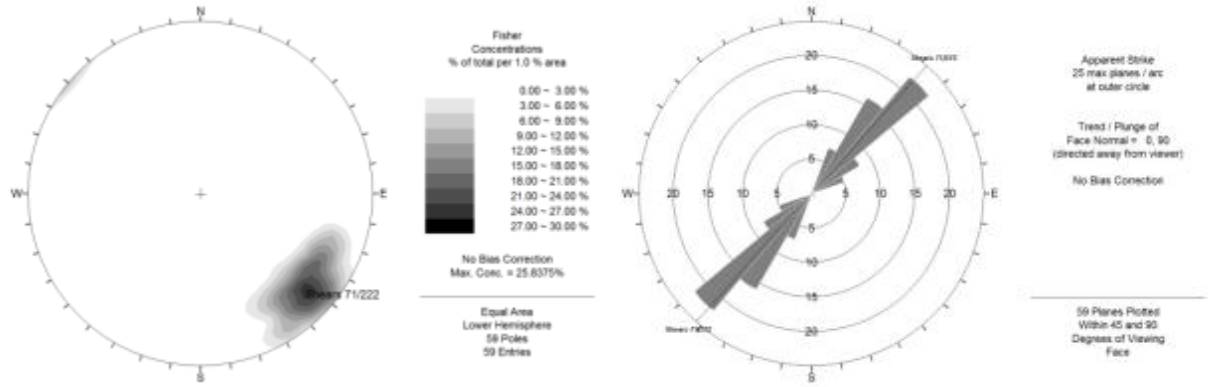
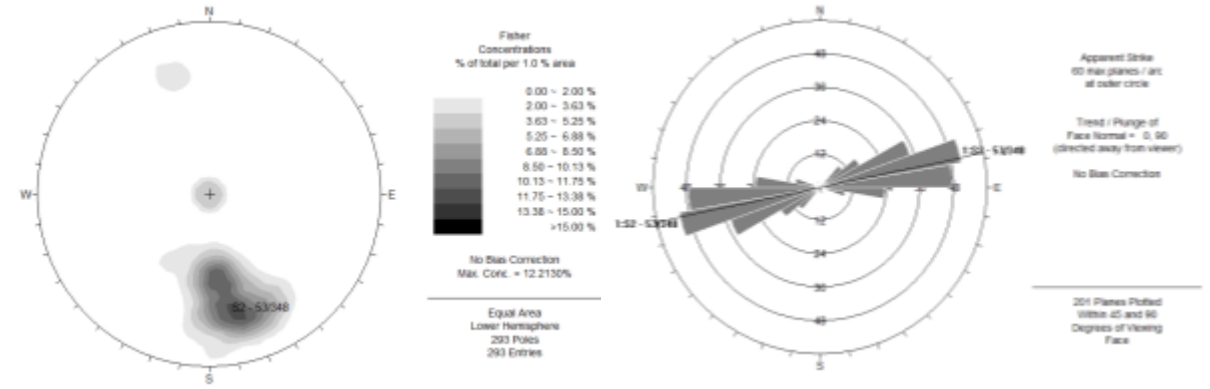


Table 5.5 Continues

Structural Volume 8 Shears: 71°/222°



Structural Volume 9: 53°/348°



5.1.3.2 Brittle Joints

Although no genetic geological evolutionary model exits for the brittle jointing their distribution and geometric occurrence are not as complex as the ductile overprint, which consists of at least four deformation events. Brittle jointing was therefore interpreted and summarised by the author. The results are presented in the form of equal area lower hemisphere stereonet and rosette plots. See Tables 5.6 and 5.7.

Two main sets, the NW trending J4/J6 and NE trending J2, are prominent. J6 is associated with the NW trending fault system. J2 and J4 are pervasive in the rock mass and the dip and strike vary slightly depending on the domain. The persistence of the joint sets is limited to one bench height, except for the J4/J6 sets in the NW fault zone, which can have a persistence of up to 3 benches (~36m). Thus the jointing will only in all likelihood impact on bench stability. This matches with current in pit observations. Limited data is available for Structural Volume 10 (Diabase dykes and sills) but from current and historic mapping one

can conclude that, depending on the location either the dominant J2 or J4 will be present. A poorly developed J8 set is also present within this volume. No data was available for Structural volumes 2, 3 and 7 and for those structural volumes the largest and closest major structural volume's data was applied in the bench analysis. See Table 5.7.

Table 5.6 Lower Hemisphere Equal Area Stereographic Projections (left) and Rosette Plots (right) for the Brittle Joints in each Structural Volume.

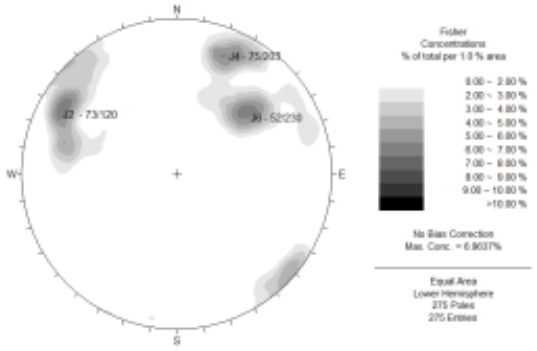
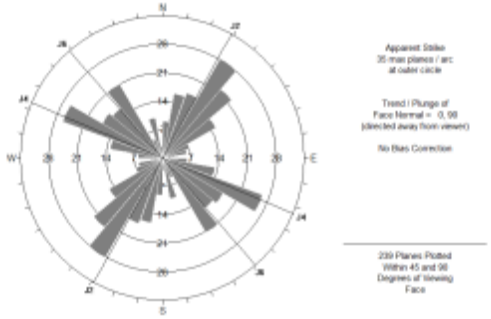
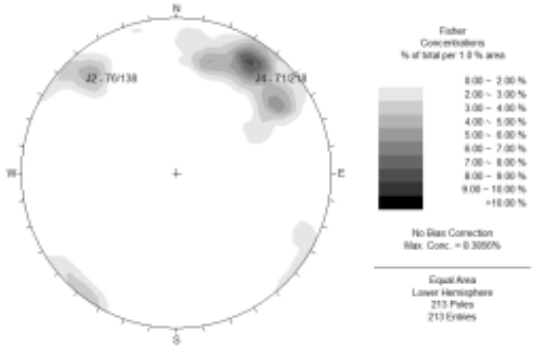
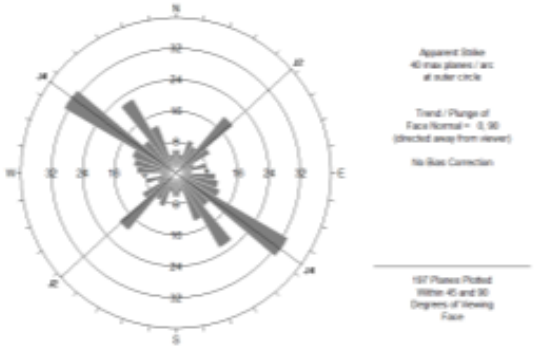
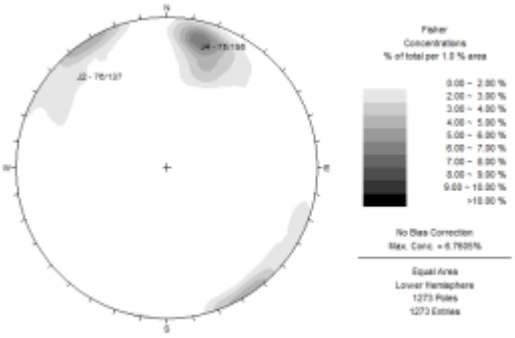
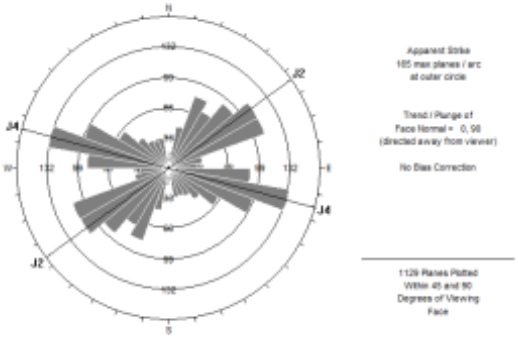
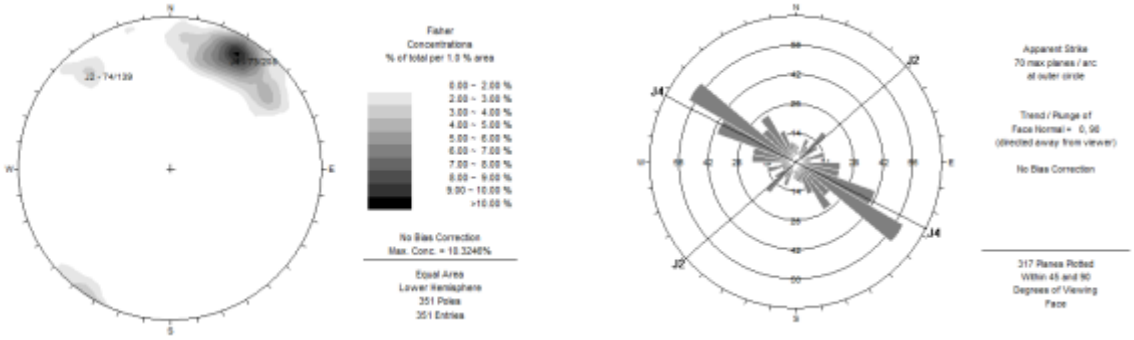
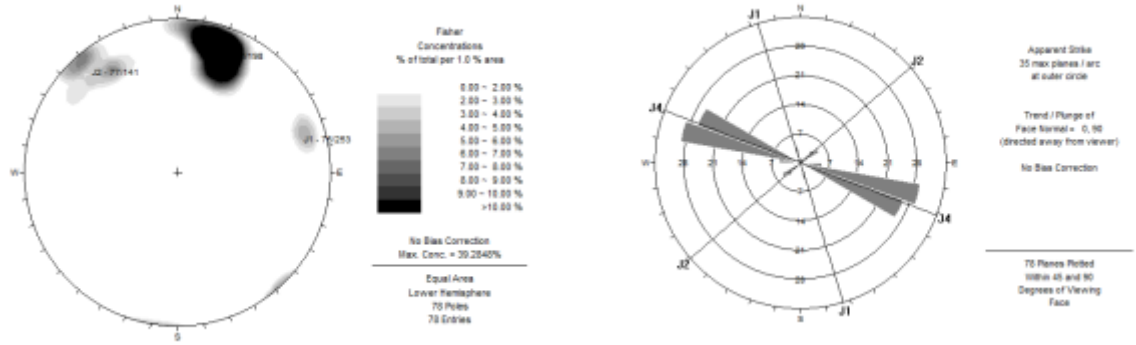
Joints	
Structural Volume 1:	
	
Structural Volume 4:	
	
Structural Volume 5:	
	

Table 5.6 Continues

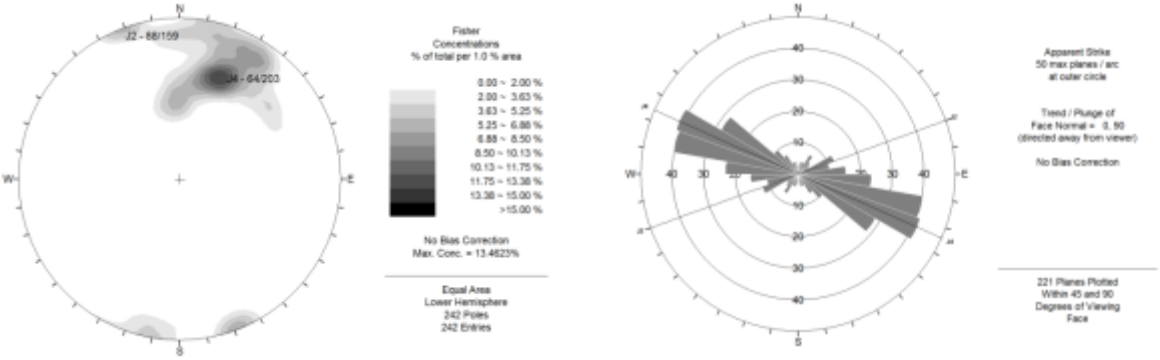
Structural Volume 6:



Structural Volume 8:



Structural Volume 9:



Structural Volume 10:

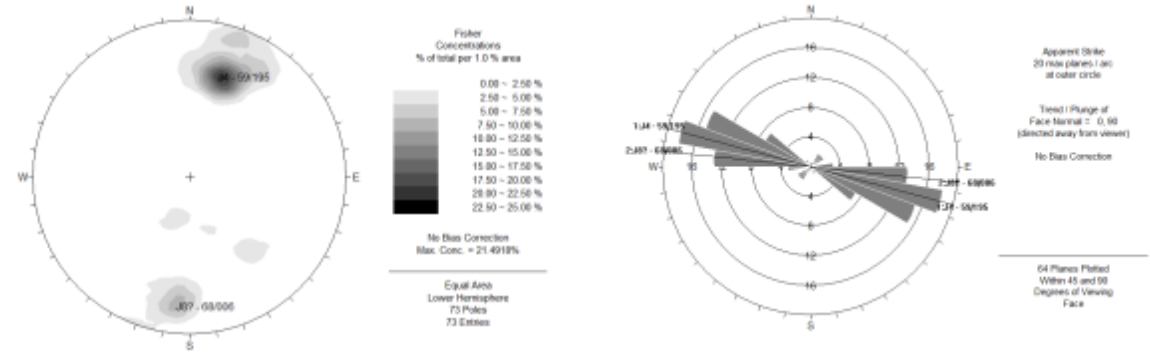


Table 5.6 Continues

Structural Volume 10:Historic Mapping (Basson, 2007)

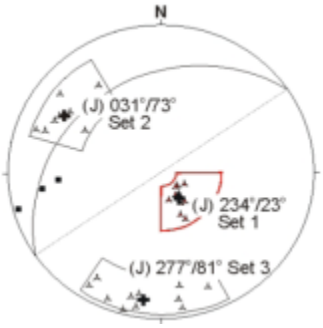


Table 5.7 The joint data for each structural volume.

Structural Volume		J2		J4		J6		J8	
		Average (Window)	Standard Deviation	Average (Window)	Standard Deviation	Average (Window)	Standard Deviation	Average (Window)	Standard Deviation
STRV1	Dip	73	5	75	6	52	7		
	Dip Direction	120	6	203	6	230	7		
STRV4	Dip	76	6	71	8				
	Dip Direction	138	5	218	13				
STRV5	Dip	76	8	75	7				
	Dip Direction	137	15	195	7				
STRV6	Dip	74	7	73	8				
	Dip Direction	139	10	208	9				
STRV8	Dip	77	9	72	9				
	Dip Direction	141	8	198	14				
STRV9	Dip	88	2	64	10				
	Dip Direction	159	2	203	8				
STRV10	Dip			59	8			68	6
	Dip Direction			195	8			006	5

5.2 HYDROLOGICAL MODEL

Inflows into the Venetia pit generally occur from the fault zones and geological contacts. The passive groundwater inflow to the current pit is estimated at about 600m^3/day. The overall hydraulic conductivity of the metamorphic country rocks is very low (~ less than 0.001m/day) and in such rocks, active dewatering from perimeter of the pit will not be successful in reducing the relatively small amount of passive inflow to the pit. No significant water bearing structures that would constitute targets for dewatering boreholes have been encountered to date (Atkinson and Shchipansky, 2008).

The first Groundwater model was done in 2008 and indicated that some natural depressurisation of the highwalls has already occurred and will continue to occur as the pit deepens due to de-stressing or relaxation of the rock mass behind the highwalls (Atkinson and Shchipansky, 2008). However the information used in that model was mainly obtained from standpipe piezometers that were located a significant distance from the toe of the slope and or zone of depressurization (Figure 8.4). The results of the groundwater and pore pressure modelling were not available in time for the first Cut 4 Design Study that was undertaken by SRK in 2008 and a best-estimate groundwater table was used in the analysis. See Figure 5.11.

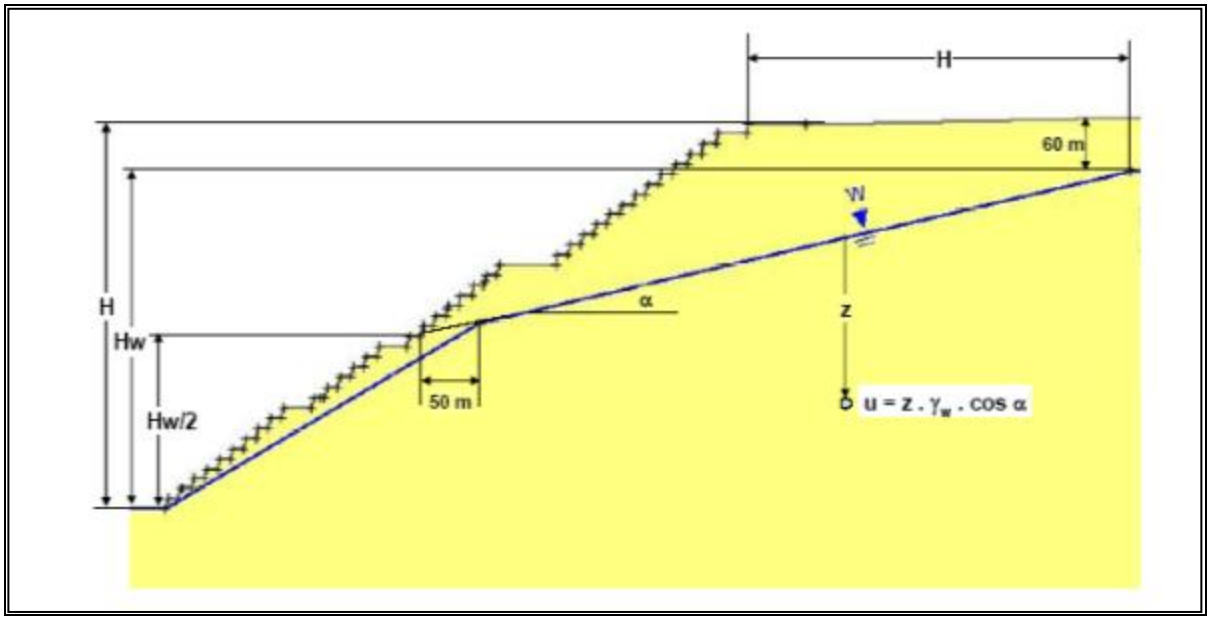


Figure 5.11 Pore pressure assumptions applied in the model (Contreras, 2008).

To address the above shortcoming the author scoped a drilling and piezometer installation programme of which the aim was install several piezometers in the toe of the slope. Three new boreholes (GDH123, DWH019 and DWH020) were drilled by Partners Drilling, and fifteen (15) VW piezometers were installed either close to the face and or toe of the current slope (Figures 5.12 and 5.14) by a sub-contractor (Terramonitoring). In each borehole three (3) VW piezometers were installed and the borehole column fully grouted. The data loggers were protected with a concrete casing and steel cap. See Figures 5.13.

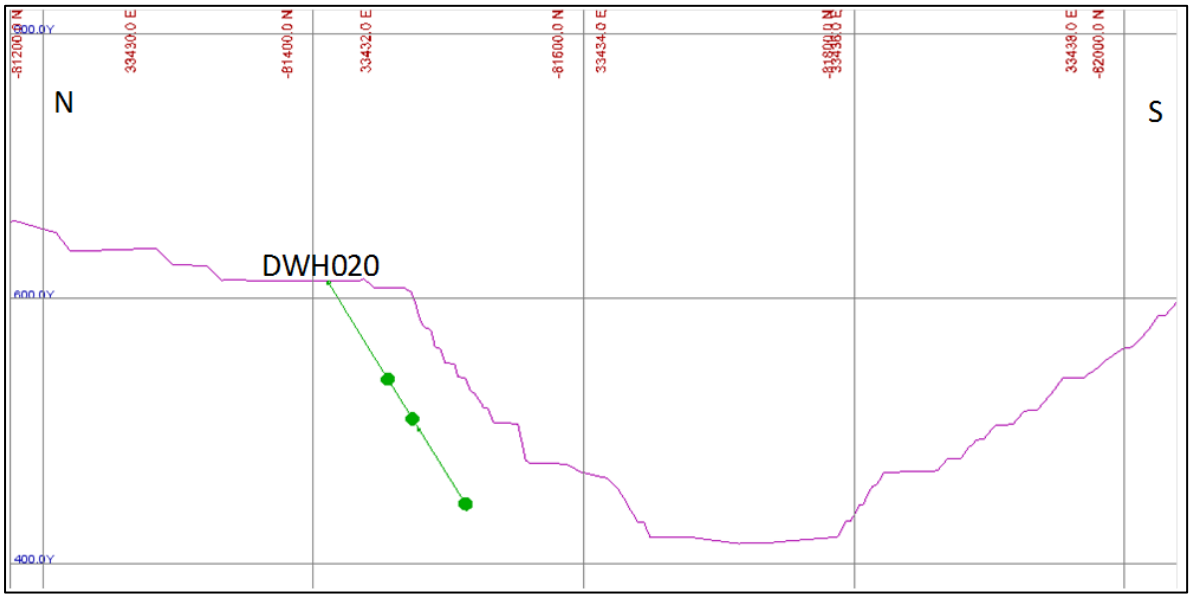


Figure 5.12 Showing a typical multi-level piezometer layout within one of the core holes (DWH020) in the North Wall.

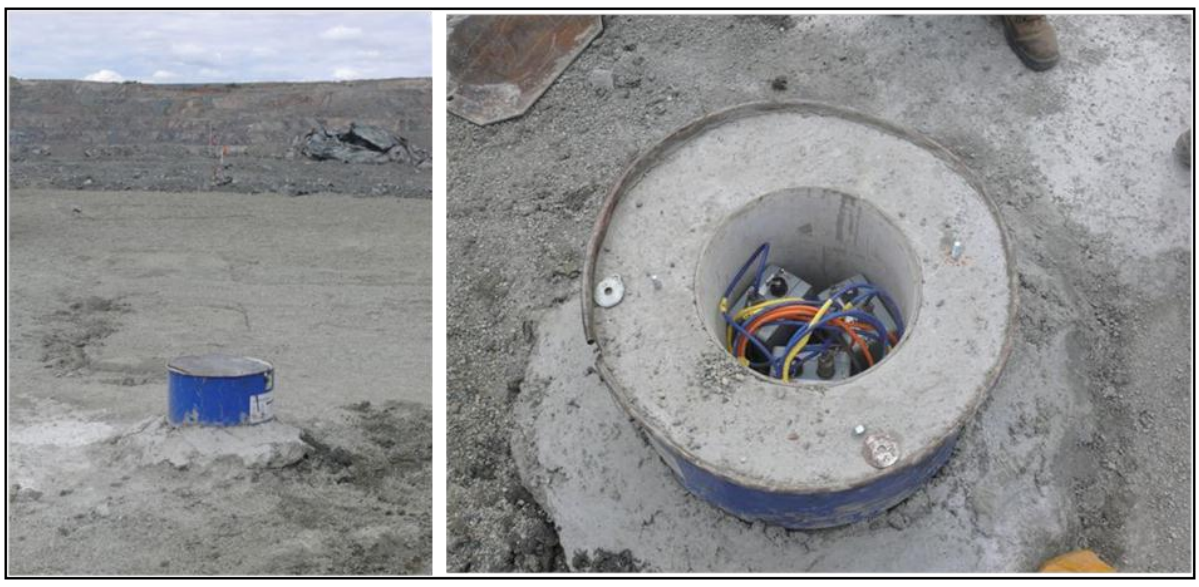


Figure 5.13 A typical multiple VW piezometer installation in an angled core hole.

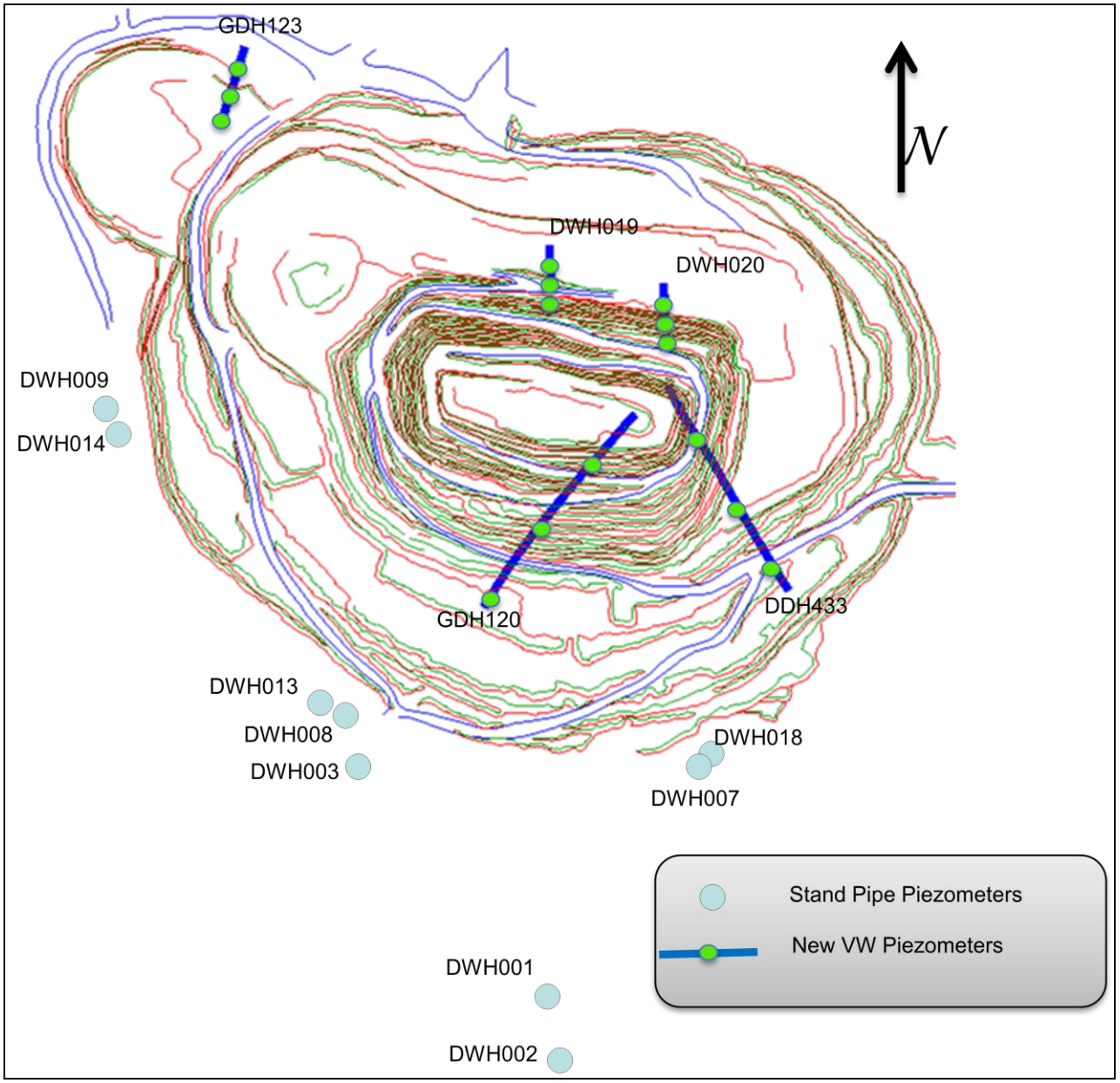


Figure 5.14 Showing the initial stand pipe piezometers and newly installed VW piezometer network.

The Itasca Office in Denver, USA, was contracted by the author to update the groundwater model for the pit. The results from the piezometer network were subsequently used by Shchipansky and Atkinson (2010) and Liu et al. (2011), from Itasca, to update the groundwater model. The modelling indicated that the best correlations between simulated and measured water levels are obtained if a 50m zone of relaxation is applied in the model to the slope. See Figure 5.15. The groundwater table on each design section line was clipped by the

author from the 3D modelled groundwater table and used in the inter-ramp and overall slope analysis. The 3D groundwater table is shown in Figure 5.16.

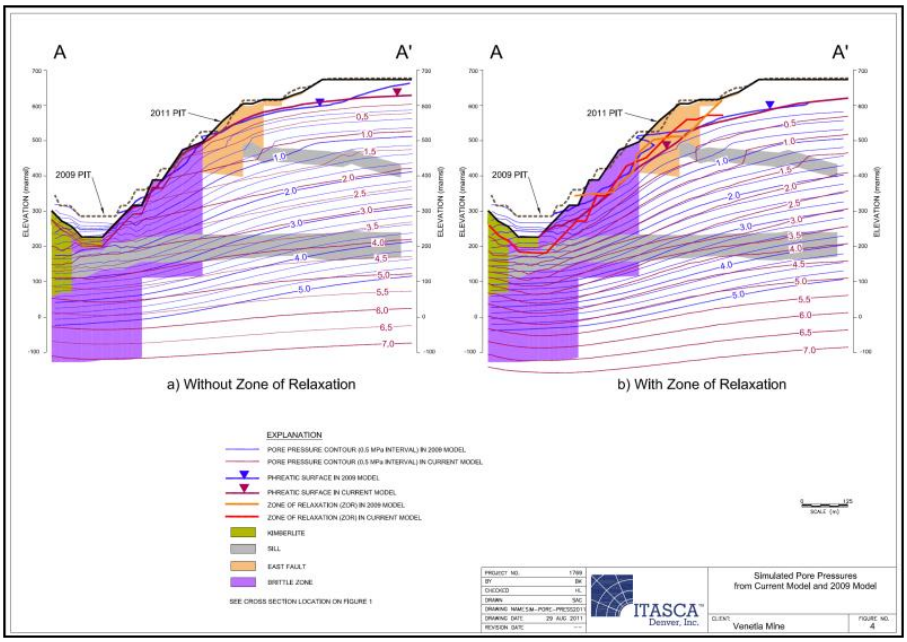


Figure 5.15 A section through the model showing the groundwater table in the North Wall with and without a zone of relaxation (Liu et al., 2011).

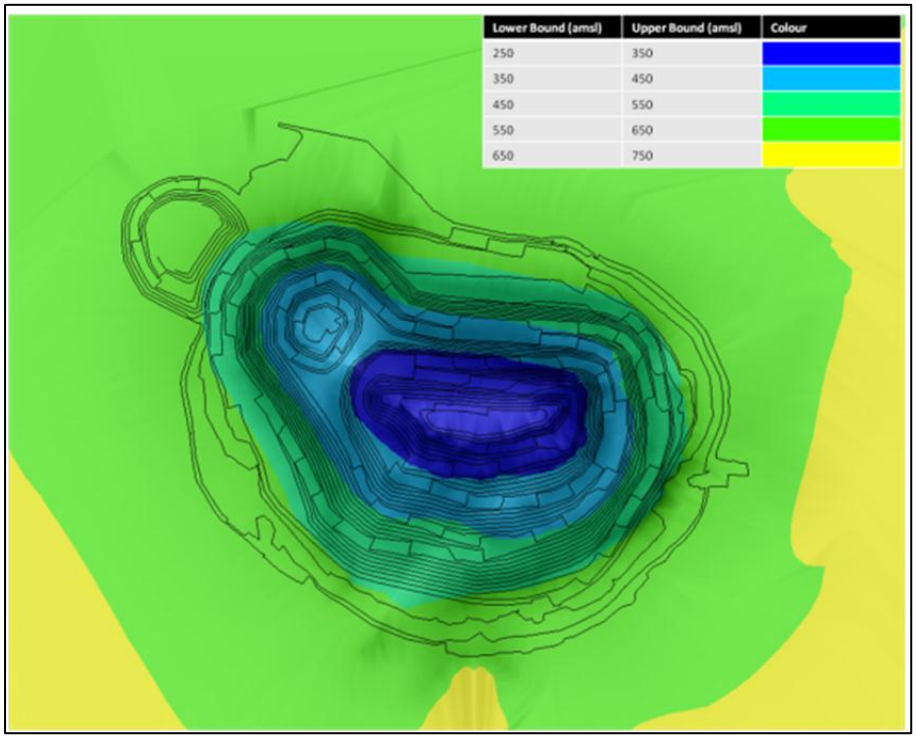


Figure 5.16 A plan view showing the 3D groundwater table as modelled by Liu et al. (2011).

5.3 SUMMARY

Phase 1 was aimed at providing initial input parameters into the SBP regarding slope angles (savings on waste stripping) (Strouth, 2009; Gomez, 2010) and bench heights (potential to increase productivity) (Contreras, 2010; Steffen and Terbrugge, 2009). The only new data for this phase was limited scan line mapping that was collected by the mine in the South-western quadrant of the pit and thus similar constraints relating to the orientation of the S2 foliation, joint sets and groundwater applied.

Phase 2 ran concurrently with the above work and was aimed at defining the orientation of the S2 foliation, joint data and pore pressures in the toe of the slope. This phase consisted of structural mapping, drilling, instrumentation installation; and modelling of the geology and ground water table by Basson (2011a) and Liu et al. (2011) respectively.

The structural data collection programme consisted of pit mapping (Scan Line and SIROVISION™) and the review and collation of available borehole information. The initial mapping consisted of conventional scan-line mapping and was subsequently replaced with a more efficient photogrammetry mapping technique, SIROVISION™. The mapping programme was scoped and supervised by the author while mapping data was collected by staff in the Venetia Geotechnical Department. In 2010 Basson was contracted by the author to: analyse the newly collected structural pit mapping information on the S2 foliation, update the geology model and further sub-divide the model into unique structural volumes. Structural volumes are characterized by an internally consistent suite of characteristics, such as a consistent fault style and orientation, consistent foliation orientation or confinement to a particular lithological unit or package. See Table 5.3 and Figure 5.10.

In order to account for pore pressures in the wall and to address the above shortcomings from the previous studies, regarding a groundwater table, the author scoped a drilling and piezometer installation programme of which the aim was install several piezometers in the toe of the slope. Three new boreholes (GDH123, DHH019 and DWH020) were drilled by Partners Drilling, and in total fifteen (15) VW piezometers were installed either close to the face and or toe of the current slope (Figure 5.12 and 5.14) by a sub-contractor. The Itasca Office in Denver, USA, was contracted by the author to update the groundwater model for the pit. The results from the piezometer network were subsequently used by Shchipansky and Atkinson (2010) and Liu et al. (2011) to update the groundwater model.

6. PHASE 3 OPTIMISATION

For the final phase of the optimisation (Phase 3) the Geotechnical domain model and slope design was updated, by the author, using the results from Phase 2 of the study. The updated design incorporated the updated groundwater table and considered the orientation of the pit slopes relative to the foliation. This phase consisted of:

- Review and analysis of fall of ground data in order to outline and define Geotechnical domains and the factors that control stability in each of those domains.
- Incorporating the findings of the literature survey in the design and re-definition of the rock mass model.
- Re-defining the rock mass model and summarise for each domain, which includes the calculation of rock mass ratings, analyses of laboratory rock testing data and calculation of rock mass and joint strengths.
- Constructing and collating the critical Geotechnical data in a 3D Block model.
- Kinematic/Stereographic Analysis to demonstrate failure mechanisms.
- Empirical analysis of inter-ramp angles.
- Bench, inter-ramp and overall slope analysis: Probabilistic limit equilibrium bench analyses were conducted by the author for every practical orientation of each domain, at various bench heights, using SWISA™ and PFISA™. For the inter-ramp and overall slope design limit equilibrium probabilistic analysis were conducted using the programme SLIDE™. The anisotropic strength model in SLIDE™ was used to account for the S2 foliation. The numerical finite difference code, FLAC™, was used to validate the results of the limit equilibrium stack analysis.

Design parameters and factors that control the stability for each of the domains are presented in this chapter.

6.1 ROCK MASS MODEL

6.1.1 Intact strength

The uni-axial compressive strength (UCS) data set consists of 1107 samples (See Table 6.1) and was analysed according to Jaeger (1960) to ascertain the effects of anisotropy and discontinuities on the UCS. The results are presented in Figure 6.1 showing the Gneissic Rocks (Biotite Gneiss, Biotite Schist and Amphibolite). From the results it is clear that a definitive trend is not visible as postulated by Jaeger (1960). This could be for reasons as noted by Brady and Brown (2004) [See previous sections].

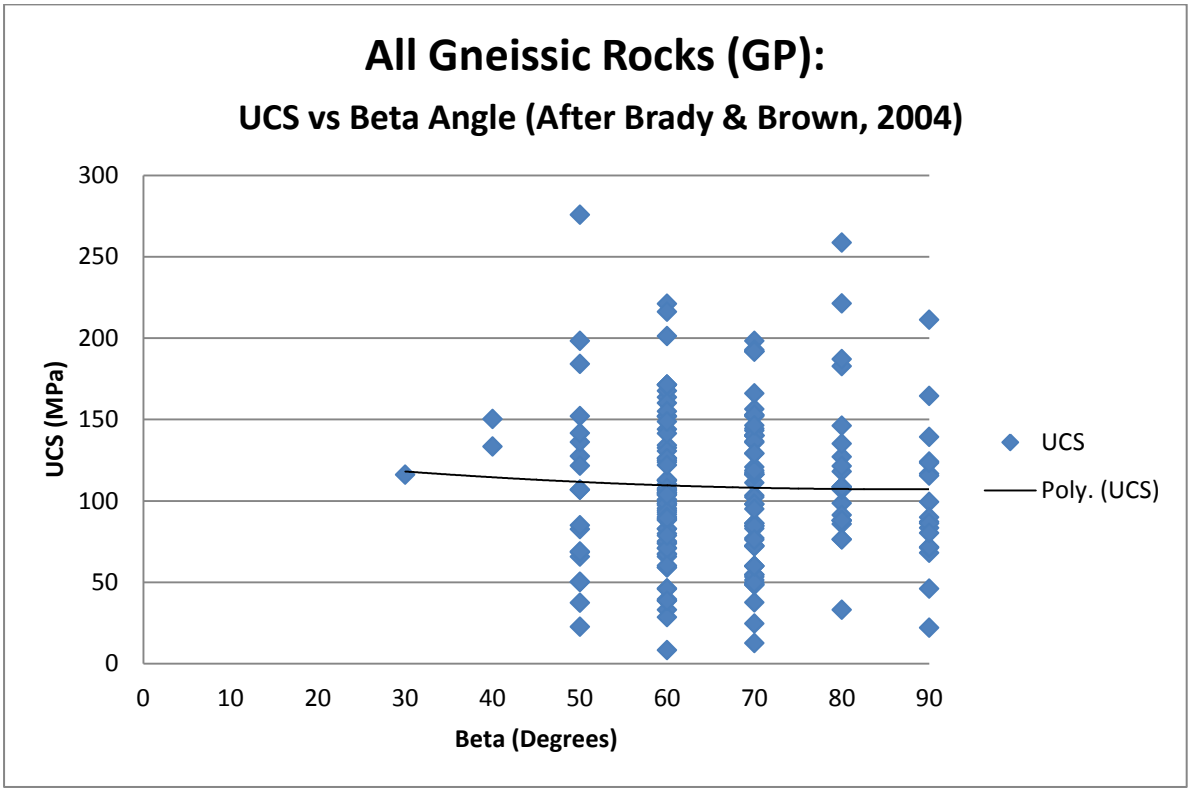


Figure 6.1 Plot of Beta angle after Jaeger (1960) versus uniaxial compressive strength for samples that failed on a discontinuity.

The layering within metamorphic rocks is called foliation and the intensity of the foliation is dependent on the mineral assemblage and intensity of the metamorphic process (heat and pressure). The intensity of the foliation on a lab sample scale varies and could be another

reason why the scatter in the data is observed. Thus two samples with the same Beta angle could have different results purely based on the intensity of the metamorphic foliation. The site is also affected by several brittle deformation events thus failure will not only occur on the foliation but also on brittle discontinuities within the rock mass (laboratory samples). The plane of failure was not described and thus it is not clear on what type of discontinuity a sample failed.

Table 6.1 The UCS results for all the country rock types and their mode of failure.

	Average of UCS (MPa)					Count of UCS				
Rock Type	Discontinuity	Intact as per Read and Stacey (2009,) / Brady and Brown (2004)	Not Recorded	Tri-axial (calculated)	Grand Total	Discontinuity	Intact as per Read and Stacey (2009,) / Brady and Brown (2004)	Not Recorded	Tri-axial (calculated)	Grand Total
AM	115	162	146		142	67	84	31		182
BG	112	160	110		137	86	119	21		226
BS	90	123	95		105	93	90	30		213
DOL	161	268	254	173	231	30	53	17	5	105
FQ	104	162	176		130	14	7	3		24
GP				104	104				30	30
MBL	111	125	135	138	126	37	119	23	36	215
MC	93	181	128		121	3	1	4		8
MP	101	147	133	117	123	32	19	32	21	104
Grand Total	110	157	139	124	136	362	492	161	92	1107

The results of the UCS testing for all the rock types, of which Amphibolite (AM), Biotite Gneiss (BG), Biotite Schist (BS), Marble (MBL) and Metapelite (MP) are the most dominant, are presented in Table 6.1. The results are split into four main categories:

- Discontinuity: this category represents all the samples that failed on a discontinuity.
- Intact as per Read and Stacey (2009) / Brady and Brown (2004): Commonly only intact rock strength is used in rock mass classifications and as such only UCS samples that failed through intact rock and which was not affected by discontinuities is to be used for UCS. This category contains samples that only failed through intact rock.

- Not recorded: The failure mode was not recorded for this set. Mostly applicable to historic data sets on the mine.
- Tri-axial (calculated): Calculated as per Hoek (2002) and is the intercept of the line (Beta) as derived from the σ_1 and σ_3 values, on the σ_1 axis.

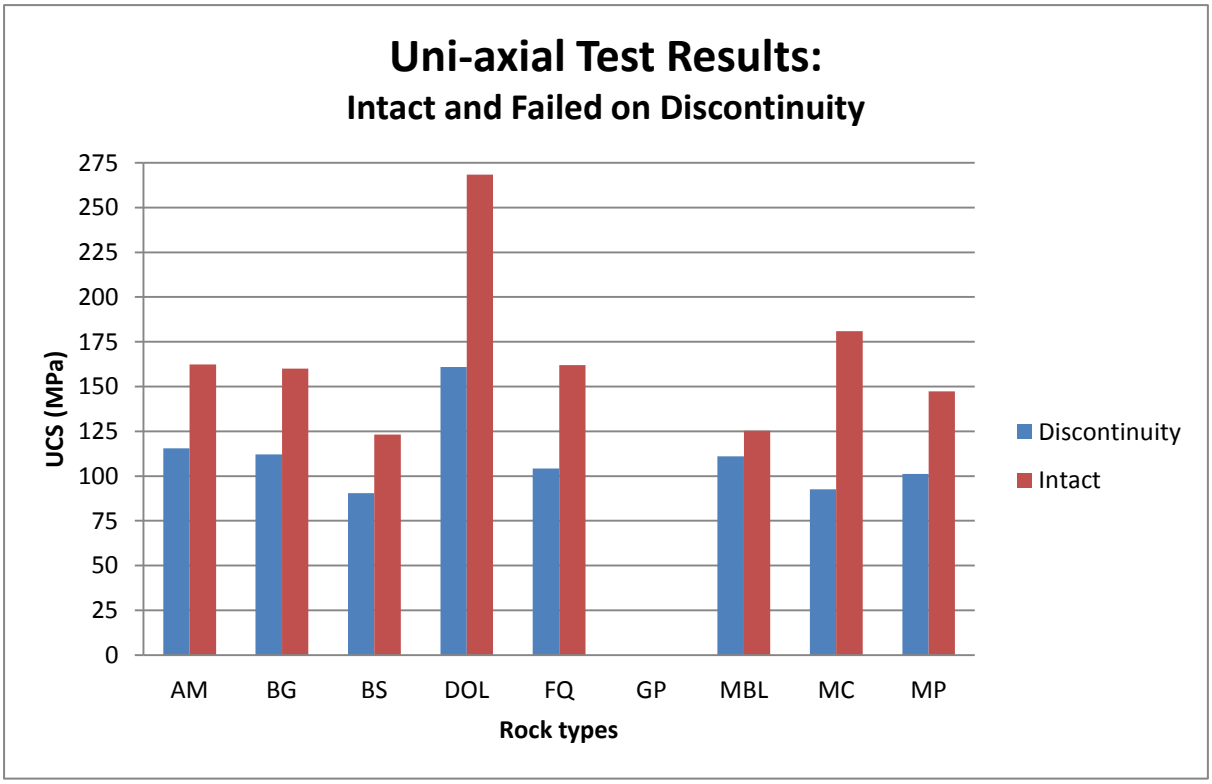


Figure 6.2 Showing the Uni-axial Test Results for those samples that failed through intact rock and on discontinuities.

The results (Table 6.1 and Figure 6.2) indicate that the UCS for the samples that failed on intact rock (Foliated rocks: AM, BG, BS, MP, etc.) are between 36%-95% higher.

However the rock mass has been affected by a number of ductile deformation events (D1 to D4), resulting in several ductile planar fabrics (S1-S3), and brittle events. Based on field observations the rock mass, on a meter/lab-sample level, can be divided into the following categories:

- S2a: planar fabric NOT separated ("closed" foliation)
- S2b: planar fabric separated ("open" foliation)

- Massive rock not dominated by biotite and or other mineral assemblage banding. See Figure 6.3

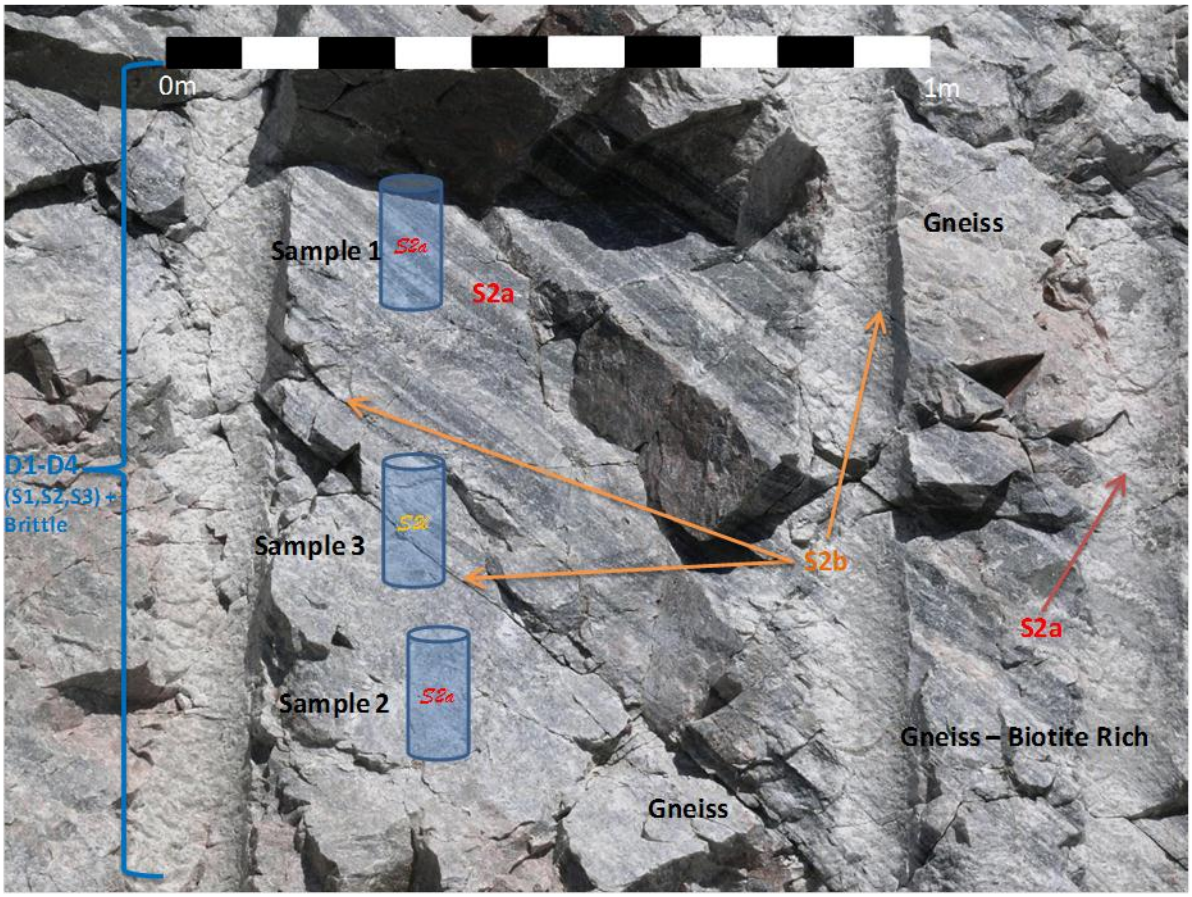


Figure 6.3 Photograph of a Gneiss unit in the Venetia Pit showing the Biotite banding/foliation in the Gneiss.

Thus if three samples are collected each from the above units the following can be assumed:

- **Sample 1:** Will have medium strength in MPa
    - UCS samples are often characterised by lab as failed on "discontinuity"
    - This does not imply an open "joint". Rather failure occurred on the dominant intact S2a fabric ("closed" foliation).
    - For example in the case of Biotite Gneiss the UCS will equal 112 MPa.
- **Sample 2:** Has very little Biotite rich fabric and is massive.
    - Lab will characterize sample as "intact failure".
    - For example in the case of Biotite Gneiss the UCS will equal 160 MPa

- **Sample 3:** Has “open” S2b foliation going through it.
    - Strength will be determined by the strength of the “open joint”.
    - Shear testing on “joints” (S2b) would have been ideal to describe the strength of this sample (not available). Alternatively Saw-cut shear testing and the Barton-Bandis Criterion can be used to calculate the strength of the open planar fabric (S2b). This was also used successfully in the past by SRK at Venetia (Contreras, 2008). The strength of open S2b foliation, referred to as S2 foliation hence forth, is described in subsequent sections of this project. This is consistent with the scale effects demonstrated by Hoek and Karzulovic (2000) and Karzulovic (2006) which noted that the Hoek Brown criterion does not apply to a single planar feature.

Thus if only the intact testing results are used, as noted by Read and Stacey (2009) and Brady and Brown (2004), and the effect of the “closed” fabric in the rock will be ignored and thus the strength on a lab scale will be overestimated. Therefore UCS results were not filtered and the UCS, that contains the intact and failed on discontinuity/fabric data sets, was used for this project. See Table 6.1.

6.2 Weathering Horizon

Historically a 60m weathering horizon was incorporated into the Venetia slope designs with angles being adjusted empirically to cater for the effect of paleo-weathering.

No historic strength data was available and or calculated for this horizon. In order to address this UCS results were sub-divided into two horizons: A weathered horizon (0-60m) and fresh (60m and below). The results confirms the historical empirical estimate of the weathered horizon with UCS values in the weathered horizon being up to 39% lower (BS) than in the fresh horizon. The biotite rich rocks (BG and BS) are the most affected by weathering. See Table 6.2.

Table 6.2 The UCS results summarised for the fresh and weathered horizons.

	Average of UCS (MPa)		
Rock Type	**Fresh**	**Weathered**	**Average**
AM	143	133	142
BG	140	83	137
BS	108	66	105
DOL	231		231
FQ	130		130
GP	118	64	104
MBL	126	119	126
MC	127	85	121
MP	123	125	123
Average	138	97	136

6.3 Weighting of Data

The geology of the country rock is complex and the 3D model only contains the main packages (Gneiss, Metasediments, Marble and Dolerite). However each of these units consists of interbedded units of various quantities; see Figure 1.6 and Table 1.1 (After Rigby et al., 2011). Extensive drilling was conducted in the country rock and a total of 142 682m of core is available consisting of 21920 country rock Geotechnical intervals.

Biotite Schist is for example 20.4% of the laboratory UCS dataset, however in Structural Volume 4 (Gneiss Rocks – GP) it makes up 34.6% of the Gneiss package. Thus if the average strength of only the laboratory samples were to be used the strength in a package could be incorrectly estimated and it would not be possible to estimate the variability of the UCS in a specific domain. See Table 6.3. The following was done to weight the data:

- The data (UCS, GSI, etc.) for each rock type was applied to the relevant drilling interval, according to the geology logs to account for the variability in the geology.
- The 2011 3D model as constructed by Basson (2011a) was used to tag each drilling interval in the dataset with the structural volume type.
- Subsequently the Hoek-Brown Criterion (Hoek et al., 2002) was used to calculate the strength for each interval.
- Data was then summarised (average, standard deviation, etc.) per domain.

The average values for each domain are summarised in Table 6.4 for reference purposes.

Table 6.3 Percentage of each Rock per Geotechnical Domain (Structural Volume).

	% of each Rock per Geotechnical Domain (Structural Volume)														
Domain	AM	BG	BIF	BS	CAL	CLS	CRBR	DOL	FQ	GP	MBL	MC	MP	PEG	UN
STRV1	26.9	32.3	0.0	31.5	0.3	1.0	0.9	0.2	0.1	5.8	0.0	0.1	0.7	0.0	0.0
STRV10	2.4	0.9		1.5	0.0	0.0	0.5	92.4	0.1		0.2	0.2	1.8	0.0	
STRV2	7.9	82.0		10.1											
STRV3	2.1		0.4	7.1	0.5	0.3	0.4	3.8	23.1	0.0	15.3	11.8	34.9	0.0	
STRV4	28.0	28.7		34.6	0.1	0.6	0.9	1.0	0.9	5.0			0.2	0.1	
STRV5	29.1	29.8		33.5	0.7	0.3	0.8	0.9	0.1	4.5			0.3	0.0	
STRV6	3.9			12.4		0.1	1.8	1.5	29.4		9.5	5.4	35.4	0.1	
STRV7	11.3			24.5		0.0		3.8	17.5		4.1	2.1	36.6		
STRV8	22.1	17.9		29.9	0.1	0.4	0.4	2.1	6.2	3.6	1.7	2.8	12.7	0.1	
STRV11	7.8	1.4		2.3	0.5	0.1	0.0	3.4	0.2		54.2	25.2	4.8	0.0	
Grand Average (%)	18.7	18.1	0.0	23.2	0.2	0.4	0.7	13.4	4.9	3.1	5.6	3.4	8.2	0.0	

Table 6.4 The Average UCS and related Standard deviation for each Structural Volume (Domain) and sub-domain (weathered and fresh).

	Average of UCS (MPa)		**Standard Deviation of UCS (MPa)**	
Structural Volume	FRESH	WEATHERED	FRESH	WEATHERED
STRV1	131	91	18	33
STRV2	141	76	1	9
STRV3	129	77	22	26
STRV4	131	90	22	29
STRV5	132	85	24	35
STRV6	130	79	26	19
STRV7	128	82	28	17
STRV8 GP	134	88	22	35
STRV8 MBL	160		46	
STRV8 MP	129	76	28	18
STRV10	210	106	45	33
STRV11	140	94	34	34

6.4 Shear Strength of the Foliation

The shear strength testing dataset, for the foliation at Venetia, consists of Triaxial shear (Goodman, 1989) and direct shear tests on saw-cut dry surfaces.

The tri-axial shear testing dataset was reviewed and results were discarded if the samples for the testing suite did not originate from the same borehole and or did not have the same rock

code. The filtered results are presented in Table 6.5. In addition the uniaxial compressive strength was calculated for each suite in RocData™ as per Hoek (2002). The results indicate that the strength of the "closed" foliation (S2a) is high and matches the observation made in the previous section regarding the strength of the closed foliation (S2a).

The shear testing on saw cut surfaces indicated that the basic friction angles of the units are in the medium to high category (Wyllie and Mah, 2005) with the lowest values occurring in the Marble and Metasediment Packages. See Table 6.6.

Table 6.5 Tri-axial shear testing on closed foliation (S2a).

Sample No.	Borehole No.	Package	Rock Type (Mapped Unit)	Rock Code	No of Samples in Testing Suite	Calculated strength at σ_3=0 in MPa
DHG154	GDH123	Gneiss	BS	BS	3	60.21
DHG251	GDH124		AM	BAM	5	228.47
DHG259	GDH124			BAM	5	302.07
DHG263	GDH124			BAM	4	133.17
DHG275	GDH124		BG	BG	3	132.67
DHG281	GDH124			BG	5	180.75
DHG316	GDH121			BG	5	220.69
DHG290	GDH122	Metasediments	MC	MC	5	120.57
DHG173	GDH122		MP	MP	6	130.58
DHG250	GDH124			MP	4	114.16
DHG300	GDH122			MP	4	126.57
Total					**49**	

Table 6.6 Results for shear tests on dry saw-cut surfaces.

Package	Basic Friction Angle			Rock Type	Basic Friction Angle		
	Average	Standard Deviation	Count		Average	Standard Deviation	Count
Gneiss (GP)	36.1	4.1	90	AM	37.8	3.3	29
				BG	37.1	3.3	27
				BS	34.0	4.3	34
Dolerite (DOL)	38.4	2.9	10	DOL	38.4	2.9	10
Marble(MBL)	30.2	8.9	5	MBL	30.2	8.9	5
Metasediments (MP)	33.2	2.8	8	MP	29.7	0.3	2
				QTZ	34.4	2.3	6
Total			**113**				**113**

Joint roughness (JRC) values were collected during scan line and SIROVISION™ mapping. JRC values during the scan line mapping were visually estimated. The main issue with the visual estimation method is that roughness is scale dependant and roughness was thus not consistently correctly estimated. For the SIROVISION™ programme roughness or unevenness amplitudes were measured using a ruler at a constant scale of 500mm. Roughness or unevenness amplitudes were then converted to the corresponding JRC value as per the method described by Barton and Bandis (1982). See Table 6.7.

The Metasedimentary units have smoother profiles (lower JRC values) when compared to the Gneissic units. The mapping also indicated that the foliation has no infilling and thus the UCS can be assumed to be the same as the JCS.



Figure 6.4 Illustrating how the roughness or unevenness amplitudes were measured on a 500mm scale.

Table 6.7 Joint roughness coefficient for all the rock types as obtained from pit mapping.

Package			Rock Type			Rock Type: Sub-Unit		
	Average	Count		Average	Count		Average	Count
GP	14.0	2795	AM	17.9	588	AM	18	588
			BG	12.5	1602	BBG	8	299
						BG	6	92
						QFG	14	1211
			BS	15.2	605	BS	15	554
						GBS	17	38
						SBS	6	13
MP	11.5	745	BIF	5.0	15	BIF	5.0	15
			FQ	13.0	571	FQ	15	443
						QTZ	6	128
			MC	3.0	4	MC	3.0	4
Total		3540	MP	6.7	155	PHY	7	155
					3540			

The largest planar failure in the history of the mine occurred on 2 July 2003 when a 280 000 tonne fall of ground occurred in the Cut 3 south wall (Tsheko, 2010). The failure exposed a plane with a persistence of approximately 50m down dip. Values were thus scaled from the mapping (500mm) to 50 000mm. See Figure 6.5.



Figure 6.5 The largest failure to date in the Venetia pit (Tsheko, 2010) on 2 July 2003 in Cut 3.

The JCS, JRC and Basic Friction Angles Results were used to calculate the scaled strength of the foliation. Similar to the UCS analysis the results for each drilling interval was calculated in order to take into account the variability in the rockmass and subsequently summarised for each domain and sub-domain (fresh and weathered). See Table 6.8 for the results.

Using the above mentioned inputs (UCS, BFA and JCS) values around 40° (friction angle) and 50 kPa (cohesion) is calculated at a norma1 stress of 1 MPa. This is consistent with previous studies undertaken by Cabrera et al. (2011) at Venetia. See Table 6.8.

Table 6.8 The strength results of the foliation.

Normal Stress (MPa)	Structural Volume (Domain)	Sub-Domain: FRESH				Sub-Domain: WEATHERED			
		Average		Standard Deviation		Average		Standard Deviation	
		Friction Angle (ϕ)	Cohesion (kPa)	Friction Angle (ϕ)	Cohesion (kPa)	Friction Angle (ϕ)	Cohesion (kPa)	Friction Angle (ϕ)	Cohesion (kPa)
1	STRV1	39.1	49.4	1.8	4.1	38.5	48.4	2.0	3.9
	STRV2	40.6	52.9	0.4	3.9	38.1	50.0	2.1	4.3
	STRV3	35.4	40.6	2.0	9.2	34.7	42.3	1.9	6.4
	STRV4	38.9	48.9	1.8	3.9	39.1	50.1	1.6	3.7
	STRV5	39.0	49.2	1.8	4.1	38.4	48.7	2.0	3.9
	STRV6	35.9	44.1	2.0	6.1	35.0	42.7	2.0	6.4
	STRV7	36.3	44.8	2.1	4.2	34.8	44.0	1.8	4.0
	STRV8 GP	39.2	49.5	1.7	4.1	38.2	47.7	1.9	3.2
	STRV8 MP	36.8	44.9	2.3	5.8	35.3	42.2	2.1	8.3

6.5 Tensile Strength

A total of 1865 Brazilian Tensile Strength results were present in the database. The results were summarised per rock type and are presented in Tables 6.9 and 6.10.

Table 6.9 The Brazilian tensile strength for the country rock units.

Rock Type	Average Tensile Strength (MPa)	Count
AM	13	178
BG	12	160
BS	10	190
DOL	19	139
FQ	13	36
GP	12	325
MBL	7	168
MC	9	8
MP	13	133
Total		1337

Table 6.10 The Brazilian tensile strength for the kimberlite units.

Rock Type	Average Tensile Strength (MPa)	Count
K01CMVK	4	6
K01CRBW	10	12
K01DVK	10	134
K01MVK	8	80
K01RVK	9	8
K02CRBE	10	22
K02MVK	6	42
K02VKBR	6	51
K02VKBRL	9	161
K04	8	12
Total		528

6.6 Triaxial testing and calculation of m_i

The triaxial database contains 239 suites of samples, each consisting of 3-5 samples per suite. The m_i value and coefficient of determination (r^2) for each suite was calculated as recommended by Hoek (2002). In addition m_i values were also calculated using the method described by Cai (2009).

The r^2 values for the tri-axial testing in general was low (0.5 range) with only some of the rocks having r^2 values of 0.83. The low r^2 values might be due to sub-standard historic sample selection. Hoek noted that values with r^2 of 0.9 and higher are considered as high

quality. In general the results for Hoek (2002) and Cai's (2009) methods indicated very similar results for the major rock types with the only noticeable difference occurring in the non-foliated units (Marble and Dolerite). The results are presented in Tables 6.11 and 6.12.

Table 6.11 The m_i results for the country rocks using Hoek (2002) and Cai (2009) methods.

Rock Type	(Hoek, 2002)			(Cai, 2009)		
				Fresh	Weathered	Global Average
	m_i	Average of r2	Count	m_i	m_i	m_i
AM	9	0.48	25	11	10	11
BG	18	0.54	28	12	7	12
BS	7	0.50	34	10	6	10
DOL	18	0.44	17	12		12
GP	11	0.52	17	10	5	8
MBL	13	0.83	44	18	17	18
MC				13	9	13
MP	8	0.56	22	9	10	9
QTZ	10	0.70	7	10		10
Total			194			

Table 6.12 The m_i results for the kimberlite rocks using Hoek (2002) and Cai (2009) methods.

Rock Type	(Hoek, 2002)			(Cai, 2009)		
				Fresh	Weathered	Global Average
	m_i	Average of r2	Count	m_i	m_i	m_i
K01CKNE	10	0.87	2	9		9
K01CKNW	6	0.51	2	8		8
K01CKS	5	0.54	2	4		4
K01CRBW	10	0.53	2	12		12
K01DVK	6	0.53	25	7		7
K01MVK	4	0.63	9	8		8
KIM	3	0.31	1	9		9
Total			43			

6.7 Density and Elastic Properties (Young's Modulus and Poisson's Ratio)

Density testing was done on the UCS and Tri-axial dataset and consists of 3848 samples in the country rock and 1522 in the kimberlite. For consistency the densities and elastic properties were weighted and summarised per domain. See Tables 6.13 to 6.17 for the density and elastic properties.

Table 6.13 Density of the country rock units.

Rock Type	Fresh		Weathered		Total	
	Density (t/m^3)	Count	Density (t/m^3)	Count	Density (t/m^3)	Count
AM	2.91	581	2.89	38	2.91	619
BG	2.64	563	2.62	54	2.64	617
BS	2.83	736	2.79	37	2.82	773
DOL	2.91	387	2.89	15	2.91	402
GP	2.77	357	2.82	22	2.78	379
MBL	2.85	525	2.78	27	2.84	552
MP	2.83	362	2.81	23	2.83	385
QTZ	2.71	108	2.66	13	2.70	121
Total		3619		229		3848

Table 6.14 Weighted density for each country rock structural volume (domain).

Structural Volume (Domain)	Fresh	Weathered
	Density (t/m^3)	Density (t/m^3)
STRV1	2.79	2.76
STRV2	2.79	2.76
STRV3	2.80	2.76
STRV4	2.79	2.76
STRV5	2.79	2.76
STRV6	2.80	2.76
STRV7	2.80	2.76
STRV8 GP	2.79	2.76
STRV8 MBL	2.85	2.78
STRV8 MP	2.80	2.76
STRV10	2.91	2.89
STRV11	2.85	2.78

Table 6.15 Density of the kimberlite units.

Rock Type	Total	
	Density (t/m^3)	Count
K01CKNE	2.73	45
K01CKNW	2.76	26
K01CKS	2.71	56
K01CMVK	2.52	13
K01CRBW	2.76	48
K01DVK	2.72	721
K01MVK	2.64	231
K01RVK	2.56	25
K02CRBE	2.72	37
K02MVK	2.61	83
K02VKBR	2.60	87
K02VKBRL	2.70	333
KIM	2.82	5
Total		1522

Table 6.16 Elastic properties (Young's Modulus and Poisson's ratio) of the country rock units.

Rock Type	Young's Modulus (GPa)	Poisson's Ratio	Count
AM	73	0.28	181
BG	64	0.26	226
BS	58	0.26	213
DOL	86	0.28	100
FQ	67	0.18	24
MBL	81	0.34	179
MC	77	0.32	8
MP	65	0.32	83
Grand Total			1014

Table 6.17 Elastic properties (Young's Modulus and Poisson's ratio) of the kimberlite units.

Rock Type	Young's Modulus (GPa)	Poisson's Ratio	Count
K01CKNE	56	0.33	20
K01CKNW	47	0.31	15
K01CKS	36	0.28	15
K01CMVK	12	0.22	4
K01DVK	37	0.28	306
K01MVK	20	0.22	97
K01RVK	14	0.23	20
K02CRBR	50	0.25	3
K02MVK	15	0.18	36
K02VKBR	18	0.21	23
K02VKBRLOW	30	0.24	88
K03CRBSW	52	0.16	6
Grand Total			633

6.8 Rock Mass Ratings

Laubscher's (1990) rock mass rating (MRMR) was calculated from the drilling dataset and contains approximately 30 000 Geotechnical intervals (country rock and kimberlite) that were derived from 368 boreholes. In general the rocks are within the fair to good category with the RMR always lower in the weathered domains when compared to the fresh. See Tables 6.18 and 6.19. The weighted MRMR's are presented in Table 6.20.

Table 6.18 Mining Rock Mass Ratings for the country rock units with no mining adjustments applied (Laubscher, 1990).

Rock Type	Average		Standard Deviation	
	Fresh	Weathered	Fresh	Weathered
AM	67	63	10	12
BG	66	55	9	11
BIF	52	53		2
BS	66	58	10	10
CAL	70	61	4	11
CLS		61		
DOL	69	64	10	10
FQ	64	51	10	11
GP	69	67	9	9
MBL	70	64	10	11
MC	69	65	10	10
MP	61	54	11	11
PEG	62		8	

Table 6.19 Mining Rock Mass Ratings for the kimberlite units with no mining adjustments applied (Laubscher, 1990).

Rock Type	Average MRMR		Standard Deviation	
	Fresh	Weathered	Fresh	Weathered
CRBR	66	45	10	1
K01CKN				
K01CKNE	78		8	
K01CKNW	69		6	
K01CKS	66		7	
K01CMVK				
K01CRBNW	64		6	
K01CRBW	55	50	9	1
K01DVK	66		10	
K01MVK	62		8	
K01RVK	62		10	
K02CRBE				
K02CRBR	67		8	
K02CRBRNW	64		9	
K02MVK	67		8	
K02VKBR	69		8	
K02VKBRLOW	70		9	
K03CK	66	56	9	8
K03CRBLOWE	72		9	
K03CRBS	63		6	
K03CRBSW	67		9	
K03VK	67	51	9	12
K03VKBN	69	47	8	
K03VKBSE	65		8	
KIM	66	56	10	10

Table 6.20 Weighted Mining Rock Mass Ratings for the country rock units with no mining adjustments applied (Laubscher, 1990).

Rock Type	Average MRMR		Standard Deviation	
	Fresh	Weathered	Fresh	Weathered
STRV1	68	60	10	12
STRV2	66	52	4	6
STRV3	68	56	10	12
STRV4	69	58	9	11
STRV5	66	60	9	11
STRV6	64	54	11	11
STRV7	60	49	9	11
STRV8 GP	65	62	10	14
STRV8 MBL	67		9	
STRV8 MP	64	53	11	13
STRV10	68	51	10	13
STRV11	67	65	11	9

Window mapping for rock mass rating purposes was revived, and subsequently supervised by the author, in 2009 and conducted by staff in the Venetia Geotechnical Department. Unlike the drilling campaigns, the foliation data in the pit window mapping was always noted correctly separately from other joint sets. The foliation was removed from the mine's window mapping dataset and MRMR's calculated to ascertain the effect of foliation on the MRMR. See Table 6.21.

The results indicate that the MRMR is between 10 to 20 points higher when the foliation is removed from the calculation. Structural Volume 6 data is unchanged since it consists of only 3 data points that were captured in a massive BS in the weathered horizon. There is also a good correlation between the drilling and mapping datasets considering that the mapping data set only contains 393 entries compared to the almost 30 000 in the drilling data set.

Table 6.21 Showing the results for the 2009 – 2011 window mapping dataset with and without foliation (no mining adjustments applied to the MRMR).

Structural Volume (Domain)	MRMR per Horison		Average MRMR			Count
	Fresh	Weathered	With Foliation	No Foliation	Difference	
STRV1	71	60	67	77	+10	111
STRV2		59	59	79	+20	4
STRV3	66	59	62	75	+13	91
STRV4	69	48	62	72	+10	33
STRV5	68	67	67	78	+10	87
STRV6		51	51	51	0	3
STRV8	55	65	62	73	+11	40
STRV10	65	64				24
Total						393

6.9 Rock Mass Strength Properties

The rock mass strength properties were calculated by the author using the Hoek-Brown criterion and related input parameters (Hoek et al., 2002). The RMR's with the effect of foliation were used. This could be considered as conservative since:

- The RMR's without foliation are 10 to 20 points higher.
- Strength anisotropy (due to the S2 foliation) was simulated using an anisotropic model in SLIDE™ and ubiquitous joint model in FLAC™ resulting in the effect of the foliation being double accounted for in the design.

For the purpose of this study, and based on the work done by Terbrugge et al. (2004), Laubscher's RMR (1990) was assumed to be equal to Bieniawski's RMR (1989). The effect of effective cohesion (Jennings, 1972 as discussed by Karzulovic and Read, 2009) was not considered and the foliation was assumed to be continuous along the dip of the slope with no rock bridges.

The slope was modelled in FLAC™ to ascertain the confining stress range and indicated that a failure surface will most likely be located in a zone of relatively low confining stress (0-1MPa). See Figure 6.6. The equivalent linear Mohr-Coulomb parameters were then subsequently calculated, from the Hoek-Brown criterion, at 1MPa confining stress.

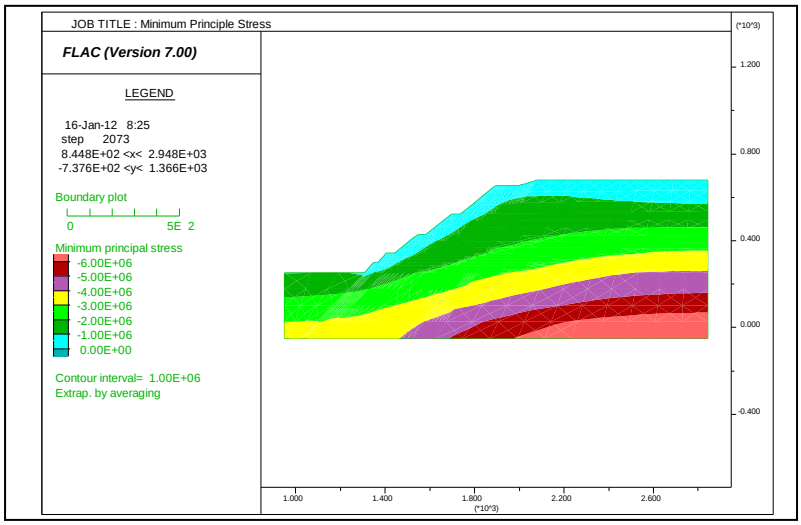


Figure 6.6 FLAC plot showing the minimum principal stress distribution in the south slope.

Damage factors of 1 for shallow conditions and 0.5 for deep conditions were used to estimate the values. This could also be considered as conservative since:

- Hoek (2009) noted that the depth of the blast damage zone is limited. Using the guidelines provided by Hoek (2009) and Lorig (2011); and taking into account that all final faces are excavated using trim blasting techniques (trim blast block = 20 -30m wide) the blast damage zone should be between 15 – 50m deep.
- All final faces are excavated using trim blasting techniques and a D factor = 1 is applicable to very large open pit slopes that suffer significant disturbance due to heavy production blasting (Hoek, 2002). See Tables 6.22 and 6.23 for the rock mass strength properties.

Table 6.22 Rock Mass Strength Properties for the various country rock domains

Structural Volume (Domain)	FRESH								WEATHERED							
	Average				Standard Deviation				Average				Standard Deviation			
	Damaged		No Damage		Damaged		No Damage		Damaged		No Damage		Damaged		No Damage	
	friction angle (°) (D=1,sig3=1)	cohesion (MPa) (D=1,sig3=1)	friction angle (°) (D=0.5,sig3=1)	cohesion (MPa) (D=0.5,sig3=1)	friction angle (°) (D=1,sig3=1)	cohesion (MPa) (D=1,sig3=1)	friction angle (°) (D=0.5,sig3=1)	cohesion (MPa) (D=0.5,sig3=1)	friction angle (°) (D=1,sig3=1)	cohesion (MPa) (D=1,sig3=1)	friction angle (°) (D=0.5,sig3=1)	cohesion (MPa) (D=0.5,sig3=1)	friction angle (°) (D=1,sig3=1)	cohesion (MPa) (D=1,sig3=1)	friction angle (°) (D=0.5,sig3=1)	cohesion (MPa) (D=0.5,sig3=1)
STRV1	50	0.894	56	1.397	1.9	0.141	1.8	0.222	39	0.516	47	0.837	8.2	0.226	8.2	0.362
STRV2	51	0.909	57	1.422	0.2	0.056	0.4	0.090	37	0.354	46	0.583	0.6	0.003	0.9	0.000
STRV3	49	0.804	56	1.259	3.5	0.227	2.6	0.334	38	0.363	48	0.576	8.5	0.167	8.6	0.254
STRV4	50	0.895	56	1.398	1.7	0.166	1.5	0.261	39	0.487	48	0.792	7.2	0.211	7.1	0.335
STRV5	50	0.900	56	1.407	1.7	0.177	1.5	0.280	38	0.449	46	0.731	9.1	0.213	9.3	0.341
STRV6	49	0.787	56	1.240	3.3	0.244	2.4	0.367	39	0.362	48	0.579	4.7	0.144	4.2	0.224
STRV7	48	0.785	55	1.242	3.2	0.243	2.7	0.373	40	0.368	50	0.581	5.7	0.144	4.3	0.205
STRV8 GP	50	0.919	56	1.436	1.7	0.174	1.5	0.273	39	0.513	47	0.832	8.5	0.226	8.5	0.361
STRV8 MBL	52	1.074	58	1.683	2.5	0.363	1.9	0.572								
STRV8 MP	49	0.818	56	1.287	2.8	0.240	2.2	0.368	38	0.374	48	0.600	5.5	0.138	5.4	0.211
STRV10	54	1.473	59	2.313	3.0	0.358	2.3	0.562	44	0.556	53	0.879	6.3	0.227	4.7	0.353
STRV11a	54	0.981	59	1.485	3.1	0.209	2.5	0.331	44	0.569	52	0.877	12.6	0.218	12.6	0.332
STRV11b	53	1.034	59	1.573	2.7	0.254	2.1	0.412								
STRV11c	53	1.027	59	1.566	2.9	0.260	2.3	0.419	44	0.549	51	0.858	3.3	0.118	2.2	0.177

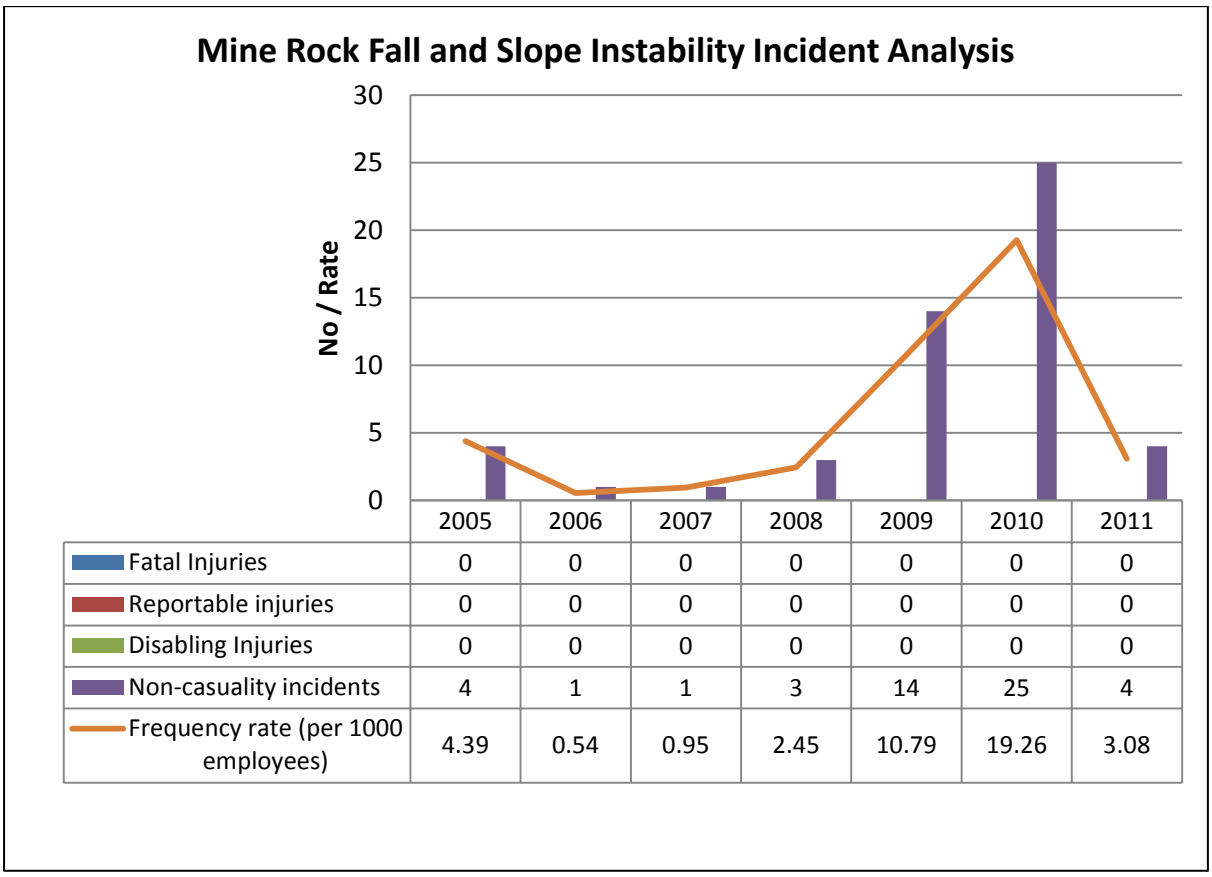
Table 6.23 Rock Mass Strength Properties for the various kimberlite units. No weathered kimberlite present (mined out).

Structural Volume (Domain)	Average		Standard Deviation	
	friction angle (°) (D=1,sig3=1)	cohesion (MPa) (D=1,sig3=1)	friction angle (°) (D=1,sig3=1)	cohesion (MPa) (D=1,sig3=1)
K01CKNE	53	2.827	1.5	1.404
K01CKNW	45	1.348	2.0	0.629
K01CKS	40	0.886	2.4	0.434
K01CRBNW	36	0.356	2.6	0.071
K01CRBW	31	0.249	5.2	0.106
K01DVK	45	0.863	4.7	0.542
K01MVK	40	0.496	4.3	0.215
K01RVK	28	0.361	4.7	0.242
K02CRBR	51	1.070	3.2	0.668
K02CRBRNW	50	0.871	4.3	0.479
K02MVK	39	0.540	4.0	0.325
K02VKBR	41	0.617	4.1	0.282
K02VKBRLOW	47	1.074	3.5	0.752
K03CK	41	0.727	5.7	0.706
K03CRBLOWE	46	1.260	3.4	0.634
K03CRBS	43	0.617	2.4	0.211
K03CRBSW	44	0.932	3.5	0.648
K03VK	43	0.920	5.5	0.779
K03VKBN	44	0.957	4.5	0.522
K03VKBSE	43	0.788	3.3	0.478

6.10 GEOTECHNICAL MODEL AND DOMAINS

6.10.1 Fall of Ground Analysis

Analysis of rock fall and slope instability incidents indicated that the rock fall frequency rate peaked in 2009 and 2010 at Venetia Mine. This is mainly due to poor mining practices in Cut 3 from 2006 to 2008. The result was an increase in the rock fall frequency in the following years as mining progressed below these areas. See Figure 6.7.



	2005	2006	2007	2008	2009	2010	2011
Fatal Injuries	0	0	0	0	0	0	0
Reportable injuries	0	0	0	0	0	0	0
Disabling Injuries	0	0	0	0	0	0	0
Non-casuality incidents	4	1	1	3	14	25	4
Frequency rate (per 1000 employees)	4.39	0.54	0.95	2.45	10.79	19.26	3.08

Figure 6.7 Mine rock fall and slope instability incident analysis

Analysis of all the fall of ground statistics indicated the following:

- The majority of incidents (67%) are structurally controlled. This is mainly due to the structural geology in the pit. However poor blasting practices up to 2008 promoted the occurrence of kinematic failures.
- Rock falls (12%) are mainly because of poor mining practices (side casting, uncontrolled blasting and insufficient cleaning and barring practices). A number of

these historic rock falls were actually incorrectly classified and can be attributed to steep wedges that are formed between the J2 and J4/J6 joint sets.

- Slumping or shearing (21%) occurs in the kimberlite and is due to weathering and over mining (triple and quadruple benches) of the kimberlite up to 2008. The over mining was due to a waste stripping bottle neck. This mining practice has been stopped and the waste bottleneck mined out. The operational controls are discussed in latter sections of this project.

Thus the bulk of failures in the pit are either structurally controlled and or the cause of poor historic mining practices. See Figure 6.8.

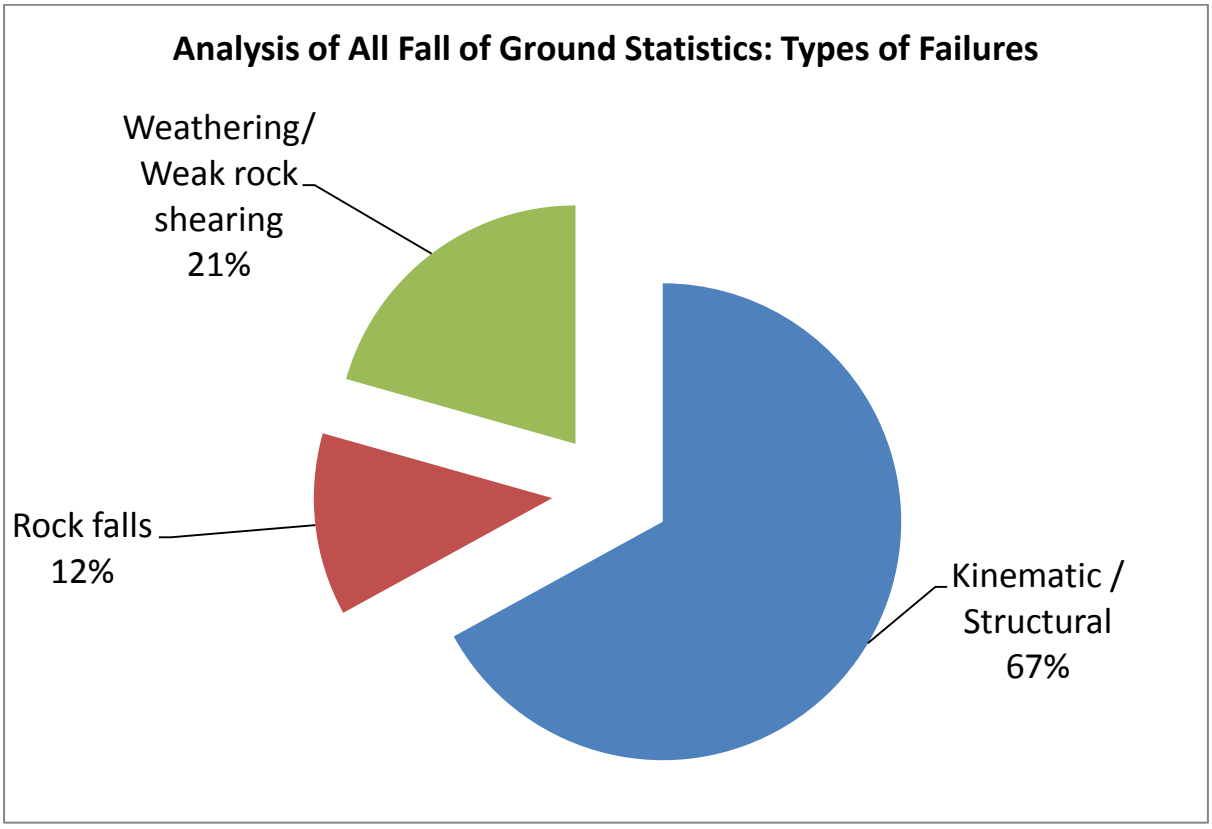


Figure 6.8 Analysis of All Fall of Ground Statistics: Types of Failures

6.10.2 Domain Boundaries

The Geotechnical domains at Venetia are primarily based on the dominant orientation of the primary metamorphic fabric, lithological boundaries, weathering profile and the overall

stability performance of the pit slope; and take into consideration the dominant failure mechanism. The domains can be divided into three tiers:

- Tier 1: Major Domains: The pit shell geometry dictates their location and extent.
- Tier 2: Structural Volumes as defined by Basson (2011a) in Table 5.3 which is based on geological package and the orientation of the S2 foliation in that unit.
- Tier 3: Weathering (Fresh or Weathered).

6.10.3 Tier 1 Major Domains

The positions of the tier 1 domain boundaries are approximate and change with depth, pit face position and orientation. The boundaries have evolved as the pit shell geometry changed and information regarding the Geotechnical conditions in the Cut 4 slope became available:

- The first Cut 4 design was done in July 2008 by SRK (Contreras, 2008). The analysis was conducted on the c4v25 and c5v5 pit designs for Cuts 4 and 5 respectively and consisted of overall slope and inter-ramp limit equilibrium analyses. Essentially only two domains were identified during this study (North and South). Limited information regarding the orientation of the S2 foliation could be supplied to the design consultant and the orientation of the S2 foliation was largely based on old data collected in Cut 2 and 3. A groundwater table had to be inferred since no information was available the time.
- The second update to the boundaries occurred in 2008 and was based on pit mapping in the South-eastern (SE) section of the pit. This resulted in the inclusion of the SE domain with the inter-ramp angle being increased from 40° to 48° (Armstrong, 2008). The author was not involved in the scoping and/or commissioning of the two above mentioned studies.
- In 2009 the author conducted a survey of bench performance in the Southern slopes. The survey indicated that bench performance is the Southern slope could be isolated to distinct areas (Figure 2.1). Since the previous Cut 4 design, 5 benches have also been developed in Cut 4 South. The newly exposed faces and geometrical changes (New shell: cut4v27) necessitated the review of the slope angle in this portion of the pit. Therefore the author initiated and supervised a scan line mapping programme in the South-western (SW) quadrant of Cut 4 South which resulted in a total of 1.5km of

scan line mapping data being collected. Thus the southern slope was divided into additional sectors considering bench performance, slope orientation and geology:

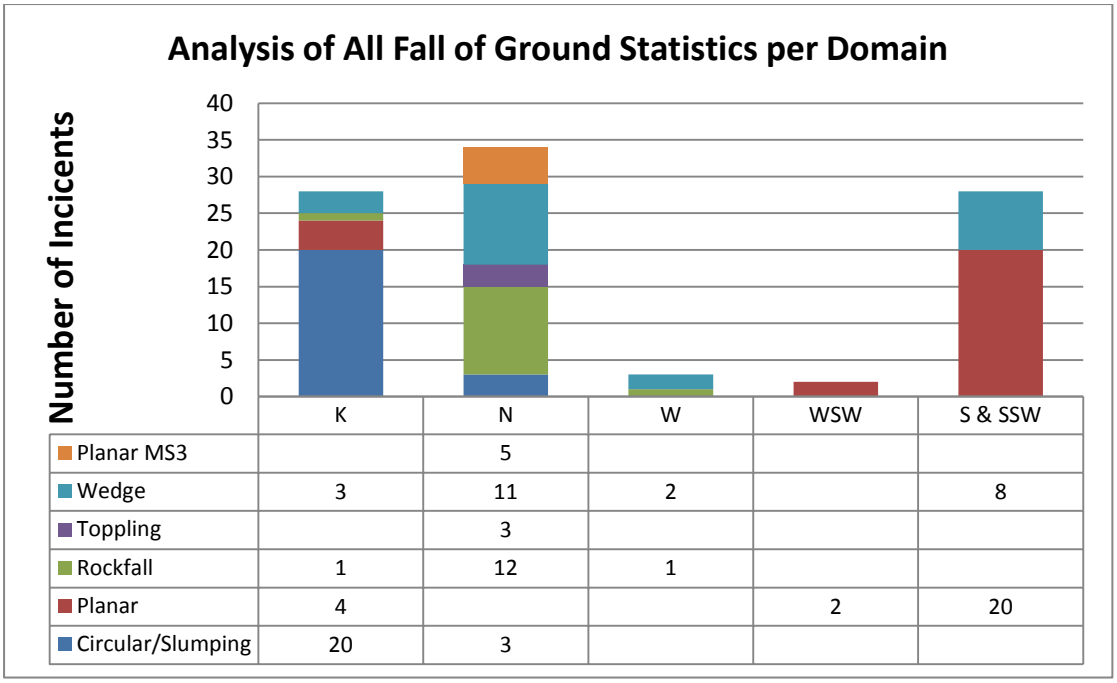
- SSW: Metasediments, Dip direction of slope = approximately 35° – 45°, Eastern boundary is the contact between Gneiss and Metasediments. Poor bench performance
- WSW: Metasediments, Dip direction of slope = approximately 60° – 70°, Northern contact with the Gneiss. Good bench performance.

Itasca was contracted by the author in 2009 to conduct an interim bench and inter-ramp scale analyses on the new domains. The kinematic wedge-and-planar analysis tools, developed by Itasca: SWISA™ and PFISA™ were used for this design (Strouth, 2009). The inter-ramp angle increased from 40° to 41° for the SSW; and 40° to 53° for the WSW. Analysis were conducted for 12m and 15m bench heights. Overall slope analyses were conducted by Itasca using the finite difference code FLAC™ on a representative design section. UDEC was not considered since all structures in the domain were parallel to the design sections (perpendicular to the face) and FLAC™, with a ubiquitous joint model, was deemed the most appropriate tool for the analysis (Gomez, 2010).

Considering the above and historic fall of ground data (See Figure 6.9) the Tier 1 domain boundaries can be summarised as follow:

- North Domain (N): The foliation is steeply dipping into the face. The main failure mechanisms in this domain are wedge type failures and rock falls. For design purposes the East and North domains have been combined (Armstrong, 2008). In the East of this domain the S2 foliation angles are oblique to the pit wall. This is a favourable relationship between the metamorphic fabric and the pit walls. Local planar failures occur exclusively on the MS3 Fault. Two of the three toppling incidents are related to poor loading practices on the upper levels (Bench 1-2) in the weathered Phyllite where benches were undercut during loading.
- Southeast Domain (SE): This is a transitional zone between the South domain and North domain. The difference in strike between the S2 foliation and pit walls are in excess of 20 degrees. Local wedge failure can however still occur. No falls of ground have been recorded in this domain to date.

- South Domain (S): In this sector the foliation strike and the pit wall are within 20° of each other. This varies and is dictated dependant on the orientation/geometry of the pit shell. The dominant failure modes are planar, wedge and step-path type failures along the foliation and consist mainly of rocks from the Gneiss Package,
- South-southwest Domain (SSW): This domain is characterised by both a change in rock type and is dominated by the rocks of the Lezel-Tina Shear zone. The S2 foliation changes in dip direction and as a result the pit walls and foliation are still parallel (within 20 degrees) to each other in this domain. Planar failure is still the dominant failure mechanism.
- West-southwest Domain (WSW): This is a transitional domain between the North and South-southwest domains. Historically this domain has the lowest rock fall history and the difference in strike between the pit walls and foliation is in excess of 30°. Localised wedge failure can still however occur. One incident of planar failure was recorded in 2011 but this was on the interim split shell face that was striking parallel to the foliation and not on the final wall.
- Kimberlite Domain: This domain is holistically used for all the kimberlites in the pit. This domain is characterised by slumping and/or circular failures. See Figures 6.9 and 6.10.



	K	N	W	WSW	S & SSW
Planar MS3		5			
Wedge	3	11	2		8
Toppling		3			
Rockfall	1	12	1		
Planar	4			2	20
Circular/Slumping	20	3			

Figure 6.9 Analysis of fall of ground statistics for each tier 1 domain.

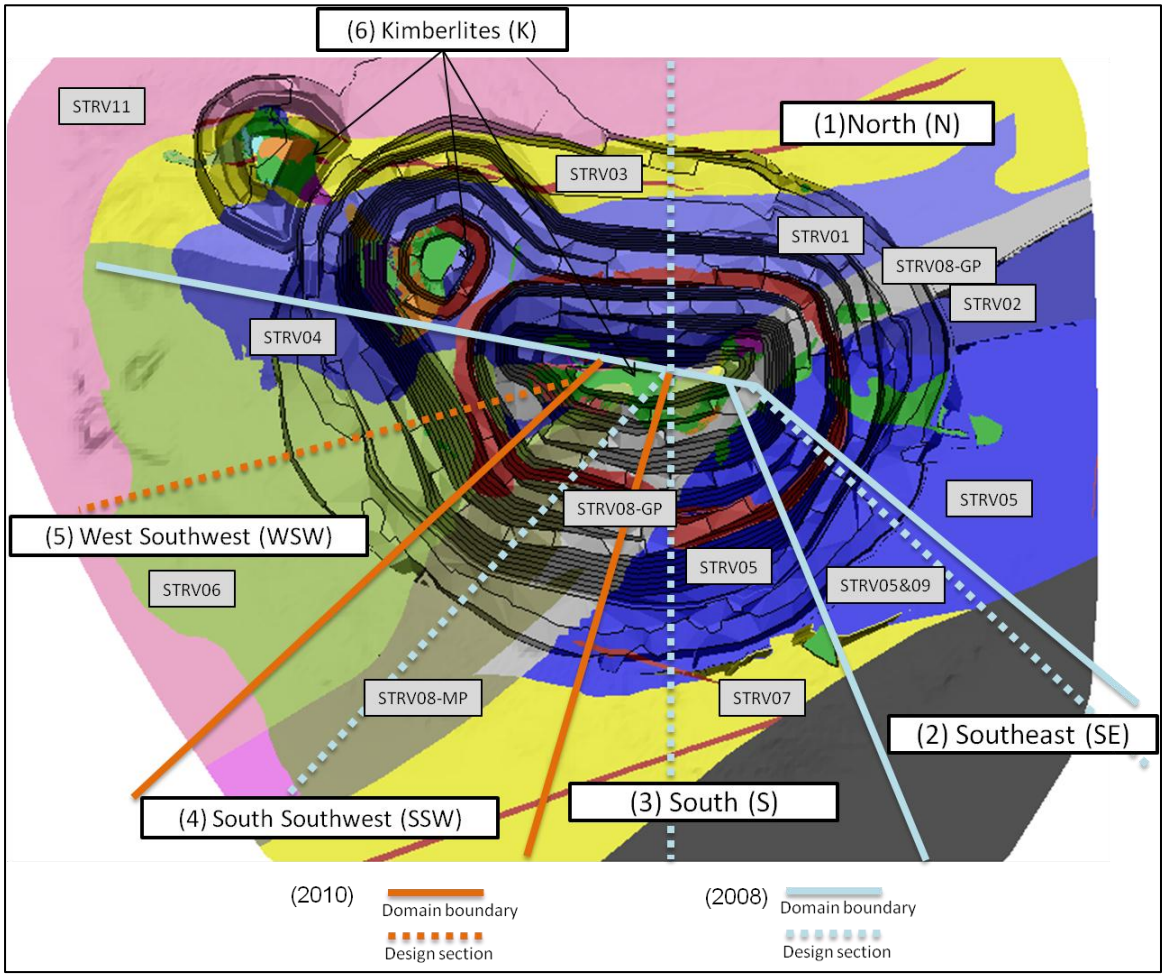


Figure 6.10 Tier 1 and 2 Geotechnical domains.

6.10.4 Tier 2 and 3 Domains

The tier 2 domains are based on the structural volumes as defined by Basson (2011a) and are defined by their lithological composition, orientation of the S2 foliation and their relation to the fold axial plane (FAP3); and Lezel-Tina Fault. The tier 2 domains are further sub-divided into "fresh" and "weathered" based on the results presented in Table 6.2. See Table 6.24 for a summary of the Tier 1 to 3 domains.

Table 6.24 Summary of the tier 1, 2 and 3 domains.

Tier 1	Tier 2	Tier 3	Horison	In Relation to Fold Axis (FAP3)	Lithological Package	In Relation to Lezel-Tina Fault
N	STRV1	STRV1-FRESH	Below 60m	North	Gneiss	West
		STRV1-WEATHERED	0-60m			
N	STRV2	STRV2-FRESH	Below 60m	North	Gneiss	East
		STRV2-WEATHERED	0-60m			
N	STRV3	STRV3-FRESH	Below 60m	North	Metasediment	West
		STRV3-WEATHERED	0-60m			
WSW	STRV4	STRV4-FRESH	Below 60m	South	Gneiss	West
		STRV4-WEATHERED	0-60m			
N / SE	STRV5	STRV5-FRESH	Below 60m	South	Gneiss	East
		STRV5-WEATHERED	0-60m			
SSW	STRV6	STRV6-FRESH	Below 60m	South	Metasediment	West
		STRV6-WEATHERED	0-60m			
SE	STRV7	STRV7-FRESH	Below 60m	South	Metasediment	East
		STRV7-WEATHERED	0-60m			
SSW	STRV8	STRV8-GP -FRESH	Below 60m	N/A	Gneiss	N/A
		STRV8-GP - WEATHERED	0-60m			
		STRV8-MP -FRESH	Below 60m	N/A	Metasediment	N/A
		STRV8-MP - WEATHERED	0-60m			
		STRV8-MBL -FRESH	Below 60m	N/A	Marble	N/A
		STRV8-MBL - WEATHERED	0-60m			
SE	STRV9	STRV9 -FRESH	Below 60m	N/A	N/A	N/A
		STRV9-WEATHERED	0-60m			
ALL	STRV10	STRV 10 -FRESH	Below 60m	N/A	Diabase	N/A
		STRV 10-WEATHERED	0-60m			
ALL	STRV11	STRV 11 -FRESH	Below 60m	N/A	Marble	N/A
		STRV 11-WEATHERED	0-60m			

6.10.5 Geotechnical Block Model

A block model, with the various domains and their related properties was constructed in the GEMS ™ software and is located on the mine servers. See Table 6.25, Figures 6.11 and 6.12.

Table 6.25 The geometric properties of the Geotechnical block model.

Criteria		Value
Number of Blocks	Columns	118
	Rows	104
	Levels	128
Origin and Rotation	X	31500
	Y	-83200
	Z	738
	Rotation	0
Block Size	Column Size	25
	Row Size	25
	Level Size	12

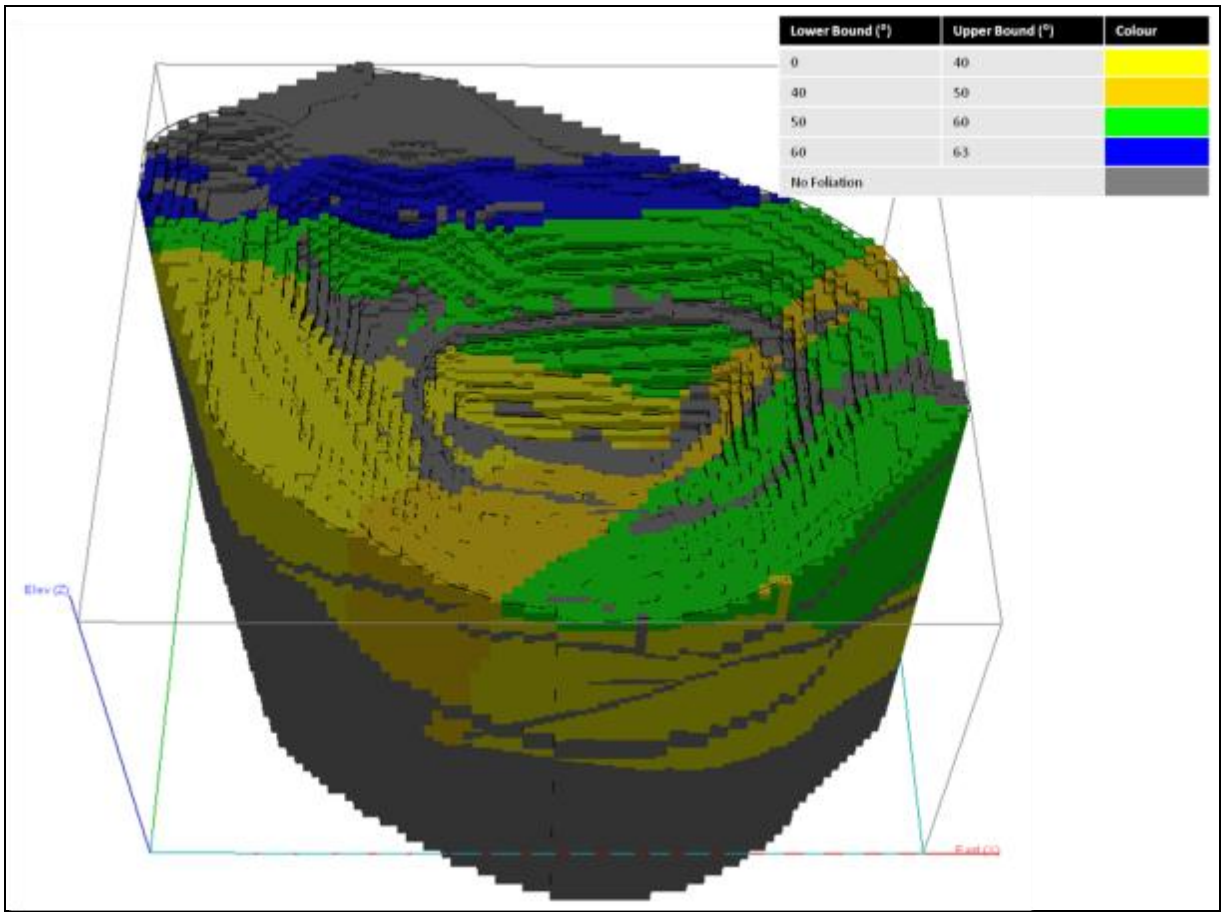


Figure 6.11 Showing the dip of the foliation in the Geotechnical block model.

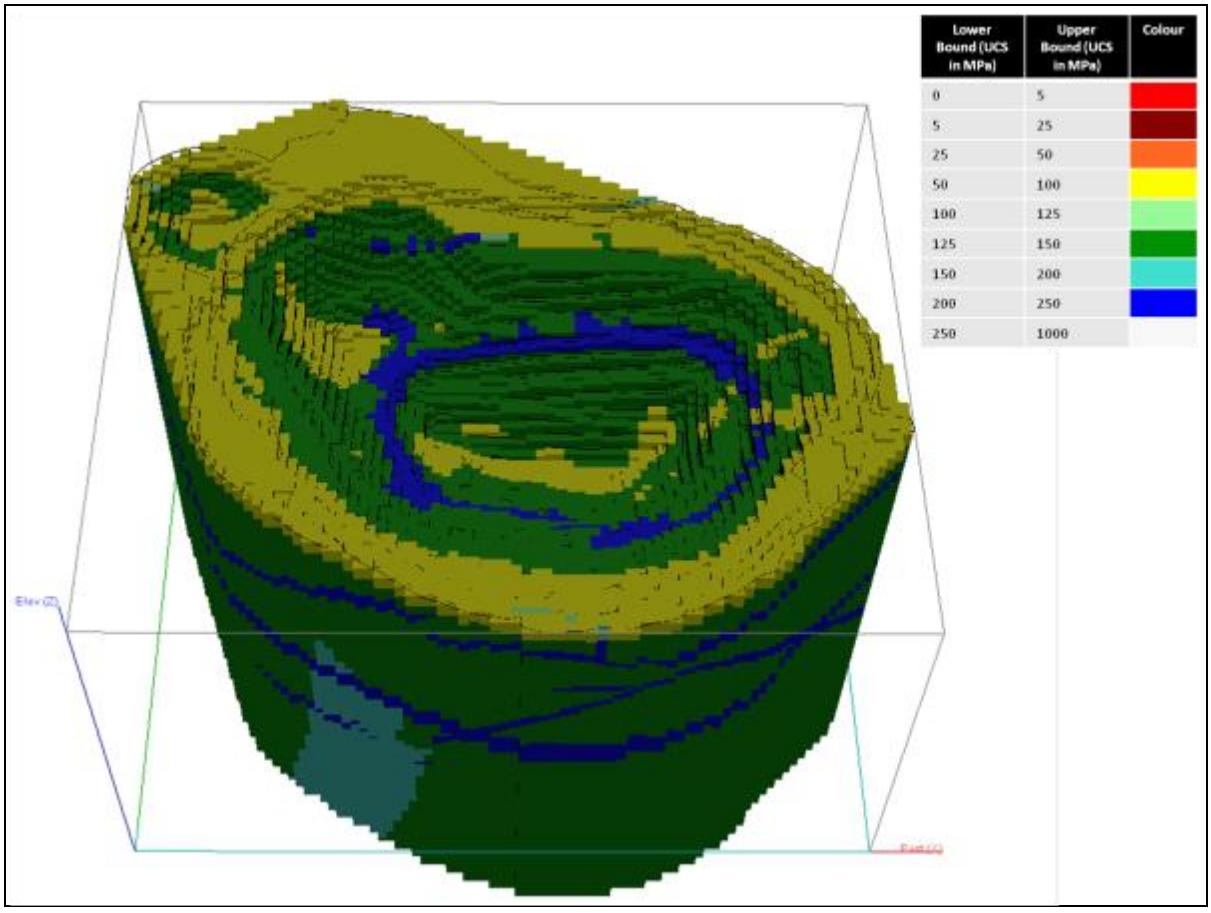


Figure 6.12 Showing the intact rock strength of the various units in the Geotechnical block model.

6.11 SLOPE DESIGN AND OPTIMISATION

6.11.1 Bench height risk assessment

A bench height risk assessment study was commissioned by the author in 2009 and was eventually completed by SRK (Contreras, 2010) in 2010. The study suffered from the same short comings as previous design studies for Cut 4, i.e. no joint and foliation orientation data for the new cut was available, however very valuable principles regarding bench heights could be deduced from this study. The analysis consisted of SWEDGE™ and ROCPLANE™ analysis of which the results were incorporated into a risk model. The results indicated that the probability of a fatality will:

- Increase significantly beyond 1 in 10 000 with an increase in bench height beyond 12m for the old Southern Domains (now called STRV4-STRV9). This is because the Southern Domains are characterised by planar failures and increasing bench heights will increase the consequences of failure.
- Decrease with an increase in bench height for the Northern Domains (S1-S3). This is because the North is characterised by rock falls and an increase in berm width will mitigate the risk of rock fall. See Figure 6.13.

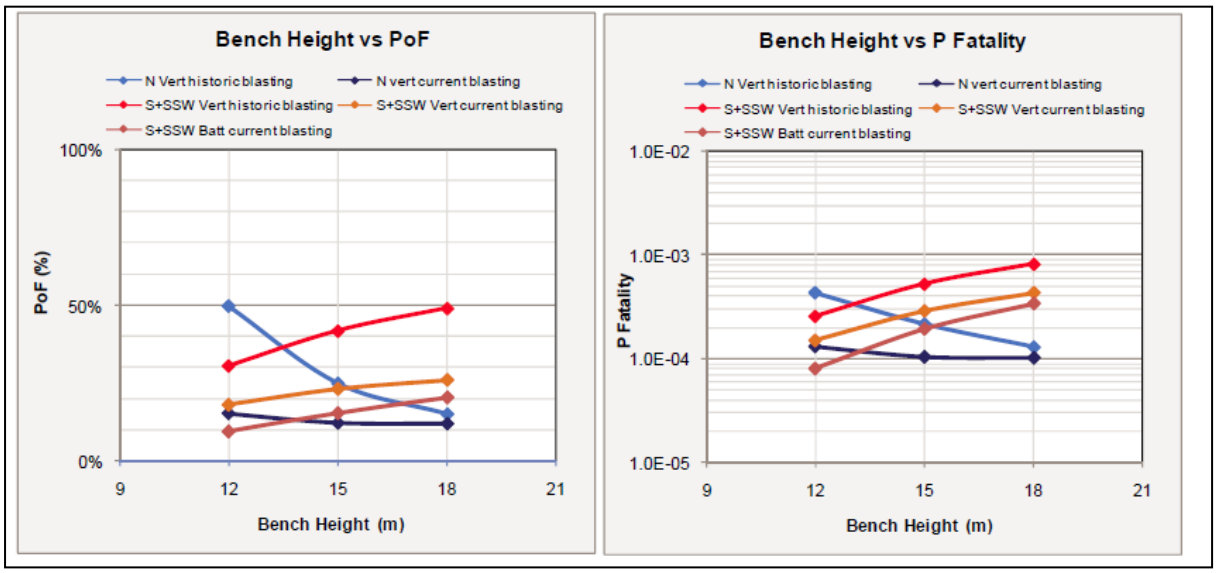


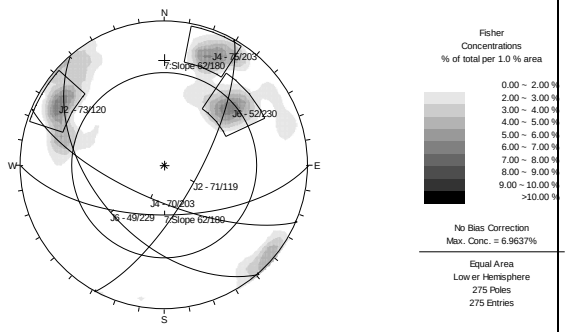
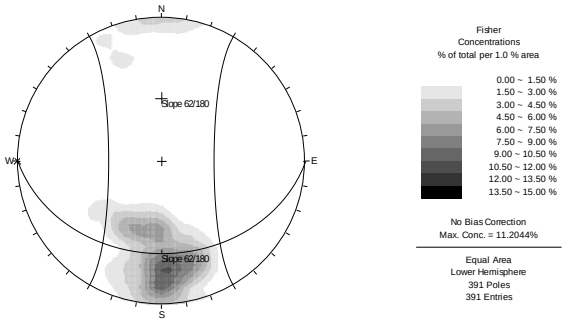
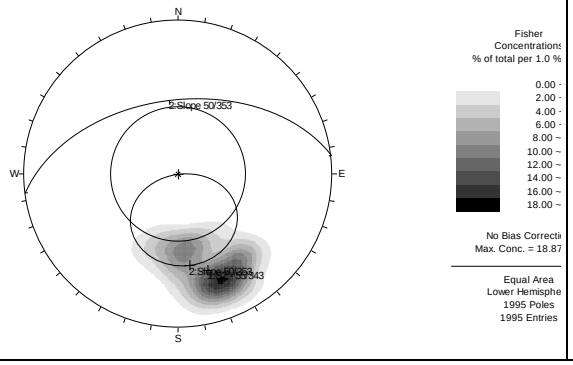
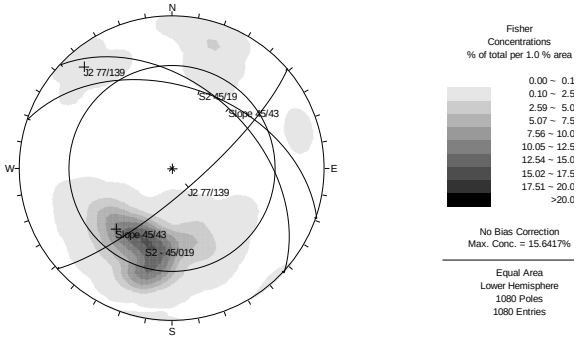
Figure 6.13 The 2010 SRK bench height risk assessment study (Contreras, 2010).

6.11.1.1 Stereographic Analysis

The kinematic impact and interaction of each set was assessed by means of probabilistic limit equilibrium analysis using SWISA™ and PFISA™. The below stereographic kinematic analysis was done by the author only to demonstrate the failure mechanisms that are practically and theoretically present in the pit. These are:

- Wedge failures on brittle jointing
- Wedge failures on the interaction of brittle jointing with S2 Foliation
- Planar failures on the S2 foliation
- Theoretical Toppling failure on the S2 foliation. This mechanism is not prevalent in the pit as demonstrated by the fall of ground analysis in Figure 6.9. See Table 6.26.

Table 6.26 DIPS™ plots showing the major bench scale failure mechanisms in the pit.

STRV1: Wedge failures on brittle jointing	**STRV1: Theoretical Toppling failure on the S2 Foliation.**
	
STRV5: Planar failures on the S2 foliation	**STRV8 – MP: Wedge failures on the interaction of brittle jointing with S2 foliation**
	

6.11.1.2 Empirical Analysis

The Modified Ritchie's Criterion width (Ryan and Prior, 2000) was used to estimate the maximum inter-ramp angle considering the minimum berm width that is required to retain rock falls (Contreras, 2010). The method has limitations since it does not take into account:

- The spill width
- The failure mechanism.
- The plunge of the line of intersection of the wedges in relation to the face and therefore cannot demonstrate the benefit of battering bench faces.

These types of empirical estimates are however valuable since they provide a first pass estimate of the viability of increasing bench heights and or stack heights in the early phases of a project. The analysis indicated that inter-ramp angles 60° and higher can be achieved. See Figure 6.14.

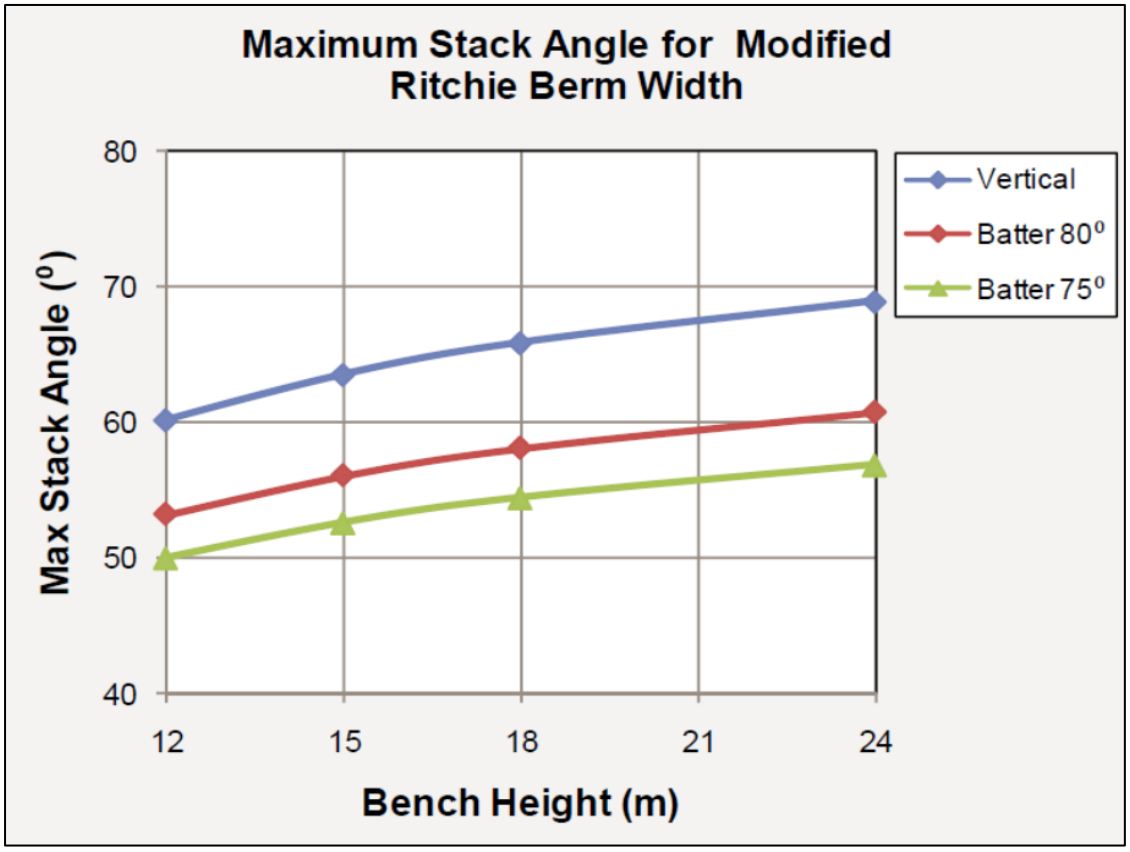


Figure 6.14 Maximum inter-ramp angle calculated using the Ritchie Modified Criterion (Contreras, 2010).

6.11.1.3 Probabilistic Limit Equilibrium Bench Analysis

Probabilistic limit equilibrium bench analyses were conducted by the author for every practical orientation of each domain, at various bench heights, using SWISA™ and PFISA™ and applying the foliation and joint data that was collected during this study.

The spill widths were calculated on a Factor of safety of 1.1 and a probability of failure of 25%. Twenty Five Percent (25%) is the minimum probability of failure, for bench designs, stipulated by the Open Pit Design Guidelines (Read and Stacey, 2009). Each analysis consisted of 10 000 Montecarlo simulations.

The current pit is mined in 12m benches and the requirement from the mine planning section was that the benches had to link in with the current 12m design (15m linked in every 4 benches, 18m every 3 benches and 24m every second bench). Eighteen meter (18m) benches were not considered since the maximum single pass loading height, taking into account bench floor variation, for the current loading fleet was deemed to be 16m (Steffen and Terbrugge, 2009). The 24m option is a double bench option and was considered since it can be efficiently loaded in a double pass. Double benching was conducted at the mine in the past and the double bench designs for the North domain were recommended as far back as 1999 by SRK (Terbrugge, 2000). Thus for every orientation an analysis was conducted for 12m, 15m and 24m high benches. The orientation for each domain is given in graphical format in Table 6.27.

The cumulative spill width distribution for each respective probability of failure (25%) was used to calculate the maximum inter-ramp angle required in order to retain the spill. Thus it is accepted that failure will occur and therefore benches are designed on the probability of retaining a spill (Lorig et al., 2009). The results are presented in Tables 6.29 and 6.30.

The basic friction value as given in previous sections was used in the analysis. The cohesion for all the sets was conservatively assumed to be zero to account for blast vibration.

Table 6.27 The various orientations of the slope for each Tier 2 domain that were considered in the bench analysis by the author.

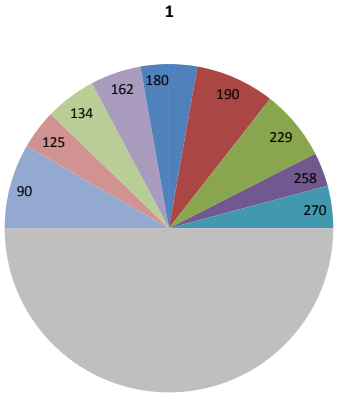
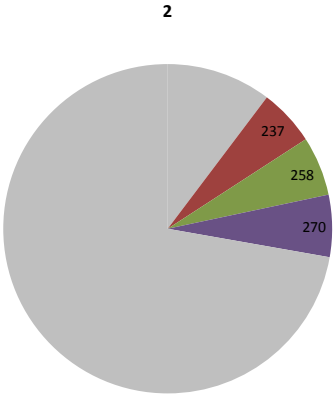
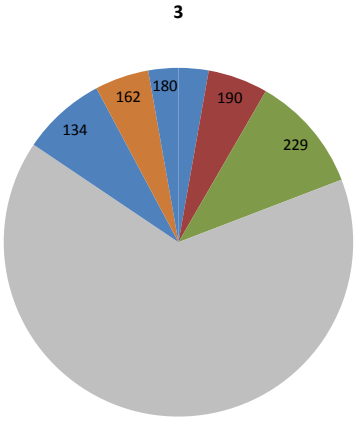
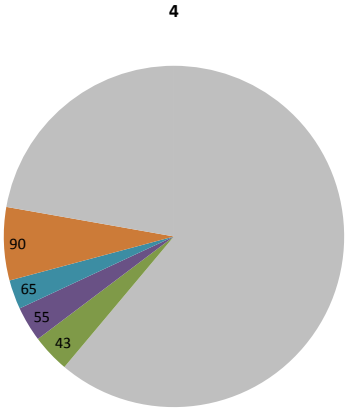
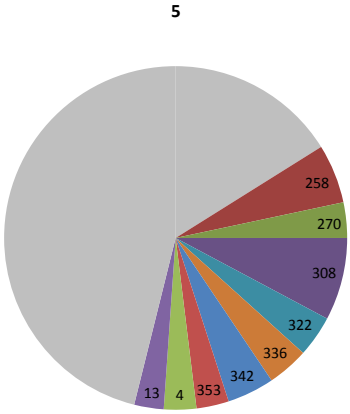
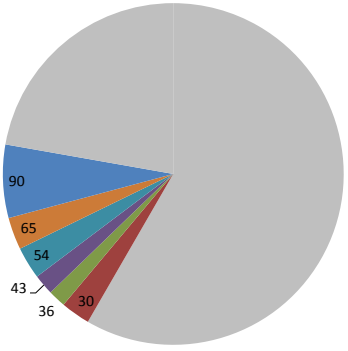
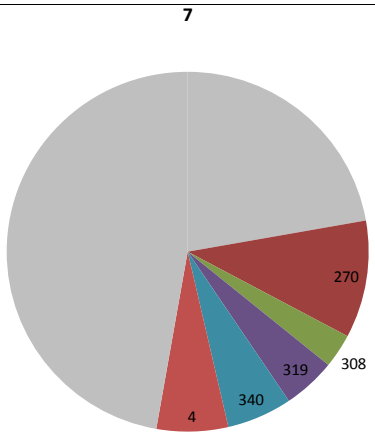
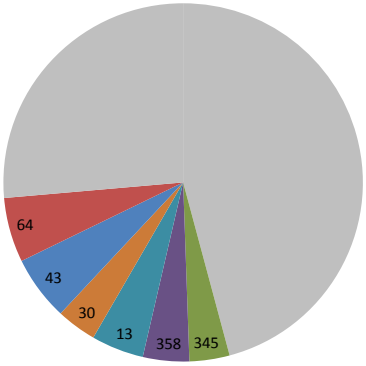
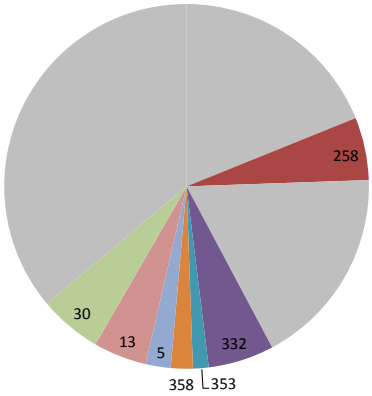
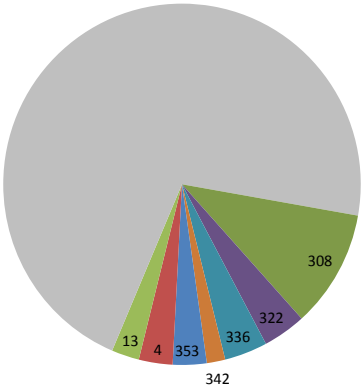
Slope Dip Directions Considered in the Bench Analysis	
Structural Volume 1:	**Structural Volume 2:**
	
Structural Volume 3:	**Structural Volume 4:**
	
Structural Volume 5:	**Structural Volume 6:**
	

Table 6.27 Continuous

Structural Volume 7:	Structural Volume 8: Metasediments
	
Structural Volume 8: Gneiss	**Structural Volume 9:**
	

The bench analysis indicated that the probability of wedge failure is much larger in the Northern domains (STRV1and3) when compared to the Domains in the South (STRV4-STRV8) with the lowest FoS (0.36) and highest PoF (99.86%) occurring on the J2 and J4/J6 wedges. The highest probability of wedge failure in the Southern domains (STRV4-8) occurs in STRV8-MP (34.97%) in the SSW domain with inter-ramp angles as low as 41 degrees required to retain the spillage. The survey of the bench performance, chapter 2 (See Figure 2.1), indicated that this domain has the highest percentage complete bench failures (43%). Thus the results compare well with field observations. See Table 6.28. See Appendices C and D for all the results.

The various bench heights (12m, 15m and 24m) gave similar maximum inter-ramp angles. This is because PFISA™ and SWISA™ do not take joint/structure persistence into account and wedge volumes subsequently increase proportionally with an increase in bench height. Joint persistence normally does not exceed one bench height. See Figure 6.15.

The PFISA™ analysis indicated that all the planar failures (apart from STRV9) occur on the foliation and that the probability of failure is high (higher than 25%). The analysis however indicated that relative small catch berms are required to retain the spill when compared to the North. This correlates well with the current on site experience which indicates that rock fall is not a major risk on the Southern domains due to the relatively shallow line of intersection of the foliation and wider berms. See Table 6.29.

The major risks in the Southern domains are back break and the impact thereof on the ramps and drilling patterns. The analysis confirmed that the results of the bench risk assessment study are still applicable and indicated that an increase in bench height for the Southern domains will result in an increase in back break. See Figure 6.16.

Based on the results, and assuming a 25% probability of retaining the spill, the minimum bench widths and related maximum inter-ramp angle are given in Table 6.28 and compared to those of previous studies. The analysis indicated that the maximum inter-ramp angle, as obtained from the bench analysis, in the S and SE is steeper than the current inter-ramp angle for those domains. The impact of increasing these angles on stability at an inter-ramp scale will be assessed in the following sections.

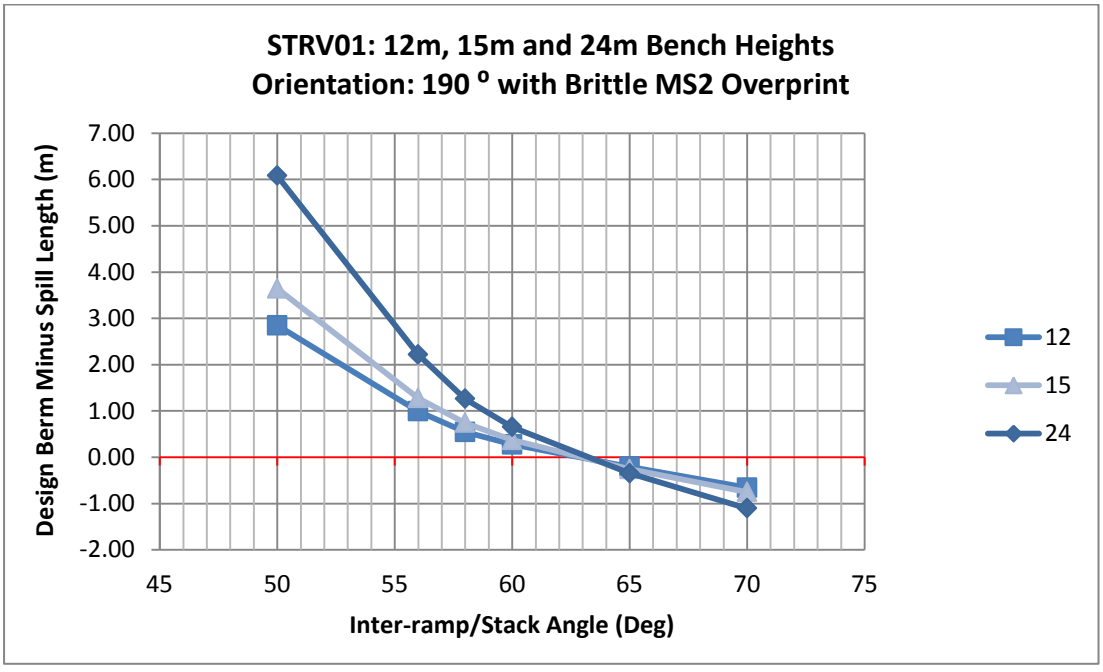


Figure 6.15 Bench analysis results for 12m, 15m and 24m benches in STRV01 with an MS2 overprint.

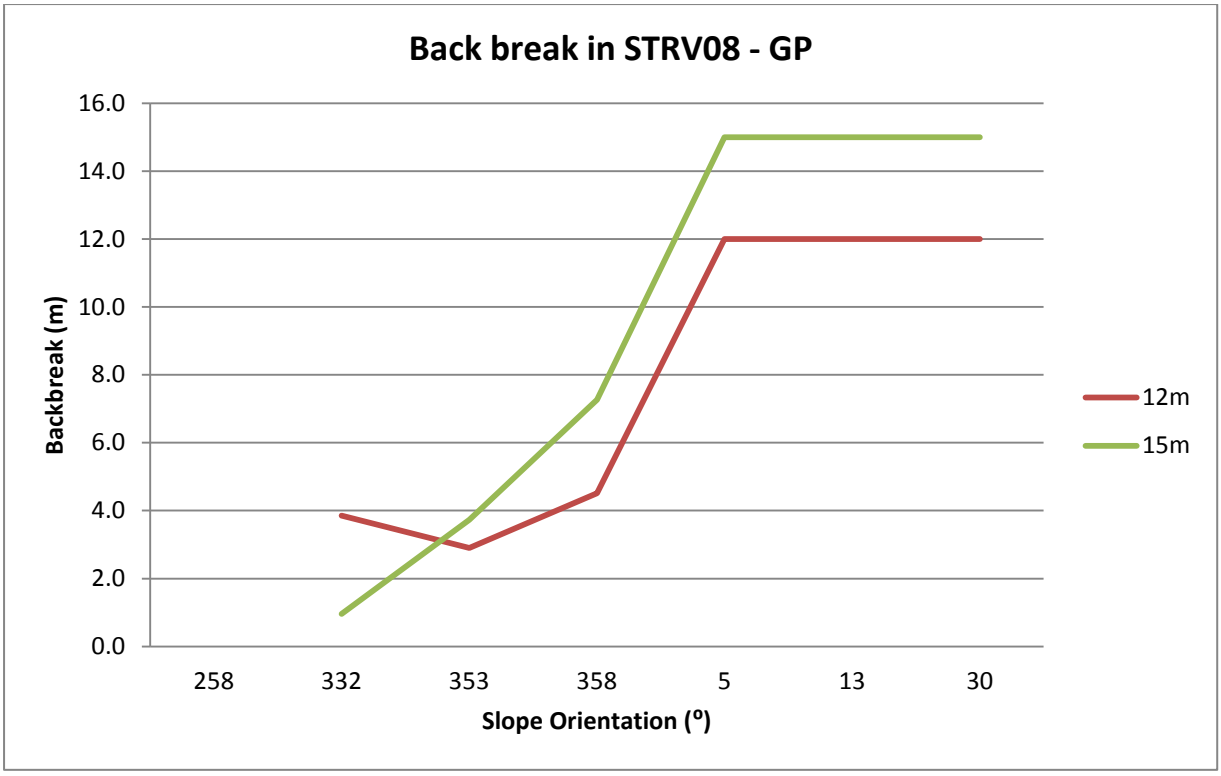


Figure 6.16 Back break in STRV08.

Table 6.28 Maximum inter-ramp angle as obtained from the bench analysis. Results of the largest Tier 2 units are assumed for the Tier 1 domains for comparative purposes only.

Tier 1	Previous		Current	
	Inter-ramp Angle (°)	Maximum bench Height (m)	Maximum Inter-ramp Angle from Bench Analysis (°)	Maximum bench Height (m)
N	58	24	63	24
SE	48	12	62	12
S	40	12	60	12
SSW	41	12	40	12
WSW	53	12	53	12

Table 6.29 SWISA™ results of the bench analysis where wedges failed and where lower than the acceptability criteria. See Appendix C for the complete set of results.

Tier 2 Domain	Orientation	Wedge Set	Average of % Prob. Kinematically Valid Wedge (PK)	Average of % Prob. Sliding (PS)	Average of % Prob. Failure (PF = PK x PS)	Average FoS	Stack Angle at 25% PoF Distribution
STRV1	162	J2-J4	99.86	100.00	99.86	0.36	67
	180	J2-J4	91.62	100.00	91.62	0.36	65
	90	J2-FOL	63.83	57.34	36.60	1.13	65
STRV1 with the NW Brittle Overprint	162	J2-J4	99.86	100.00	99.86	0.36	65
	180	J2-J4	91.62	100.00	91.62	0.36	66
	190	J2-J6	100.00	61.66	61.66	1.01	63
	90	J2-FOL	63.83	57.34	36.60	1.13	63
STRV2	237	J4-FOL	59.11	29.74	17.58	1.60	
	258	J4-FOL	100.00	22.12	22.12	1.60	
	270	J4-FOL	100.00	22.12	22.12	1.60	
STRV3	162	J2-J4	99.83	100.00	99.83	0.33	67
	180	J2-J4	91.63	100.00	91.63	0.33	67
STRV4	90	J2-FOL	98.34	22.47	22.10	1.47	
	43	J2-FOL	100.00	23.07	23.07	1.47	
	55	J2-FOL	100.00	21.83	21.83	1.47	
	65	J2-FOL	100.00	21.97	21.97	1.47	
STRV6	36	J2-FOL	98.80	23.37	23.09	1.56	
	43	J2-FOL	99.47	21.64	21.53	1.56	
	65	J2-FOL	99.54	20.72	20.62	1.56	
	90	J2-FOL	91.51	20.51	18.77	1.56	
	54	J2-FOL	99.54	20.71	20.61	1.56	
STRV8 GP	258	J2-J4	22.80	86.67	19.76	0.04	
STRV8 MP	43	J2-FOL	99.41	35.18	34.97	1.29	41
	64	J2-FOL	99.90	34.88	34.85	1.29	53

Yellow >15% PoF; Red >25% PoF

Table 6.30 PFISA™ results of the bench analysis where wedges failed and where lower than the acceptability criteria. See Appendix D for the complete set of results.

Tier 2 Domain	Orientation	Average of % Prob. Kinematically Valid Wedge (PK)	Average of % Prob. Sliding (PS)	Average of % Prob. Failure (PF = PK x PS)	Average of FOS	Stack Angle at 25% PoF Distribution
STRV4	43	45.41	72.21	32.79	0.42	60
	55	29.21	72.13	21.07	0.43	
STRV5	4	47.68	96.06	45.80	0.09	61
	13	27.92	95.63	26.70	0.10	61
	308	18.81	95.59	17.98	0.10	
	322	47.68	95.57	45.57	0.10	62
	336	73.13	95.84	70.09	0.51	62
	342	76.76	95.84	73.57	0.51	62
	353	69.45	95.94	66.63	0.52	62
STRV6	30	52.23	83.76	43.75	0.84	58
	36	45.41	84.23	38.25	0.40	58
	43	36.36	83.88	30.50	0.40	58
	54	21.05	83.94	17.67	0.41	
STRV7	4	45.09	66.60	30.03	0.17	60
	308	31.33	67.44	21.13	0.16	
	319	39.22	66.83	26.21	0.17	60
	340	46.48	66.46	30.89	0.81	60
	353	43.54	66.72	29.05	0.83	60
STRV8 GP	5	54.52	87.05	47.46	0.75	60
	13	60.85	86.97	52.92	0.73	60
	30	57.40	86.92	49.89	0.74	60
	353	39.66	86.18	34.18	0.27	60
	358	48.25	86.47	41.72	0.27	60
STRV8 MP	13	60.85	92.80	56.47	0.66	61
	30	57.41	93.14	53.47	0.67	60
	43	41.96	93.33	39.16	0.27	60
	345	26.94	92.95	25.04	0.25	61
	358	48.26	92.58	44.68	0.26	60
STRV9	4	47.68	96.06	45.80	0.09	61
	13	27.92	95.63	26.70	0.10	61
	308	18.81	95.59	17.98	0.10	
	322	47.68	95.57	45.57	0.10	61
	336	73.13	95.84	70.09	0.51	61
	342	76.76	95.84	73.57	0.51	62
	353	69.45	95.94	66.63	0.52	62

Yellow > 15% PoF; Red >25% PoF

6.11.2 Inter-ramp Analysis

6.11.2.1 Empirical Inter-ramp Analysis

The empirical method as described by Haines and Terbrugge (1991) was used, by the author, to estimate the inter-ramp angles for a 120m high stack in each of the Tier 2 and selected kimberlite domains. Adjustments for weathering (slight after 4 years = 96%), blasting (smooth wall blasting = 97%) and orientation (maximum adjustment for units in the South = 70%) were applied to the RMR. The results are presented in Table 6.31. The results from the bench and empirical inter-ramp analysis were used as initial inputs into the inter-ramp limit equilibrium probabilistic analysis.

Table 6.31 Empirical Estimate for the inter-ramp angles (Haines and Terbrugge, 1991).

Type	Tier 2 Domains	Average RMR		Adjustments			Adjusted MRMR		Stack Angle (°) @ FoS of 1.2	
		Fresh	Weathered	Weathering	Blasting	Orientation	Fresh	Weathered	Fresh	Weathered
Country Rock	STRV1	68	60	96%	97%		63	56	64	56
	STRV2	66	52	96%	97%		61	48	63	52
	STRV3	68	56	96%	97%		63	52	64	55
	STRV4	69	58	96%	97%	70%	45	38	53	47
	STRV5	66	60	96%	97%	70%	43	39	52	48
	STRV6	64	54	96%	97%	70%	42	35	51	46
	STRV7	60	49	96%	97%	70%	39	32	48	45
	STRV8-GP	65	62	96%	97%	70%	42	40	50	49
	STRV8-MBL	67		96%	97%	70%	44		51	
	STRV8-MP	64	53	96%	97%	70%	42	35	50	46
	STRV10	68	51	96%	97%		63	47	64	47
	STRV11	67	65	96%	97%		62	61	63	63
Kimberlite	K01DVK	66		70%	97%		45		53	
	K01MVK	62		70%	97%		42		50	
	K01RVK	62		70%	97%		42		50	

6.11.2.2 Limit equilibrium probabilistic analysis

For the inter-ramp design limit equilibrium probabilistic analysis were conducted, by the author, using the programme SLIDE™. Selected sections were verified by using the finite difference code: FLAC™. The consequence of inter-ramp failure was assumed to be high and thus a FoS = 1.20-1.30 and a maximum probability of failure of 10% was deemed to be acceptable for the inter-ramp design (Wesseloo and Read, 2009).

The anisotropic strength model in SLIDE™ was used to account for the S2 foliation. Spencer's method was applied since it satisfies force (x and y) and moment equilibrium. Each probabilistic analysis consisted of 10 000 simulations using the Monte Carlo method. Various inter-ramp heights were analysed for each tier 2.

Groundwater modelling by Liu et al. (2011) indicated that the stacks (inter-ramps) higher up in the final Cut 4 slope will be depressurised. However for the inter-ramp analysis the highest water table, from the bottom stack in the slope, was used on each design section. See Figure 6.17.

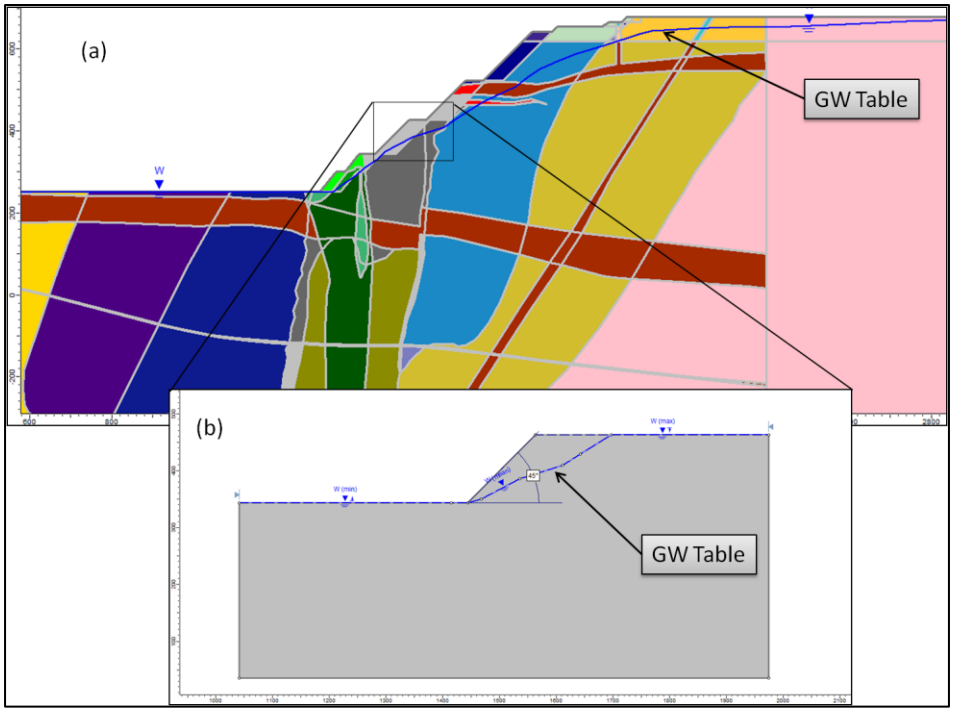


Figure 6.17 (a) Design section South (S) showing the modelled GW table and Tier 2 domains in the South slope (b) the highest water table, from the lower most stack, that were used in the inter-ramp analysis.

All final faces are excavated using trim blasting techniques however a Damage factor (D) of 1 was applied to the inter-ramp values.

The inter-ramp analysis indicated that inter-ramp angles in excess of 67 degrees can be achieved in the North domain (STRV1and3). However bench analysis indicated that a maximum stack angle of 63 degrees can be obtained if the minimum berm width to retain rock falls is taken into account. Thus rock strength is not the dominant factor that controls the maximum stack angle in the North Domain but rather the ability of the benches to retain rock falls from wedge failures. See Figure 6.18

Bench analyses have indicated high maximum inter-ramp angles in STRV5 and STRV8 GP. However inter-ramp analysis indicated that the orientation of the S2 foliation severely impacts on the stability at an inter-ramp scale with lower angles required to achieve an acceptable inter-ramp design. See Figure 6.19. The only exception to this rule is STRV8 MP where the interaction of the brittle jointing and foliation determines the maximum achievable inter-ramp angle.

The analysis also indicated that:

- Inter-ramp design is not highly sensitive to a change in stack height.
- The same stack angle for the fresh tier 2 domains can be applied to the tier 3 domains on condition that the stack height is limited to 60m.
- The inter-ramp angle at FoS = 1.20-1.30 and PoF = 10% along with the limit factors are given in Table 6.32. The complete results, including the above stack height sensitivity analysis are given in Appendix E.

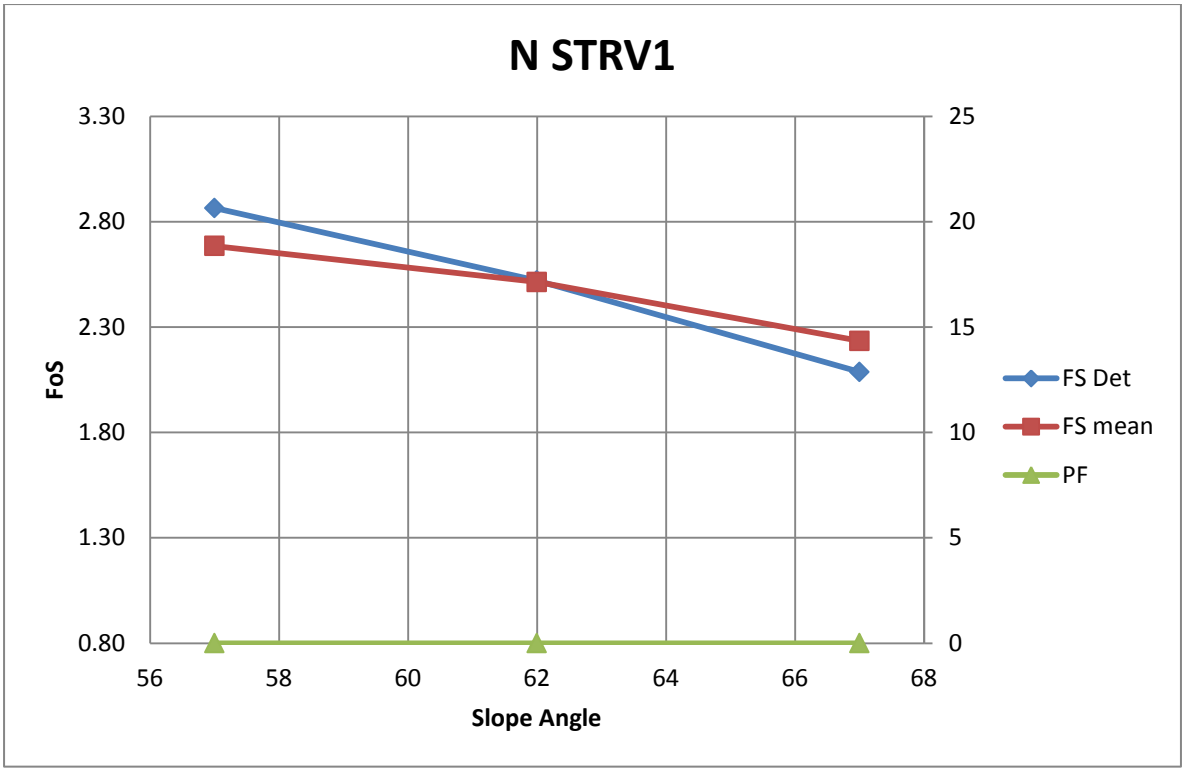


Figure 6.18 The inter-ramp analysis for STRV1 in the North Domain.

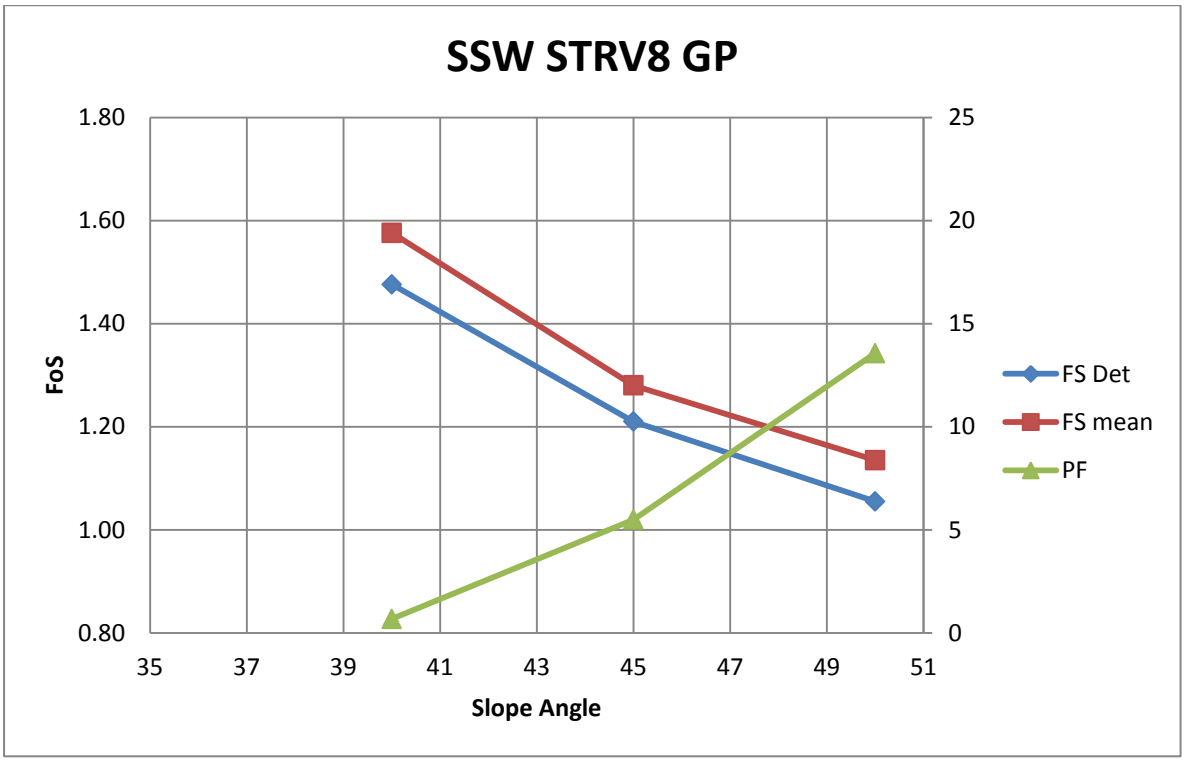


Figure 6.19 The inter-ramp analysis for STRV8 GP indicating the lower inter-ramp angles are required to achieve the proposed acceptance criteria (FoS = 1.20-1.30 and PoF = 10%).

Table 6.32 Inter-ramp angles obtained from Bench and Inter-ramp scale analysis with the controlling factors on stability.

Domains		Bench Analysis	Inter-ramp Analysis	Limiting Angle/Factor	
Tier 1	Tier 2			Final Angle	Factor
N	STRV1	63	67	63	Rock falls / catch berm width
SE	STRV5	62	49	49	Inter-ramp failure on S2 Foliation
S	STRV5	61	49	49	Inter-ramp failure on S2 Foliation
	STRV8 GP	60	45	45	Inter-ramp failure on S2 Foliation
SSW	STRV8 GP	60	45	45	Inter-ramp failure on S2 Foliation
	STRV8 MP	41	43	41	Catch berm to retain wedge failures on J2 and S2 Foliation
WSW	STRV6	58	60	58	Catch berm to retain spillage from planar failures below 43° Slope dip direction
	STRV4	60	60	52	Inter-ramp failure on slightly steeper 22 ° S2 Foliation

The FLAC™ and SLIDE™ verification and comparison was conducted on one of the Tier 2 stacks (STRV8 – GP) and consisted of two scenarios:

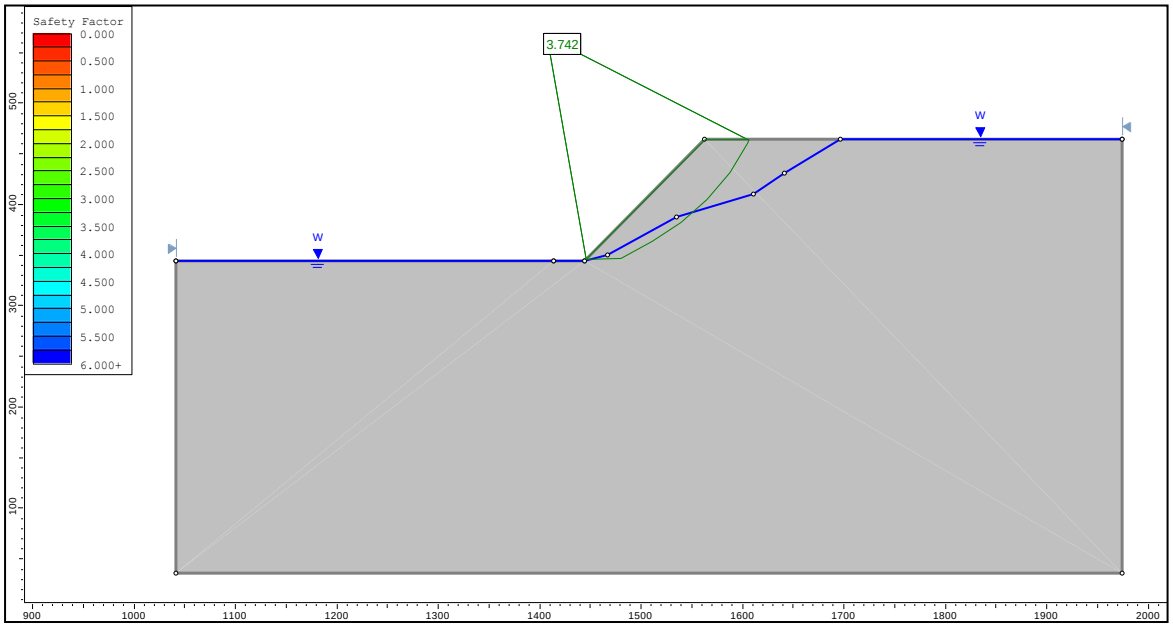
- Isotropy. Only the strength of the rockmass was considered and the effect of S2 foliation ignored.
- Anisotropy: The effect of the foliation was simulated in FLAC™ with a ubiquitous joint model and in SLIDE™ with the anisotropic strength model.

The verification indicated that:

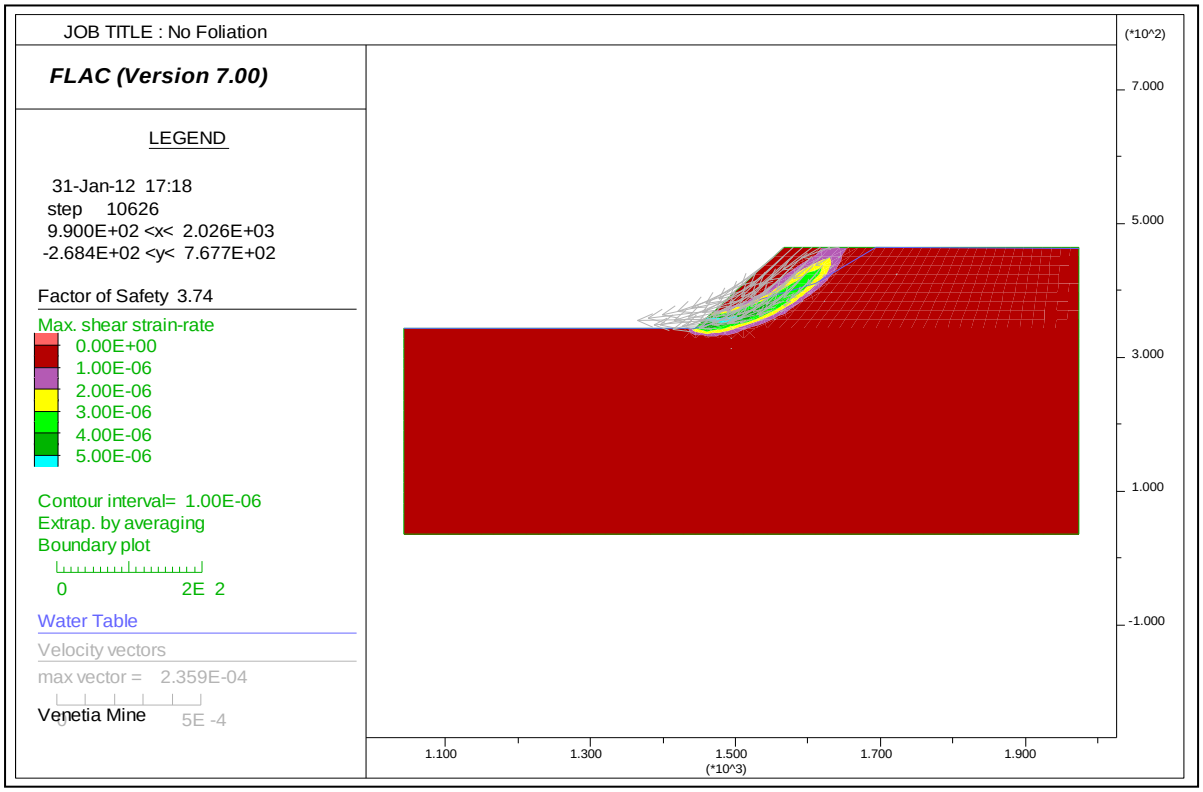
- There is a good correlation between FLAC™ and SLIDE™ where the models account for isotropy.
- The result of SLIDE™ anisotropic strength model is significantly lower than the FLAC™ ubiquitous joint model thus the proposed inter-ramp angles can be considered as conservative. Future studies should consider using the response surface methodology by Chiwaye and Stacey (2010) whereby numerical modelling is used to estimate the risk (probability of failure). See Table 6.33 and Figures 6.20 and 6.21.

Table 6.33 FLAC ™ and SLIDE ™ verification scenarios

Scenario		Factor of Safety
FLAC™	- No Anisotropy	3.74
SLIDE™	- No Anisotropy	3.74
FLAC ™	- Ubiquitous Joint Model	2.45
SLIDE™	- Anisotropic Strength Model	1.21



Figures 6.20 Limit Equilibrium Results (SLIDE™) for a 120m stack with no foliation.



Figures 6.21 Numerical Modelling Results (FLAC™) for a 120m stack with no foliation.

6.11.3 Overall Slope Analysis

A similar methodology as the inter-ramp analyses was followed by the author for the overall slope design. The consequence of inter-ramp failure was assumed to be high and thus a FoS = 1.30 and a maximum probability of failure of 5% or less was deemed to be acceptable for the inter-ramp design (Wesseloo and Read, 2009).

The opportunity to optimise an overall slope is limited since the overall angle is determined by the ramp systems and ramp width. The results for the North are high as expected. Using a stack angle of 58° in the WSW domain resulted in a lower FoS/higher PoF than the acceptance criteria and subsequently the stack angle in this domain had to be reduced to 53° in order to meet the overall slope acceptance criteria. See Figure 6.22.

The minimum slip surface for the South (S) Domain is in the STRV5 stack at the top of the slope. A sensitivity analysis indicated that the FoS in the rest of the slope exceeds 1.30 with the overall slope slip surface having a factor of safety of 1.64. Thus the overall slope in this domain meets the required acceptance criteria. See Figure 6.23. See Table 6.34 and Appendix F for the results of the other design sections.

Table 6.34 The results for overall slope analysis.

Tier 1 Domain	FoS Det.	FoS mean	PoF (%)	Depth (m)	Overall Slope Angle (°) measured to new push back	Overall Slope Angle (°) measured to old V25 push back
N	2.46	2.41	0	425	47	38
SE	1.30	1.37	0.1	425	38	35
S	1.23 1.64	1.39	0.6	425	38	30
SSW	1.46	1.52	0	425	33	33
WSW	1.31	1.34	0	425	36	30

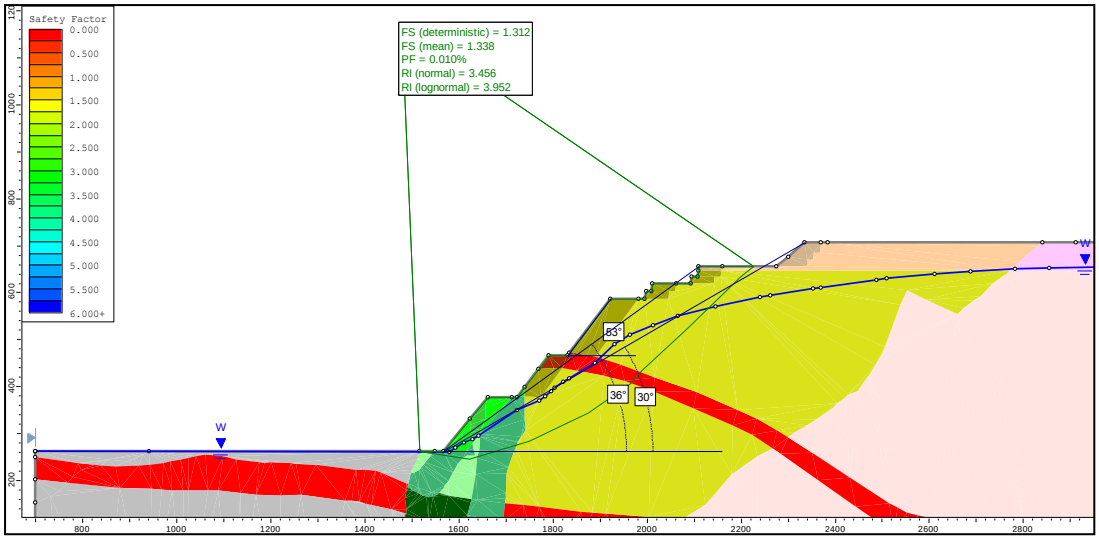


Figure 6.22 Overall slope limit equilibrium analyses for the WSW domain

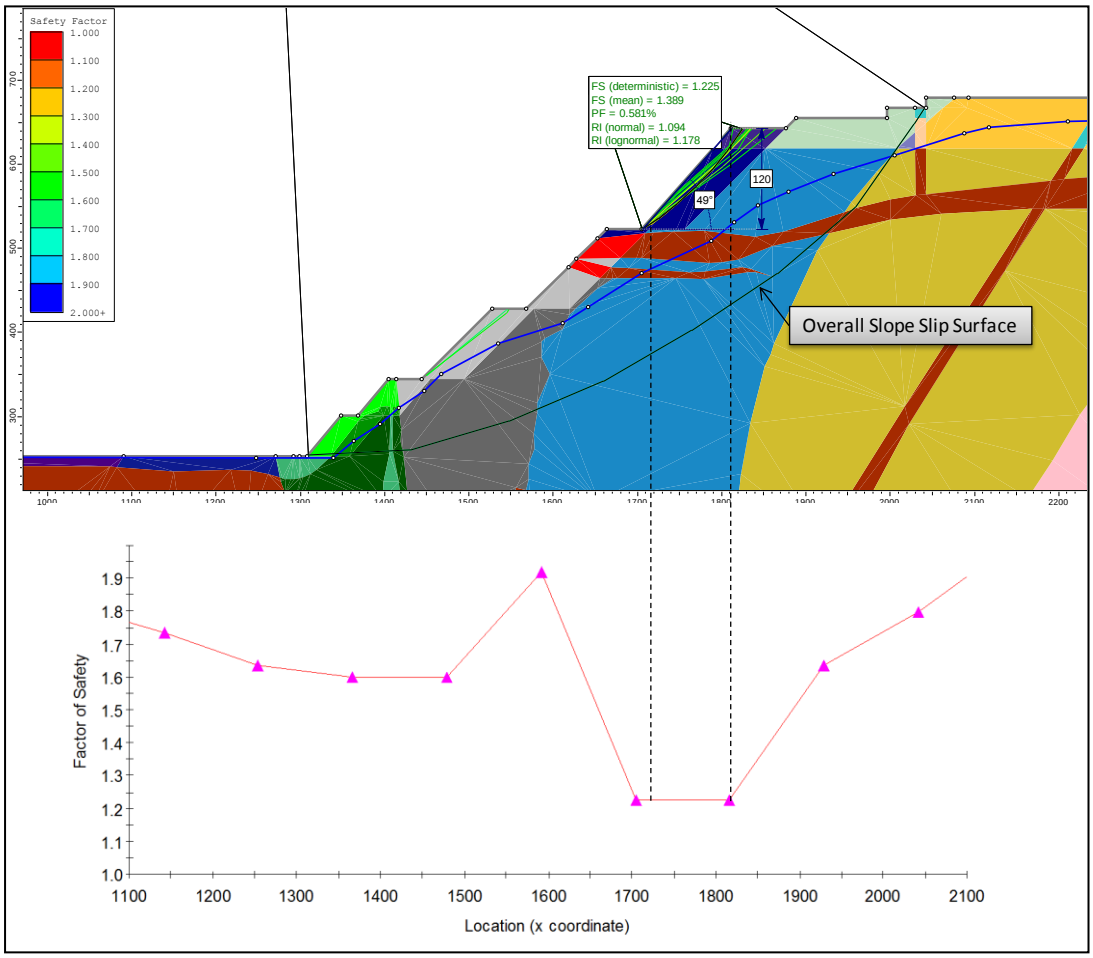


Figure 6.23 Overall slope limit equilibrium and sensitivity analyses for the South domain.

6.11.4 Ramp Width Design

A ramp system has a major impact on the angle of the overall slope and subsequent waste stripping. Thus as part of the optimisation in 2009 the widths of the ramps were reviewed. Venetia currently has single lane ramp access to the bottom of Cut 3. This was mainly due to poor mining that resulted in significant overbreak, kinematic failures and an increase in size of the hauling fleet (upgraded from 785 Caterpillar trucks to 793D Caterpillar trucks which are wider). Three main aspects that impact on the required ramp width were identified:

- Minimum travelling width for double lane access considering equipment size
- The minimum earthen safety berm required on the crest of the ramp
- Geotechnical conditions (overbreak due to mining practices and kinematic failures).

The US Mines Safety and Health handbook (Elam et al., 1999) was used by Mompati (2009) as guideline to determine the minimum tramming width and earthen berm requirements. Based on the guideline the following was recommended:

- In the case of Venetia mine the width of the largest haul truck (CAT793) is 8.36m, therefore the total haul road travel/tramming width required is 29.3m (3.5 times the width of the largest truck.
- Earthen berms (safety berms) are placed on ramps to give the driver a visual indication of the road edge and to provide restraint to the vehicle to give the driver/operator the opportunity to regain control and keep the vehicle from leaving the roadway, and to keep the vehicle from the road edge by a distance equal to the base of the earthen berm. To satisfy the above the earthen berm should be 1.8m high with a width of 5m assuming an angle of repose of 37^0. See Figure 6.24.

The methodology to determine the percentage catch berm and maximum overbreak, as described in chapter 7, was used to determine what allowance should be made for Geotechnical conditions (overbreak and kinematic failures). A survey of the highwall using the abovementioned method indicated that the average maximum-overbreak is approximately 2m in the North domain. Thus an additional 2m, to cater for overbreak was added by the author to the ramp width. See Figure 6.24.

However the current bench analysis indicated that the overbreak is higher (up to 4m) in the North. The over or back break in the South (STRV8 MP) is also significantly more than for

the North (up to 14m) and correlates with observations in the pit. Thus the risk of losing tramming width and subsequent double pass hauling capacity in the South is high. It is therefore recommended that a ground support study be undertaken to assess the viability of using artificial ground support to retain tramming width in the Southern domains. See Figures 6.25 and Table 6.35.

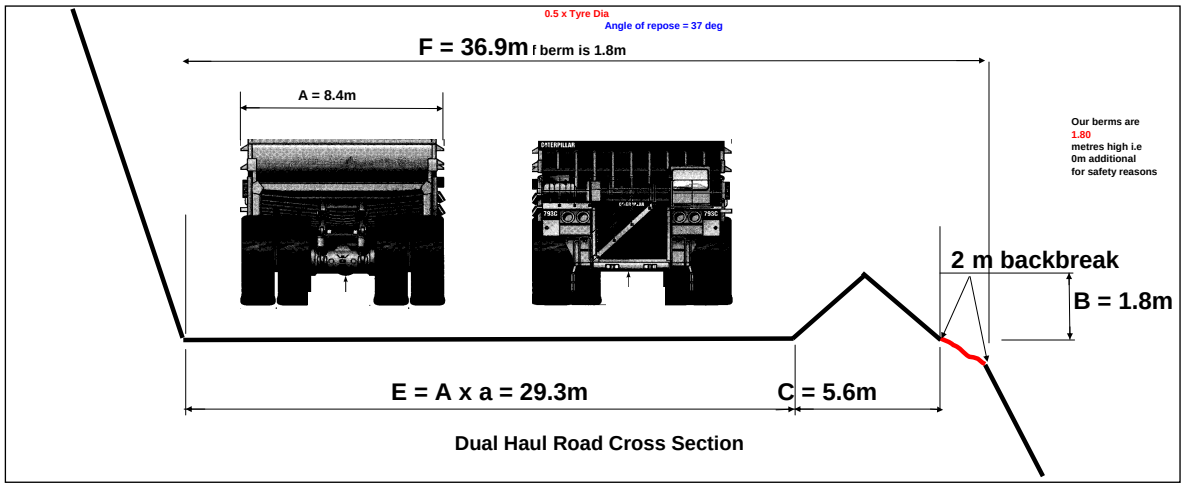
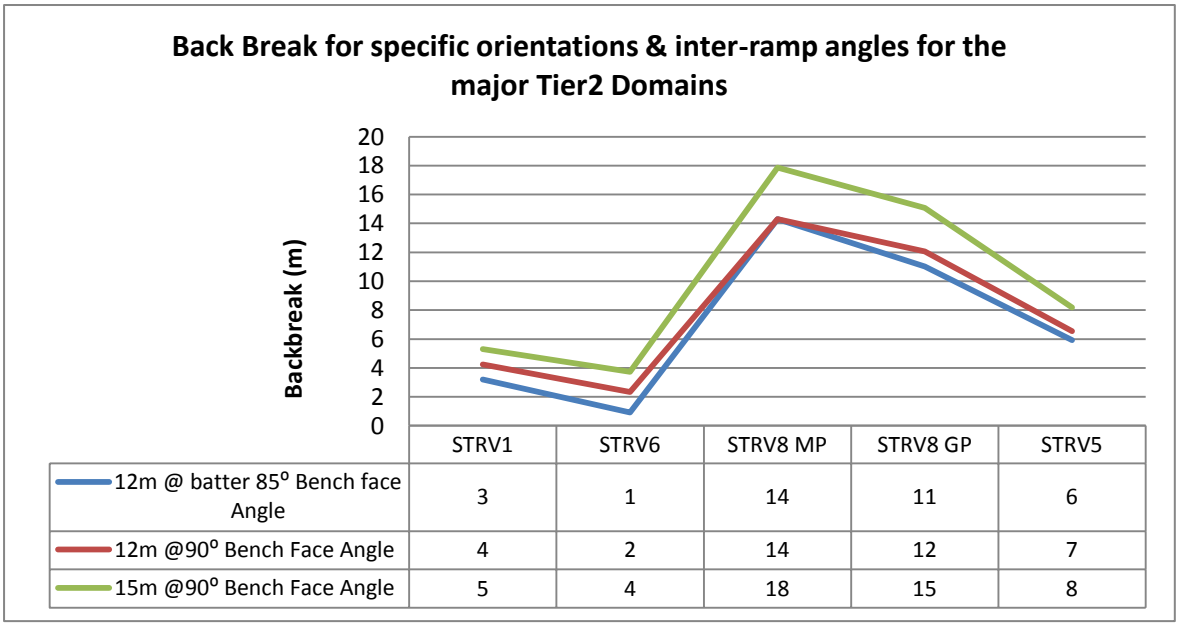


Figure 6.24 Venetia mine ramp width design methodology (Mompati, 2009)



	STRV1	STRV6	STRV8 MP	STRV8 GP	STRV5
12m @ batter 85° Bench face Angle	3	1	14	11	6
12m @90° Bench Face Angle	4	2	14	12	7
15m @90° Bench Face Angle	5	4	18	15	8

Figure 6.25 Back break results.

Table 6.35 Conceptual ramp widths taking into consideration back break from the bench analyses.

Tier 2 Domain	Tramming Width (m)	Earthen Berm Width (m)	Back break (m)	Final Ramp Width (m)	Current Ramp Width (m)
STRV1	29.3	5.6	4	39	37
STRV6	29.3	5.6	2	37	40
STRV8 MP	29.3	5.6	14	49	40
STRV8 GP	29.3	5.6	12	47	40
STRV5	29.3	5.6	9	44	40

6.12 SUMMARY

For the final phase of the optimisation (Phase 3) the Geotechnical domain model and slope design was updated, by the author, using the results from Phase 2 of the study. The updated design incorporated the updated groundwater table and considered the orientation of the pit slopes relative to the foliation; and consisted of bench, inter-ramp and overall slope analyses.

The author used the new geological model from Basson (2011a) in conjunction with a review of pit slope performance and fall of ground data to outline and define new Geotechnical domains for the Venetia Pit. See Figure 6.10. The domains were upgraded from the initial two (2) domains in 2008 to twenty six (26) and can be broadly divided into three levels or tiers (1–3):

- Tier 1: Major Domains: The pit shell geometry dictates their location and extent.
- Tier 2: Structural Volumes as defined by Basson (2011a) in Table 5.3 which is based on geological package and the orientation of the S2 foliation in that unit.
- Tier 3: Weathering (Fresh or Weathered). See Table 6.24 for a summary of the Tier 1 to 3 domains.

The rock mass model (Geotechnical) data was subsequently re-defined and summarised for each domain. This included the calculation of rock mass ratings, analyses of laboratory rock testing data and calculation of rock mass and joint strengths.

The rock mass strength properties were calculated by the author using the Hoek-Brown criterion and related input parameters (Hoek et al., 2002). The technique as described by Barton and Bandis (1982, 1990) was used to calculate the strength of the foliation. Ratios of JCS_F/JCS_O and JRC_F/JRC_O for this project are lower than those prescribed by Karzulovic and Read (2009) (JCS_F /JCS_O < 0.3 or JRC_F /JRC_O < 0.5) and can be therefore considered as conservative. See Appendix G. Strength values were calculated for each drilling interval, and summarised per domain, to take account for the variability of the metamorphic rockmass.

Commonly only intact rock strength is used in rock mass classifications and as such only UCS samples that failed through intact rock is to be used for UCS (Read and Stacey, 2009; Brady and Brown, 2004). However the rock mass at Venetia has been affected by a number of ductile deformation events (D1 to D4), resulting in several ductile planar fabrics (S1-S3), and brittle events. Based on field observations the rock mass, on a meter/lab-sample scale, can be divided into S2a: planar fabric ("closed" foliation), S2b: planar fabric ("open" foliation) and massive rock not dominated by biotite and or other mineral assemblage banding. See Figure 6.3. Triaxial shear testing conducted on S2a samples have demonstrated that several samples preferentially fail on this "closed" foliation and thus could be mistakenly recorded as samples that failed on a discontinuity in the rockmass. Therefore if the effect of the "closed" fabric; and all samples described by the lab as failed on discontinuity, were discarded the strength on a lab scale will be overestimated. Therefore UCS results were not filtered and the UCS, that contains the intact and failed on discontinuity/fabric data sets, was used for this project. See Table 6.1.

The RMR's with the effect of foliation was used. This could be considered as conservative since: the RMR's without foliation are 10 to 20 points higher; and strength anisotropy (due to the S2 foliation) was simulated using an anisotropic model in SLIDE™ and ubiquitous joint model in FLAC™ resulting in the effect of the foliation being double accounted for in the design. It was also assumed that the S2 foliation is continuous and the positive effect of rock bridges and effective cohesion, as described by Terzaghi (1962), Jennings (1972) and Karzulovic and Read (2009), was not accounted for in the design.

A 50m deep damage zone was applied to the slope and correlates with the findings of the 2011 groundwater modelling (Liu et al., 2011) and those of Lorig et al. (2009). Key Geotechnical data were collated and stored in a 3D block model.

The consequence of inter-ramp failure was assumed to be high for bench, inter-ramp and overall slopes and associated acceptance criteria as defined by Wesseloo and Read (2009) were applied.

Probabilistic limit equilibrium bench analyses were conducted by the author for every practical orientation of each domain, at various bench heights, using SWISA™ and PFISA™. For the inter-ramp and overall slope design limit equilibrium probabilistic analysis were conducted using the programme SLIDE™. The anisotropic strength model in SLIDE™ was used to account for the S2 foliation.

The cumulative spill width distribution for each respective probability of failure (25%) was used to calculate the maximum inter-ramp angle required in order to retain the spill. While the cohesion for all the foliation/joint sets were conservatively assumed to be zero to account for blast vibration. The limitations of the current load and haul fleet was taken into consideration and bench analyses were only conducted on 12m, 15m and 24m bench heights.

The analysis indicated that an increase in bench height for the Southern domains will result in an increase in back break. The various bench heights (12m, 15m and 24m) gave similar maximum inter-ramp angles. This is because PFISA™ and SWISA™ do not take joint/structure persistence into account and failure volumes subsequently increase proportionally with an increase in bench height. Joint persistence normally does not exceed one bench height and thus in practice higher benches (wider catch berms) in the North will be more effective. Although not part of the initial scope of the project the effect of back break on tramming width (ramp width) was estimated. The risks of losing tramming width and subsequent double pass hauling capacity in the Southern domains are high. It is therefore recommended that a ground support study be undertaken to assess the viability of using artificial ground support to retain tramming width in the Southern domains

The bench analysis indicated that the probability of wedge failure is much larger in the Northern domains (STRV1 and 3) when compared to the Domains in the South (STRV4 to STRV8). The stack angles in the North domain are not controlled by the S2 foliation and/or rock mass strength. Here the interaction between brittle jointing controls the maximum catch berm and subsequent stack angle. Analysis of fall of ground data and probabilistic bench analysis confirm that the dominant failure mechanism in the North is wedges that form on the intersection of the J2 and J4/J6 joint sets. Bench analysis indicated that steeper angles are viable in this domain.

The stability of the pit walls in the Southern domains is not only controlled by their orientation in relation to the major S2 foliation but also by the interaction of jointing with the foliation. The highest probability of wedge failure in the Southern domains (STRV4 to 8) occurs in STRV8-MP (34.97%) on the intersection of the J2 set with the S2 foliation. The field survey of the percentage complete bench failures (See Figure 2.1) also indicated that this domain has the highest incidence of bench failures (43%). Thus the results compare well with field observations.

In STRV4, STRV5 and STRV8-GP the dominant factor that drive stability is inter-ramp scale failure on the S2 foliation compared to STRV6 where the maximum inter-ramp angle is limited by failure at the overall slope scale. The bench and inter-ramp kinematic analyses indicated that steeper angles are viable where there is a major difference in strike between the S2 foliation and pit walls. Where the dip direction of the slope and foliation is within 20° the maximum inter-ramp angle is controlled by the dip of the foliation. It is thus critical that the dip of the foliation be confirmed by continuous pit mapping as faces are exposed during mining. The Phase 3 results are compared to the first design and initial phases of optimisation in Table 6.36.

The numerical finite difference code, FLAC™, was used to validate the results of the limit equilibrium stack analysis. The validation indicated that the limit equilibrium modelling is conservative when compared to numerical modelling and it is recommended that future studies use the response surface methodology by Chiwaye and Stacey (2010), whereby numerical modelling is used, to estimate the risk (probability of failure).

The final design parameters for each major tier 2 domain are given in Table 6.37. Historically stack heights at the mine was limited to 120m. Therefore Inter-ramp angles are stated at a maximum stack height of 120m.

Domains at Venetia were for the first time designed from the bench scale and upwards and conform to the acceptance criteria as stipulated in the 2009 Open Pit Design Guidelines (Read and Stacey, 2009).

Table 6.36 Comparison between the initial design, phase 2 and phase 3 inter-ramp angles.

Domains		Previous Design		Limiting Angle/Factor	
Tier 1	**Tier 2**	**Inter-ramp Angle (°)**	**Author**	**Final Inter-ramp Angle (°)**	**Factor**
N	STRV1	56	Contreras (2008)	63	Rock falls / catch berm width
SE	STRV5	48	Armstrong (2008)	49	Inter-ramp failure on S2 Foliation
S	STRV5	40		49	Inter-ramp failure on S2 Foliation
	STRV8 GP	40	Contreras (2008)	45	Inter-ramp failure on S2 Foliation
SSW	STRV8 GP	40		45	Inter-ramp failure on S2 Foliation
	STRV8 MP	41	Strouth (2009)	41	Catch berm to retain wedge failures on J2 and S2 Foliation
WSW	STRV6	53		53	Overall slope failure on S2 Foliation
	STRV4	53		52	Inter-ramp failure on S2 Foliation

Table 6.37 Final proposed inter-ramp angles and bench heights.

Domains		Inter-ramp Angle (°)	Maximum Stack Height (m)	Maximum Bench Height (m)
Tier 1	**Tier 2/3**			
N	STRV1 - WEATHERED	63	60	24
	STRV1 - FRESH	63	120	24
SE	STRV5 - WEATHERED	49	60	12
	STRV5 - FRESH	49	120	12
S	STRV5 - WEATHERED	49	60	12
	STRV5 - FRESH	49	120	12
	STRV8 GP - WEATHERED	45	60	12
	STRV8 GP - FRESH	45	120	12
SSW	STRV8 GP - WEATHERED	45	60	12
	STRV8 GP - FRESH	45	120	12
	STRV8 MP - WEATHERED	41	60	12
	STRV8 MP - FRESH	41	120	12
WSW	STRV6 - WEATHERED	53	60	12
	STRV6 - FRESH	53	120	12
	STRV4 - WEATHERED	52	60	12
	STRV4 - FRESH	52	120	12

7. IMPLEMENTATION STRATEGIES AND CONTROLS

Excavating the highwalls with conventional production blasting techniques and related poor mining practices (side casting, uncontrolled blasting and insufficient cleaning and barring practices) resulted in extremely poor highwall conditions, poor bench retention values and a significant increase in the rock fall frequency rate. See Figure 6.7. In 2008 this practice was ceased and the mine started experimenting with limit blasting techniques on the final pit limits. As part of the optimisation programme effective measures had to be put in place that will flag poor mining practices and the related rock fall risks. The aim was therefore:

- Measure blasting damage/ success and cleaning practices on the final limit:
- Define a programme to access manage and communicate rock fall risk.

7.1 MEASURE BLASTING DAMAGE/ SUCCESS AND CLEANING PRACTICES ON THE FINAL LIMIT

The new pre-split and trim blast programme has significantly improved highwall conditions however no method was in place before 2009 to effectively measure blasting successes. A final wall blasting damage study was undertaken in 2009 and 2010, of which the aim was to define an effective method to measure blasting damage/ success and cleaning practices on the final limit. Great strides were made in the implementation of controlled blasting at Venetia however a degree of damage is still observed on the highwalls. Andrieux (2010) was contracted by the author to assess mechanisms that initiate the current observed blast damage.

7.1.1 Crest Lost on Benches in the Southern Domains

In the Southern Domains (STRV 4, 5, 6 and 8) the foliation dips out of the face. The instability observed behind the presplit lines is mainly in the form of crest damage/loss. See Figure 7.1.



Figure 7.1 Photograph looking at the south wall, showing recent presplit results. The quality of the wall is very good, but the crest integrity could not be maintained.

This is mainly caused by pressurised detonation gases acting on the foliation. When an insufficient collar length is implemented (Figure 7.2), the detonation gases can easily vent through foliation planes near the bench floor and destabilise them. If enough confinement is provided, it becomes easier for the detonation gases to vent through the borehole itself, rather than the foliation. As gases travel upwards inside the blast hole towards the surface, their volume expands and their temperature cools, which effectively lowers their pressure. When the gases reach foliation planes near the surface (which are under low confinement levels), the remaining pressure will be insufficient to disturb the strata. Thus the damage could be minimised by increasing the collar lengths (Andrieux, 2010).

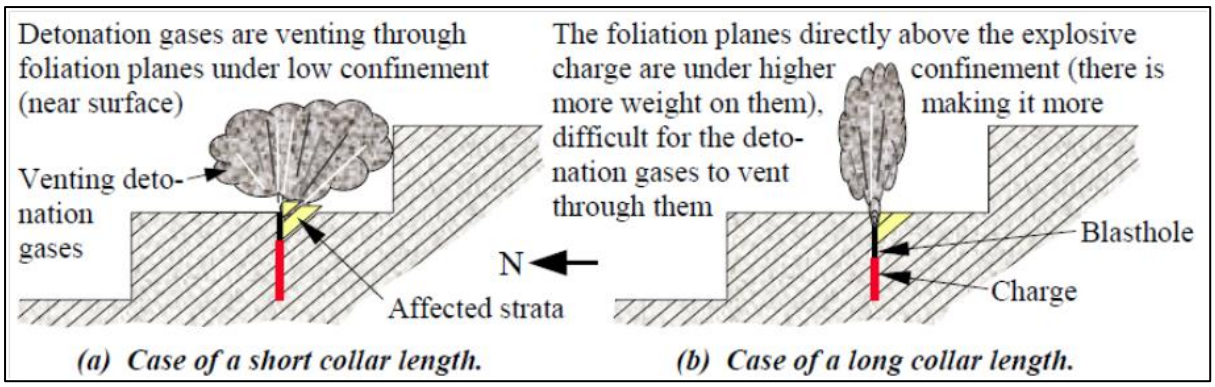


Figure 7.2 Conceptual cross-sections showing how an increased collar length reduces the risk of damaging the crest of the bench behind a presplit line on the south pit wall (Andrieux, 2010).

7.1.2 Crest Damage on Benches in the Northern and Southern Domains

In the Northern and Southern Domains cracking is observed in the crests of the benches on the final limits. See Figure 7.3. This is due to damage caused to the floor of the previous bench (the one above) when it was blasted. Figure 7.4 illustrates this mechanism. The practice of not sub-drilling the production blast holes located in the vicinity of future final walls in the bench below does minimise the extent of this damage. However the amount of crest damage is usually associated with over drilling of the design depth on the previous pattern.

Adding coarse crushed rock (20 mm) at the bottom of these blast holes prior to loading them would also act as a cushion and could reduce the floor damage to a certain extent. Good drilling depth control must be maintained in order to mitigate the effect of this damage mechanism (Andrieux, 2010).



Figure 7.3 Photograph of a well pre-splitted and cleaned final limit bench in Structural Volume 1. Note the damage near the crest of the bench.

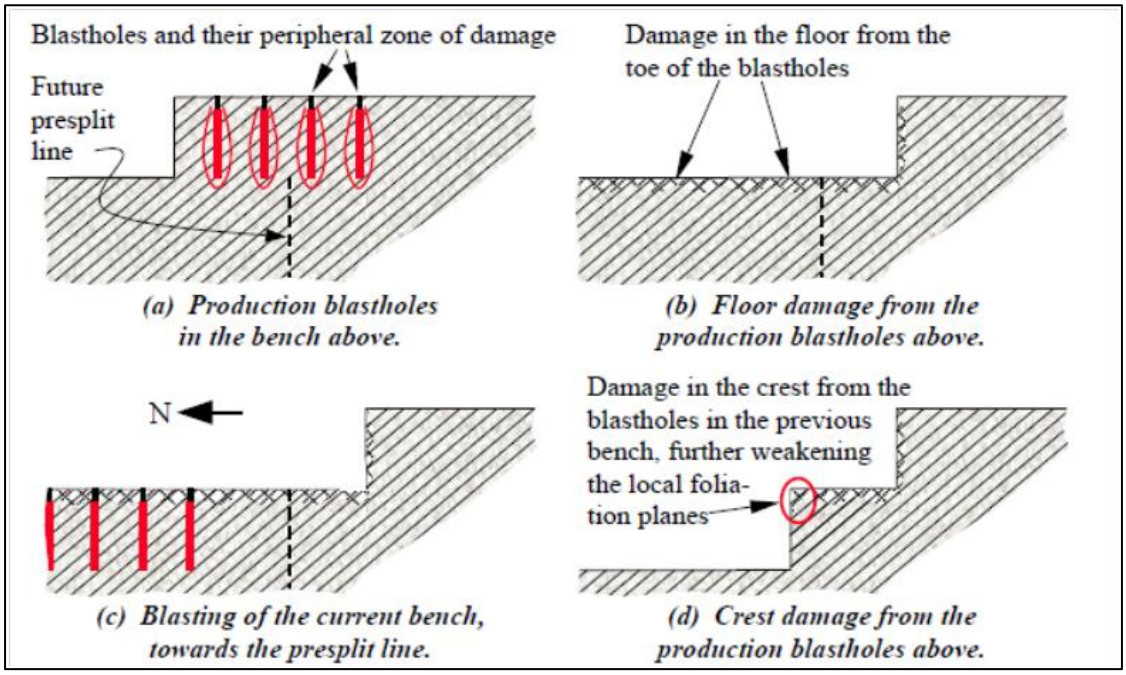


Figure 7.4 Conceptual cross-sections (not to scale) looking east, showing how the blast holes in the previous (upper) bench have damaged the crest of the final wall in the lower bench (Andrieux, 2010).

7.1.3 Measuring Blasting and Final Pit Wall Excavation Effectiveness

From the previous section it is clear that blasting damage will still occur on final pit wall benches due to:

- Geological conditions,
- Operational issues.

It is thus important that blasting effectiveness and specifically the condition of the final wall be measured so that:

- The blasting can be optimised and final wall damaged be minimised,
- Poor Mining practices and potential rock fall risk areas are identified.

A blasting rating study was initiated in 2009 to address the above purpose. Two approaches were followed:

- Detailed rating system of benches,
- Crest and Toe Methods based on actual surveyed bench geometries.

Each of the above is discussed below.

7.1.3.1 Detailed rating system of benches

The author imitated and oversaw the development of a detailed rating system for the benches (Final Limit Blasting and Cleaning Quality Assessment). This rating system was developed by considering the critical parameters that are required for a well-developed bench. These are:

- Drilling Quality
- The level of damage to the bench
- The quality of the loading and bench scaling. See Table 7.1 showing the Final Limit Blasting and Cleaning Quality Assessment form with the ratings from each parameter.

Ngoro (2009) rated several patterns in the pit using this system. It quickly became apparent that a good correlation could be made between the ratings and actual in pit conditions. See Figures 7.5 to Figure 7.7. However the system had the following main drawbacks:

- The rating is time consuming since it involves counting all the half-cast pre-split barrels
- The rating could only be conducted on benches with access. Thus historical benches could not be rated and no comparison between current and historical performance could be deduced.

Table 7.1 The Final Limit Blasting and Cleaning Quality Assessment Form.

DE BEERS
A DIAMOND IS FOREVER

Final Limit Blasting and Cleaning Quality Assessment

Venetia Mine

				Presplit	Trim-Buffer	Trim-Production
Block Id		**Spacing**				
		Distance to Pre-split				
Cut No		**Halfcast Factor**				
Rock Type		**Hole Diameter**				
Bench No		**Burden x Spacing x Rows**				
Date of Blast		**Explosive Charge**				
Date of Assessment		**Explosive Type**				
Blasting Index Rating		**Depth**				

Drilling Quality Rating (S, L, A)				**DQR**	**Pre-split**	**Trim**
V. Good (75-100)	**Moderate (50-75)**	**Poor (25-50)**	**V. Poor (0-25)**	**Spacing**		
On design	Slightly out of design <100mm	Did not achieve design 100-200mm	Did not achieve design >200mm	**Line**		
25-33	17-25	8-17	0-8	**Angle**		
TOTAL RATING (Max 100)						

Basis of Assessment	**V. Good (75-100)**	**Moderate (50-75)**	**Poor (25-50)**	**V. Poor (0-25)**	**Assessment Rating**	**Description/ observations**
Blasting Damage						
Blasthole Barrels exposure quality	Barrels fully exposed on the face.	Barrels largely exposed on the face. Up to 10% not exposed due to over or under break	Barrels moderately exposed on the face. 10% - 50% not exposed due to over or under break	Barrels poorly exposed on the face. >50% not exposed due to over or under break		
	15-20	10-15	5-10	0-5		
Bedding/joints condition	Joints / bedding closed/tight	Occasional joints / bedding opened up	Frequent joints / bedding open and blocks dislodged.	Joints / bedding dislocated blocks / wedges shattered		
	15-20	10-15	5-10	0-5		
Cracking	No cracking behind crest line.	Hairline cracking evident within berm.	Open cracks evident within berm.	Large cracks open along structure.		
	15-20	10-15	5-10	0-5		
Crest Condition - Back break	Minimal back break (0-10%) North: 0-0.8m South: 0-1.43m	Minimal back break, berm largely intact - 10-20% North: 0.8-1.6m South:1.43-2.86m South	Severe Back break (20-50%)	Extensive berm loss, possibly with bench slump (>50%)		
	15-20	10-15	5-10	0-5		
Toe Condition - Underbreak	No toe (0-10%)	Within 10-20% of design	Within 20-50% of design	>50% from design.		
	15-20	10-15	5-10	0-5		
TOTAL RATING (Max 100)						
Cleaning and Barring						
Bench Floor Condition	No humps/completely flat, on design line, No loose material, (0')	Few humps,slightly out of design line,some loose material (<5')	Several humps, several loose material, did not achieve design (5-10')	Frequecy/many humps, many loose material, did not achieve design (>10')		
	40-50	25-40	15-25	0-15		
Face Condition	Not loading past presplit, completely visible, no loose blocks on the face	Many half barrels visible on the face, few loose block hanging on the face	Few half barrels visible on the face, several loose blocks	Presplit not exposed, loading past presplit, Many loose blocks on the face		
	40-50	25-40	15-25	0-15		
TOTAL RATING (Max 100)						



Blast Damage	Values	Cleaning and Barring Quality	Values
Barrels	18	Bench Floor Condition	48
Joints Condition	18		
Cracking Condition	16		
Back Break	17	Face Condition	42
Toe Condition	15		
Total Blasting Quality	84%	Total Cleaning Quality	90%

Figure 7.5 Good Quality Blasting Example 2 (Meta-sedimentary rock type) (Ngoro, 2009).



Blast Damage	Values	Cleaning and Barring Quality	Values
Barrels	8	Bench Floor Condition	30
Joints Condition	10		
Cracking Condition	14		
Back Break	10	Face Condition	20
Toe Condition	14		
Total Blasting Quality	56%	Total Cleaning Quality	50%

Figure 7.6 Moderate Quality Blasting Example (Dolomite Rock type) (Ngoro, 2009).



Blast Damage	Values	Cleaning and Barring Quality	Values
Barrels	2	Bench Floor Condition	30
Joints Condition	14		
Cracking Condition	14		
Back Break	6	Face Condition	20
Toe Condition	8		
Total Blasting Quality	44%	Total Cleaning Quality	50%

Figure 7.7 Poor Quality Blasting Example (Kimberlite rock type) (Ngoro, 2009).

7.1.3.2 Crest and Toe Methods based on actual surveyed bench geometries

The second method is based on actual toe and crest positions that are compared to the design limits. The definition as described by Ryan and Prior (2000) was used by the author to define the actual catch berm width for the benches in the North domain. See Equation [7.1] for the definition of the percentage catch berm:

% Catch berm = actual catch berm width / design catch berm width x 100 [7.1]

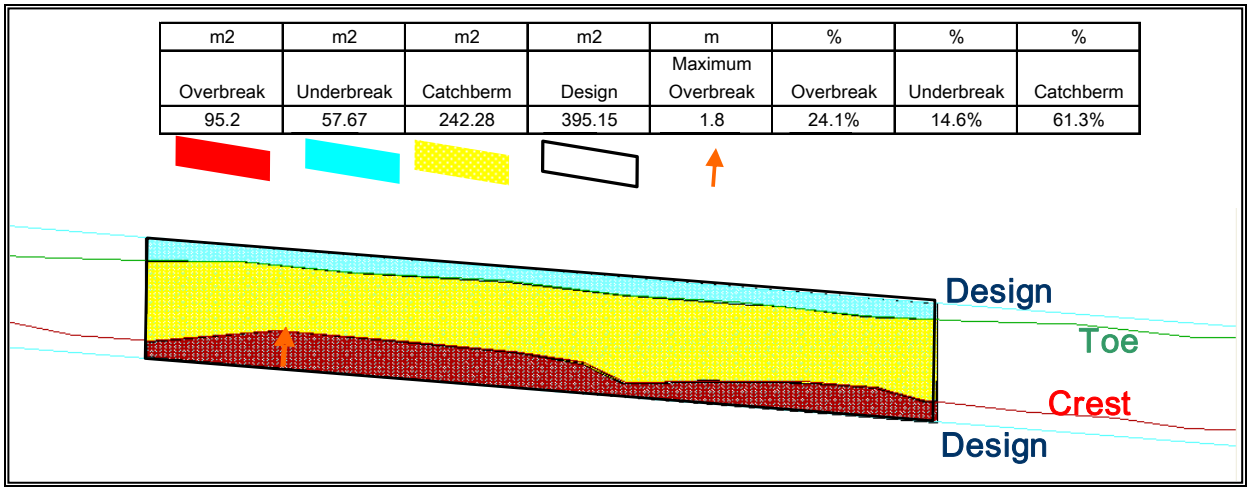


Figure 7.8 Showing an actual design limit in the 3D Mine Design and Modelling Package (GEMS) that contains the Geotechnical block model and mine design amongst others.

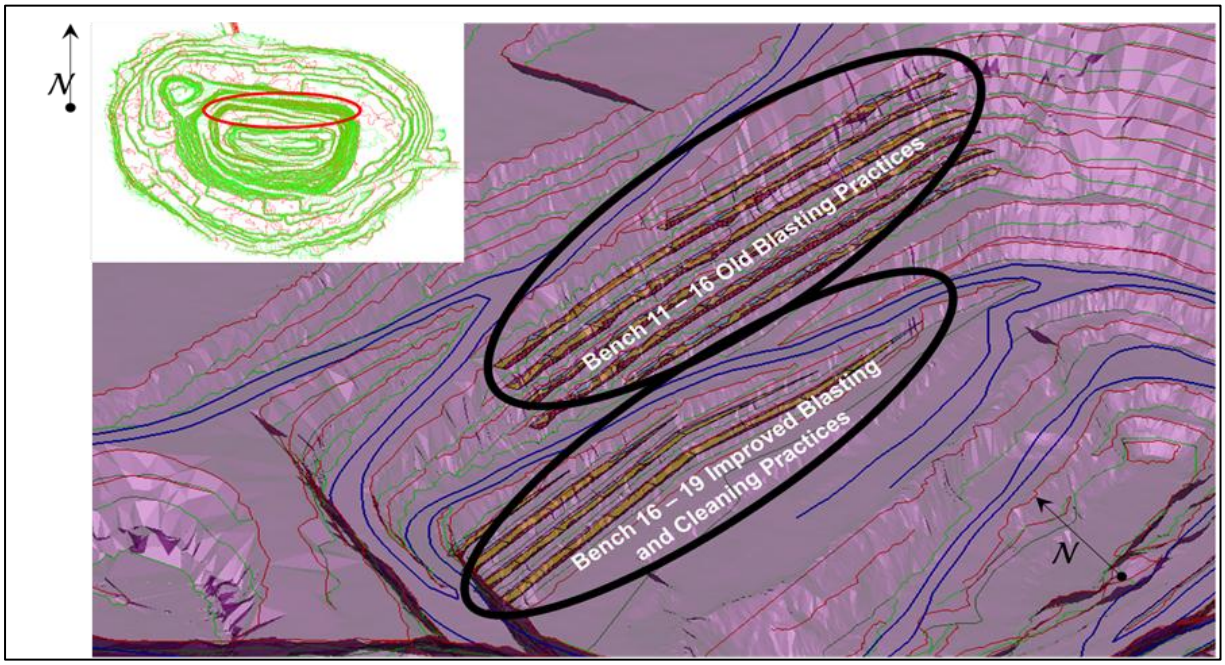


Figure 7.9 Showing the Polygons in 3D dimensions for a historic and current wall in the GEMS software.

The definitions are visually explained in Figures 7.8. This system has the following advantages:

- Not subjective and not dependant on the experience of the user.
- Can be applied to any section of the pit (current or historical) where surveyed crest and positions are available. See Figure 7.9.
- Stored electronically in the mine's integrated mine design and modelling system (GEMS™).
- Allows for a quick assessment of final wall quality.

The only disadvantage of this system is that it requires very accurate toe and crest positions. Initially toe and crest positions were surveyed in by means of a differential global positioning system (DGPS). This however required that the surveyors walk directly below the toe and adjacent to the crest which was seldom the case. From 2010 all toe and crest positions are either surveyed in with a laser scanner or Theodolite Total Station System.

It was found that a direct visual correlation could be made between a well blasted / cleaned face and a high % catch berm value. Thus considering the advantages this system was adopted as the mine standard for measuring bench and blasting performance.

Anglo American in 2009 drafted guidelines for Slope Stability Management of which one aspect was bench retention. H. The ratings as defined by that guideline are given in Table 7.2. However no technique to quantify or clearly define this rating was defined at that stage. The average % catch berm for each year since 2008 was calculated. See Figure 7.10. From the results it is clear that blasting has improved resulting in a significant increase in catch berm potential (% catch berm).

Table 7.2 The draft Anglo American Guideline for Bench Retention (Author unknown, 2009)

Area	Good	Average	Poor	Unacceptable
Bench Retention	> 85% width	60 to 85 % width	40 to 60 % width	< 40%

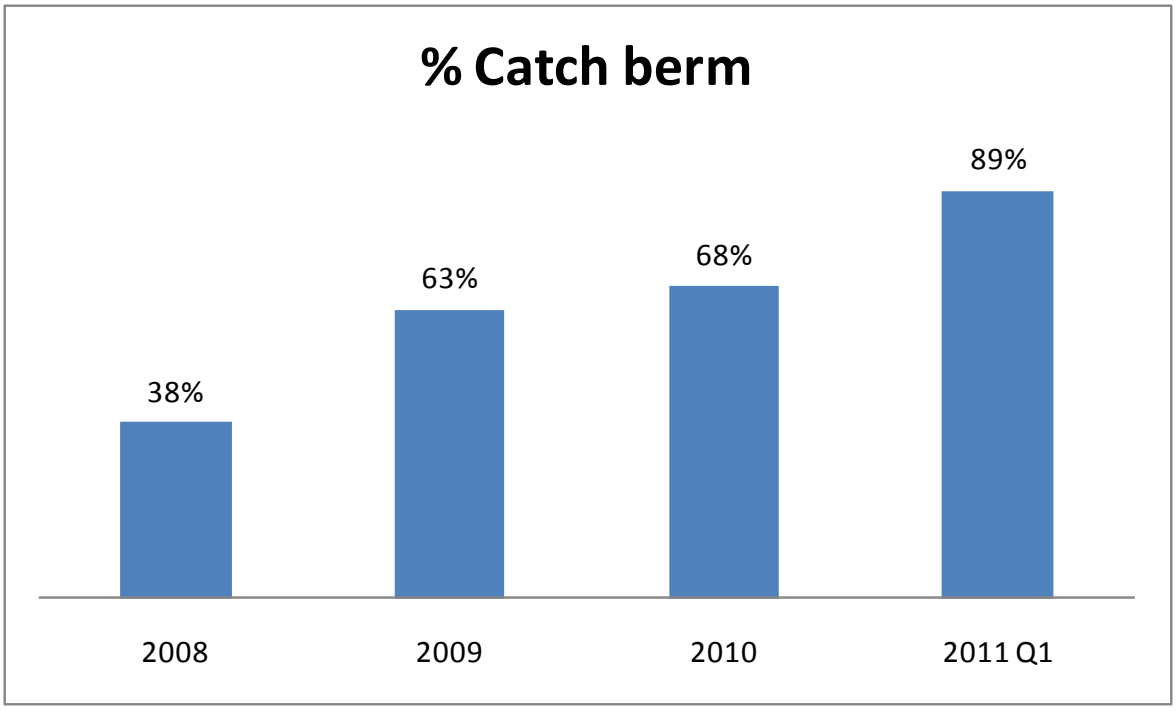


Figure 7.10 % Catch berm since 2008 demonstrating the improvement in blasting practices.

7.1.4 Blast Pattern Selection

In 2009 the author implemented Lilly's 1986 blast index at the mine with the aim of defining blast design parameters (burden, spacing and powder factor). "Lilly (1986) developed a rock mass classification system for use in blast engineering, called the Blastability Index (BI), which is based on four main rock mass parameters which contribute significantly to the performance of a blast:

- Structural nature of the rock mass, e.g. whether it is powdery , blocky or massive (RMD);
- The spacing (JPS); and orientation (JPO); of planes of weakness such as joints, bedding planes, schistosity and foliation;
- The specific gravity of the material (RDI);
- And the hardness/strength of the material (S)" (Lilly, 1992).

Blastability index (BI) is calculated as follows (See also Table 7.3):

RDI = (25*DENSITY) – 50 [7.2]

S = 0.05*(UCS in MPa) [7.3]

BI = 0.5*(RMD + JPS +JPO + RDI +S) [7.4]

Table 7.3 Rating values for the RMD, JPS and JPO components of the BI (Lilly, 1992).

Rock Mass Description (RMD)	RMD Rating	Joint Plane Spacing (JPS)	JPS Rating	Joint Plane Orientation Rating (JPO)	JPO Rating
Powdery or Friable	10	Close (<0.1m)	10	Horizontal	10
Blocky	20	Intermediate (0.1 to 1.0m)	20	Dip out of face	20
Massive	50	Wide (>1.0m)	50	Strike normal to face	30
				Dip into face	40

Extensive BI mapping was conducted by the Geotechnical Department in the pit however the application of a distinct single number to define a specific burden, spacing and powder factor did not prove to be effective for limit blasting. The use of BI to define controlled blasting parameters at Venetia was not effective for the following reasons:

- This method was initially developed to ensure optimal fragmentation and not for controlled blasting purposes.
- It was developed in a vastly different geological setting,
- Due to the variability in the rockmass the application of a single number for a 50 - 100m pattern was not practical.

However what was noted was that a range of BI numbers could be correlated empirically with a specific rock mass condition. These rockmass conditions were termed hard, medium and soft and blast patterns with the optimum burden, spacing was empirically developed by Taljaardt (2010) for each type of rock mass condition. The blasting indices below serve as a guideline and will be developed further as the database is expanded. See Table 7.4. The Blast design for each type of blasting technique and related ground condition is given in Table 7.5.

Table 7.4 Blasting Index Guidelines for Hard, Medium and Soft Rock Mass Conditions in the Venetia Pit.

Domain	BI
Soft	36-46
Medium	47-60
Hard	>60

Table 7.5 Blasting Index Guidelines (Taljaardt, 2010).

Type			Hardness Classification	Hole Diam. (mm)	Burden (m)	Spacing (m)	Standoff to Pre-split (m)	Explosives		Stemming	
								kg/m	kg/m2	Kg/m	Kg/hole
Limit	Pre-split		Soft	127		0.8			0.25		
			Medium						0.40		
			Hard						0.50 - 0.70		
	Trim	Buffer Rows	Soft Kim	127	2.5	3.0	1.9	17		22	77
			Soft Waste		2.3	2.8	1.7				
			Medium		2.2	2.6	1.5				
			Hard		2.1	2.5	1.0				
		Production Rows	Soft	165	4.8	5.8		28		36	130
			Medium		4.5	5.4					
			Hard		4.2	5.0					
Production	Waste	Block	Soft	251	7.5	9.0		64		84	420
			Medium		6.5	7.8					
			Hard		6.0	7.2					
		Box Cut	Soft		7.0	7.0					
			Medium		6.0	6.0					
			Hard		5.5	5.5					
	Kimberlite	Block	Medium	127	2.8	3.2		17		22	77
			Hard		2.5	2.9					
		Box Cut	All	251	5.0	5.0		64		84	420

Stemming material: 15mm to 25 mm aggregate or in kimberlite DMS tailings.

7.2 QUANTIFICATION AND COMMUNICATION OF ROCK FALL RISK

Based on Venetia mine standards a rock fall is defined as any failure smaller than 5 tonnes. Read and Stacey (2009) in turn classify it as any failure smaller than $10m^3$ (18 tonnes at a broken density of $1.8t/m^3$). See Table 7.6 for the size classification of failures.

Table 7.6 Venetia mine size classification of failures (Ekkerd, 2010).

CLASSIFICATION	TONNAGE
Rock fall	< 5
Small	> 5 - 5000
Medium	> 5000 - 50000
Large	> 50000
Catastrophic	> 2800000

The mine currently makes use of slope stability radar (GROUNDPROBE™ SSR) and geodetic monitoring (LEICA GEOMOS™) to monitor the highwalls for any signs of instability. However none of these systems are effective at detecting rock falls. Thus rock fall risks need to be proactively identified by means of regular inspection. Rock fall risk assessment and hazard communication at Venetia mine was done in a haphazard and subjective manner which often resulted in the over or under estimation of rock fall risk in a specific mining area.

The aim of this study was therefore to define an effective risk classification and communication strategy to mining personnel that:

- Is not subjective and highly user dependant,
- Is repeatable, auditable and will consistently identify high risk areas.
- Is applicable to a dynamic mining environment.

7.2.1 Rock Fall Rating Systems

Defining which area requires remedial action or closure to date has been subjective and inconsistent. It was therefore recommend that a standard rock fall rating system be investigated in order to address the above mentioned concerns. This section presents a summary of the comparative studies of rock fall rating and classification systems and a justification for the best suitable system for Venetia mine.

Various systems for rock fall risk assessment and rating have been developed over the years: the Rock Fall Hazard Rating System (RHRS) (Pierson et al., 1990), the Rock Fall Hazard Rating for Ontario (RHRON) (Senior, 2003) and the Rock Fall Risk Assessment for Quarries and Open Pits (ROFRAQ) (Alejano et al., 2008).

The Rock Fall Hazard Rating System (RHRS) was developed by Oregon State Highway Division and takes into account the slope height, catch ditch effectiveness, exposure to vehicles, current climatic and geology conditions to name a few. A summary of the system with all the categories and ratings is given in Table 7.7. Hoek (2002) demonstrates how each category is rated and provides various field case studies.

The Rockfall Hazard Rating for Ontario (RHRON) was developed for the Canadian state of Ontario by Franklin and Senior (1997) and further modified by Senior (2003). RHRON is calculated by answering four basic questions, corresponding to the factors described, Table 7.8. Each factor is rated on a scale from 0 (good) to 9 (bad). The final value for RHRON is calculated as (See Equation 7.5):

$$RHRON = \frac{F1+F2+F3+F4}{4} \qquad [7.5]$$

Table 7.7 Rock Fall Hazard Rating System (RHRS) (Hoek, 2002)

CATEGORY			RATING CRITERIA AND SCORE			
			POINTS 3	POINTS 9	POINTS 27	POINTS 81
SLOPE HEIGHT			25 FT	50 FT	75 FT	100 FT
DITCH EFFECTIVENESS			Good catchment	Moderate catchment	Limited catchment	No catchment
AVERAGE VEHICLE RISK			25% of the time	50% of the time	75% of the time	100% of the time
PERCENT OF DECISION SIGHT DISTANCE			Adequate site distance, 100% of low design value	Moderate sight distance, 80% of low design value	Limited site distance, 60% of low design value	Very limited sight distance, 40% of low design value
ROADWAY WIDTH INCLUDING PAVED SHOULDERS			44 feet	36 feet	28 feet	20 feet
GEOLOGIC CHARACTER	CASE 1	STRUCTURAL CONDITION	Discontinuous joints, favorable orientation	Discontinuous joints, random orientation	Discontinuous joints, adverse orientation	Continuous joints, adverse orientation
		ROCK FRICTION	Rough, irregular	Undulating	Planar	Clay infilling or slickensided
	CASE 2	STRUCTURAL CONDITION	Few differential erosion features	Occasional erosion features	Many erosion features	Major erosion features
		DIFFERENCE IN EROSION RATES	Small difference	Moderate difference	Large difference	Extreme difference
BLOCK SIZE ——— QUANTITY OF ROCKFALL/EVENT			1 FT ——— 3 cubic yards	2 FT ——— 6 cubic yards	3 FT ——— 9 cubic yards	4 FT ——— 12 cubic yards
CLIMATE AND PRESENCE OF WATER ON SLOPE			Low to moderate precipitation; no freezing periods, no water on slope	Moderate precipitation or short freezing periods or intermittent water on slope	High precipitation or long freezing periods or continual water on slope	High precipitation and long freezing periods or continual water on slope and long freezing periods
ROCKFALL HISTORY			Few falls	Occasional falls	Many falls	Constant falls

Table 7.8 RHRON – Ontario Rock Hazard Rating (Franklin and Senior, 1997)

Name	Factor	Questions to be answered
F1	Magnitude	How much rock is stable?
F2	Instability	How Soon or often is it likely to come down?
F3	Reach	What are the chances of this rock reaching the highway?
F4	Consequences	How serious are the consequences of the blockage?

The Rock Fall Risk Rating (ROFRAQ) method was specifically developed for open pit and quarry mining and takes into consideration not only the geotechnical conditions but also conditions that are unique to an open pit mine (blasting, cleaning of benches, etc.) (Alejano et al., 2008). See Table 7.9. ROFRAQ recognizes that a rock fall incident occurs as a result of five sequential events, as follows:

(A) a detached block/rock mass exists on a slope,
(B) the block/rock mass is close to equilibrium (under any given instability mechanism),
(C) a triggering phenomenon makes the block/rock mass unstable,
(D) the block/rock mass fall path is such that one or more blocks reach the mine bottom and finally
(E) at least one block hits a worker or a machine.

The probability of occurring, which is the probability of these five events taking place sequentially, can be calculated by multiplying the individual factor probabilities. In the method, a score of between 0-10 is assigned to each of these possible events (Assigned labels A-E) on the basis of an assessment and weighting of all the factors that affect the occurrence of the rock fall. The product of all the factors, plus a final corrective value based on the rock fall history of the mine (rating F in the proposed method), yields an empirical final value for ROFRAQ index, which provide a yearly estimate of the likelihood of a rock fall-related accident occurring on any given pit slope, see Table 7.9 for details of each individual rating A-E (Alejano et al., 2008). The ROFRAQ value is updated as remedial and safety measures are implemented or as new risks are identified.

Table 7.9 Template for collecting data for Rock Fall Risk Rating for Open Pit and Quarry Mines (ROFRAQ) (Alejano et al., 2008).

Rockfall Risk Assessment for Quarries (ROFRAQ)

Quarry: _____ Slope: _____ Date: _____

ARE THERE POTENTIAL FALLING BLOCKS? a	Joint sets (a)		Joint continuity (b)		Faults (c)		Observed overblasting damage (d)		Bench & berm cleanup (e)		Blocks on slopes (f)		Slope height (g)		A={[[(a*b)+c+d+e+f]/2}*g 0<A<10
	0-1	0.5	<1 m	0.6	NO	0	Pre-split	-2	Very regular	-3	Many	7-10	<25 m	0.5	
	2	1	1-3 m	0.8	Small x 1	0.5	Half-barrels	-0.5	Regular	-1	Several	3-7	50 m	0.8	
	3	3	3-10 m	1	Large x 1	1	None	0	Occasional	0	Some	1-3	100 m	1	
	4	5	10-20 m	1.2	2	1.5	Slight	1	Infrequent	1	Few	0.1-1	150 m	1.3	
	>5	7	>20 m	1.4	>2	2	Excess. overbreak	2.5	Little/none	3	None	0.0-0.1	>250 m	1.5	

ARE THE BLOCKS POTENTIALLY UNSTABLE? b	GEOTECHNICAL STUDY + JOINT DATA INTERPRETATION + IN SITU OBSERVATION/RECORDING OF SLOPE LOCAL AND GENERAL INSTABILITY MECHANISMS									
	Mechanism type (observed or estimated)							Affected slope area (%)			
	SIMPLE	B* (*0.8)	COMPLEX	B* (*1.1)	EVOLUTIVE	B* (*1.4)		IN-SITU OBS.	GEOTECH. STUDY	FALLEN BLOCKS AT SLOPE TOE	AVERAGE (correct. B*) P_i
	Plane failure		Ravelling		Block toppling		A				
	Wedge failure		Many blocks		Flexural toppling		B				
	Circular failure		Free blocks		Footwall slopes		C				
	B* is a correction factor according to failure mechanism complexity						D				

Where *Pi* is the corrected average for the affected slope area %. Rating (B) is calculated as: $B = 10 \times \left\{1 - \left[\prod_{i=1}^{n}\left(1 - \frac{P_i}{100}\right)\right]\right\}$ **0<B<10**

IS A TRIGGERING EFFECT LIKELY TO PRODUCE INSTABILITY? Triggering Phenomena c	Max. 24h rainfall for a 50-year return period (a)		Average 0ºC frost-free period (days) (b)		Slope water (c)		Weathering/erosion (d)		Blasting vibration (specific load) (e)		C=a+b+c+d+e 0<C<10
	<50 mm	0.1	>300	0.1	Dry	0	Unweathered	0	<250 gr/m³	0.1	
	50 – 80 mm	0.5	250–300	0.4	Damp	0.1	Slightly weathered	0.1	250–400 gr/m³	0.5	
	80 – 110 mm	1.5	200–250	1	Wet	0.3	Weathered	0.3	400–550 gr/m³	1	
	110- 150 mm	4	150-200	2	Dripping	0.7	Very weathered	0.7	550–700 gr/m³	1.5	
	>150 mm	6	<150	2.5	Flowing	1	Extremely weathered	1	>700 gr/m³	2	

ARE THE BLOCKS LIKELY TO REACH THE MINE BOTTOM? d	Bench height (m) & Berm/catch-bench width [BW] (m)										General slope dip (a)		Berm conditions & cleanup (b)		Face irregularity (c)		D=(D_b+a+b+c)*d 0<D<10 Estimated probability of block reaching mine bottom (RockFall)
	5		10		12		15		20						High	+2	
	BW	D_b	BW.	D_b	BW	D_b	BW	D_b	BW	D_b					Medium	+0.5	
	<1	10	<1	10	<2	10	<3	10	<4	10	40º	+2	Optimal	0	Low	0	
	1.5	7	2	9	3	8	4	9	5	9.5	48º	+1	Good	+0.5	Mesh / ditches (d)		
	2	4	3	6	4	5	5	6	6	7.5	56º	+0.5	Limited	+1			
	2.5	1	4	2	5	2.5	6	3	7.5	2.5	60º	0	Poor	+1.5			
	>3	0	5	0.2	6	1	7	1	9	0.5	72º	-0.5	Very poor	+3	Yes	0	
			>5.5	0	7 >	0	>8.5	0	10	0	80º	-1			No	1	

ARE BLOCKS LIKELY TO IMPACT ON WORKERS OR MACHINERY? e	Block size (1 falling block) (a_1)		Rock volume (>1 falling blocks) (a_2)		Time spent at slope toe by machinery/ workers (%) (b)	Space occupied by machinery/workers vs. slope length (%) (c)	Position of machinery/ workers in relation to slope toe (d)		E_{mach} = (b/100) *(c-mach/100)* (a_1 or a_2)*d*10 E_{pers} = (b/100) *(c-pers/100)* (a_1 or a_2)*d*10 E=10-[(10- E_{mach})*(10-E_{pers})/10] 0.00025<E<10
	<0.001 m³	0.9	<0.1 m³	1	Days/year shifts/day hours/shift % time under slope	Space occupied by machine vs. slope length (c_{mach})	Very close (x/H < 10 %)	1	
	0.001-0.1 m³	1	0.1–5 m³	1.5			Close (x/H < 25 %)	0.5	
	0.1–1 m³	1.2	5–50 m³	2		Space occupied by persons (1 m) vs. slope length (c_{pers})	Average (x/H < 50 %)	0.1	
	>1 m³	1.5	>50 m³	2.5			Far (x/H < 100 %)	0.01	
							Very far (x/H >100 %)	0.001	

f	SLOPE ROCKFALL HISTORY					
No recorded rockfalls	Very few rockfalls	No data Unreliable observations	Occasional rockfalls	Several rockfalls No accidents	Some rockfalls 1 reported accident	Frequent rockfalls >1 reported accident
0.75	0.9	1.0	1.1	1.2	1.4	1.5

ROFRAQ = (A x B x C x D x E x F) = **$ROFRAQ_{BASIC}$ = (A x B x C x D) =**

$ROFRAQ_{pers}$ = (A x B x C x D x E_{pers} x F) = **$ROFRAQ_{mach}$= (A x B x C x D x E_{mach} x F) =**

Estimated probability of an accident due to rockfall occurring on the slope = ROFRAQ / 100,000 =

Preliminary assessment of the quarry face hazard according to ROFRAQ results					
Less than 10	10-25	25-100	100-250	250-1000	More than 1000
VERY LOW RISK No special measures required.	LOW RISK Simple precautionary measures required (inc. regular observation)	LOW TO AVERAGE RISK Some simple safety precautions required e.g. avoid traffic under slope during rainy periods, etc.	AVERAGE RISK Important safety measures required. Improve berms and catch-benches, cleanup, blasting control techniques, etc.	HIGH RISK Highly hazardous. Redraft mining plan, enlarge catch-benches, redesign locally, etc.	VERY HIGH RISK Redesign quarry, install meshes, build ditches, etc.

Rankhododo and Ekkerd (2009) conducted a comparative study in the Venetia pit and compared the results of the above-mentioned rock fall ratings. The pit was sub-divided into individual nodes as follows: N1-N6 on the North, and S1-S6 on the South. See Figures 7.11 to 7.14. Each of these areas were then rated using ROFRAQ, RHRON and RHRS systems.

The ROFRAQ results compared well with the perceived in pit conditions and rock fall history and ROFRAQ was subsequently recommended as the preferred method for assessing rock fall risk in the Venetia pit (Rankhododo and Ekkerd, 2009).

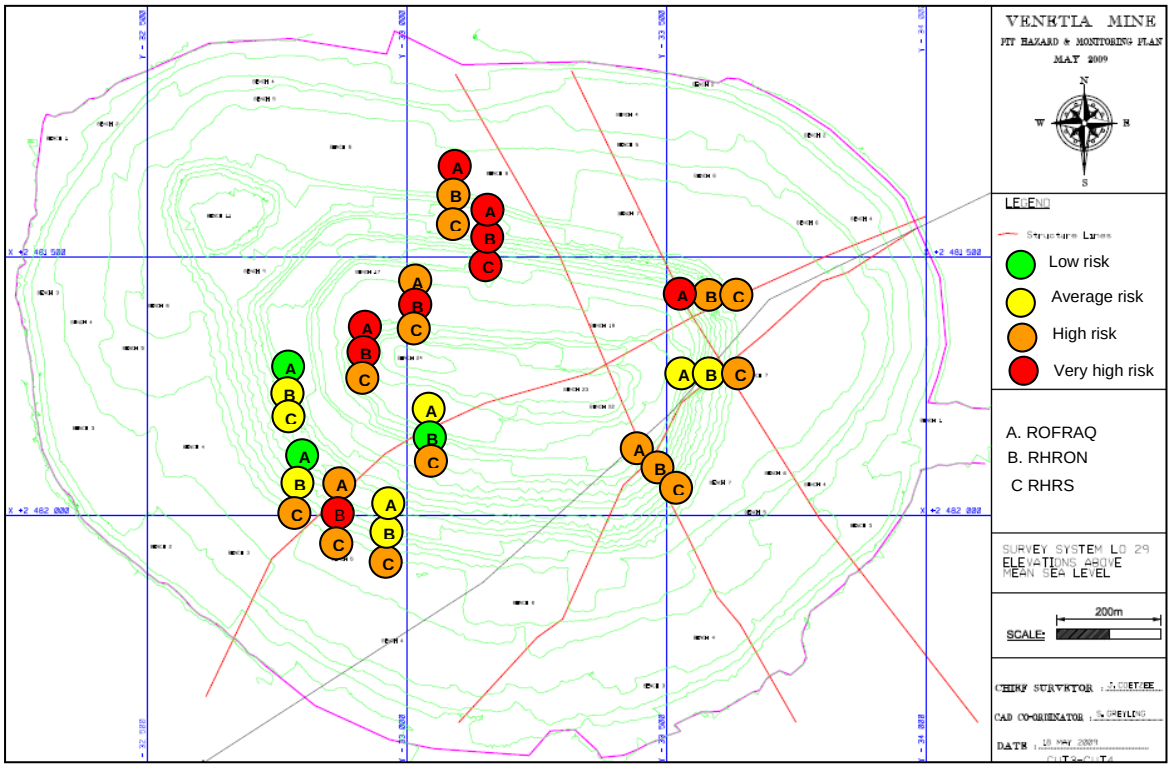


Figure 7.11 Rockfall Hazard Risk Assessment and Classification for Venetia Mine-a comparison of the ROFRAQ, RHRON, RHRS systems (Rankhododo and Ekkerd, 2009).

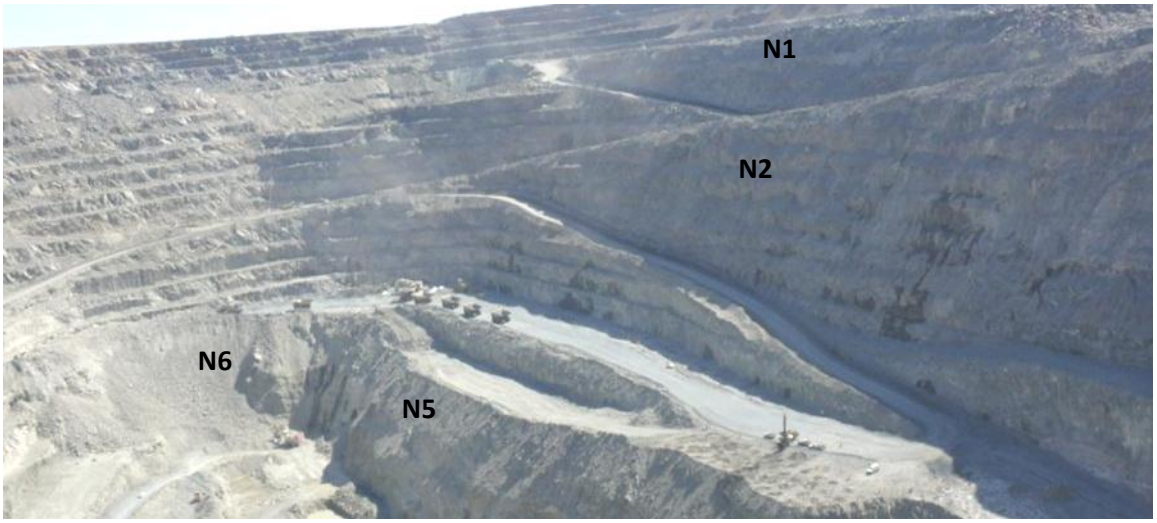


Figure 7.12 Photograph Looking North-West (Rankhododo and Ekkerd, 2009).

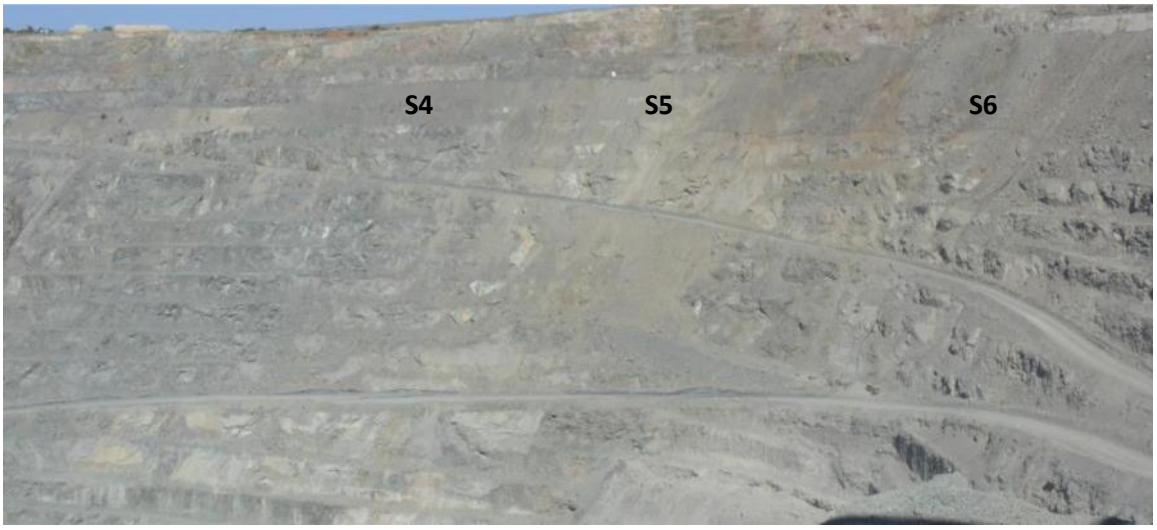


Figure 7.13 Photograph, Looking South-East (Rankhododo and Ekkerd, 2009).



Figure 7.14 Photograph, Looking East (Rankhododo and Ekkerd, 2009).

7.2.2 Application of ROFRAQ rating and Communication of Risk

Subsequent to the implementation of the ROFRAQ system it was quickly noted that users seldom conducted a rating in the same area over time. This made it very difficult to establish a rock fall risk history for an area. The mine therefore adopted a sector based risk identification and design validation philosophy whereby all the domains in the pit (See Figure 7.15) are sub-divided into risk sectors. The sector based philosophy has the following advantages:

- It eliminates the ad hoc inspection of only certain portions of the pit.
- Allows for a risk history to be established for a specific area of the pit.
- Facilitates and eases communication of risk for the Geotechnical risk sectors. See Figure 7.15.

The sectors should:

- Be located within the relative Geotechnical Domain and not cross cut domain boundaries.
- Be approximately 150m in length.
- Cover all the major stacks in the pit.
- Be named as follows: Domain_Grid number. See Figure 7.5 for a complete Pit Hazard and Monitoring map with the grid.

This systematic approach has allowed Rankhododo and Ekkerd (2009) to develop a database over several months of rock fall performance and the effectiveness of various remedial actions. Based on actual in pit performance and the recommended application of ROFRAQ by Alejano et al. (2008) a risk classification guideline was developed.

Thus the ROFRAQ risk rating is used as a guideline to classify an area and remedial action is applied depending on the classification. See Table 7.10 for details of the classification and associated remedial action. The ROFRAQ medium and high risk sectors, with their remedial actions, along with the other Geotechnical risks in the pit, are then captured on the monthly Pit Hazard and Monitoring Map and distributed to mining production personnel and management. See Figure 7.16.

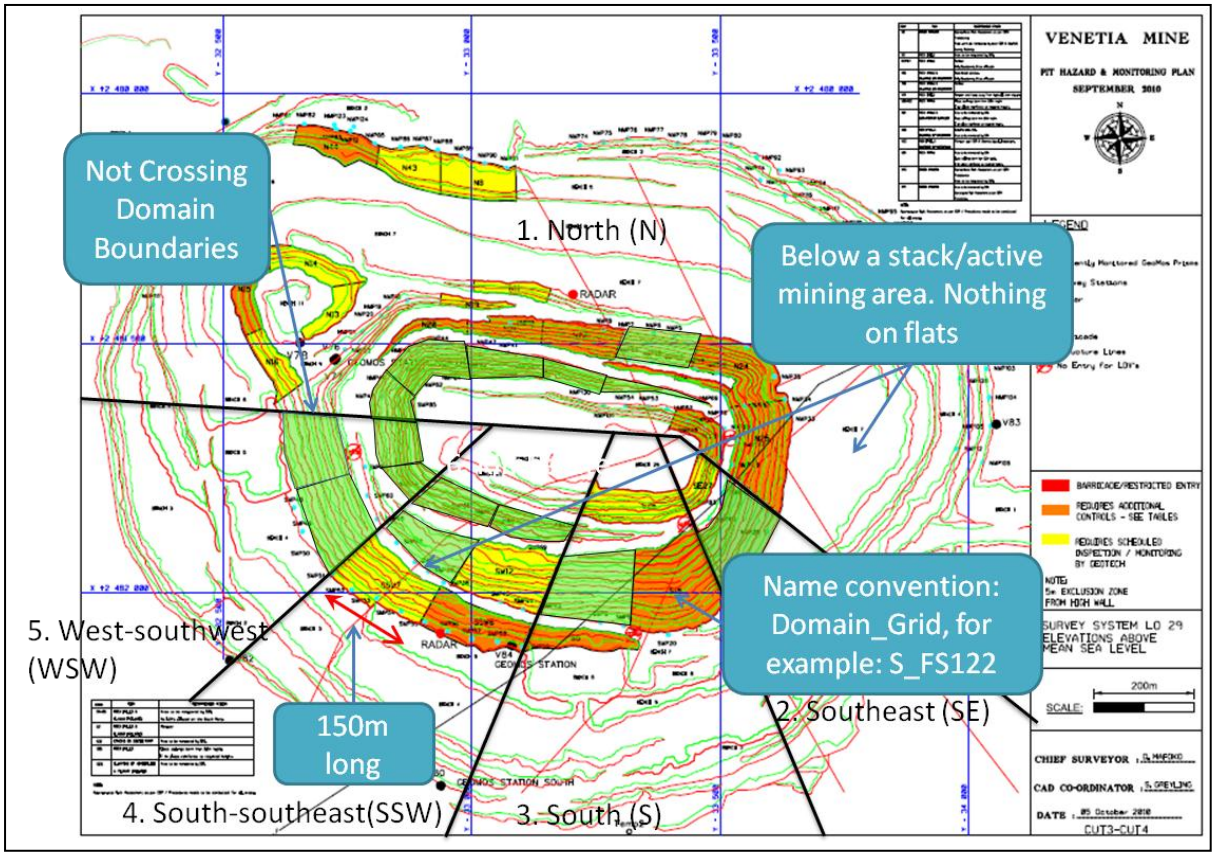


Figure 7.15 Example of the Geotechnical Risk Sectors

Table 7.10 ROFRAQ classification and guideline for remedial actions

Preliminary Assessment of the slope face hazard according to ROFRAQ results			
Classification	**Yellow**	**Orange**	**Red**
Rating	**100 - 250**	**250 – 1000**	**>1000**
Proposed Action	Inspect Weekly / Communicate regression of conditions	Require Remedial Actions like tailings berms or only rock fall protected vehicles	No Entry / Eliminate or Redesign / Special Instruction

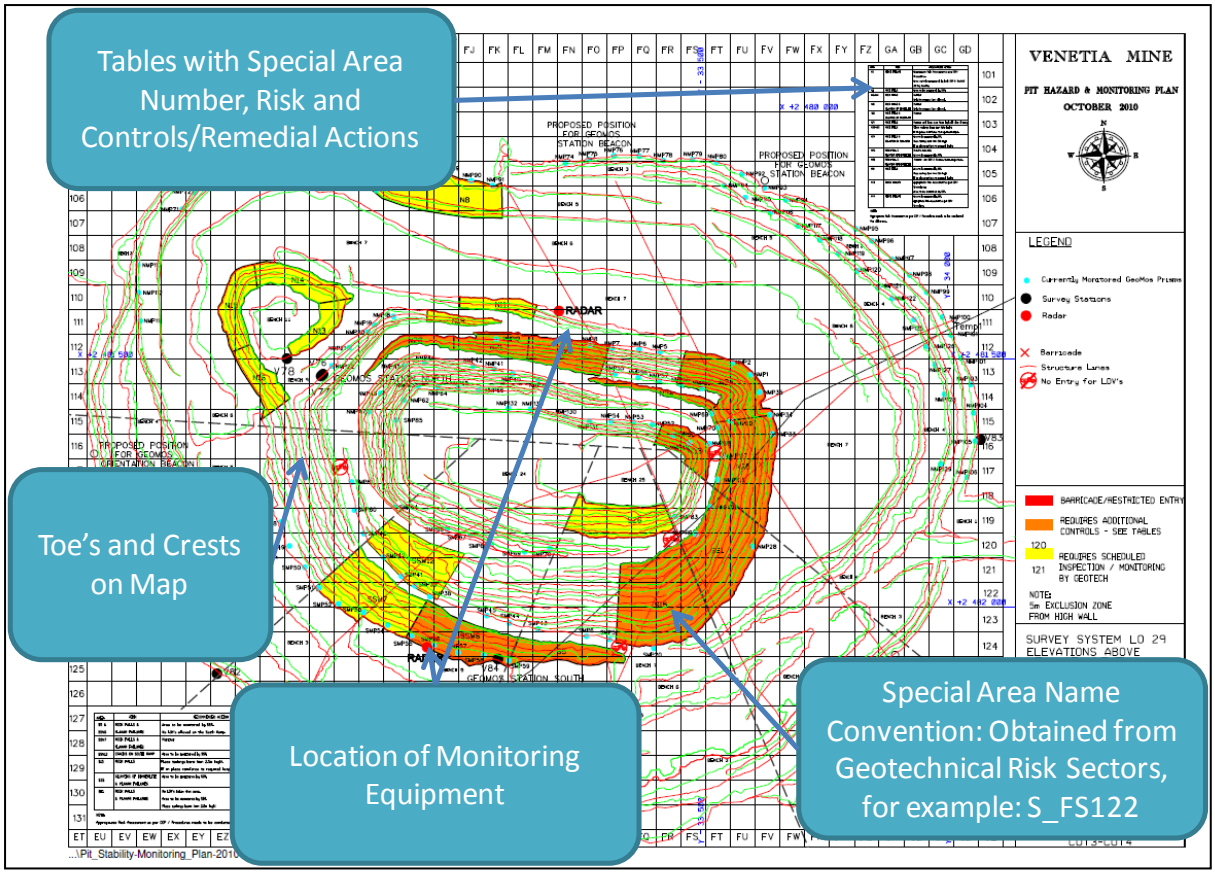


Figure 7.16 Example of a Pit Hazard and Monitoring Map that is updated and distributed to mining production personnel on a monthly basis

7.3 SUMMARY

Excavating the highwalls with conventional production blasting techniques and related poor mining practices (side casting, uncontrolled blasting and insufficient cleaning and barring practices) resulted in extremely poor highwall conditions, poor bench retention values and a significant increase in the rock fall frequency rate. See Figure 6.7. In 2008 this practice was ceased and the mine started experimenting with limit blasting techniques on the final pit limits. As part of the optimisation programme effective measures had to be put in place that will flag poor mining practices and the related rock fall risks.

The author oversaw the investigation and development of techniques (bench rating system, modified %catch berm method after Ryan and Prior (2000) and rock fall rating) to monitor the condition of final walls and related mining practices. The detailed rating system of benches (The Final Limit Blasting and Cleaning Quality Assessment) was developed by

considering the critical parameters that are required for a well-developed bench (drilling quality, the level of damage to the bench, the quality of the loading and bench scaling). This technique was very onerous and time-consuming. The modified %catch berm method after Ryan and Prior (2000) proved effective and faster in highlighting areas of poor bench performance and was adopted by the mine to monitor the condition of final walls and related mining practices.

Individual blasting indices are not effective in blast pattern selection at Venetia Mine. This is due to the complex and heterogeneous nature of the metamorphic rocks that make up the pit walls. A range of blasting index values (See Table 7.4) can be used to describe soft, medium and hard ground conditions. Taljaardt (2010) has developed blasting patterns for each of those ground conditions and excellent results have been achieved to date. See Figure 7.10 and Table 7.5.

Various systems for rock fall risk assessment and rating systems were evaluated in the pit: (RHRS) (Pierson et al., 1990), the Rock Fall Hazard Rating for Ontario (RHRON) (Senior, 2003) and the Rock Fall Risk Assessment for Quarries and Open Pits (ROFRAQ) (Alejano et al., 2008). The ROFRAQ results compared well with the perceived pit conditions and were subsequently recommended as the preferred method for assessing rock fall risk in the Venetia pit (Rankhododo and Ekkerd, 2009). The implementation of the abovementioned systems allowed for the effective identification of poor mining practices and facilitated the communication of risk.

8. SUMMARY AND CONCLUSIONS

The geology of Venetia mine is complex because it had a long and protracted geological evolution that was earmarked by various magmatic and metamorphic events. Thus ample and reliable information regarding the rock mass is required for slope design purposes.

The country rock assemblages at Venetia are part of the Limpopo Mobile Belt and mainly consist of metamorphic and intrusive igneous rocks. The stability of the pit is structurally controlled and the structure can be divided into two main components, ductile structure (S2 foliation) and brittle structures (major structures, MS1–3, and joints, J2, J4 and J6). The pit has been affected by several ductile deformation events, termed D1 to D4. However a dominant metamorphic foliation (S2) cross cuts all the geology which results in an anisotropic rock mass strength. The interaction between the brittle jointing (J2, J4 and J6) and S2 foliation also locally impacts on bench stability and subsequent bench performance. The slope design is therefore highly dependent on the orientation of the pit slopes relative to structural features. See Figures 1.7 and 1.8.

No significant water bearing structures that would constitute targets for dewatering boreholes have been encountered to date however piezometer data have indicated the presence of significant pore pressures within the pit walls. Active dewatering is however not deemed as viable due to the low permeability of the metamorphic rocks.

Up to 2009 Venetia mine employed high energy blasting techniques, mainly focused on achieving high production rates and optimum fragmentation, to develop the final walls of the pit. Excavating the highwalls with conventional production blasting techniques resulted in extremely poor highwall conditions. In 2009 this practice was ceased and the mine started experimenting with limit blasting techniques on the final pit limits. The benefit of the limit blasting was however not quantified. That same year a revision and optimisation of the business plan was undertaken of which one aspect was the review of the slope angles and design sectors. The acceptance criteria, as recommended by the Guidelines for Open Pit Slope Design (Read and Stacey, 2009) were used by De Beers to determine the acceptable level of risk for the optimisation programme.

Rigorous reviews of actual pit slope performance were conducted by the author for the North and Southern slopes. This indicated that the bench performance in the Southern slopes can be

isolated to distinct areas. The South-western portion of the slope had the highest incidence of complete bench failures (43%) followed by the Southern section (17%). See Figure 2.1. In turn rock falls were prevalent in the North domain. This was aggravated by poor blasting resulting in the catch berms not being retained and thus not being effective at retaining rock falls. The mechanisms that initiated the variable bench performance and rock fall risk were not well understood at that stage.

The author used the definition as described by Ryan and Prior (2000) to define the actual catch berm width for the benches in the North domain. The survey indicated that the new blasting techniques and improved mining practices were effective resulting in a significant increase in the catch berm potential (% catch berm). See Figure 2.2.

Initial the pit design was conducted in 2008 and defined on only two major domains [North: mined at 56 degrees, South: mined at 40 degrees] (Contreras, 2008). The South slope design assumed a slope striking parallel to the orientation of the foliation. This study indicated that steeper stack angles are achievable in the North domain however a lower slope angle was recommended due to the perceived rock fall risk and the mining practices at the mine. The rock fall risk was however not quantified. Review of the data supplied by the operation to the consultant indicated that the orientation of the S2 foliation and joint populations were extrapolated from old exposures in Cut 2. In addition to the above no groundwater table was available for the first design in 2008.

Thus considering the improvement in mining practices, lack of understanding regarding the actual in pit performance and extrapolated data that was used in the design the author deemed it appropriate to re-evaluate the Cut 4 design in 2009. The optimisation study was scoped by the author and consisted of various phases (1 – 3).

Phase 1 was aimed at providing initial input parameters into the SBP regarding slope angles (savings on waste stripping) (Stroth, 2009; Gomez, 2010) and bench heights (potential to increase productivity) (Contreras, 2010; Steffen and Terbrugge, 2009). The only new data for this phase was limited scan line mapping that was collected by the mine in the South-western quadrant of the pit and thus similar constraints relating to the orientation of the S2 foliation, joint sets and groundwater applied.

Phase 2 ran concurrently with the above work and was aimed at defining the orientation of the S2 foliation, joint data and pore pressures in the toe of the slope. This phase consisted of

structural mapping, drilling, instrumentation installation; and modelling of the geology and ground water table by Basson (2011a) and Liu et al. (2011) respectively.

The Phase 2 structural data collection programme consisted of pit mapping (Scan Line and SIROVISION™) and the review of available borehole information. The initial mapping consisted of conventional scan-line mapping and was subsequently replaced with a more efficient photogrammetry mapping technique, SIROVISION™. The mapping programme was scoped and supervised by the author while mapping data was collected by staff in the Venetia Geotechnical Department. In 2010 Basson was contracted by the author to: analyse the newly collected structural pit mapping information on the S2 foliation, update the geology model and further sub-divide the model into unique structural volumes. Structural volumes are characterized by an internally consistent suite of characteristics, such as a consistent fault style and orientation, consistent foliation orientation or confinement to a particular lithological unit or package. See Table 5.3 and Figure 5.10.

In order to account for pore pressures in the wall and to address the above shortcomings from the previous studies, regarding a groundwater table, the author scoped a drilling programme of which the aim was install several piezometers in the toe of the slope. Three new boreholes (GDH123, DWH019 and DWH020) were drilled by Partners Drilling, and in total fifteen (15) VW piezometers were installed either close to the face and or toe of the current slope (Figure 5.12 and 5.14) by a sub-contractor. The Itasca Office in Denver, USA, where contracted by the author to update the groundwater model for the pit. The results from the piezometer network were subsequently used by Shchipansky and Atkinson (2010) and Liu et al. (2011) to update the groundwater model. The modelling indicated that the best correlations between simulated and measured water levels are obtained if a 50m zone of relaxation is applied in the model to the slope.

For the final phase of the optimisation (Phase 3) the Geotechnical domain model and slope design was updated, by the author, using the results from Phase 2 of the study. The updated design incorporated the updated groundwater table and considered the orientation of the pit slopes relative to the foliation; and consisted of bench, inter-ramp and overall slope analyses.

The author used the new geological model from Basson (2011a) in conjunction with a review of pits lope performance and fall of ground data to outline and define new Geotechnical domains for the Venetia Pit. See Figure 6.10. The domains were upgraded from the initial

two (2) domains in 2008 to twenty six (26) and can be broadly divided into three levels or tiers (1–3):

- Tier 1: Major domains – The pit shell geometry dictates their location and extent.
- Tier 2: Structural volumes as defined by Basson (2011a) in Table 5.3 which is based on geological package and the orientation of the S2 foliation in that unit.
- Tier 3: Weathering (Fresh or Weathered). See Table 6.24 for a summary of the Tier 1 to 3 domains.

The rock mass model (Geotechnical) data was subsequently re-defined and summarised for each domain. This included the calculation of rock mass ratings, analyses of laboratory rock testing data and calculation of rock mass and joint strengths.

The rock mass strength properties were calculated by the author using the Hoek-Brown criterion and related input parameters (Hoek et al., 2002). The technique as described by Barton and Bandis (1982, 1990) was used to calculate the strength of the foliation. Ratios of JCS_F/JCS_O and JRC_F/JRC_O for this project are lower than those prescribed by Karzulovic and Read (2009) (JCS_F /JCS_O < 0.3 or JRC_F /JRC_O < 0.5) and can be therefore considered as conservative. See Appendix G. Strength Values were calculated for each drilling interval, and summarised per domain, to take account for the variability of the metamorphic rockmass.

Commonly only intact rock strength is used in rock mass classifications and as such only UCS samples that failed through intact rock is to be used for UCS (Read and Stacey, 2009; Brady and Brown, 2004). However the rock mass at Venetia has been affected by a number of ductile deformation events (D1 to D4), resulting in several ductile planar fabrics (S1-S3), and brittle events. Based on field observations the rock mass, on a meter/lab-sample scale, can be divided into S2a: planar fabric (“closed” foliation), S2b: planar fabric (“open” foliation) and massive rock not dominated by biotite and or other mineral assemblage banding. See Figure 6.3. Triaxial shear testing conducted on S2a samples have demonstrated that several samples preferentially fail on this “closed” foliation and thus could be mistakenly recorded as samples that failed on a discontinuity in the rockmass. Therefore if the effect of the “closed” fabric; and all samples described by the lab as “failed on discontinuity”, were discarded the strength on a lab scale will be overestimated. Therefore UCS results were not filtered and the UCS, that contains the intact and failed on discontinuity/fabric data sets, was used for this project. See Table 6.1.

The RMR's with the effect of foliation was used. This could be considered as conservative since: the RMR's without foliation are 10 to 20 points higher; and strength anisotropy (due to the S2 foliation) was simulated using an anisotropic model in SLIDE™ and ubiquitous joint model in FLAC™ resulting in the effect of the foliation being double accounted for in the design. It was also assumed that the S2 foliation is continuous and the positive effect of rock bridges and effective cohesion, as described by Terzaghi (1962), Jennings (1972) and Karzulovic and Read (2009), was not accounted for in the design.

A 50m deep damage zone was applied to the slope and correlates with the findings of the 2011 groundwater modelling (Liu et al., 2011) and those of Lorig et al. (2009). Key Geotechnical data were collated and stored in a 3D block model.

The consequence of failure was assumed to be high for bench, inter-ramp and overall slopes and associated acceptance criteria as defined by Wesseloo and Read (2009) were applied.

Probabilistic limit equilibrium bench analyses were conducted by the author for every practical orientation of each domain, at various bench heights, using SWISA™ and PFISA™. For the inter-ramp and overall slope design limit equilibrium probabilistic analysis were conducted using the programme SLIDE™. The cumulative spill width distribution for each respective probability of failure (25%) was used to calculate the maximum inter-ramp angle required in order to retain the spill. While the cohesion for all the foliation/joint sets were conservatively assumed to be zero to account for blast vibration. The limitations of the current load and haul fleet was taken into consideration and bench analyses were only conducted on 12m, 15m and 24m bench heights.

The analysis indicated that an increase in bench height for the Southern domains will result in an increase in back break. The various bench heights (12m, 15m and 24m) gave similar maximum inter-ramp angles. This is because PFISA™ and SWISA™ do not take joint/structure persistence into account and failure volumes subsequently increase proportionally with an increase in bench height. Joint persistence normally does not exceed one bench height and thus in practice higher benches (wider catch berms) in the North will be more effective.

The bench analysis indicated that the probability of wedge failure is much larger in the Northern domains (STRV1 and 3) when compared to the Domains in the South (STRV4 to STRV8). The stack angles in the North domain are not controlled by the S2 foliation and/or

rock mass strength. Here the interaction between brittle jointing controls the maximum catch berm and subsequent stack angle. Analysis of fall of ground data and bench analyses confirm that the dominant failure mechanism in the North is wedges that form on the intersection of the J2 and J4/J6 joint sets. Bench analyses indicated that steeper angles are viable in this domain.

The bench and inter-ramp analyses indicated that stability of the pit walls in the Southern domains is not only controlled by their orientation in relation to the major S2 foliation but also by the interaction of jointing with the foliation. The highest probability of wedge failure in the Southern domains (STRV4 to 8) occurs in STRV8-MP (34.97%) on the intersection of the J2 set with the S2 foliation. The field survey of the percentage complete bench failures (See Figure 2.1) also indicated that this domain has the highest incidence of bench failures (43%). Thus the results compare well with field observations.

In STRV4, STRV5 and STRV8-GP the dominant factor that drive stability is inter-ramp scale failure on the S2 foliation compared to STRV6 where the maximum inter-ramp angle is limited by failure at the overall slope scale. The bench and inter-ramp kinematic analyses indicated that steeper angles are viable where there is a major difference in strike between the S2 foliation and pit walls. Where the dip direction of the slope and foliation is within 20^0 the maximum inter-ramp angle is controlled by the dip of the foliation. It is thus critical that the dip of the S2 foliation be confirmed by continuous pit mapping as faces are exposed during mining.

The numerical finite difference code, FLAC™, was used to validate the results of the limit equilibrium stack analysis. The validation indicated that the limit equilibrium modelling is conservative when compared to numerical modelling and it is recommended that future studies use the response surface methodology by Chiwaye and Stacey (2010), whereby numerical modelling is used, to estimate the risk (probability of failure). The final design parameters for each major tier 2 domain are given in Table 6.37.

In this project the effect of poor mining practices on highwall conditions and related rock fall frequency was demonstrated. Maintaining good mining standards are thus critical if steeper stack angles are considered. The author oversaw the investigation and development of techniques (bench rating system, modified %catch berm method after Ryan and Prior (2000) and rock fall rating) to monitor the condition of final walls and related mining practices. The detailed rating system of benches (The Final Limit Blasting and Cleaning Quality

Assessment) was developed by considering the critical parameters that are required for a well-developed bench (drilling quality, the level of damage to the bench, the quality of the loading and bench scaling). This technique was very onerous and time-consuming. The modified %catch berm method after Ryan and Prior (2000) proved effective and faster in highlighting areas of poor bench performance and was adopted by the mine to monitor the condition of final walls and related mining practices. Various systems for rock fall risk assessment and rating systems were evaluated in the pit: (RHRS) (Pierson et al., 1990), the Rock Fall Hazard Rating for Ontario (RHRON) (Senior, 2003) and the Rock Fall Risk Assessment for Quarries and Open Pits (ROFRAQ) (Alejano et al., 2008). The ROFRAQ results compared well with the perceived pit conditions and ROFRAQ was subsequently recommended as the preferred method for assessing rock fall risk in the Venetia pit (Rankhododo and Ekkerd, 2009). The implementation of the abovementioned systems allowed for the effective identification of poor mining practices and facilitated the communication of risk.

The project resulted in re-defining Geotechnical domains for the Venetia pit (K01 and K02 pits) and indicated that steeper stack angles are viable in a number of domains. The pit was designed, for the first time, at bench, inter-ramp and overall slope scale; and conforms to the acceptance criteria as stipulated in the 2009 Open Pit Design Guidelines (Read and Stacey, 2009). Design parameters for the main country rock domains that will be intersected by the Cut 4V27 pit has been presented. The failure mechanisms, which initiate instability and control the maximum inter-ramp angle, in each domain was also successfully identified and correlated with actual pit conditions.

The results from this study was incorporated into the strategic business plan for the operation and desktop studies, undertaken by Venetia's Mine Planning Department, indicated that a one degree change in overall slope angle results in a potential saving of US$ 50 million.

9. REFERENCES

Alejano, L.R., Stockhausen, H.W., Alonso, E., Bastante, F.G. and Ramirez Oyanguren, P., (2008) ROFRAQ: A statistic-based empirical method for assessing accident risk from rockfalls in quarries, International Journal of Rock Mechanics and Mining Sciences 45, pp. 1252–1272.

Andrieux, P., (2010) Report on the Itasca Canada Site Visit of 07-10 June 2010 at Venetia Mine. Site visit report by Itasca Consulting Canada, Inc., to the De Beers Consolidated Mines Corporate Headquarters, Sudbury, Ontario, Canada, pp. 1 – 28.

Armstrong, R., (2008) Evaluation and Recommendations for the Venetia Cut 4 24DD Design, SRK Consulting, October.

Atkinson, L. and Shchipansky, A., (2008) Updated Three-Dimensional Groundwater Flow Model of Venetia Mine and Predicted Groundwater Conditions During Future Mining, Report no: HCI-1769, HCItasca Denver (Now trading as Itasca Denver).

Author unknown, (2009) Anglo major risk guideline - slope stability, received from Marc Ruest.

Bandis, S., Lumsden, A. and Barton, N., (1981) Experimental studies on scale effects on the shear behaviour of rock joints. International Journal of Rock Mechanics and Mining Science and Geomechanics Abstracts 18(1), pp.1–21.

Barnett, W.P., (2002) Venetia Mine Code of Practice to Combat Rock Falls, De Beers Internal Report.

Barnett, W.P., (2003) Geological control on slope failure mechanisms in the open pit at the Venetia Mine, South African Journal of Geology, Vol. 106(2/3), pp. 149 – 164.

Barnett, W.P., (2004) Venetia Rock type Descriptions: A Guide for the On-Site Rock Library. Internal Company Report No. GSC04/0037, De Beers GeoScience Centre, pp. 1 – 24.

Barnett, W.P., (2007) Venetia Mine Country Rock Model Report, De Beers Internal Report.

Barton, J.M., Barnett, W., Barton, E.S., Barnett, M., Doorgapershad, A., Twiggs, C., (2003) The geology of the area surrounding the Venetia kimberlite pipes, Limpopo Belt, South Africa: a complex assembly of terranes and granitoid magmatism. South African Journal of Geology 106, pp. 109–128.

Barton, N., (1973) Review of a new shear strength criterion for rock joints. Engineering Geology 7, pp. 287–332.

Barton, N., (1974) A Review of the Shear Strength of Filled Discontinuities in Rock. Norwegian Geotechnical Institute, Publication, no. 105.

Barton, N. and Choubey V., (1977) The shear strength of rock joints in theory and practice. Rock Mechanics 12(1), pp. 1–54.

Barton, N., (1980) Estimation of in situ joint properties, Nasliden Mine. In Application of Rock Mechanics to Cut and Fill Mining, Proceedings of International Conference (eds O Stephansson and MJ Jones), Lulea, Sweden, pp.186–192, IMM, London.

Barton, N., (1982) Shear strength investigations for surface mining, In Stability in Surface Mining, Proceedings of 3rd International Conference (ed. CO Brawner), Vancouver, British Columbia, Society of Mining Engineers, AIME, New York, pp. 171–196.

Barton, N. and Bandis, S.C., (1982) Effects of block size on the the shear behaviour of jointed rock, 23rd U.S. symposium on rock mechanics, Berkeley, pp. 739-760.

Barton, N. and Bandis, S.C., (1990) Review of predictive capabilities of JRC-JCS model in engineering practice. In Rock joints, proc. int. symp. on rock joints, Loen, Norway, (eds N. Barton and O. Stephansson), Rotterdam: Balkema, pp. 603-610.

Basson, I.J, (2005) Structural Mapping, Analysis and 3-D GEMCOM Modelling of Country Rock Surrounding the Venetia Kimberlite Pipes, Prepared For: Venetia Mine De Beers Consolidated Mines, Tect Consulting, pp. 1 – 192.

Basson, I.J., (2007) Summary of Major Structural Features and Observations on Crenulation Zones in the Venetia Pit, Prepared For: Venetia Mine De Beers Consolidated Mines, Tect Consulting, pp. 1 – 62.

Basson, I.J., (2011a) The Delineation of 3D Structural Volumes and Dominant Discontinuities at Venetia Mine as an Aid to Geotechnical Design and Finite Element Modelling, Report Prepared For: Venetia Mine De Beers Consolidated Mines, Tect Consulting, pp. 1 – 28.

Basson, I.J, (2011b) Main Deformation Events, Informal Communications, Prepared For: Venetia Mine De Beers Consolidated Mines, Tect Consulting, p. 1.

Basson, I.J, (2011c) Summary of S2 Foliation Data within 3D Structural Volumes as an Aid to Geotechnical Design and Finite Element Modelling, Report Prepared For: Venetia Mine De Beers Consolidated Mines, Tect Consulting, July 2011, pp. 1 – 28.

Bieniawski, Z.T., (1973) Engineering classification of jointed rock masses. Trans South African Institute of Civil Engineering 15(12), pp. 335–344.

Bieniawski, Z.T., (1974) Geomechanics classification of rock masses and its application in tunnelling. In Proceedings of 3rd Congress of International Society of Rock Mechanics, Denver, vol. 2A, National Academy of Sciences, Washington DC, pp. 27–32.

Bieniawski, Z.T., (1976) Rock mass classification in rock engineering. In Exploration for Rock Engineering (ed. ZT Bieniawski), volume 1, Balkema, Cape Town, pp. 97–106.

Bieniawski, Z.T., (1989) Engineering Rock Mass Classifications. John Wiley and Sons, New York.

Brady, B.H.G. and Brown, E.T., (2004) Rock Mechanics for Underground Mining, 3rd edition, Kluwer, Dordrecht.

Brandl, G., (2000) Sheet 2228 Alldays, Geological Series, S. Afr. Counc. Geoscience 1:250 000 scale.

Brown, E.T. (ed.), (1981) Rock Characterization, Testing and Monitoring. ISRM Suggested Methods, Pergamon Press, Oxford.

Cabrera A, Gómez P., Lorig L., (2011) Three-dimensional Stability Analysis of the K2 and K3 Open Pits at Venetia Mine, Project ISA-556/002 Rev.1, May.

Cai, M., (2009) A simple method to estimate tensile strength and Hoek-Brown strength parameter m_i of brittle rocks, Proceedings of the 3rd CANUS Rock Mechanics Symposium, Toronto, May.

Chiwaye, H.T. and Stacey T.R., (2010) A comparison of limit equilibrium and numerical modelling approaches to risk analysis for open pit mining, The Journal of The Southern African Institute of Mining and Metallurgy, Volume 110, pp. 571-580.

Contreras, L., (2008) Venetia Open Pit Slope Design Cut 4 and 5, Report to De Beers Consolidated Mines Ltd, No. 173849, SRK Consulting, June.

Contreras, L., (2010) Venetia Mine – Bench Height Study – Geotechnical Risk, SRK Consulting, Report No 173849, July.

Curran, J., (2007) Rocscience Training Course Notes, Johannesburg, South Africa.

Dight, P.M., (2006) Pit wall failures on ‘unknown’ structures, The Journal of The South African Institute of Mining and Metallurgy, Volume 106, July, pp. 451 – 458.

DIPS™ 5.0, Rocscience Inc., (1998) Dips Version 5.0 - Graphical and Statistical Analysis of Orientation Data, www.rocscience.com, Toronto, Ontario, Canada.

Doorgapershad, A., Barnett, M., Twiggs, C., Martin, J., Millonig, L., Zenglein, R., Klemd, R., Barnett, W.P., Barton, J.M., (2003) Procedures used to produce a digitized geological mapping database of the area around the Venetia kimberlite pipes, Limpopo Belt, South Africa. South African Journal of Geology 106 (2/3), pp. 103–108.

Duncan, J.M. and Wright S.G., (2005) Soil Strength and Slope Stability. John Wiley and Sons, New Jersey.

Ekkerd, J.N., Ruest, M.R., Rankhododo, N.R. (2011) De Beers Cut 4 Optimisation, Slope Stability 2011, Vancouver, Canada.

Ekkerd, J.N., (2010) Venetia Mine Code of Practice to Combat Rock Falls, De Beers Internal Report.

Elam, R.A., Teaster, E.C and Lawless Jnr, M.J., (1999) Haul Road Inspection Handbook, MSHA Handbook Series, Handbook Number PH99-I-4, U. S. Department of Labor.

Field, M., Stiefenhofer, J., Robey, J. and Kurszlaukis, S., (2008) Kimberlite-hosted diamond deposits of southern Africa: A review, Ore Geology Reviews 34, pp. 33–75.

FLAC 7.0., (2011) Fast Lagrangian Analysis of Continua, Itasca Consulting Group, Minneapolis, USA.

Franklin, J.A. and Dusseault, M.B., (1989) Rock Engineering.McGraw-Hill, New York.

Franklin, J.A. and Senior, S.A., (1997) The Ontario rockfall hazard rating system. In: Conference on Engineering Geology Environment, Athens, 1997. pp. 647–56.

Gallagher, M.S. and Kear, R.M., (2001) Split shell open pit design concept applied at De Beers Venetia Mine South Africa using the Whittle and GEMCOM software. Journal of the South African Institute of Mining and Metallurgy, 101, pp. 401 – 408.

GEMS™, (2011) Gemcom Enterprise Management System, www.gemcomsoftware.com

Gibson, W.H., de Bruyn, I.A., Walker D.J.H., (2006) Considerations in the optimisation of bench face angle and berm width geometries for open pit mines, Stability of rock slopes in open pit mining and civil engineering situations, The South African Institute Of Mining And Metallurgy Symposium Series S44, pp. 557–578.

Gomez, P., (2010) Two dimensional Slope Stability Assessment for SW Quadrant at Venetia Mine, Itasca S.A, January.

Goodman, R. E. and Bray, J., (1976) Toppling of rock slopes. ASCE, Proc. Specialty Conf. on Rock Eng. for Foundations and Slopes, Boulder, CO, 2, pp. 201–234.

Goodman, R.E., (1989) Introduction to Rock Mechanics, 2nd edn, Wiley, New York.

Google Maps (2011) http://maps.google.co.za, Google Inc., USA.

Grasselli, G. and Egger P., (2003) Constitutive law for the shear strength of rock joints based on three-dimensional surface parameters, International Journal of Rock Mechanics and Mining Sciences 40 (2003), pp. 25–40.

Grobler, H.P., (2008) De Beers SIROVISION ™ Training Course, Internal report

GROUNDPROBE™ (2011) Groundprobe Slope Stability Radar, www.groundprobe.com.

Haines, A. and Terbrugge, P.J., (1991) Preliminary estimate ofrock slope stability using rock mass classification systems. In 7th Congress of International Society of Rock Mechanics, Aachen, Germany, pp. 887–892.

Haverland, M.L. and Slebir, E.J. (1972) Methods of performing and interpreting in situ shear tests. In Stability of Rock Slopes. Proceedings of 13th US Symposium on Rock Mechanics (ed. EJ Cording), Urbana, Illinois, ASCE, New York pp. 107–137.

Hencher, S.R. and Richards, L.R., (1982) The basic frictional resistance of sheeting joints in Hong Kong granite. Hong Kong Engineer 11(2), pp. 21–25.

Hencher, S.R. and Richards, L.R., (1989) Laboratory direct shear testing of rock discontinuities. Ground Engineering, March, pp. 24–31.

Hoek, E. and Brown, E.T., (1980a) Underground Excavations in Rock, IMM, London.

Hoek, E. and Brown, E.T., (1980b) Empirical strength criterion for rock masses. Journal of Geotechnical Engineering Div.

Hoek, E. and Bray, J., (1981) Rock Slope Engineering, 3rd edition, Inst. Mining and Metallurgy, London, UK.

Hoek, E. and Kaiser, P.K. and Bawden, W.F., (1995) Support of Underground Excavations in Hard Rock. Balkema, Rotterdam.

Hoek, E., Read J., Karzulovic, A., Chen, Z., (2000) Rock Slopes in Civil and Mining Engineering, International Conference on Geotechnical and Geological Engineering, GeoEng2000, 19-24 November, 2000, Melbourne.

Hoek, E. and Karzulovic, A., (2000) Rock mass properties for surface mines, Published in Slope Stability in Surface Mining, (Edited by W.A. Hustralid, M.K. McCarter and D.J.A. van Zyl), Littleton, Colorado: Society for Mining, Metallurgical and Exploration (SME), pp. 59–70.

Hoek, E., (2002) Practical Rock Engineering, www.rocsience.com.

Hoek, E., Carranza-Torres, C. and Corkun, B., (2002) Hoek-Brown failure criterion, 2002 edn. In Mining and Tunnelling Innovation and Opportunity. Proceedings of 5th North American Rock Mechanics Symposium and 17th Tunnelling Association of Canada Conference (eds R Hammah,W Bawden, J Curran and M Telesnicki), Toronto, vol. 1, University of Toronto Press, Toronto, pp. 267–273.

Hoek, E. and Diederichs, M.S., (2006) Empirical estimation of rock mass modulus, International Journal of Rock Mechanics and Mining Sciences 43, pp. 203–215.

Hoek, E., (2009) Fundamentals of slope design. Keynote address at Slope Stability 2009, Santiago, Chile, 9 – 11 November.

Itasca, (2011) www.itascacg.com, Itasca Consulting Group, Minneapolis, USA

Jaeger, J. C., (1960) Shear fracture of anisotropic rocks. Geol. Mag., 97, pp. 65–72.

Jennings, J.E, (1972) An approach to the stability of rock slopes based on the theory of limiting equilibrium with a material exhibiting anisotropic shear strength, Stability of Rock Slopes. Proceedings of 13th US Symposium on Rock Mechanics (ed. EJ Cording), Urbana, Illinois, ASCE, New York, pp. 269–302.

Karzulovic, A., (2006) Fundamentals of Geomechanics (in Spanish), lecture notes. Universidad de los Andes.

Karzulovic, A., Read, J., (2009) Guidelines for Open Pit Slope Design. Chapter 5: Acceptance Criteria, CSIRO Publishing, Collingwood, pp. 83–140.

Kear, R.M., (2010) Personal Communication with the author.

Laubscher, D.H., (1977) Geomechanics classification of jointed rock masses – mining applications. Transactions of Institute of Mining and Metallurgy, Section A: Mining.

Laubscher, D.H., (1990) A geomechanics classification system for the rating of rock mass in mine design. Journal of South African Institute of Mining and Metallurgy 90(10), pp. 279–293.

Laubscher, D.H., (1993) Planning mass mining operations, Comprehensive Rock Engineering: Principles, Practice and Projects, ed J Hudson, Pergamon Press, Vol 2, pp. 547-583.

LEICA GEOMOS™, (2011) Leica GeoMos, www.geosystemsafrica.com.

Lilly, P.A., (1986) An Empirical Method of Assessing Rock Mass Blastability, Alrge Open Pit Mining Conference.

Lilly, P.A., (1992) The use of the blastability index in the design of blasts for open pit mines. Proceedings of the Western Australian Conference on Mining Geomechanics, Curtin University of Technology, pp. 421–4 26.

Liu, H., Kaya, B.S. and Sterrett, R., (2011) Model Update and Comparison of Simulated Pore Pressure Between the 2010 Model and the Current Model, Technical Memorandum - 1769/10-02, Itasca Denver, USA, August.

Lorig, L., Stacey, P. and Read, J., (2009) Guidelines for Open Pit Slope Design. CSIRO Publishing, Collingwood, Chapter 10, pp. 235–260.

Lorig, L., (2011) Solving today's slope stability problems using tomorrow's technology, FLAC/DEM Symposium, 14 February.

Marinos, V., Marinos. P. and Hoek, E., (2005) The geological strength index: applications and limitations, Bull Eng Geol Environ, 64: 55–65 DOI 10.1007/s10064-004-0270-5.

Mompati, T., (2009) Venetia Mine Ramp Design Philosophy, De Beers Internal Document.

Ngoro, W., (2009) Final Limit Blasting and Cleaning Quality Control Assessment, Fourth Year Project at Wits University.

Orpen, J., (2007) Analysis of Venetia Drill Hole Data (38 Boreholes), Ground Modelling Technologies, Electronic Dataset.

Orpen, J., (2011) https://www.groundmodellingtechnologies.com.

Patton, F.D., (1966) Multiple modes of shear failure in rock, Proceedings of 1st Congress of International Society of Rock Mechanics, Lisbon, 1, pp. 509–513.

PHASE2™ 7.0, Rocscience Inc., (2008) Phase2 Version 7.0 - Finite Element Analysis for Excavations and Slopes, www.rocscience.com, Toronto, Ontario, Canada.

PFISA™, (2011) Planar Failure Itasca S.A., Itasca Consulting Group, Minneapolis, USA.

Phillips, D., Kiviets, G.B., Barton, E.S., Smith, C.B., Viljoen, K.S. and Fourie, L.F., (1999) $^{0}Ar/^{39}Ar$ dating of kimberlites and related rocks: problems and solution.

Pierson, L.A., Davis, S.A. and van Vickle, R., (1990) Rockfall Hazard Rating System implementation manual. Federal Highway Administration report FHWA-OR-EG-90-01, US Department of Transportation.

Rankhododo, N.R. and Ekkerd, J.N., (2009) Quantification and Communication of Rock Fall Risk at Venetia Mine, Internal Report

Read, J,.Jakubec, J. and Beale, G., (2009) Field data collection in Guidelines for Open Pit Slope Design. CSIRO Publishing, Collingwood, pp. 15 – 52.

Read, J., Stacey, P., (2009) Guidelines for Open Pit Slope Design. CSIRO Publishing, Collingwood.

Rigby, M.J., Mouri, H. and Brandl, G., (2008) A review of the P–T–t evolution of the Limpopo Belt: constraints for a tectonic model. Journal of African Earth Sciences 50, pp. 120–132.

Rigby, M.J., Basson I.J., Kramers, J.D., Gräser, P. and Mavimbela, P.K., (2011) The structural, metamorphic and temporal evolution of the country rocks surrounding Venetia Mine, Limpopo Belt, South Africa: Evidence for a single palaeoproterozoic tectono-metamorphic event with implications for a tectonic model, Precambrian Research 186, pp. 51–69.

ROCDATA™ 4.0, Rocscience Inc., (2005), RocData Version 4.0 - Rock, Soil and Discontinuity Strength Analysis, www.rocscience.com, Toronto, Ontario, Canada.

ROCPLANE™ 2.0, Rocscience Inc., (2001), RocPlane Version 2.0 - Planar Sliding Stability Analysis for Rock Slopes, www.rocscience.com, Toronto, Ontario, Canada.

Romero, S.U., (1968) In situ direct shear tests on irregular surface joints filled with clayey material. In Proceedings of ISRM International Symposium of Rock Mechanics, Madrid, 1, pp. 189–194.

Ryan, T.M. and Prior, P.R, (2000) Designing Catch Benches and Inter-ramp Slopes, Slope Stability in Surface Mining, SME, pp. 27 – 46.

Senior, S.A., (2003) Ontario Rockfall Hazard Rating System. Field procedures manual. Report draft, Materials Engineering and Research Office, Ont., pp. 36.

Shchipansky, A. and Atkinson, L., (2010) Pore Pressures in North Highwall of Venetia Mine Predicted by Groundwater Flow Model Calibrated to Multi-Level Piezometer Data, Technical Memorandum, Itasca Denver, USA, July.

Simmons, J.V. and Simpson, P.J., (2006) Composite failure mechanisms in coal measures' rock masses—myths and reality, The Journal of The South African Institute of Mining and Metallurgy, Volume 106, July, pp. 459 – 469.

Simons N., Menzies, B. and Matthews, M., (2001) A Short Course in Soil and Rock Slope Engineering, Tomas Telford, London.

SIROVISION™, (2011) CAE Mining, www.sirovision.com.

Sjoberg, J., (1996) Large Scale Slope Stability in Open Pit Mining – A review, issn 0349 – 3571.

Sjoberg, J., (2000) Failure Mechanisms for High Slopes in Hard Rock, Slope Stability in Surface Mining, SME, pp. 71 – 80.

Skinner, E.M.W. and Clement, C.R., (1979) Mineralogical classification of southern African kimberlites. Second International Kimberlite Conference, Santa Fe. American Geophysical Union, p. 129–139.

SLIDE 6.0, Rocscience Inc., (2010) SLIDE Version 6.0 - 2D Limit Equilibrium Slope Stability Analysis, www.rocscience.com, Toronto, Ontario, Canada.

Stacey, P., (2010) Personal Communication with the author during site visit and design review.

Stacey, T.R., (2001) Best practice rock engineering handbook for "other" mines, Safety in Mines Research Advisory Committee, OTH 602.

Stead, D., Eberhardt, E., Coggan, J., Benko, B. (2001) Advanced Numerical Techniques In Rock Slope Stability Analysis - Applications And Limitations Landslides – Causes, Impacts and Countermeasures.

Stead, D., Eberhardt E., Coggan J.S. (2006) Developments in the characterization of complex rock slope deformation and failure using numerical modelling techniques, Engineering Geology 83, pp. 217– 235.

Steffen, O., Terbrugge P.J., (2009) Venetia Bench Height Study – Site Visit Feedback Letter, SRK Consulting, 12 October

STEREOCORE™, (2011) https://www.groundmodellingtechnologies.com.

Strouth, A., (2009) Bench-Scale and Inter-Ramp Configuration Analysis for Venetia Southwest Design Sectors. Itasca S.A. Report to DeBeers Consolidated Mines. December.

SWEDGE™ 5.0, Rocscience Inc. (2006) Swedge Version 5.0 - 3D Surface Wedge Analysis for Slopes. ww.rocscience.com, Toronto, Ontario, Canada.

SWISA™, (2011) A Kinematic Wedge Analysis Tool, Itasca Consulting Group, Minneapolis, USA

Tait, M.A., (2007) Update to the three dimensional geological model of the K01 and K02 kimberlite pipes: Venetia kimberlite cluster, Limpopo, RSA, De Beers Internal Report.

Taljaardt J., (2010) Blast Design Parameters for Venetia Mine, Table received via email. De Beers Internal Document.

Tapia, A., Contreras, L.F., Jefferies, M.G. and Steffen, O., (2007) Risk evaluation of slope failure at Chuquicamata Mine. Proc. Int. Symp. Rock Slope Stability in Open Pit Mining and Civil Engineering, Perth, Australian Centre for Geomechanics, ISBN 978 0 9756756 8 7, pp. 477–485.

Terbrugge, P., (2000) Determination of Slope Angles for the Northern Slopes of Cut 3. Report for De Beers Consolidated Mines Limited - Venetia Open Pit Diamond Mine, Report No. 173849/2, April

Terbrugge, P., Harvey F., Venter J. and Mulville D. (2004) Geotechnical Evaluation and Slope Design for the 200 m Pit Feasibility and 400 m Pit Pre-Feasibility Study, Voorspoed Mine, Nov.

Terbrugge, P.J., Steffen O.K.H., Wesseloo, J. and Venter, J., (2006) A risk consequence approach to open pit slope design. In Proceedings of International Symposium on Stability of Rock Slopes in Open Pit Mining and Civil Engineering,Cape Town, South African Institute of Mining, p. 81–96.

Terzaghi, K., (1946) Rock defects and loads on tunnel support, In Rock Tunnelling with Steel Supports (eds RV Proctor and T White), Commercial Shearing, Youngstown, Ohio, pp. 15–99.

Terzaghi, K., (1962) Stability of steep slopes on hard unweathered rock, Ge´otechnique 12, pp. 251–270.

Tsheko, P., (2010) Venetia Mine Code of Practice to Combat Rock Falls and Slope Instability Training Module, Internal Document.

Wesseloo, J. and Read, J., (2009) Guidelines for Open Pit Slope Design. Chapter 9: Acceptance Criteria, CSIRO Publishing, Collingwood, pp. 219–234.

Wikipedia, (2011), The definition of Nappe and Terranes, www.wikipedia.com.

Williams, P., Floyd J., Chitombo G. and Maton, T., (2009) Design implementation, Guidelines for Open Pit Slope Design. CSIRO Publishing, Collingwood, Chapter 11, pp 261–324.

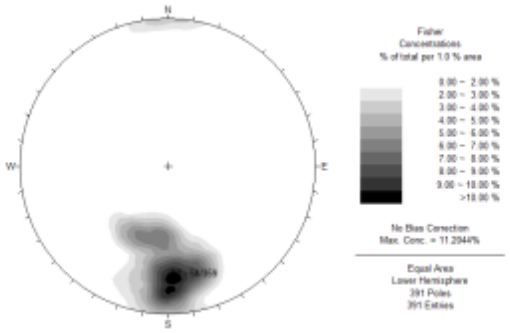
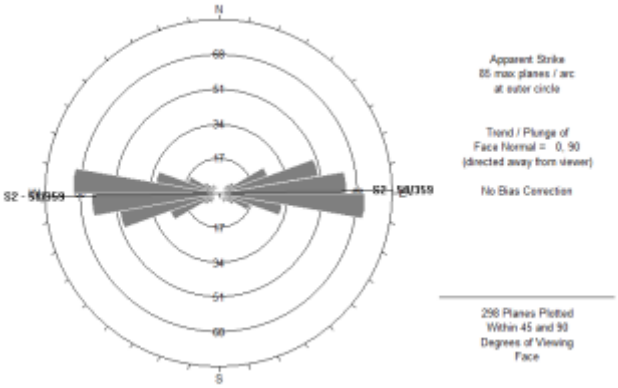
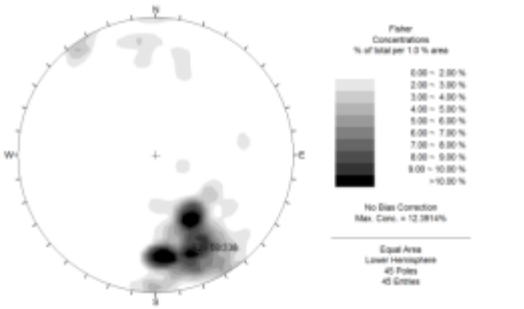
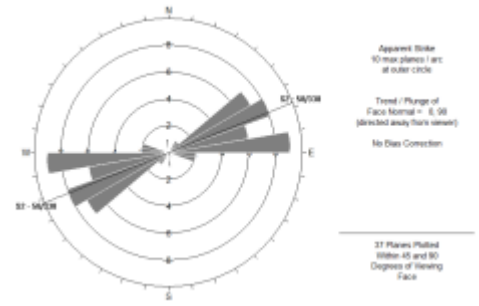
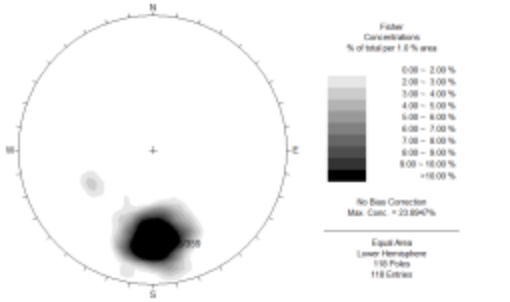
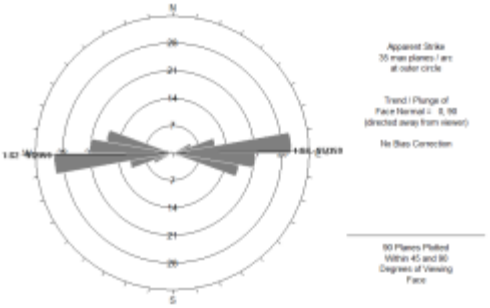
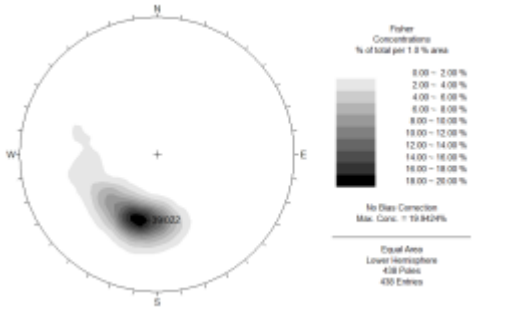
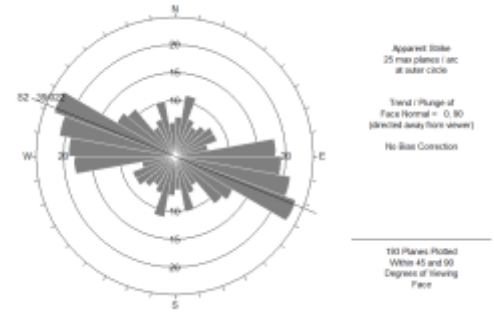
Wittke, W., (1990) Rock Mechanics. Theory and Applications with Case Histories. Springer-Verlag, Berlin.

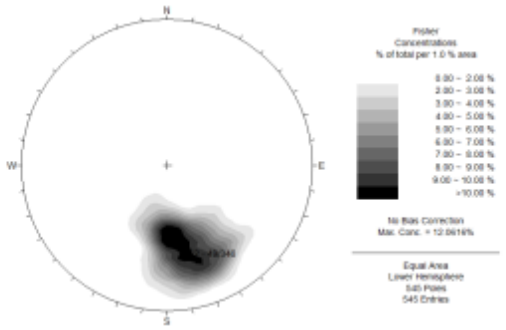
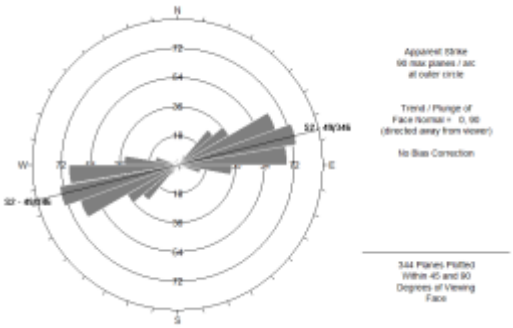
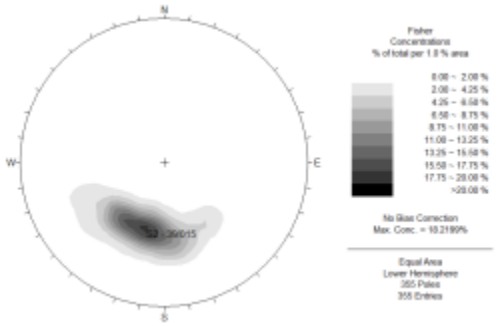
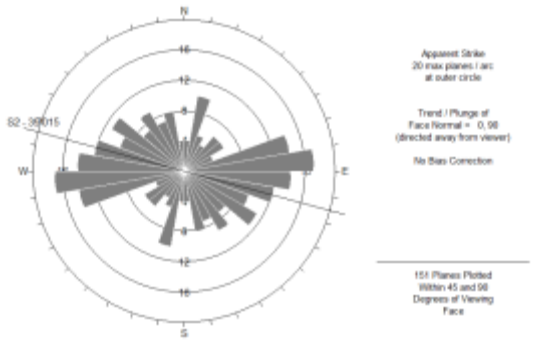
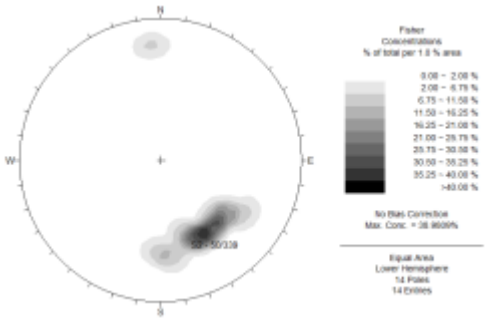
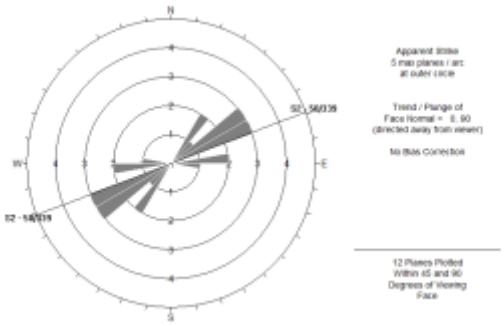
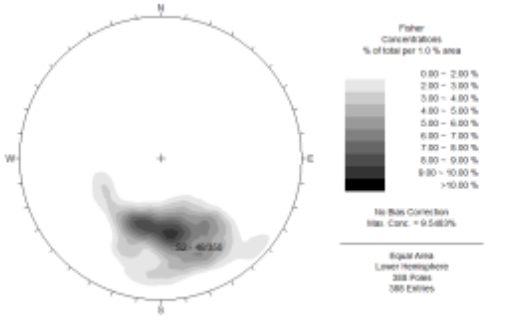
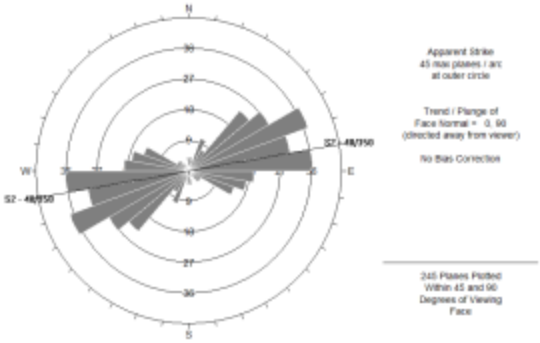
Wyllie, D.C. and Mah C.W., (2005) Rock Slope Engineering, Civil and Mining, 4th edition. Spon Press, London.

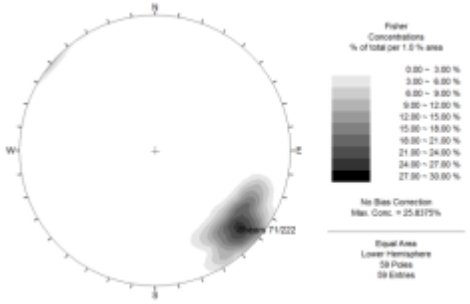
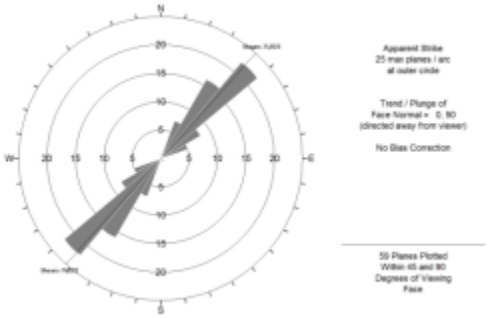
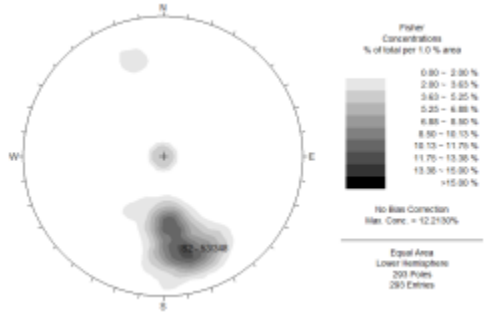
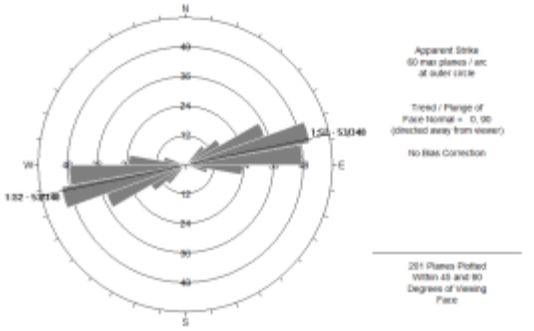
Wyllie, D.C., and Norrish N.I., (1996) Rock strength properties and their measurement. In Landslides Investigation and Mitigation, Special Report 247 (eds AK Turner and R Schuster), pp. 372–390. Transportation Research Board, NRC, National Academy Press, Washington DC.

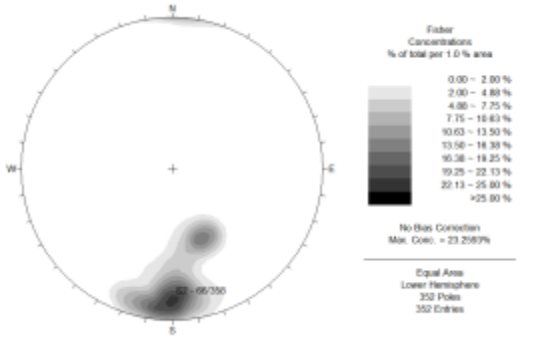
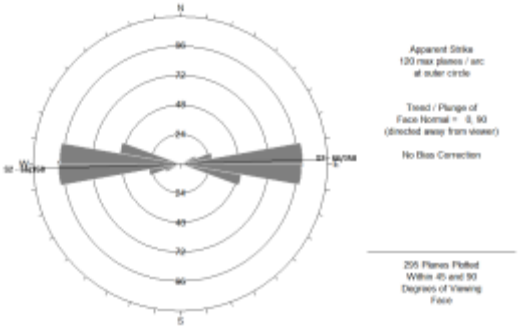
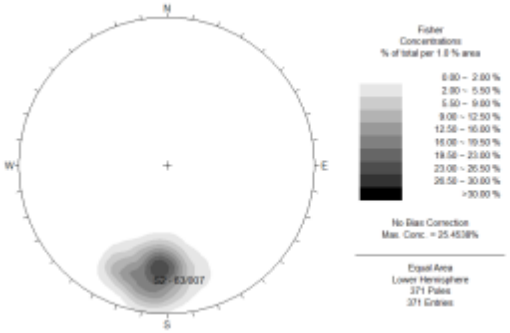
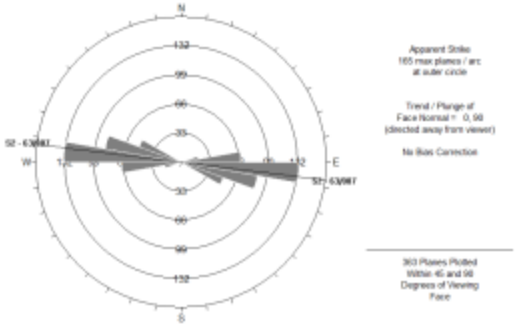
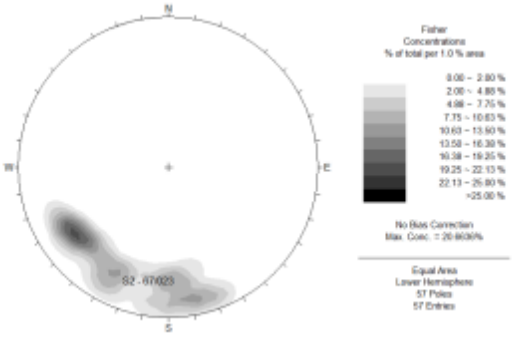
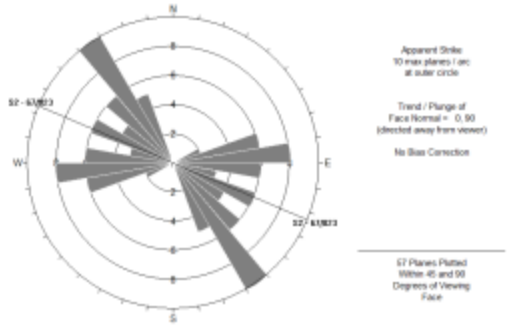
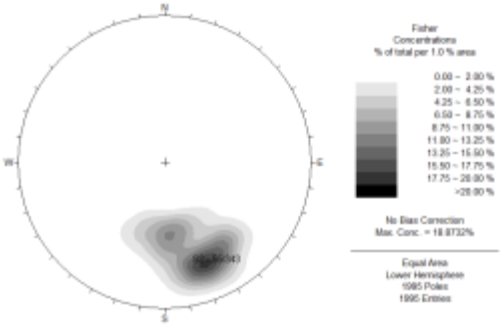
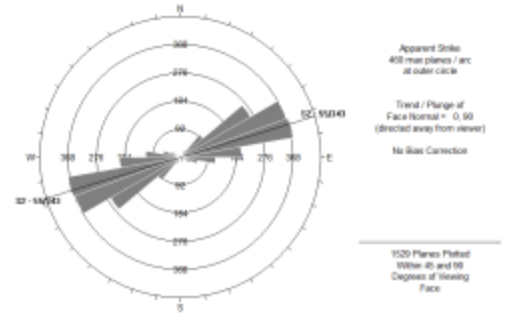
Wyllie, D.C., (1992) Foundations on Rock. E and FN Spon, London.

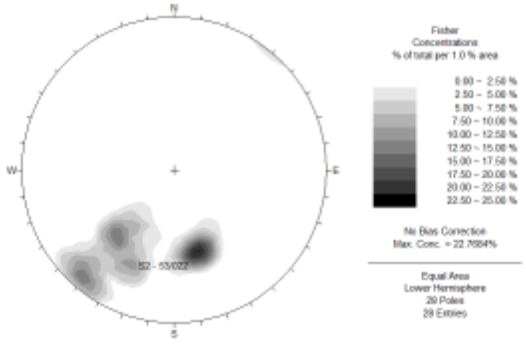
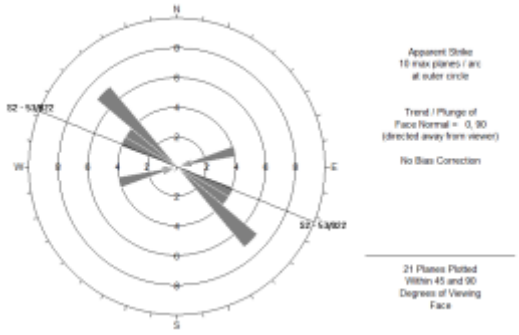
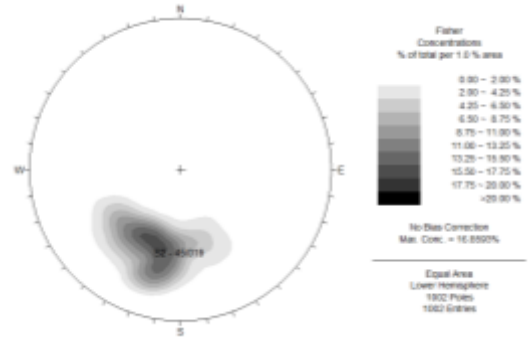
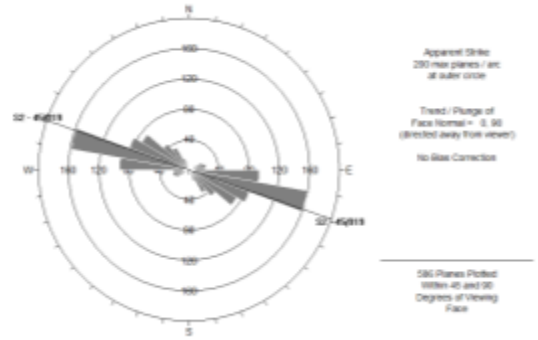
Appendix A: Stereographic projections of data constructed by author

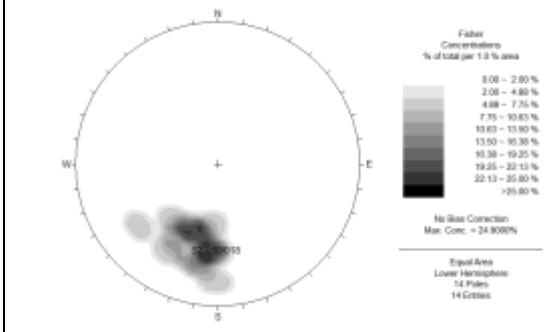
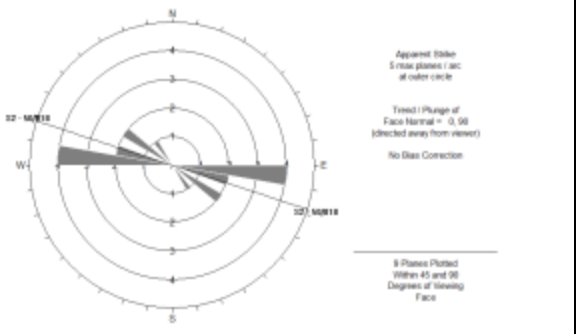
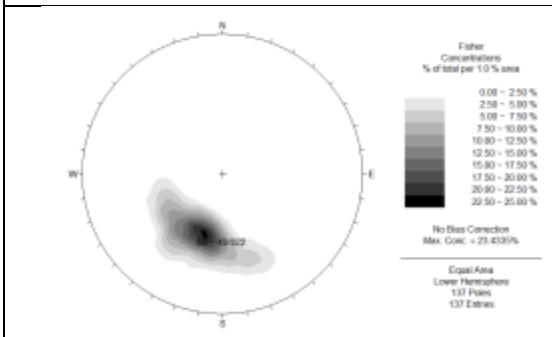
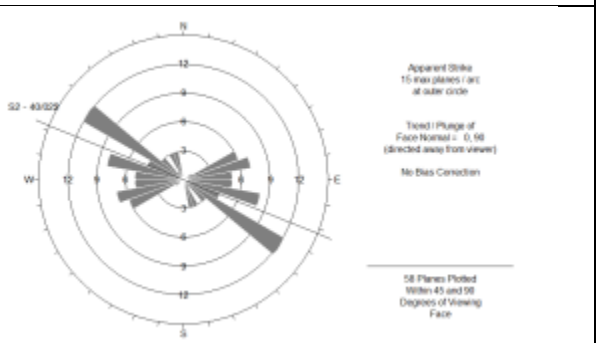
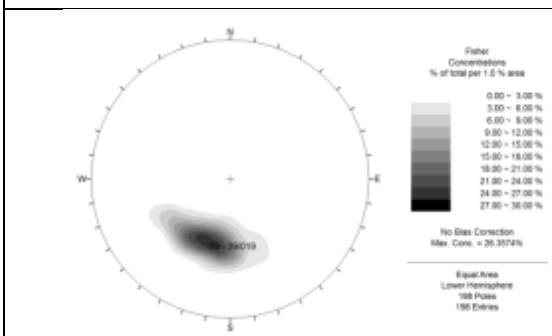
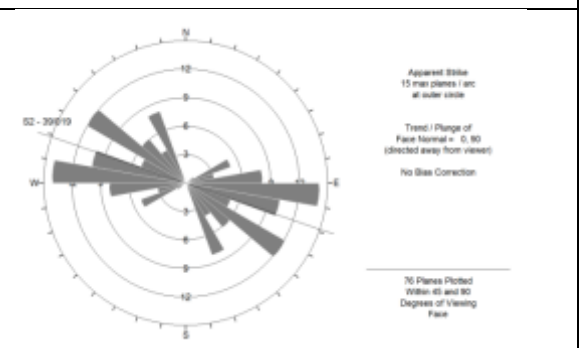
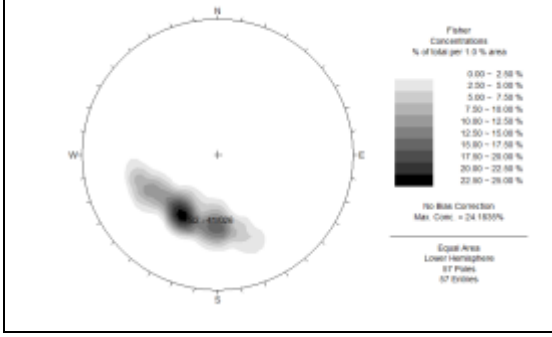
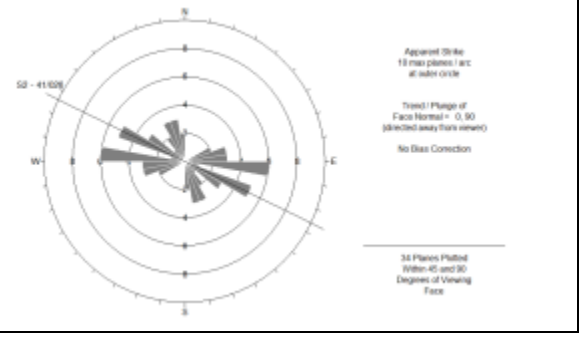
Ian Basson Face Mapping Data: S2 Foliation	
Structural Volume 1: 58°/359°	
	
Structural Volume 2: 58°/338°	
	
Structural Volume 3: 55°/359°	
	
Structural Volume 4: 39°/022°	
	

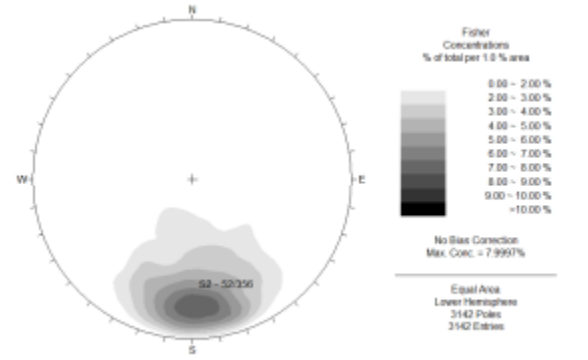
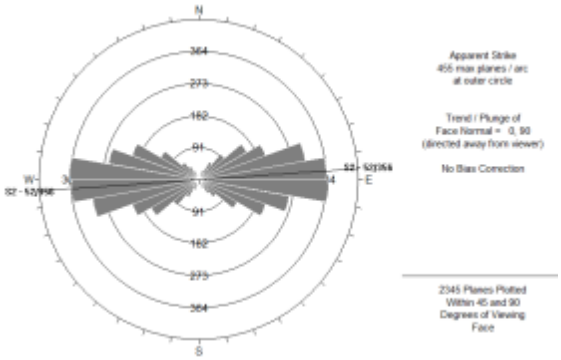
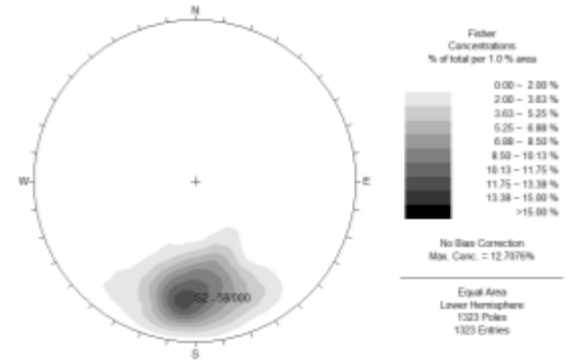
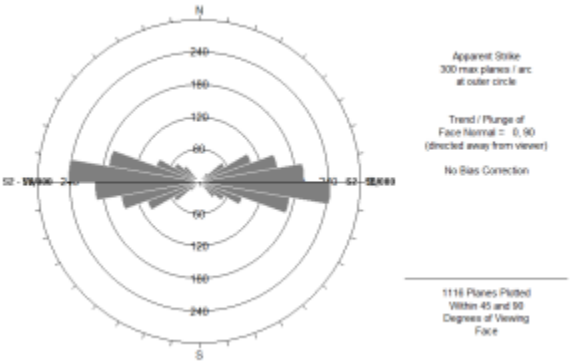
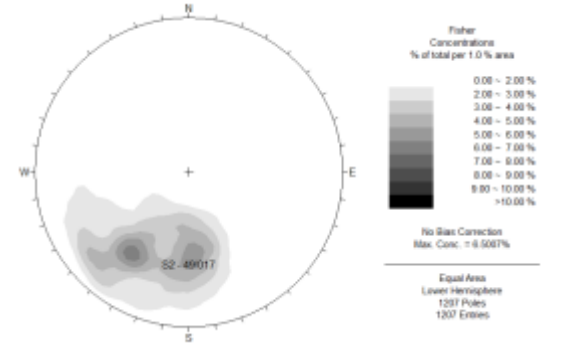
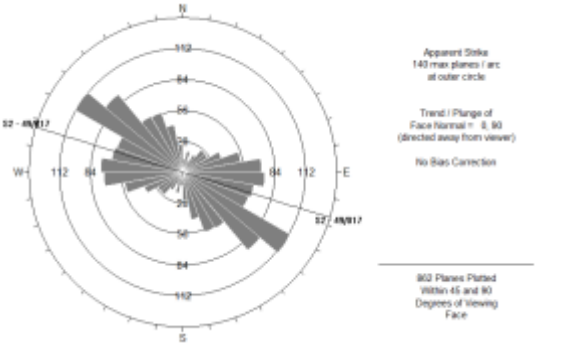
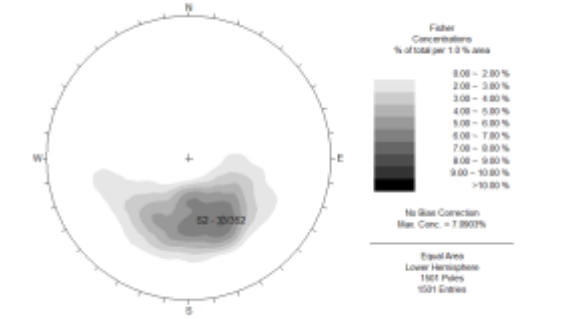
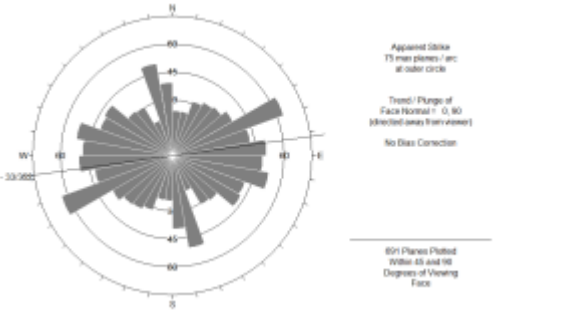
Structural Volume 5: 49°/346°	
	
Structural Volume 6: 39°/015°	
	
Structural Volume 7: 50°/339°	
	
Structural Volume 8: 48°/350°	
	

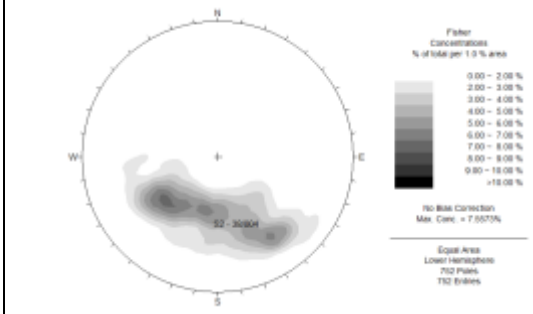
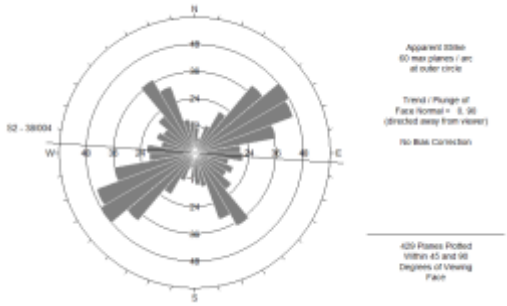
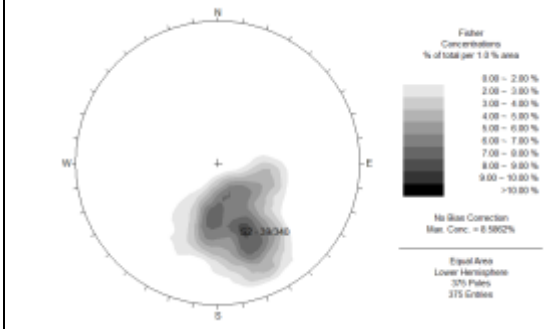
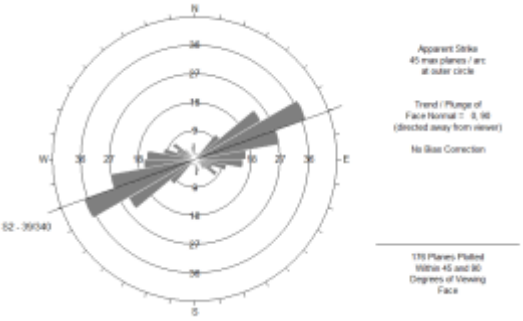
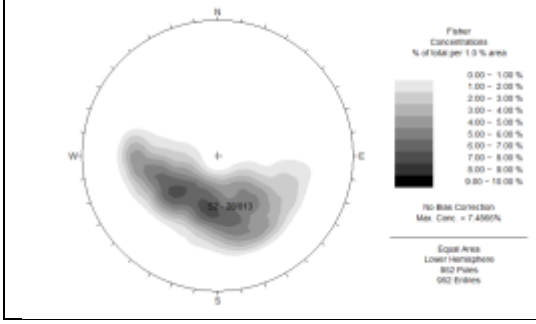
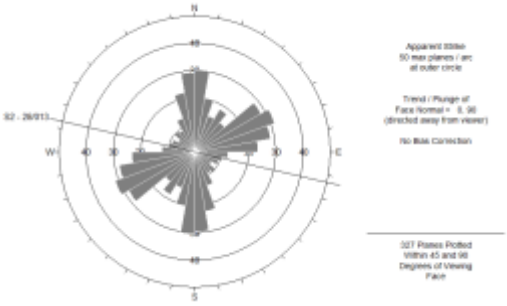
Structural Volume 8 Shears: 71°/222°	
	
Structural Volume 9: 53°/348°	
	

Venetia Mine SIROVISION Data: S2 Foliation	
Structural Volume 1: 66°/358°	
	
Structural Volume 3: 63°/007°	
	
Structural Volume 4: 67°/023°	
	
Structural Volume 5: 55°/343°	
	

Structural Volume 6: 53°/022°	
	
Structural Volume 8: 45°/019°	
	

Venetia Mine Scan Line Data: S2 Foliation	
Structural Volume 1: 50°/018°	
	
Structural Volume 4: 40°/022°	
	
Structural Volume 6: 39°/019°	
	
Structural Volume 8: 41°/026°	
	

John Orpen STEREOCORE Borehole Data: S2 Foliation	
Structural Volume 1: 52°/356°	
	
Structural Volume 3: 58°/000°	
	
Structural Volume 4: 49°/017°	
	
Structural Volume 5: 33°/353°	
	

Structural Volume 6: 38°/004°	
	
Structural Volume 7: 39°/340°	
	
Structural Volume 8: 28°/013°	
	

Appendix B: Data Compact Disc

Appendix C: SWISA™ Bench Analysis

Tier 2 Domain	Orientation with Wedge Set	Average of % Prob. Kinematically Valid Wedge (PK)	Average of % Prob. Sliding (PS)	Average of % Prob. Failure (PF = PK x PS)	Average of FOS	Stack Angle at 25% PoF
STRV1						
	125					
	J4-FOL	4.50	0.00	0.00	4.38	
	134					
	J4-FOL	4.50	0.00	0.00	4.38	
	162					
	J2-J4	99.86	100.00	99.86	0.36	67
	J4-FOL	0.07	0.00	0.00	44.95	
	180					
	J2-J4	91.62	100.00	91.62	0.36	65
	229					
	J2-J4	3.68	100.00	3.68	0.16	
	J4-FOL	5.85	20.34	1.19	0.29	
	258					
	J4-FOL	95.49	2.75	2.63	3.51	
	270					
	J4-FOL	95.50	2.75	2.63	3.51	
	90					
	J2-FOL	63.83	57.34	36.60	1.13	65
	J2-J4	8.38	100.00	8.38	0.09	
	J4-FOL	4.50	0.00	0.00	4.38	
STRV1 with the NW Brittle Overprint						
	125					
	J4-FOL	4.50	0.00	0.00	4.38	
	134					
	J4-FOL	4.50	0.00	0.00	4.38	
	162					
	J2-J4	99.86	100.00	99.86	0.36	65
	J2-J6	98.86	61.49	60.79	1.01	
	J4-FOL	0.07	0.00	0.00	44.95	
	J4-J6	0.01	100.00	0.01	0.77	
	180					
	J2-J4	91.62	100.00	91.62	0.36	66
	J2-J6	100.00	61.66	61.66	1.01	
	J4-J6	0.20	100.00	0.20	0.25	
	190					
	J2-J6	100.00	61.66	61.66	1.01	63
	229					
	J2-J4	3.68	100.00	3.68	0.16	
	J4-FOL	5.85	20.34	1.19	0.29	

	258					
	FOL-J6	86.00	9.85	8.47	1.77	
	J4-FOL	95.49	2.75	2.63	3.51	
	J4-J6	99.88	6.88	6.87	2.53	
	270					
	FOL-J6	99.67	8.58	8.55	1.77	
	J4-FOL	95.50	2.75	2.63	3.51	
	J4-J6	99.80	6.74	6.73	2.53	
	90					
	J2-FOL	63.83	57.34	36.60	1.13	63
	J2-J4	8.38	100.00	8.38	0.09	
	J4-FOL	4.50	0.00	0.00	4.38	
STRV2						
	237					
	J2-FOL	0.06	0.00	0.00	41.48	
	J2-J4	0.63	100.00	0.63	0.21	
	J4-FOL	59.11	29.74	17.58	1.60	
	258					
	J2-FOL	0.06	0.00	0.00	41.48	
	J4-FOL	100.00	22.12	22.12	1.60	
	270					
	J4-FOL	100.00	22.12	22.12	1.60	
STRV3						
	134					
	J4-FOL	8.06	0.00	0.00	4.48	
	162					
	J2-J4	99.83	100.00	99.83	0.33	67
	J4-FOL	0.15	0.00	0.00	32.43	
	180					
	J2-J4	91.63	100.00	91.63	0.33	67
	229					
	J2-J4	3.47	100.00	3.47	0.15	
	J4-FOL	0.88	0.00	0.00	1.13	
STRV4						
	90					
	J2-FOL	98.34	22.47	22.10	1.47	
	J2-J4	0.83	100.00	0.83	0.13	
	J4-FOL	22.47	0.00	0.00	1.44	
	43					
	J2-FOL	100.00	23.07	23.07	1.47	
	55					
	J2-FOL	100.00	21.83	21.83	1.47	
	65					
	J2-FOL	100.00	21.97	21.97	1.47	
	J4-FOL	1.55	0.65	0.01	0.96	
STRV5						

	4				
	J2-FOL	33.34	12.33	4.11	0.21
	13				
	J2-FOL	58.53	9.07	5.31	3.29
	258				
	J2-FOL	10.79	0.00	0.00	1.57
	J2-J4	11.51	91.48	10.53	0.05
	J4-FOL	97.34	7.18	6.99	2.59
	270				
	J2-FOL	10.17	0.00	0.00	1.57
	J2-J4	5.34	83.13	4.44	0.08
	J4-FOL	97.34	7.18	6.99	2.59
	308				
	J4-FOL	91.90	5.70	5.24	2.59
	322				
	J4-FOL	46.33	6.09	2.82	0.17
STRV6					
	36				
	J2-FOL	98.80	23.37	23.09	1.56
	43				
	J2-FOL	99.47	21.64	21.53	1.56
	65				
	J2-FOL	99.54	20.72	20.62	1.56
	J2-J4	0.06	83.33	0.05	0.37
	J4-FOL	4.49	0.00	0.00	1.65
	90				
	J2-FOL	91.51	20.51	18.77	1.56
	J2-J4	5.87	99.83	5.86	0.07
	J4-FOL	29.72	0.00	0.00	1.34
	54				
	J2-FOL	99.54	20.71	20.61	1.56
STRV7					
	270				
	J2-FOL	16.85	1.54	0.26	0.45
	J2-J4	5.52	87.49	4.83	0.07
	J4-FOL	85.96	13.97	12.01	2.64
	308				
	J2-J4	0.01	100.00	0.01	0.07
	J4-FOL	81.44	13.64	11.11	2.64
	319				
	J4-FOL	61.00	11.97	7.30	2.64
	4				
	J2-FOL	33.79	13.50	4.56	0.20
STRV8 GP					
	258				
	J2-FOL	0.05	0.00	0.00	41.84

	J2-J4	22.80	86.67	19.76	0.04	
	J4-FOL	44.11	0.23	0.10	0.94	
	332					
	J2-J4	0.01	100.00	0.01	0.04	
	J4-FOL	26.94	0.48	0.13	0.57	
	353					
	J4-FOL	1.56	3.21	0.05	0.55	
	358					
	J4-FOL	0.17	5.88	0.01	0.80	
STRV8 MP						
	345					
	J4-FOL	7.41	2.16	0.16	0.30	
	358					
	J4-FOL	0.17	0.00	0.00	2.79	
	43					
	J2-FOL	99.41	35.18	34.97	1.29	41
	J2-J4	0.07	71.43	0.05	0.27	
	J4-FOL	1.41	3.55	0.05	0.36	
	64					
	J2-FOL	99.90	34.88	34.85	1.29	53
	J2-J4	1.88	83.00	1.56	0.05	
	J4-FOL	27.88	1.47	0.41	92.44	
STRV9 (S5 with NW Brittle Over Print)						
	4					
	J2-FOL	33.34	12.33	4.11	0.21	
	13					
	J2-FOL	58.53	9.07	5.31	3.29	
	308					
	FOL-J6	92.76	22.69	21.05	1.32	
	J4-FOL	91.90	5.70	5.24	2.59	
	J4-J6	67.88	4.27	2.90	1.71	
	322					
	FOL-J6	72.26	15.87	11.47	1.32	
	J4-FOL	46.33	6.09	2.82	0.17	
	J4-J6	27.41	0.40	0.11	0.87	
	336					
	J4-J6	1.72	0.00	0.00	1.77	
	342					
	J4-J6	0.07	0.00	0.00	2.53	

Appendix D: PFISA™ Bench Analysis

Tier 2 Domain	Orientation with Wedge Set	Average of % Prob. Kinematically Valid Wedge (PK)	Average of % Prob. Sliding (PS)	Average of % Prob. Failure (PF = PK x PS)	Average of FOS	Stack Angle at 25% PoF	Stack Angle at 15% PoF
STRV4							
	43	45.41	72.21	32.79	0.42	60	54
	55	29.21	72.13	21.07	0.43		54
	65	16.35	71.93	11.76	0.43		
	90	0.49	61.22	0.30	0.51		
STRV5							
	4	47.68	96.06	45.80	0.09	61	58
	13	27.92	95.63	26.70	0.10	61	58
	258						
	270						
	308	18.81	95.59	17.98	0.10		58
	322	47.68	95.57	45.57	0.10	62	58
	336	73.13	95.84	70.09	0.51	62	58
	342	76.76	95.84	73.57	0.51	62	58
	353	69.45	95.94	66.63	0.52	62	58
STRV6							
	30	52.23	83.76	43.75	0.84	58	50
	36	45.41	84.23	38.25	0.40	58	50
	43	36.36	83.88	30.50	0.40	58	50
	54	21.05	83.94	17.67	0.41		52
	65	9.67	83.45	8.07	0.44		
	90						
STRV7							
	4	45.09	66.60	30.03	0.17	60	60
	270	5.03	65.81	3.31	0.16		
	308	31.33	67.44	21.13	0.16		56
	319	39.22	66.83	26.21	0.17	60	55
	340	46.48	66.46	30.89	0.81	60	54
	353	43.54	66.72	29.05	0.83	60	58
STRV8GP							
	5	54.52	87.05	47.46	0.75	60	57
	13	60.85	86.97	52.92	0.73	60	57
	30	57.40	86.92	49.89	0.74	60	57
	258						
	332	11.26	87.30	9.83	0.28		
	353	39.66	86.18	34.18	0.27	60	58
	358	48.25	86.47	41.72	0.27	60	58
STRV8MP							
	13	60.85	92.80	56.47	0.66	61	55
	30	57.41	93.14	53.47	0.67	60	55

	43	41.96	93.33	39.16	0.27	60	55
	64	13.20	92.35	12.19	0.28		
	345	26.94	92.95	25.04	0.25	61	55
	358	48.26	92.58	44.68	0.26	60	56
STRV9							
	4	47.68	96.06	45.80	0.09	61	58
	13	27.92	95.63	26.70	0.10	61	58
	258	10.88	99.91	10.87	0.29		
	308	18.81	95.59	17.98	0.10		58
	322	47.68	95.57	45.57	0.10	61	58
	336	73.13	95.84	70.09	0.51	61	58
	342	76.76	95.84	73.57	0.51	62	58
	353	69.45	95.94	66.63	0.52	62	58

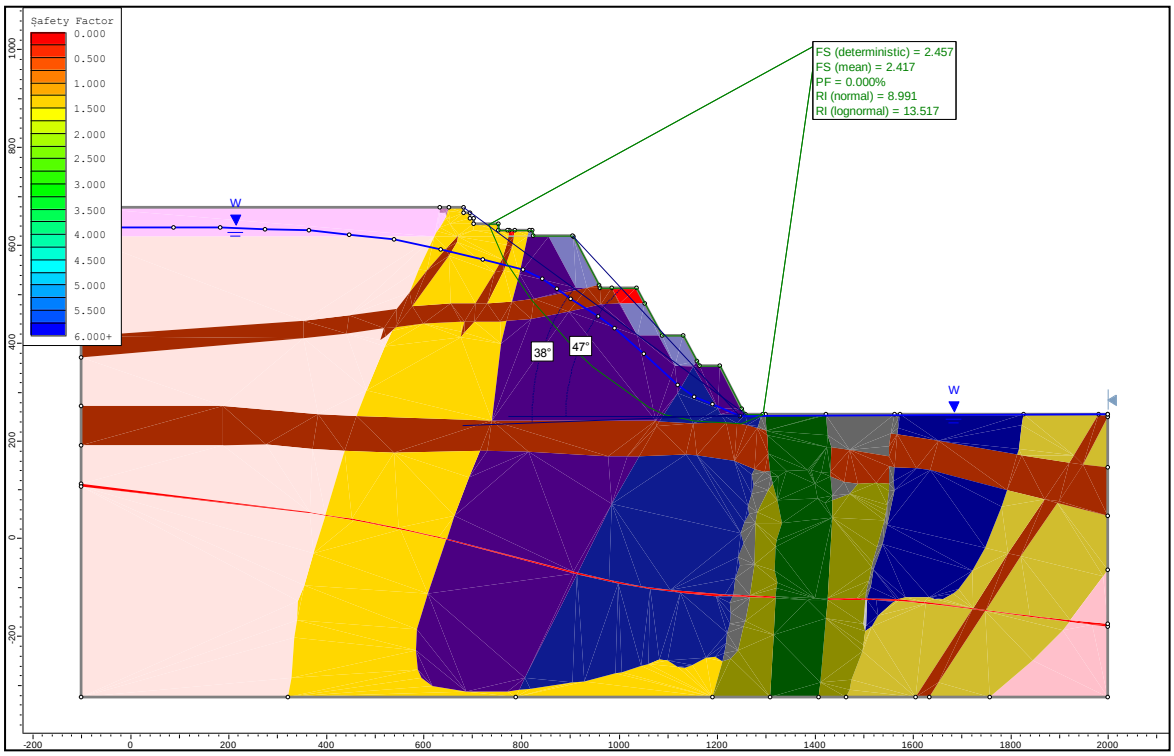
Appendix E: SLIDE™ Stack Analysis

Overall Slope Design Section	Tier 2/3 Domain	Stack Height (m)	Stack Angle (°)	FoS Det.	FoS mean	PoF (%)
N	STRV3 FRESH	120	57	2.583	2.475	0
	STRV3 FRESH	120	62	2.37	2.25	0.1
	STRV3 FRESH	120	67	1.98	2.00	0.1
	STRV3 WEATHERED	60	62	2.11	2.02	1.7
	STRV3 WEATHERED	120	62	1.36	1.32	17.3
	STRV1 FRESH	120	57	2.87	2.69	0.0
	STRV1 FRESH	120	62	2.52	2.51	0.0
	STRV1 FRESH	120	67	2.09	2.23	0.0
	STRV1 FRESH	150	62	2.31	2.33	0.0
	STRV1 FRESH	180	62	2.17	2.03	0.0
	STRV1 WEATHERED	60	62	2.39	3.69	0.0
	STRV1 WEATHERED	120	62	1.66	1.56	7.2
S	STRV5 FRESH	120	44	1.46	1.60	1.1
	STRV5 FRESH	120	49	1.20	1.36	4.5
	STRV5 FRESH	120	54	0.97	1.13	38.5
	STRV5 WEATHERED	60	49	1.34	1.43	2.2
	STRV5 WEATHERED	120	49	1.08	1.14	16.4
	STRV5 FRESH	150	47	1.20	1.31	6.74
	STRV5 FRESH	135	48	1.20	1.33	5.72
	STRV8 GP FRESH	120	40	1.46	1.57	0.4
	STRV8 GP FRESH	120	45	1.21	1.33	0.6
	STRV8 GP FRESH	120	50	1.05	1.14	10.8
	STRV8 GP WEATHERED	60	45	1.38	1.45	1.2
	STRV8 GP WEATHERED	120	45	1.135	1.17	6.9
	STRV8 GP FRESH	135	45	1.20	1.29	2.6
	STRV8 GP FRESH	150	44	1.22	1.31	2.3
SE	STRV5 FRESH	120	44	1.49	1.63	1.1
	STRV5 FRESH	120	49	1.20	1.36	5.5
	STRV5 FRESH	120	54	0.99	1.15	36.8
	STRV5 WEATHERED	60	49	1.35	1.44	22.0
	STRV5 WEATHERED	120	49	1.08	1.11	23.6
	STRV5 FRESH	135	48	1.20	1.34	6.2
	STRV5 FRESH	150	47	1.21	1.33	6.7
SSW	STRV8 MP FRESH	120	38	1.47	1.56	0.6
	STRV8 MP FRESH	120	43	1.20	1.30	4.3
	STRV8 MP FRESH	120	48	1.02	1.11	22.7
	STRV8 MP WEATHERED	60	46	1.20	1.25	5.3
	STRV8 MP WEATHERED	120	43	1.08	1.09	20.1
	STRV8 MP FRESH	150	42	1.20	1.27	5.4
	STRV8 MP FRESH	135	42.5	1.20	1.28	4.9
	STRV8 GP FRESH	120	50	1.06	1.14	13.6
	STRV8 GP FRESH	120	45	1.21	1.28	5.5

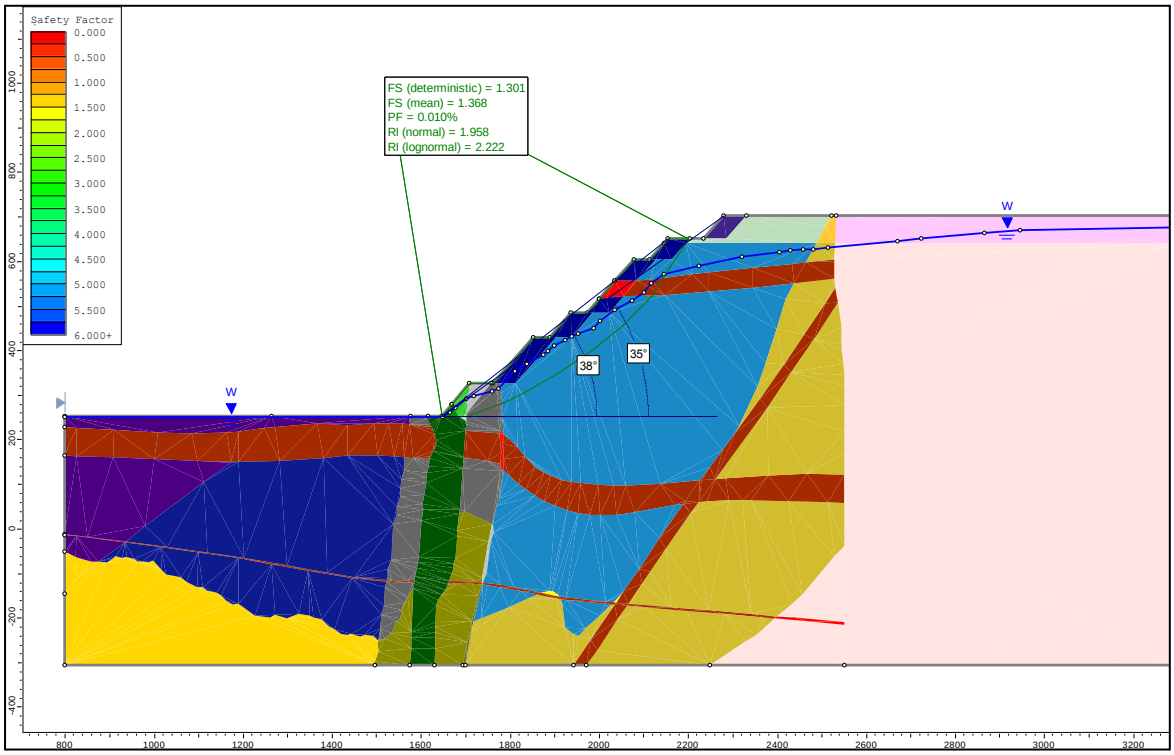
	STRV8 GP FRESH	120	40	1.476	1.58	0.7
	STRV8 GP WEATHERED	60	45	1.364	1.43	1.5
	STRV8 GP WEATHERED	120	45	1.12	1.13	16.9
	STRV8 GP FRESH	150	43	1.20	1.25	7.3
	STRV8 GP FRESH	135	44	1.20	1.27	6.4
WSW	STRV6 FRESH	120	53	1.36	1.37	3.0
	STRV6 FRESH	120	58	1.29	1.30	6.6
	STRV6 FRESH	120	63	1.27	1.23	13.7
	STRV6 FRESH	150	58	1.31	1.28	5.5
	STRV6 WEATHERED	60	58	1.23	1.15	7.7
	STRV6 WEATHERED	120	58	0.75	0.77	98.1
	STRV4 FRESH	120	47	1.27	1.30	3.7
	STRV4 FRESH	120	52	1.20	1.20	10.0
	STRV4 FRESH	120	58	1.13	1.13	22.6
	STRV4 FRESH	150	48	1.20	1.20	9.5
	STRV4 WEATHERED	60	58	1.347	1.373	3.67
	STRV4 WEATHERED	120	58	1.00	1.01	45.6
KIM	K01DVK D=1.3	60	56	2.78	2.64	0.9
	K01RVK	60	50	1.84	1.81	6.8
	K01RVK D=1.3	60	50	1.23	1.25	31.4
	K01MVK	60	50	2.61	2.63	0.0
	K01MVK D=1.3	60	50	1.82	1.85	3.0
	K02VKBR	60	50	3.11	3.20	0.0
	K02VKBR D=1.3	60	50	2.29	2.32	0.9
	K02CRBR	60	50	4.34	4.20	0.0
	K02CRBR D=1.3	60	50	3.20	2.93	1.0

Appendix F: SLIDE™ Overall Slope Analysis

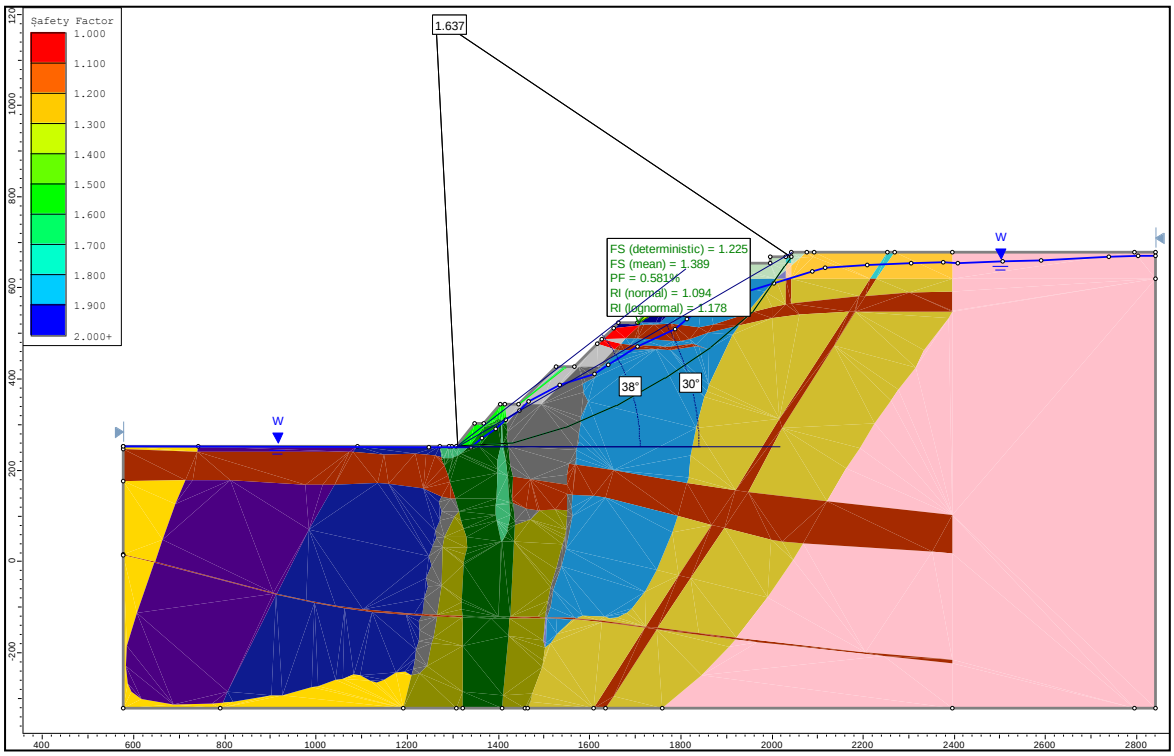
Tier 1 North Design Section (N)



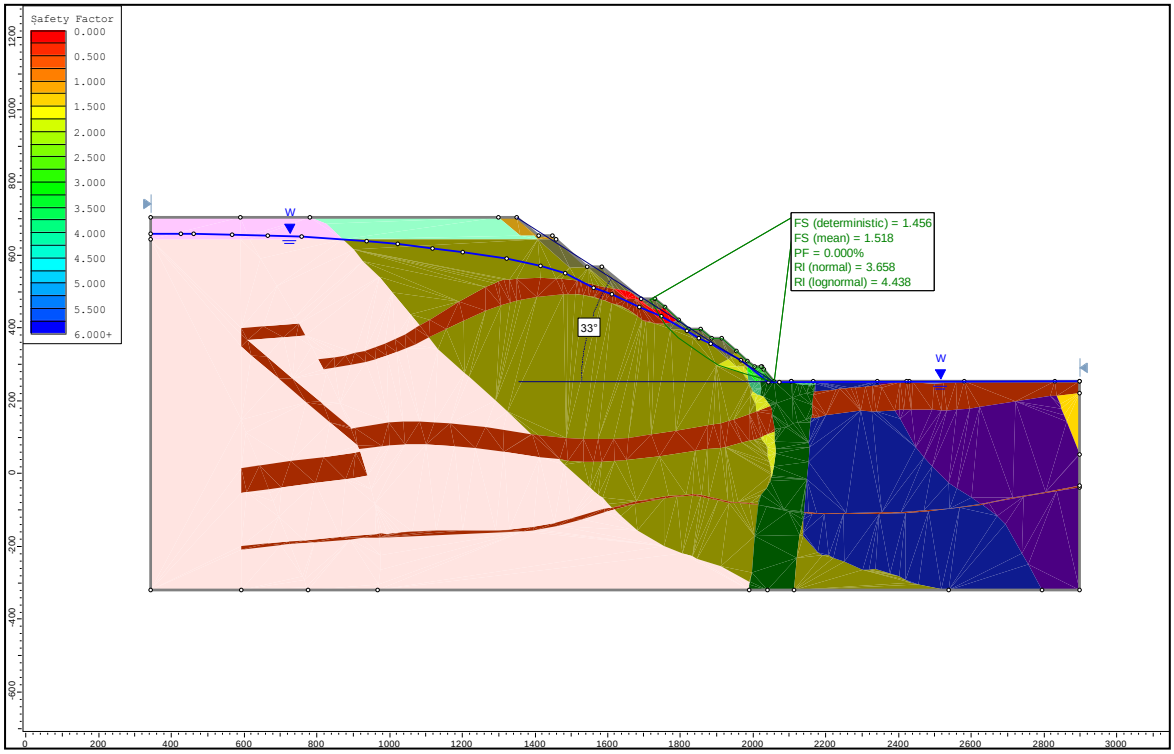
Tier 1 Southeast Design Section (SE)



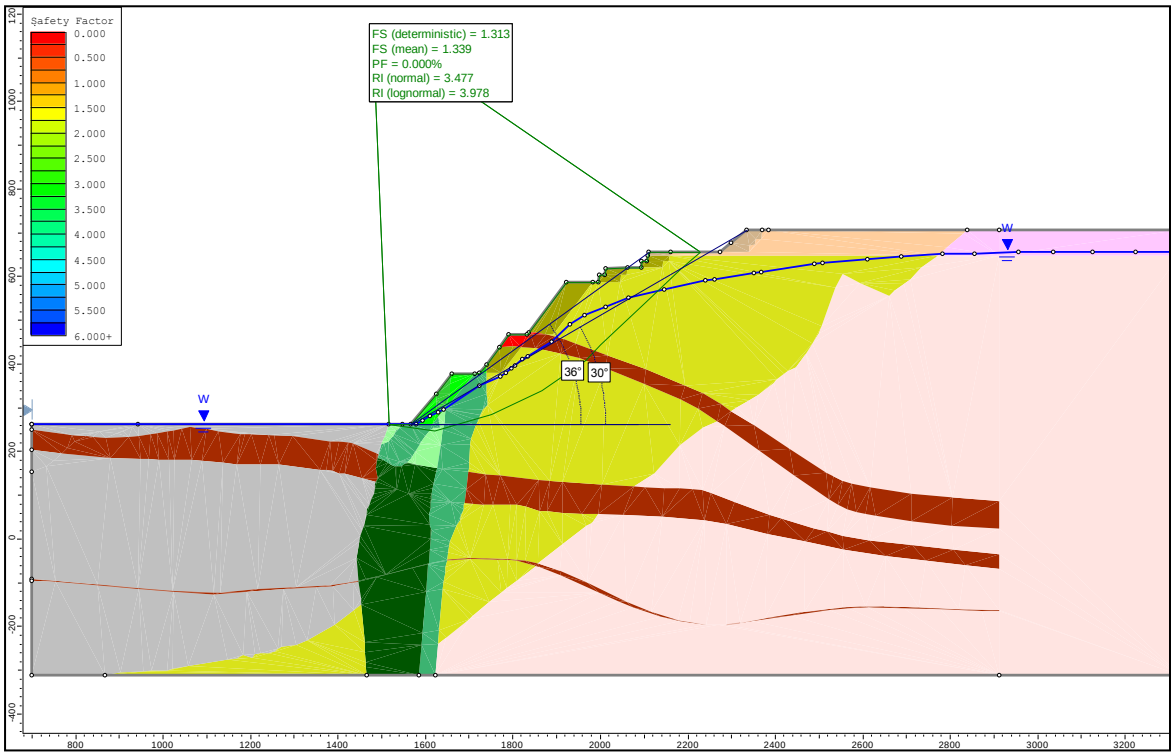
Tier 1 South Design Section (S)



Tier 1 South southwest Design Section (SSW)



Tier 1 West southwest Design Section (WSW)



Appendix G: JRC_F/JRC_O and JCS_F/JCS_O Ratios

JCS_F/JCS_O Ratios

Tier 2 Domain	Fresh JCS_F/JCS_O	Weathered JCS_F/JCS_O
STRV1	0.13	0.14
STRV2	0.15	0.16
STRV3	0.36	0.33
STRV4	0.13	0.14
STRV5	0.13	0.14
STRV6	0.28	0.30
STRV7	0.23	0.27
STRV8	0.16	0.17

JRC_F/JRC_O Ratios

Tier 2 Domain	Fresh JRC_F/JRC_O	Weathered JRC_F/JRC_O
STRV1	0.25	0.25
STRV2	0.27	0.28
STRV3	0.41	0.40
STRV4	0.24	0.26
STRV5	0.24	0.25
STRV6	0.36	0.38
STRV7	0.31	0.41
STRV8	0.27	0.26